

# **Scuola Superiore Sant'Anna di Studi Universitari e di Perfezionamento**

The International Doctoral School in Innovative Technologies of  
Information & Communication Engineering and Robotics  
*curriculum BioRobotics*



## **A BioRobotic approach towards Artificial Touch**

*by*  
*Calogero Maria Oddo*

A thesis submitted in partial fulfillment of the requirements of the Scuola Superiore Sant'Anna for the degree of Philosophiæ Doctor (Ph.D.)

Tutor: Prof. Maria Chiara Carrozza  
*Professor of Biomedical Engineering and Robotics*  
*The BioRobotics Institute, Scuola Superiore Sant'Anna*

Pisa, Italy

May 2011

*A mia moglie Elettra, con amore e stima  
mi rendi pienamente felice  
sei la mia guida, sono fiero di te  
ti amo*

*Ai miei Genitori, con gratitudine  
per ieri, oggi e domani  
e a Rosario, il mio fratellino  
vi voglio bene*

*Ai Nonni  
e a Titti e Paolo  
a varie distanze siete tutti vicini*

*... se la cosa va avanti*

## Acknowledgment

There is a fine but radical difference between a standalone technical problem, though most challenging, and a scientific investigation presenting technical challenges while addressing a higher level objective.

This is well depicted by the difference between education towards being an Engineer and the further steps towards being a Researcher. As a consequence, the studies for succeeding in both Bachelor and Master degrees were actually very different, though fundamental, with respect to the PhD program.

I progressively realized those substantial differences while addressing the challenge of publishing the research results reported in this thesis.

To publish a research study is actually an objective, but it is a mean as well, since it is one of the best ways to orient the intermediate actions so that the final outcome would have a scientific impact.

I would have never realized this, nor defined my research objectives, strategy and choices, without the guide of my Mentor, Prof. Maria Chiara Carrozza. I am very proud for having been supervised by Prof. Carrozza in my doctoral studies in BioRobotics at the Scuola Superiore Sant'Anna, as well as in all my previous theses at the University of Pisa (Bachelor and Master of Science in Electronic Engineering) and at the Scuola Superiore Sant'Anna (First and Second level Degrees in Industrial and Information Engineering), and I sincerely thank Prof. Carrozza for all the opportunities I had in these years.

I sincerely thank Prof. Paolo Dario for the competitive though familiar research environment I had the opportunity to be part of at The BioRobotics Institute, and for the motivations I got every time I listened or read one of his speeches to Researchers and PhD students.

I am indebted with researchers, colleagues and friends I encountered during my studies towards the PhD: Dr. Lucia Beccai for her major contributions in orienting the studies on artificial tactile sensing and for the reciprocal trust we established during this collaboration; Prof. Johan Wessberg for having provided non-restricted access to precious experimental sessions and datasets and for the related discussions on the human sense of touch; Dr. Fabrizio Vecchi and Dr. Stefano Roccella for their meaningful advices and peaceful smiles; Mr. Marco D'Alonzo for everyday friendly presence in the laboratory; Dr. Nicola Vitiello for the objectives and experiences we shared while always being positive and good friends regardless of the required efforts.

A particular acknowledgment is for the technical staff of The BioRobotics Institute, with particular regards to Mr. Riccardo Di Leonardo and Mr. Carlo Filippeschi, for their support in fabricating prototypes and using instruments.

Finally, I would like to thank the Scuola Superiore Sant'Anna as a whole, to which I am intimately and emotionally bonded. While being at the Scuola, I feel like at home.

## **Evaluation Committee**

**Prof. Maria Chiara Carrozza** (President of the Committee)

*Professor of Biomedical Engineering and Robotics  
Director of Scuola Superiore Sant'Anna, Pisa, Italy*

**Prof. Paolo Dario**

*Professor of Biomedical Engineering and Robotics  
Director of The BioRobotics Institute of Scuola Superiore Sant'Anna, Pisa, Italy*

**Prof. Arianna Menciassi**

*Associate Professor of Biomedical Engineering and Robotics  
The BioRobotics Institute, Scuola Superiore Sant'Anna, Pisa, Italy*

**Prof. Cecilia Laschi**

*Associate Professor of Biomedical Engineering and Robotics  
The BioRobotics Institute, Scuola Superiore Sant'Anna, Pisa, Italy*

**Dr. Cesare Stefanini**

*Assistant Professor of Biomedical Engineering and Robotics  
The BioRobotics Institute, Scuola Superiore Sant'Anna, Pisa, Italy*

**Dr. Barbara Mazzolai**

*Coordinator of the Center for Micro-BioRobotics@SSSA, Pontedera, Italy  
Istituto Italiano di Tecnologia, Genova, Italy*

**Dr. Lucia Beccai**

*Team Leader of the Center for Micro-BioRobotics@SSSA, Pontedera, Italy  
Istituto Italiano di Tecnologia, Genova, Italy*

**Prof. Sir Alfred Cuschieri**

*Professor of Surgery  
Director of the Institute of Medical Science and Technology  
Dundee and St Andrew's Universities, UK*

**Prof. Johan Wessberg**

*Associate Professor of Physiology  
Department of Physiology, University of Gothenburg, Gothenburg, Sweden*

**Prof. Chris Melhuish**

*Professor of Intelligent Autonomous Robotic Systems  
Director of Bristol Robotic Laboratory  
University of Bristol and the West of England, Bristol, UK*

**Prof. Giovanni Cioni**

*Professor in Child Neurology and Psychiatry, Faculty of Medicine, University of Pisa, Pisa, Italy  
Head of the Department of Developmental Neuroscience, IRCCS, Stella Maris, Pisa, Italy*

**Dr. Sabina Lucia**

*Researcher at the Istituto di Biofisica  
National Research Council, Section of Pisa, Pisa, Italy*

**Dr. Giovanni Cercignani**

*University Member at the Istituto di Biofisica  
National Research Council, Section of Pisa, Pisa, Italy*

## TABLE OF CONTENTS

<b>ARTIFICIAL TOUCH: A BIOROBOTIC APPROACH .....</b>	<b>7</b>
<b>1. TEXTURE ENCODING AND PERCEPTION IN DYNAMIC-TOUCH .....</b>	<b>11</b>
<b>2. TACTILE STIMULATION IN PASSIVE-TOUCH .....</b>	<b>18</b>
<b>3. PASSIVE- AND ACTIVE- ARTIFICIAL DISCRIMINATION OF TEXTURES .....</b>	<b>31</b>
<b>4. CONCLUSIONS AND FUTURE RESEARCH DIRECTIONS.....</b>	<b>67</b>
<b>BIBLIOGRAPHY .....</b>	<b>72</b>
<b>PUBLICATIONS LIST .....</b>	<b>82</b>
Published papers .....	82
1. ISI journals .....	82
2. Journals.....	82
3. Book chapters .....	82
4. International Conferences .....	83
5. National Conferences .....	83
<b>APPENDIX: COPY OF SIGNIFICANT PAPERS PUBLISHED DURING THE PHD PROGRAMME .....</b>	<b>85</b>

## Artificial Touch: a BioRobotic approach

This thesis is the result of part of the research activities carried out during a three year PhD program in BioRobotics at the Scuola Superiore Sant'Anna di Studi Universitari e di Perfezionamento, Pisa, Italy, under the supervision of Prof. Maria Chiara Carrozza.

The focus is on artificial tactile sensing, aiming at the design of a sensorized fingertip for integration into mechatronic hands within both upper limb prosthetics and humanoid robotics.

The original contributions by the PhD candidate were in the design and fabrication of bioinspired artificial tactile sensing systems, the development of mechatronic tools for their evaluation in parallel to studies on the human sense of touch, the implementation of experimental protocols, and the elaboration and assessment of models for the interpretation and critical analysis of experimental results.

The study was funded by the Scuola Superiore Sant'Anna with a dedicated doctoral scholarship, and by the EU FP6 Naniobiotact (Nano-engineering biomimetic tactile sensors) and FP7 Nanobiotouch (Nano-resolved multi-scan investigations of human tactile sensations and tissue engineered nanobiosensors) research projects under the NMP (Nanosciences, Nanotechnologies, Materials and new Production Technologies) theme. A particular collaboration, as confirmed by joint journal publications, was established with the Department of Physiology of University of Gothenburg (Prof. Johan Wessberg) and with the Bio-medical and Micro Engineering Research Centre, School of Mechanical Engineering of University of Birmingham (Prof. Mike Ward).

The development of artificial tactile systems is one of the chief open challenges in robotics and is directly linked with the findings and debate on human touch. Therefore, the research activities were undertaken with a biorobotic approach (Dario et al., 2008), merging a systematic study of state of the art of artificial tactile sensing in parallel with that of literature of neurophysiology of human touch. BioRobotics offers the possibility to develop emulator of the human subjects, with different characteristics and design parameters, to selectively evaluate the related effect. As a consequence, this approach fosters the definition of design parameters while developing bioinspired tactile sensory systems but it could be also useful to provide hints and suggestions to develop experimental protocols and models in neurophysiology.

Among the various properties that an artificial tactile system should be able to sense, texture is one of the most challenging and less established (Oddo et al., IEEE TRo 2011). This is dedicatedly addressed in this study, which investigates the (bioinspired) encoding of textural features of tactile surfaces, with a particular focus on roughness.

The development of a tactile sensory system which is able to mimic the human sense of touch in the encoding of textures, and is compact enough to be integrated into articulated artificial fingers, would significantly improve dexterous manipulation (e.g., exploited in industrial, service, or

assistive robotics) and upper limb prosthetics (Dario, 1991; Howe, 1994; Bicchi, 2000). Particularly, within prosthetics one of the main drawbacks of current commercial systems is the lack of (tactile) sensory feedback (Biddiss et al., 2007); as a consequence, the user is unable to feel an item held by the hand. Such ideal sensory feedback system is schematically composed by two main modules: the artificial sensory subsystem and the interface subsystem. While this research study targets the design, development and experimental evaluation of the former subsystem, its bioinspired implementation (with particular regards to the kind of encoding of tactile information) could also reveal to be effective in its porting to the interface subsystem.

As it will be detailed in Section 1, while addressing the encoding of textural features, in robotics the major sources of bioinspired design are human Pacinian (type-II) mechanoreceptors as an alternative to either Merkel or Meissner (both are type-I) units. These alternative options reflect the open debate in the neuroscience community with respect to human touch.

In this work, the choice (motivated and detailed in Section 3) was to get the major design inputs from the potential role that in humans has been hypothesized for high-density surface-located type-I mechanoreceptors (Vallbo and Johansson, 1984; Yoshioka et al., 2001; Johnson & Yoshioka, 2001). As a consequence, this results in the assumption that the gathering of textural information takes benefit from the implementation of an artificial tactile system which can encode dynamic events with a low threshold in sensitivity, narrow receptive field and human-like high density of surface-located taxels. To this aim, piezoresistive and capacitive MicroElectroMechanical Systems (MEMS) were used as core sensors in this research study, and their integration into tactile arrays as well as their evaluation were driven by bioinspiration and biomimetism according to such design choice, particularly for the definition of the physical features, the experimental protocols, and the data analysis techniques.

This research attempt was partitioned into a number of particular objectives, most of which resulted in the publication of the related achievements. Selected and adapted excerpts from such published results are integrated in the thesis, while the complete publications list is provided at the end of the manuscript and the significant full papers are annexed as an appendix to this work. Particularly, out of the total number of papers coauthored by the PhD candidate, the contents from six ISI journal publications and one IEEE conference paper (finalist for best student paper award) were integrated in the thesis. Below, each section of the thesis is associated to its particular research topics and to the related significant papers coauthored by the PhD candidate.

- Section 1 – investigation of methods, established findings and open debate in neuroscience with respect to the coding and perception of textural features of tactile surfaces, as a source of bioinspiration in the biorobotic study (this Section is in part unpublished, and in part is excerpted from Oddo et al., *Sensors* 2009; Oddo et al., *Mechatronics* 2011; Oddo et al., *Sensors* 2011; Oddo et al., *IEEE TRo* 2011):

- roughness as a fundamental dominant dimension of texture;
- established electrophysiological methods (with particular reference to microneurography);

- established psychophysical methods;
  - mechanoneurotransduction phenomena in the human hand, with particular references to the classes of mechanoreceptors and possible strategies for the coding of textural features of tactile stimuli;
  - role of fingerprints;
  - relevance of motion (dynamic touch) and role of kinesthesia;
  - possible perceptual strategies based on neural codes;
  - experimental protocols:
    - static- vs. dynamic- touch;
    - passive- vs. active- touch.
- Section 2 – design, development and assessment of a mechatronic tactile stimulation platform for human and artificial passive-touch studies (this Section is mostly excerpted from Oddo et al., Mechatronics 2011):
    - motivation of the need of such a robotic device in human and artificial passive-touch protocols;
    - particular requirements and reinforced constraints to guarantee platform suitability with human electrophysiological techniques such as microneurography;
    - original platform design;
    - platform assessment:
      - traditional robotic validation;
      - original validation via microneurographic recordings.
- Section 3 – bioinspired design, development and assessment of artificial tactile systems for the discrimination of textures (this Section is mostly excerpted from Oddo et al., Sensors 2009; Oddo et al., IEEE RoBio 2009; Muhammad et al., SNA 2011; Muhammad et al., MNE 2011; Oddo et al., Sensors 2011; Oddo et al., IEEE TRO 2011)
    - artificial tactile encoding of roughness via spectral cues: frequency-locking:
      - requiring constant, known or dedicatedly measured fingertip-stimulus relative tangential velocity;
      - frequency-locking dominated by spatial coarseness of tactile stimulus vs. by fingertip patterning (fingerprints), as a function of the physical design (bioinspired to type-I vs. to type II mechanoreceptors) of the artificial fingertip;

- design of artificial tactile sensory systems based on different technologies and bioinspired to particular features of the human fingertips:
  - integrating arrays of capacitive or piezoresistive MEMS sensors;
  - density and positioning of sensing units bioinspired to type I mechanoreceptors;
  - compliant packaging;
  - biomimetic fingerprints;
  - progressively going towards full integration into an anthropomorphic, articulated robotic finger;
- passive-touch evaluation, via the purposely developed mechatronic platform, with forces, velocities and tactile stimuli as for and in parallel to human-touch studies:
  - constant and known fingertip-stimulus relative tangential velocity;
  - discrimination of gratings via frequency-locking;
  - parallel human-touch study via microneurography, to evaluate the significance of the frequency-locking approach in artificial touch;
  - study of directional isotropy as a function of shape of fingerprints;
- active-touch evaluation via a robotic finger mimicking human tactile exploratory tasks:
  - stereotyped trajectory;
  - discrimination of gratings via frequency-locking;
  - discrimination suitability of textiles via frequency-locking;
- phase-locking for artificial roughness encoding:
  - providing tactile cues additional to those carried out by principal frequencies only;
  - potentially appropriate for overcoming the restrictive conditions on (constant, known, or dedicatedly measured) velocity, encountered with frequency-locking.
- Section 4 – conclusions and future directions (overviews on future directions are in part excerpted from Oddo et al., Sensors 2009; Oddo et al., Mechatronics 2011; Oddo et al., Sensors 2011 and Oddo et al., IEEE TRo 2011, and in part are unpublished):
  - summary of research strategy and objectives and of achieved results;
  - proposed modular artificial-touch model being potentially appropriate for sensory feedback in upper limb prosthetics and artificial intelligence in (humanoid) robotics.

## 1. Texture encoding and perception in dynamic-touch

Roughness is associated to the spatial modulation of the surface and has been described in the literature as the sense of spatial coarseness (Yoshioka et al., 2007); it is a major dimension of texture, together with softness to which it is orthogonal (Hollins et al., 1993); during tactile exploratory tasks, it conveys most of discrimination information with respect to the other minor textural dimensions such as stickiness, warmth, bumpiness, harshness, etc., resulting in a consolidated agreement for a primacy of the smooth-rough dimension as a descriptor, even if not unique, of surface textures (Hollins et al., 1993; Yoshioka et al., 2007; Yoshioka & Zhou, 2009); furthermore, in humans roughness is mediated by neural mechanisms which are also involved in tactile guidance during dexterous manipulation (Yoshioka et al., 2001; Johansson & Flanagan, 2009).

As regards the neurophysiologic experimental paradigms to study the human sense of touch, in the periphery the activity of single afferents in the skin can be recorded using the microneurography technique (Vallbo et al., 2004); CNS activity can be probed using electroencephalography (EEG) to reconstruct cortical sources (Grave de Peralta et al., 2001), while sensory thresholds and percepts can be assessed using psychophysical methods (Hollins & Risner, 2000).

A varied set of spatial features of tactile stimuli should be taken into account for investigating the neural coding and perception of roughness. Therefore, to reduce the dimensionality of the analysis, the features of tactile stimuli were typically investigated by separate and controlled variation of particular parameters of standardized surfaces (Jones & Lederman, 2006). As an example, considering ridged tactile stimuli (gratings), which are widely used to investigate roughness encoding in neurophysiological studies (Johnson & Yoshioka, 2001), the effect of controlled variations in groove width, ridge width, ridge orientation, ridge height, fine finishing, etc. was typically evaluated in the literature (Jones & Lederman, 2006). In human psychophysical experiments some groups highlighted the presence of a relatively narrow region where perceived roughness increases together with the groove width of ridged stimuli, followed by a flattened perception in case of very coarse gratings, up to 8.5 mm of groove width (Lawrence et al., 2007). In parallel to this, using embossed dots a monotonic function between roughness and dots spacing was presented (Meftah et al., 2000), while an inverse “U” shape was also shown since, depending on the height of the raised elements, a very coarse patterning may be perceptually considered as an almost smooth surface (Klatzky et al., 2003). Therefore, regardless on the particular differences which could be pointed out in the perceptual curves due to the specific experimental conditions and surfaces (Johnson & Yoshioka, 2001; Jones & Lederman, 2006), an established findings is that the surface patterning (at both micro- and macro- scales) of tactile stimuli is actually represented along the smooth-rough dimension of texture; definitely, the intensity of roughness perception monotonically increases together with spatial coarseness at least in a range from very fine up to medium-coarse tactile stimuli.

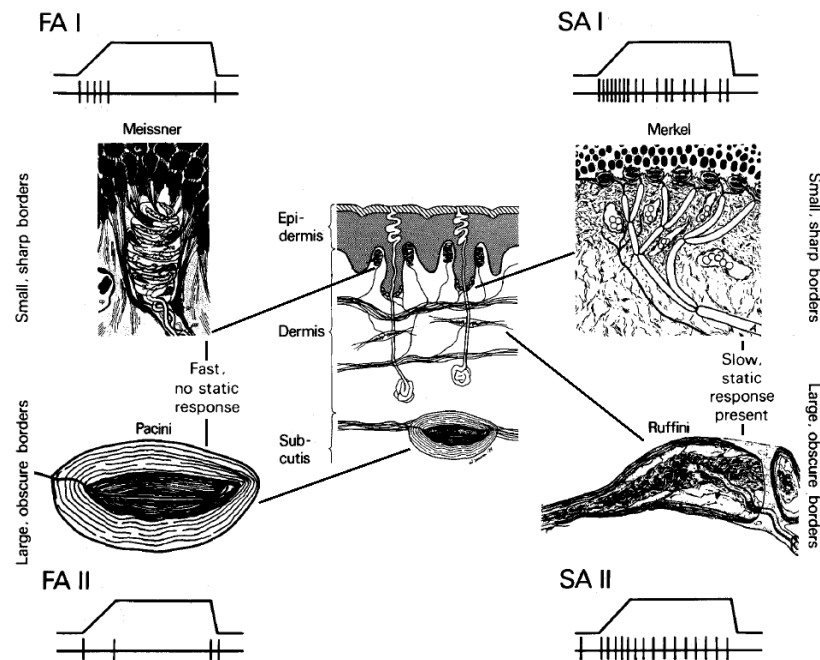


**Fig. 1.** Structure and location of tactile mechanoreceptors in a section of glabrous skin of the hand (freely adapted from Vallbo & Johansson, 1984). The Merkel cell neurite complexes (Slowly Adapting type I, SAI) have a density in the order of 70 units/cm<sup>2</sup> in the fingertips, are located at the interface between epidermis and dermis, have small receptive field with distinct borders and show static response to sustained indentations. The Meissner corpuscles (Fast Adapting type I, FAI or also Rapidly Adapting, RA) have a density in the order of 140 units/cm<sup>2</sup> in the fingertips, are located in the dermis at the interface between epidermis and dermis, have small receptive field with distinct borders and fast adaptation to varying mechanical stimulation, with no static response to sustained indentations. Ruffini endings (Slowly Adapting type II, SAII) have a density in the order of 10 units/cm<sup>2</sup> in the fingertips, are located in the dermis layer, have large receptive field with obscure borders and show static response to sustained indentations. Pacinian Corpuscles (Fastly Adapting type II, FAII or also PC) have a density in the order of 20 units/cm<sup>2</sup> in the fingertips, are deeply located (subcutis layer), have large receptive field with obscure borders and fast adaptation to varying mechanical stimulation, with no static response to sustained indentations.

Considering dynamic exploration of extremely fine textures, various researchers showed that humans can detect even up to microtextures (LaMotte & Srinivasan, 1991) and that the human perception of roughness is severely degraded in case of lack of tangential motion between the fingertip and the tactile stimuli, i.e. considering dynamic vs. static touch (Morley et al., 1983; Gardner & Palmer, 1989; Radwin et al., 1993; Jones & Lederman, 2006).

In contrast to the consolidated findings reported above, the physical determinant of perceived roughness is not yet fully understood (Jones & Lederman, 2006), and the detailed neuronal mechanisms and relative contributions of the different classes (Fig. 1) of human mechanoreceptors in the encoding of roughness remain to be identified (Yoshioka et al., 2007). Therefore, an established agreement has not been reached yet neither on the most informative mechanoreceptors (particularly as regards the role of Merkel, Meissner and Pacini corpuscles) nor on the coding strategy (e.g., temporal, spatial, spatiotemporal, intensity) used by humans to map the roughness dimension of texture.

Various studies aimed at demonstrating that roughness is encoded by the Pacinian system for fine textures (Hollins et al., 2001; Bensmaïa and Hollins, 2003-2005): Hollins and Risner supported the Katz's duplex theory, according to which roughness is supposed to be mediated by different classes of mechanoreceptors via vibrational cues for fine forms and via spatial cues for coarse textures (Hollins & Risner, 2000): particularly, PC were considered to have a key function in the coding of fine patterns. Conversely, Johnson and colleagues presented human psychophysical studies and complementary electrophysiological results with monkeys supporting a unified peripheral neural mechanism (Fig. 2) for roughness encoding of both coarse and fine stimuli, based on the spatial variation in the firing rate of slowly adapting type I (SAI; Merkel) afferents (Connor et al., 1990; Connor et al., 1992; Blake et al., 1997; Yoshioka et al., 2001).

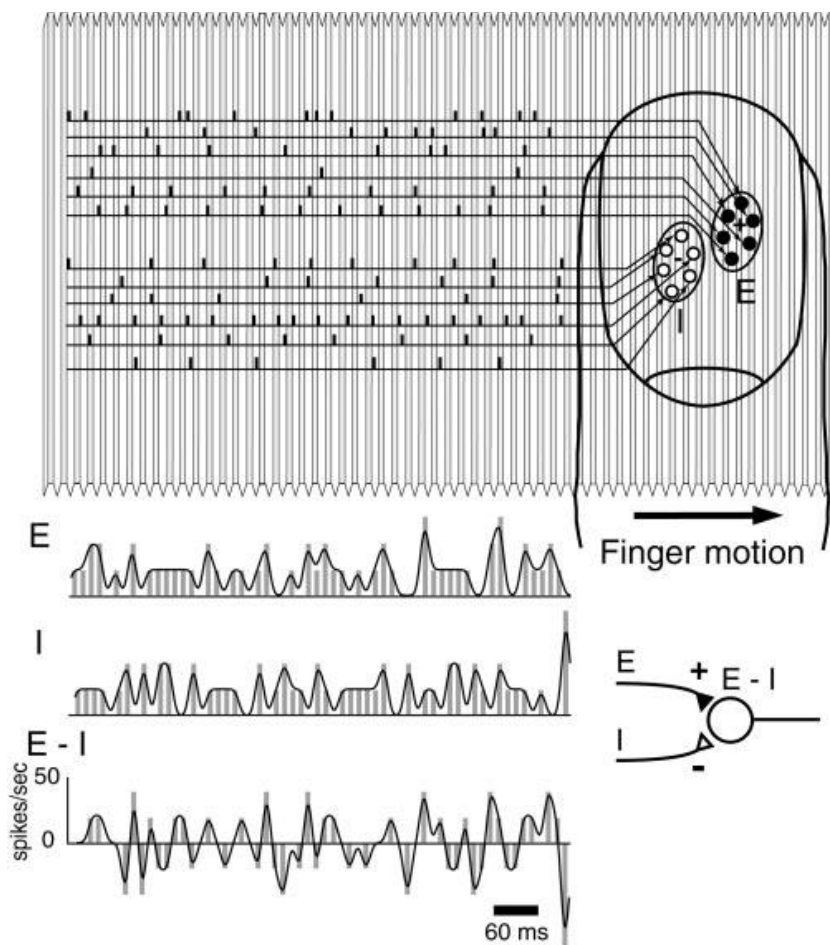


**Fig. 2.** Model by Yoshioka et al. (2001), proposing roughness encoding based on spatial variation in the firing rate of SAI units, revealed by means of excitatory (E) and inhibitory (I) afferents located in neighboring regions of the fingerpad.

As it will be detailed in the discussion of the biorobotic artificial touch studies (Sections 3 and 4), a notable hypothetical human model, based on coincidence detection of neural events (Fig. 3), was recently accounted for by Johansson and Flanagan (2009).

Such model proposes that: i) the relative timing of neural spikes elicited in (neighboring) tactile units of the fingertip conveys significant information during manipulation activities; ii) the spikes pass through neural afferents showing differentiated delays one to the other (due to dispersion of conduction velocity) in the pathways up to the second order (Cuneate) neurons; iii) second order neurons propagate the firing events to the higher stage in case that the differential delay introduced by the afferent pathways compensates the relative spike timing at the level of mechanoreceptors in the fingerpad; iv) the tactile stimulus is pre-perceptually represented through the pattern of second order neurons being activated (i.e. those detecting a coincidence of incoming neural spikes, and thus propagating the firing up to the higher stage) during finger-surface mechanical interaction.

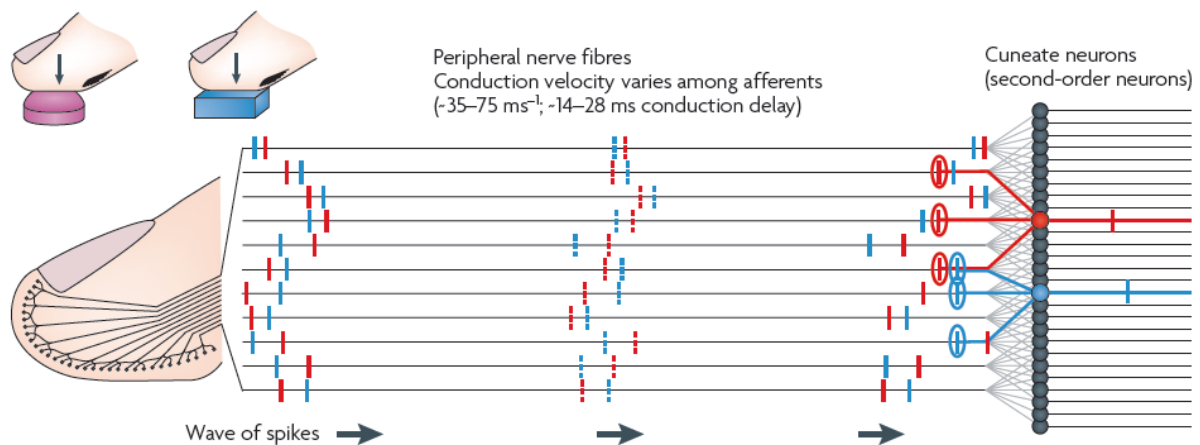


**Fig. 3.** Hypothetical model, accounted by Johansson and Flanagan (2009), based on coincidence detection of neural events for the fast processing of afferent information.

Such ongoing debate in the neuroscience community is currently represented only in part within the robotic studies on the artificial mimicry of the sense of touch.

As an example, various robotic research papers (Edwards et al., 2008; de Boissieu et al., 2009; Scheibert et al., 2009) exclusively considered the Pacinian system as a design reference, and this biorobotic research study also aims at proposing a different approach.

The following selected quotes from a milestone study by Yoshioka, colleagues and Johnson (2001), also dealing with the shift from verificationism towards falsificationism occurring to epistemology in the middle of the XX<sup>th</sup> century, better provide an insight on the open neuroscience debate (which applies to robotics as well).

*“Hollins and his colleagues have provided evidence of this hypothesis by showing that intense, high-frequency vibration can make a relatively smooth surface feel less smooth (Hollins et al., 2000). However, after it is demonstrated that the SAI hypothesis accounts for roughness perception for fine and coarse surfaces, the first hypothesis seems moot. Why (to invoke parsimony) would the nervous system use two different mechanisms when one mechanism accounts for the perceived roughness of both fine and coarse surfaces? But this is a logical, not an empirically based, argument. The empirical finding is that we could, in fact, find no correlation between any measure of the PC discharge and the subjective roughness judgments reported in the psychophysical experiments; because the PCs responded equally vigorously to fine and coarse surfaces, every PC measure yielded nearly the same predicted roughness. The neural basis for the observations by Hollins and his colleagues is unclear; the intense, high-frequency vibration could have affected the discharge of SAI and RA afferents as well as that of PC afferents, or it could have affected some central interaction between the PC and SAI systems (Tommerdahl et al., 1999).*

*... The argument that roughness perception is accounted for by variation in firing rates between SAI afferents is based on the ideas of falsification (Popper, 1959; Platt, 1964); when there are many possible explanations, one can arrive at a single explanation only by demonstrating the adequacy of that explanation and the falseness of the rest. First, consider adequacy.*

*... There are no data of which we are aware that suggest that SAI spatial variation does not account for roughness perception. Second, consider falseness. The test of the falseness of a putative neural code in these studies was inconsistency, not just that it fitted the results less well than did another hypothesis. If two surfaces evoke neural responses with the same neural coding measure (e.g., PC impulse rate) but one is perceived as smooth and the other rough, then that measure cannot be the basis for the two percepts. The consistency test has resulted in the rejection of all codes based on PC responses (Lederman et al., 1982; Connor et al., 1990; and the present study), all codes based on RA responses (Lederman et al., 1982; Johnson and Hsiao, 1994; Blake et al., 1997), all codes based on SA2 responses [by analysis of data reported in Phillips et al. (1992) and Phillips and Matthews (1993)], all codes based on mean impulse rate (Connor et al., 1990; Connor and Johnson, 1992), and all temporal codes (Connor and Johnson, 1992). Our working hypothesis is that the brain uses a single neural coding mechanism for all surfaces. An alternative possibility is that different neural codes are used for different surfaces.”*

The lack of complete understanding of the neural coding of texture via the mechanoreceptors in the human fingertip applies to the interaction between the tactile stimuli, the epidermal ridges and the mechanoreceptors as well (Gerling & Thomas, 2008). Focusing on the fingerprints, they were hypothesized as vibration promoters (Scheibert et al., 2009) and their structure was shown to increase the sensitivity in tactile activities with a major effect on surface located type I receptors (Maeno et al., 1998; Yamada et al., 2002); Pacinian Corpuscles were also considered as detectors of fingerprint-mediated stimulus-related vibrations (Srinivasan et al., 1990). Evidence was provided with monkey subjects that gratings locally oriented parallel to the finger ridges elicit stronger response than tactile stimuli oriented along the orthogonal direction (Wheat & Goodwin, 2000). However, the association of the directional anisotropy, observed in both SAI and RA

population responses, to physical phenomena is still unclear, as from the following selected quotes (Bensmaïa et al., 2006):

*“There are two hypotheses as to the cause of the observed anisotropy in afferent responses to gratings, one mechanical and the other neural. The effect of grating orientation may be due to a structural anisotropy in the skin.*

*... Another possibility is that the anisotropy in the response is due to afferent branching ...*

*The extent to which mechanical anisotropy and afferent branching play a role in producing the observed effects of grating orientation on spatial modulation is unclear.”*

To investigate those phenomena, in the final design presented in this work, the density and positioning of sensing units on the artificial fingerpad mimicked that of surface-located type-I human mechanoreceptors; the polymeric packaging layer was compliant and recovered its original shape after the application of tactile stimuli; biomimetic fingerprints were embossed onto the surface of the covering material; the effect of their shape on the encoding of tactile vibrational cues was investigated with a dedicated differential study via selective and precise variation of the curvature of ridges embossed onto the fingerpad; roughness encoding was investigated via passive stimulation of the artificial fingertip and during active exploratory tasks by a robotic finger.

Passive- and active- touch are the main experimental paradigms used in the literature to study the neuronal mechanisms of the sense of touch in the human hand, and were the common framework for the evaluation of the artificial tactile systems developed during the PhD program.

Various definitions of the passive- and active- paradigms are actually possible, and one of those involves considerations on the energy flow associated to the dynamic phases of the tactile experience (Prescott, 2011). With such a definition, similarly to passive measurement instruments, in dynamic passive-touch the (kinetic) energy required to apply the relative motion between the sensory system and the tactile surface is provided via the surface under test. Conversely, in active-touch protocols the (kinetic) energy to achieve the dynamic tactile stimulation condition is provided by an actuated mechanism closely integrated with the (human or artificial) sensory system.

A possible application of such definition to dynamic-touch studies (either passive- or active-) results in the core of the tactile stimulation sequence being characterized by a tangential relative motion between the fingerpad and the textured surface, and the difference between passive- and active- is in the body (i.e., fingertip or tactile stimulus) which actually moves with respect to an absolute reference frame. The relative motion can be obtained by sliding the tactile stimulus while the fingertip is still (passive- dynamic-touch) (Yoshioka et al., 2001), or by exploration via the finger (active- dynamic-touch) while the tactile stimulus is static (Lawrence et al., 2007).

While considering the deformation of skin tissues, established findings showed that passive- and active- passive protocols are equivalent (e.g., up to 4 N in Birznieks et al., 2001). In addition, one may wonder whether this is the same at perceptual level, considering that in passive-touch there is a lack of voluntary movement, while in active-touch the percept may be integrated by kinesthetic afferent sensory feedback or by efference copy associated to motion dynamics of the body part. However, with respect to this particular point, a dedicated study (Lederman, 1981) excluded any difference in the perception of roughness by passive- and active- touch.

In both human and artificial passive-touch studies, the presentation of tactile stimuli should be replicated several times repeatably in the same conditions to infer models based on statistical analysis of acquired data (Johansson & Birznieks, 2004); also, the passive-stimulation operation should avoid to introduce spurious information by the system delivering the tactile surfaces. To this aim, a dedicated mechatronic platform was designed, fabricated and assessed, as it will be detailed Section 2. The so developed mechatronic platform enabled a variety of electrophysiological studies on the human sense of touch via the microneurographic technique.

The PhD candidate participated in part and had direct access to such microneurography (Vallbo et al., 2004) experimental sessions and data, carried out under passive-touch protocols at the Department of Physiology of University of Gothenburg and approved by the ethics board of the University of Gothenburg.

During microneurography, the subjects were seated comfortably in a dentist's chair, the left arm resting in a vacuum cast for stabilization and maximum comfort. Tungsten needle electrodes were inserted in the left median nerve, 8 cm above the elbow. The nerve signal was band-pass filtered at 200-4000 Hz, sampled at 12.8 kHz together with analog data from a purposely developed tactile stimulation mechatronic platform, and stored on a PC using the ZOOM/SC system developed at the Department of Physiology, Umeå University, Sweden. Recorded nerve impulses were inspected off-line on an expanded time scale using in-house software implemented in MATLAB (The Mathworks) and were accepted for subsequent analyses only if they could be validated as originating from a single afferent. Before running the experimental protocol, the units' responses and receptive fields were explored using calibrated nylon filaments (von Frey hairs) and were classified as SAI, SAII, RA, or PC according to the adaptation of the response to sustained stimulation and size of the receptive field (Vallbo & Johansson, 1984; Chambers et al., 1972).

Enabled by the collaboration with the Department of Physiology of University of Gothenburg, the possibility to have access to a significant human microneurography dataset was a key element towards the development of biomimetic artificial tactile sensory systems and the elaboration of models and discrimination strategies bioinspired to the observed mechanoneurotransduction phenomena. In total, the PhD candidate had access to a dataset with impulses of single tactile afferents in the left index and middle fingers which were recorded in 36 human healthy volunteers during passive-touch protocols implemented by means of the purposely designed mechatronic tactile stimulation platform (Oddo et al., Mechatronics 2011) discussed in Section 2.

## 2. Tactile stimulation in passive-touch

To achieve standardization and repeatability, the passive-touch approach requires a robotic stimulator that enables detailed analyses of receptor response or Central Nervous System (CNS) processing in human studies, or of encoding of tactile cues in artificial touch, through controlled variation of stimulation parameters, of stimulus spatial coarseness, materials and tribological properties, to make comparisons between sessions or participants, or to average over a large number of replications.

There are a number of particular requirements in the design of such a robotic tactile stimulation device. First, to allow repeatable experiments with standardized conditions, accuracy and precision in the control of stimulation parameters, such as the contact force and the sliding velocity profile, is required. Second, the device must guarantee a range of forces and movement velocities covering those that would be used by humans in the exploration of textures, while both normal and tangential forces need to be recorded as they are fundamental for human touch investigation. Studies on discriminative touch (Johnson & Yoshioka, 2001; Jones & Lederman, 2006) suggested: for the indentation force a range of at least 100 mN–5 N, with a control accuracy of about 5% of the reference force and sensing resolution within a few mN; 100 mm of stroke along the sliding direction and velocities up to 150 mm/s with  $\mu\text{m}$  position sensing resolution and steady state control accuracy. Such requirements apply to both artificial and human touch studies but, as it is detailed in the following, the latter ones present additional constraints due to the particular neurophysiological experimental methods while dealing with the biological system. The third challenging requirement, given that some classes of tactile receptors are highly sensitive to vibration up to 400 Hz or more (Connor & Johnson, 1992), is in developing a stimulator that could get into contact with the human finger free from any spurious vibration that could interfere with the encoding of tactile stimuli. Fourth, electrophysiological methods such as microneurography and EEG involve recording of signals in the  $\mu\text{V}$  range, and electromagnetic interference from the robotic system has to be minimized. Fifth, these experiments can require the participant to sit in a natural position and to remain relaxed for hours. Hence, the subject's comfort puts stringent demands on the mounting of the device and on the control laws of each DoF so that it can be adapted in 3D space to the position of the subject's arm, hand and finger (Birznieks et al., 2001). Finally, the programming operation by the experimenter to implement the targeted protocols has to be simple and flexible, and upgradeability of the platform should be possible.

The reviewed previous works span from platforms with flat or curve extended textured stimuli for studying the application of ridged or dotted surfaces to the fingerpad, to other devices with wide or pointed probes, to pinned stimulators for applying spatio-temporal indentation profiles with an array of contact locations. Some neurophysiological studies addressed the response of single afferents to the applied stimuli, while others took into account population of mechanoreceptors. Nevertheless, as regards the studies on texture perception and its related

dimensions (e.g., roughness), one of the major limitations of most of reviewed platforms is that they were developed for experiments in monkeys rather than humans, then presenting less demanding requirements since higher level of invasiveness is tolerated in animal model studies (Goodwin and Morley, 1987; LaMotte et al., 1998). Conversely, in this research study the parallel investigation of mechanoneurotransduction phenomena of the human hand was a strategic objective to foster the effective bioinspired design of artificial tactile sensory systems.

A considerable input was given in the 70's by the availability of digital controllers (Looft and Williams, 1979) which enabled the design of mechatronic platforms with customizable motion profiles to address specific experimental paradigms. This is confirmed by the fact that in the 80's a few platforms integrated complex mechanisms (Goodwin et al., 1985) for tuning the desired stimulation parameters. Furthermore, the analog circuitry was reduced as much as possible, remaining between the sensors and the controller only, and between the controller and the actuators or, at most, for implementing low-level force (or position) servo control (Byrne, 1975; Looft and Williams, 1979; LaMotte et al., 1983). As a matter of fact, almost all the reported tactile platforms employed digital processors for data storage at least, and for the generation of force and position references. In contrast to the almost standardized architecture for the control electronics, a greater variability could be found between the core mechanisms of the reported systems.

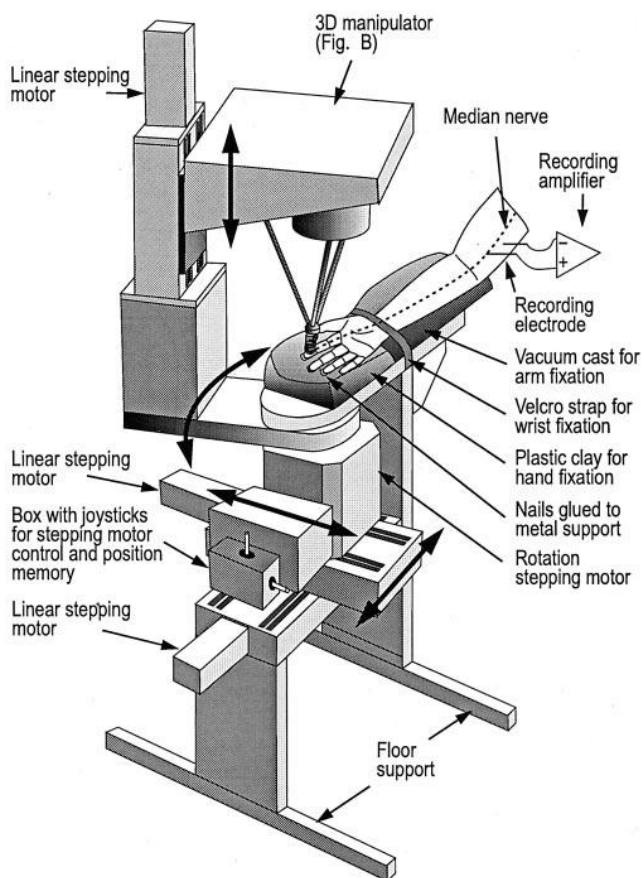


**Fig. 4.** Electromechanical tactile stimulator used by Birznieks and colleagues (2001). The design of the platform also considered ergonomic design since it was applied to human touch studies under the microneurographic technique (which requires the participant to sit relaxed for several hours in order to maintain stable electrical contact with the recorded tactile unit).

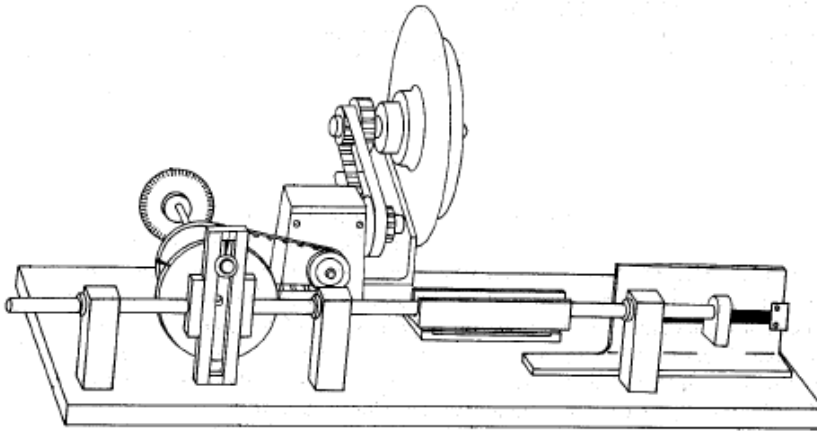


**Fig. 5.** A schematic diagram of the scotch yolk stimulator (Goodwin et al., 1985).

In the class of devices that were built to study the neural coding and perception of texture, Goodwin et al. (1985) used a scotch yolk driven by a DC motor which rotated at constant speed for producing a sinusoidal motion (Fig. 5). The stimulus was attached magnetically to a holding block mounted on a shaft actuated by the yolk. The amplitude was tuned modifying the mechanism, while the frequency could be continuously varied from 0.1 Hz to 2.0 Hz, choosing between a discrete set of reduction ratios or by modifying the driving voltage of the motor. The motion control was completely in open-loop, relying on the non-backdrivability of the mechanism in spite of subject-machine interaction. Digital electronics was integrated for storing the position of the stimulator and the finger-stimulus interaction force only, resulting in a lack of flexibility of the experimental protocol.

The advanced stimulator shown by LaMotte et al. (1983) controlled the sliding motion and the indentation position or load force of a selectable surface which, in turn, contacted and stroked the skin of the fingerpad in passive-touch studies (Fig. 6). The stimulus could be selected among eight flat plates carrying textured surfaces. The user could select the motion profiles, allowing the definition of the horizontal and vertical displacements or the load force, and the displacement velocities. The controlled Degrees of Freedom (DoFs) were moved by means of hydraulic actuators. A horizontal displacement of 50 mm and a bandwidth of 16 Hz, monitored by means of a LVDT transducer, were obtained. Similar performances were achieved for the indentation axis, whose range was limited to 6.3 mm in order to achieve higher position accuracy. Moreover, the indentation axis could be controlled with a force feedback servo by means of a force transducer. However, with respect to the objectives of the current study, such system did not guarantee suitable stroke (50 mm), maximum velocity (112 mm/s) and overshoot (3.2 mm for displacements of 40 mm) for the position controller; moreover, it was too bulky to be easily oriented in 3D space and relied on the early digital electronics available at the time.

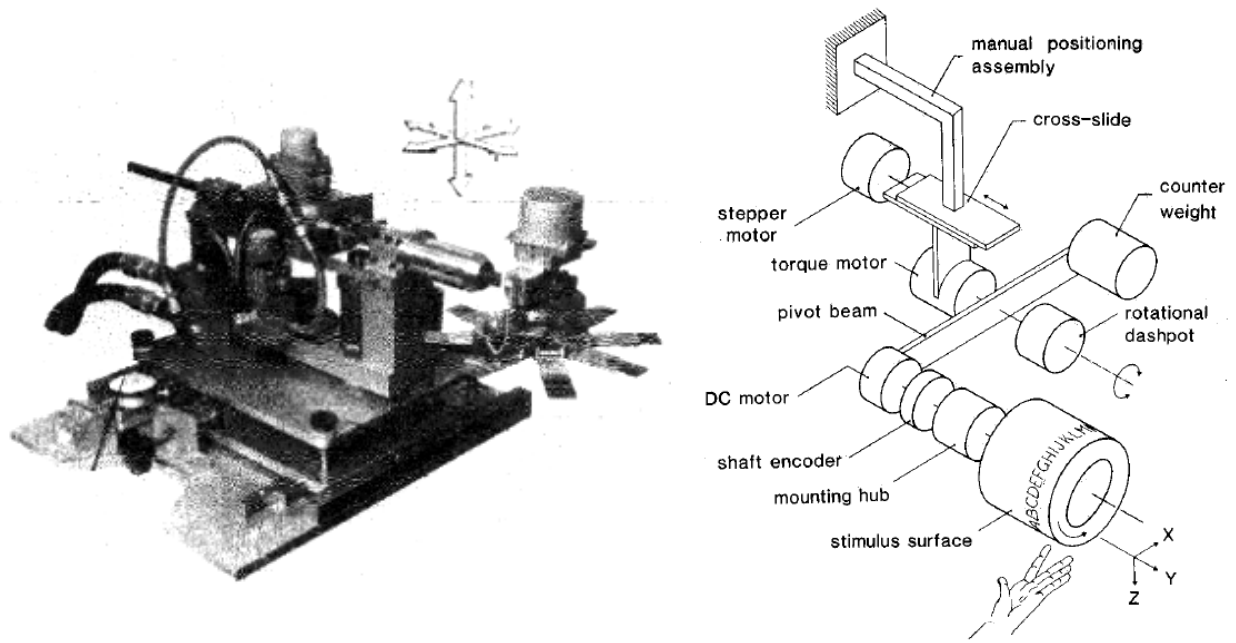


**Fig. 6.** Left: the advanced tactile stimulator by LaMotte and colleagues (1983) for controlled movements of a set of textured surfaces across the skin. Right: an example system (Johnson & Phillips, 1988) belonging to the class of rotating drum stimulators.

A number of groups (Darian-Smith & Oke, 1980; Johnson & Phillips, 1988; Romo et al., 1993; Radwin et al., 1993; Wheat et al., 2004) utilized beams for the application of stimuli to the subjects. The devices shown by Darian-Smith and Oke (1980) and by Johnson and Phillips (1988), the latter being an improved version of the stimulator described by Johnson and Lamb (1981), had a rotating drum with embossed patterns mounted at one end of a pivot beam (Fig. 6-right). The drum was rotated at constant velocity by using DC motors with speed control. Remarkably, Johnson and Phillips (1988) used a fully automated computer controlled approach, which could be changed to manual mode depending on the specific needs. As the authors state, they faced the problem of operating a compromise between the need for precision and the need to keep the processing load on the controller at a reasoning level, operating a reduction in the drum shaft-encoder resolution (to about 942  $\mu\text{m}$  respect to the original 47  $\mu\text{m}$  one) partially compensated by means of a linear interpolation. Such a problem is nowadays less evident thanks to the considerable improvements in digital electronics. A major difference between the two rotating drum platforms regards the motion along the indentation direction. Darian-Smith and Oke (1980) chose an electronically controlled solenoid for enabling the counterweight to apply the desired force, while Johnson and Phillips (1988) used a torque motor driven in open loop mode for regulating the interaction force. Conversely, here a relevant design constraint is to achieve closed-loop controlled fingertip-stimulus normal contact force, so that it could be modulated regardless of external disturbances or deviations from nominal operative conditions. This requirement suggests to avoid pivot beam structures with counterweight or open-loop torque motors (Darian-Smith & Oke, 1980; Johnson & Phillips, 1988), which rely on the static counterbalance of forces and torques without taking into account dynamic effects.

Both the rotating drums platforms used dampers, also applied to other devices (Romo et al., 1993; Wheat et al, 2004; Oddo et al., *Mechatronics* 2011), for minimizing any transient increase in the contact force at the onset of the stimulation, or to reduce the propagation of vibrations to the human subject. Considering the major limitations with respect to the objectives of this study, the rotating drum by Darian-Smith and Oke (1980) had too high minimum velocity (from 20 mm/s to 180 mm/s), together with too narrow load force range (from 196 mN to 980 mN). The similar device by Johnson and Phillips (1988) had reduced maximum velocity (up to 15 mm/s), but adequate movement range (100 mm) and resolution (2.5  $\mu\text{m}$ ).

The stimulator described by Romo et al. (1993) showed a reduced maximum velocity as well, and limited force and positioning ranges; it employed a probe (Fig. 7) which was scanned across the hand of primates in any direction with a 25 mm range, 0.5  $\mu\text{m}$  sensing resolution and 2  $\mu\text{m}$  positioning precision under digital control; the maximum indentation force was 588 mN, while velocities were from 4 mm/s to 120 mm/s.

Another class of tactile stimulators is represented by pinned systems (Bliss et al., 1970; Gardner & Palmer, 1989; Killebrew et al., 2007). A noticeable number of such devices has been reported in literature (wideband devices were shown by Summers and Chanter, 2002 and by Kyung et al., 2006), being of great interest for pointed and distributed stimulation of the fingerpad stimulation, also allowing flexible experimental paradigms with a variety of spatio-temporal stimulation profiles (Vidal-Verdú & Hafez, 2007). On the other hand, the pinned stimulator approach does not typically allow experiments with textured materials, which are addressed in this study.

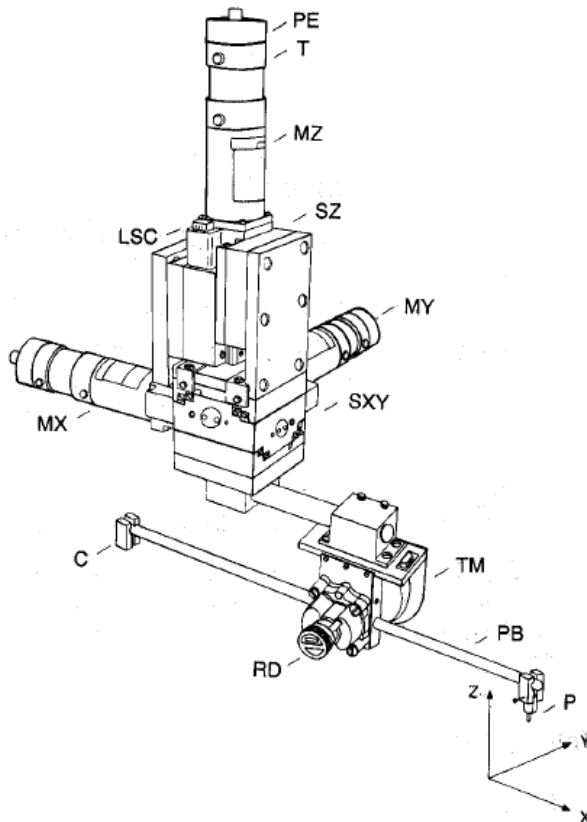


**Fig. 7.** Design of the scanning probe stimulator suitable for indenting and sliding punctuated stimuli to the fingerpad (Romo et al., 1993).

A 2 DoFs mechatronic system (Oddo et. al, Mechatronics 2011) was dedicatedly developed to enable passive-touch protocols for this research study on the sense of touch, with a common core stimulation apparatus between human and artificial experiments. The developed platform fulfils all the requirements detailed above for passive-touch tactile stimulation and was replicated in five exemplars with customizations for electrophysiological, psychophysical, and artificial touch studies and for tribological experiments on different tactile surfaces as well. It can be used to perform neurophysiological studies in humans with techniques such as microneurography and EEG (Beckmann et al., 2009) even in combination with psychophysical experimental paradigms. Also, it is suitable for tribological and artificial touch studies as well.

The platform could indent and slide sequences of textured stimuli (lodged in 77 mm x 32 mm changeable plates) to the fingerpad with feedback-controlled normal contact force and parametric sliding trajectories while recording (Smith et al., 2002; Libouton et al., 2010) the normal and tangential forces at finger-stimulus interface; a voice-coil actuator (NCC05-18-060-2X, H2W Tech.) applied the indentation force with a 12.7 mm stroke, and a linear guide (LTP 60.180.0804-02, SKF Multitec) driven by a DC motor (RE35, Maxon Motors) applied the sliding motion through a 4 mm pitch ball bearing screw, allowing a maximum velocity of 300 mm/s and a stroke of 110 mm. Linear Current Amplifier Modules (LCAM, Quanser), guaranteeing very low electromagnetic interference, were chosen for driving the actuators. Switching power devices were avoided since the typical (10–50 kHz) range for PWM carrier frequency is higher than half the microneurography sampling rate, but just outside the cutoff frequency of the bandpass filter preceding the sampling block. Hence, even introducing shielding techniques, a residual slight coupling between the PWM carrier frequency and  $\mu\text{V}$  range microneurography data could have been aliased at significant low frequencies, affecting the band of interest.

The robotic system has been devised with an open design approach since it is simple to command via a graphical user interface and is upgradable thanks to the FPGA control electronics. This design choice represented an advancement with respect to state of the art systems coherently with the trend showed in the literature of mechatronic tactile stimulators, which used digital controllers (Looft & Williams, 1979) for avoiding to integrate complex mechanisms such as in the scotch yolk stimulator (Goodwin et al., 1985) and reducing as much as possible the analog circuitry (LaMotte et al., 1983; Looft et al., 1979; Byrne et al., 1975; Schneider et al., 1995). Despite this design solution is promising, only a few mechatronic tactile stimulators were based on FPGA control electronics (Wagner et al., 2002; Pasquero et al., 2007).

For the platform presented by Oddo and colleagues (Mechatronics 2011), this choice was operated for two main reasons: i) to allow future upgradeability of the architecture of control electronics (e.g. by instantiating on the same FPGA a number of additional parallel soft-core processors, peripherals, custom digital hardware modules, etc.); ii) to achieve, via hardware-software codesign, a multi-layered hierarchical controller (Fig. 9) allowing low-level parallel (Astarloa et al., 2009) scheduling of periodic routines implementing the motion control laws and of interruptions managing the communication (commands and platform data) functions.

Therefore, the multi-layered hierarchical control architecture partitioned the tasks between a general purpose PC and the embedded FPGA hardware-programmable logics, which was interfaced to the sensors and power current drivers of the platform (Fig. 9a).

The HIGH-level layer ran a Graphical User Interface (GUI) to generate, save, load or execute buffers of HIGH-level commands and for displaying the received platform data. The MID-level layer was in charge of interpreting HIGH-level commands, of point-to-point trajectory generation for the linear guide LOW-level controller, of force target generation for the voice coil LOW-level controller, and of transmitting the platform variables to the GUI for display purposes and to the acquisition systems for electrophysiological or artificial touch experiments.

The dimensioning of the 2 DoFs LOW-level control laws took into account the mechanical characteristics of the fingertip (Serina et al., 1997; Pawluk & Howe, 1999; Nakazawa et al., 2000); both the controllers were in closed loop with integrator to reject disturbances (e.g. variable friction) or modifications of the boundary conditions (e.g. the inclination of the platform in 3D space for adapting it to the position of the subject during microneurography); also, they had ad hoc dead bands (Fig. 9b) to prevent any steady state vibration (Iskakov et al., 2007).

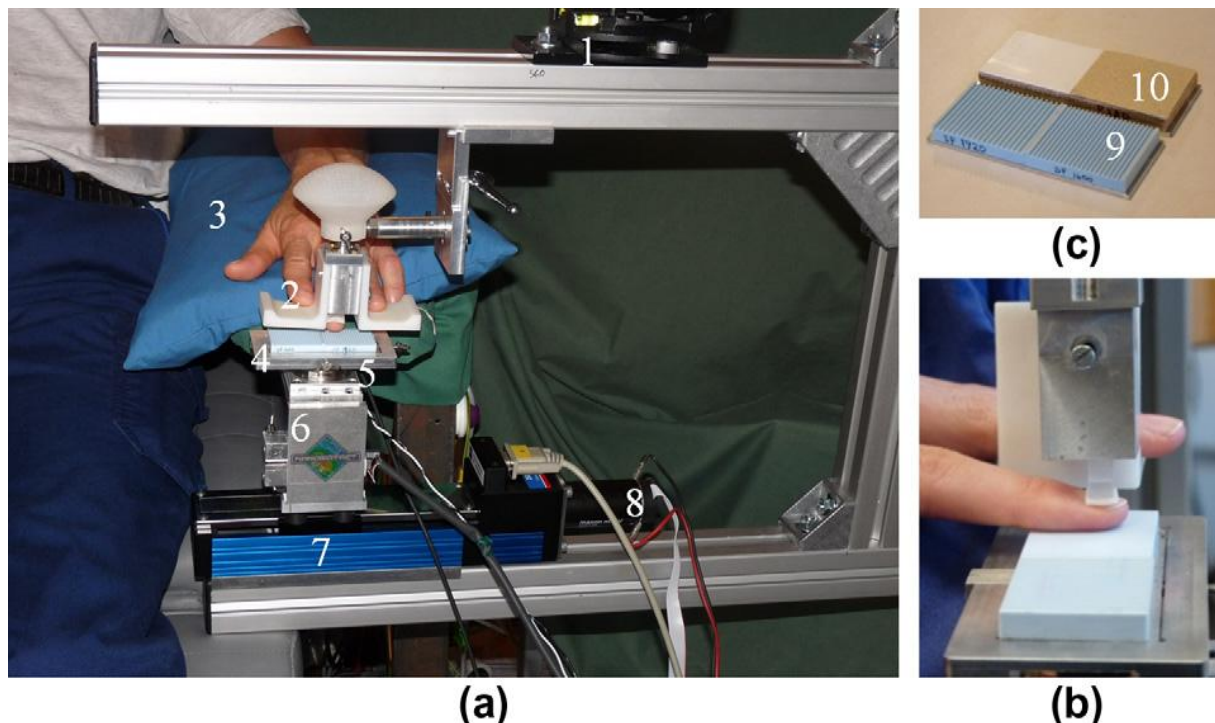


**Fig. 8.** Mechatronic tactile stimulation platform by Oddo et al. (Mechatronics 2011). (a) Experimental set-up during microneurography: frame hold by spherical joint (1), hand-finger support system (2), vacuum cast for arm support (3), carrier for stimuli (4), load cell (5), voice-coil actuator assembly for indentation of stimuli (6), linear guide for tangential sliding of stimuli (7), DC motor with encoder (8). (b) Fingerpad-stimulus interface with finger fixation system and free fingers support. (c) Examples of the used stimuli glued to a changeable aluminum plate: a couple of ridged stimuli (9), smooth plastic and rough sandpaper (10).

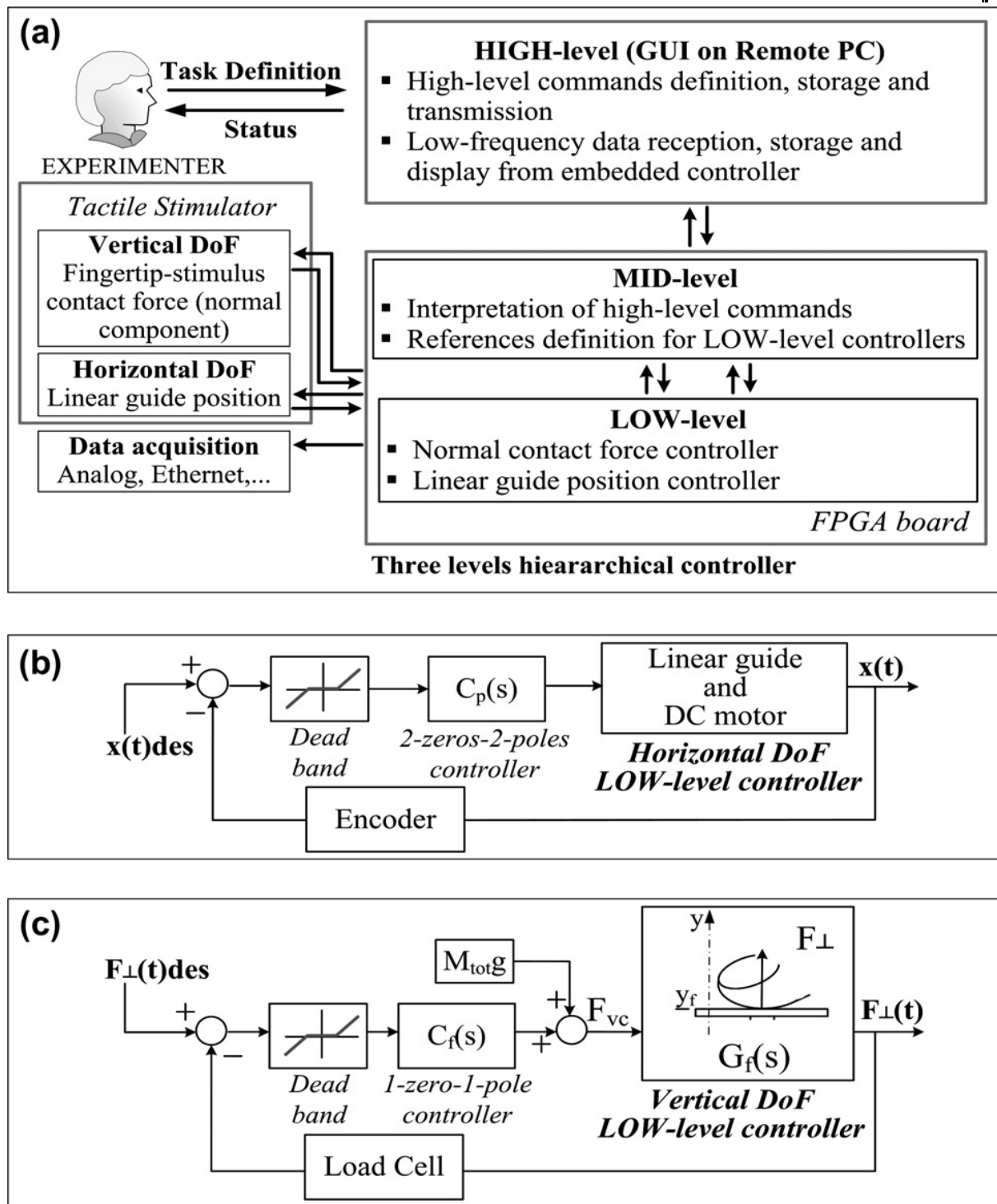


**Fig. 9.** From Oddo et al. (Mechatronics 2011). (a) Overview of the Dynamic Platform hierarchical controller. (b) Block diagram of the LOW-level closed-loop position controller along the sliding direction. (c) Block diagram of the LOW-level closed-loop force controller along the indentation direction.

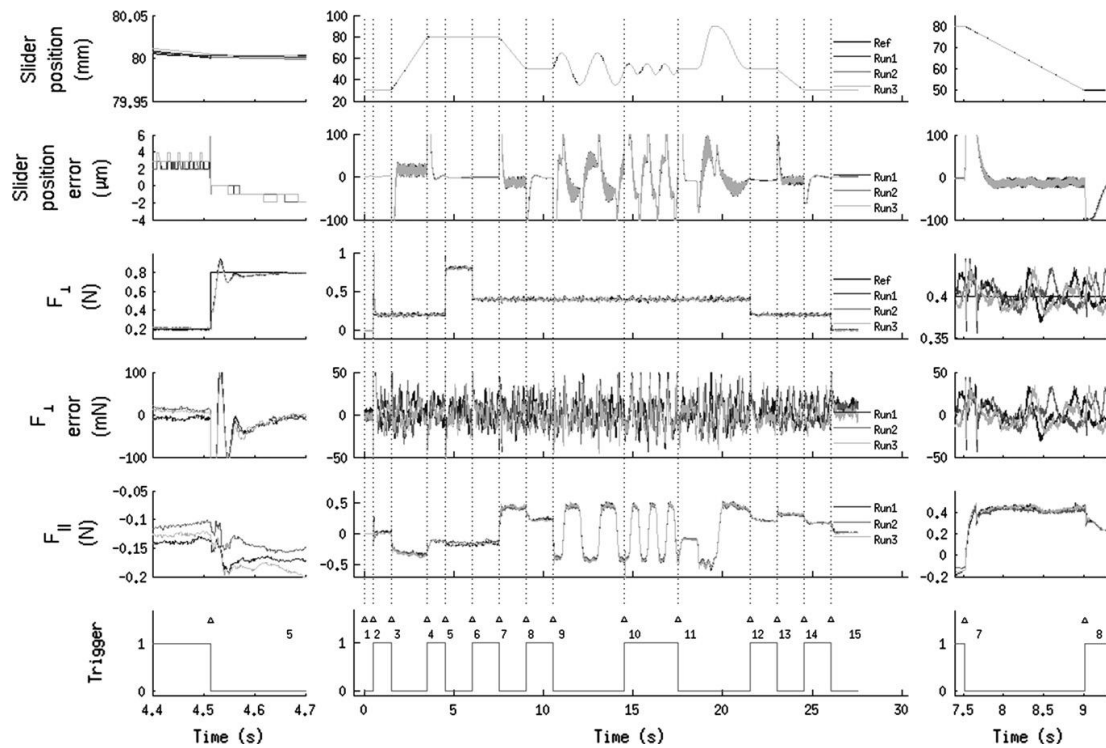


**Fig. 10.** From Oddo et al. (Mechatronics 2011). Sample protocols that can be implemented with the mechatronic platform. Three runs acquired at 5 kHz through Ethernet digital transmission, of the same sequence of commands are superimposed to show high repeatability. The plots represent, from the top: position of the translational slider (target and actual), error in tracking the reference slider position, indentation force at finger-stimulus interface (target and actual), error in tracking the reference indentation force, tangential force component along the direction of the sliding motion, Boolean channel switching each time a new high-level command is executed. Phases 2 and 15, at the beginning and at the end of the protocol, are the loading and unloading of the smooth aluminum stimulus to the finger. In phase 3 the stimulus is stroked for 50mm at 25 mm/s and normal contact force at 200 mN; phases 5 and 6 are normal contact force steps from 200 mN to 800 mN and then to 400 mN; from phase 7 to phase 11 the normal contact force is held at 400 mN, while the stimulus is stroked for 30 mm at constant speed of 20 mm/s (phase 7), while two (phase 9, 15 mm amplitude at 0.5 Hz) or three (phase 10, 5 mm amplitude at 1 Hz) sine waves are executed, or while a fifth order polynomial trajectory is followed (phase 11). Phase 13 is a position ramp from 50 mm to 30 mm in 1.5 s and normal contact force set to 200 mN. The left inset shows a zoom on the transitory between phase 4 and phase 5. The right inset shows a zoom on dynamic phase 7.

Traditional indices (tracking error along the 2 DoFs and confidence intervals to evaluate repeatability) were calculated for assessing the controllers of the 2 DoFs over repeated tactile stimulation runs. Such quantitative indexes confirmed adequate control performances (example protocols are shown in Fig. 10): the reference slider position is tracked with an error lower than 28  $\mu\text{m}$  for ramps (phases 3, 7 and 13 in Fig. 10); reference sine waves (phases 9 and 10) having peak velocities up to 47.1 mm/s are followed with error lower than 68  $\mu\text{m}$ ; and 5th order polynomial trajectories (phase 11) present a Tracking Error lower than 43  $\mu\text{m}$ . As regards the regulation of the indentation force, all the calculated parameters showed absolute Tracking Error lower than 20 mN, while the normalized error was comprised between 1.6% and 6.6%. As a further relevant result, the extremely reduced values of the confidence intervals (typically in the order of few permille points of the reference target) confirm that the developed mechatronic platform guarantees excellent repeatability in the presentation of tactile stimuli (Oddo et al., Mechatronics 2011).

This achievement is fundamental in touch studies: even if the tracking of the reference curves may get relatively worse in certain conditions, the actual trajectories under feedback control are almost coincident among different runs.

Apart for the particular design choices and results for traditional robotic assessment, the research work presented by Oddo et al. (Mechatronics 2011) also provided methodological contributions on the possibility to use the human mechanoreceptors as instrumental sensors, to assess platform compatibility with the exacting demands of electrophysiological methods, specifically the lack of electromagnetic interference and absence of spurious vibrations.

The lack of significant electromagnetic interference coupling with the electrode for microneurography due to the platform was investigated by means of analysis of neural recordings from a SAI unit (left index finger), under three experimental conditions: i) Manual Stimulation (MS)-mode: while the platform was not actuated, the experimenter manually stimulated the finger of the subject (test subject) from which neural data was recorded; ii) Closed Loop (CL)-mode: a 1600  $\mu\text{m}$  periodic ridged stimulus was indented and scanned across the fingertip of a second subject (control subject), in close proximity to the fingertip of the test subject (from which neural data was recorded), with 500 mN feedback controlled contact force, sliding distance of 20 mm and velocity set to 20 mm/s; iii) Open Loop (OL)-mode: to double check whether or not the time varying driving current (related to the indentation DoF actuator in feedback force control) affected the microneurography results, the same protocol of point ii) was operated apart for the fact that the indentation was in open loop by supplying a constant current to the voice-coil actuator, resulting in a normal contact force of about 750 mN before the onset of stimulus sliding motion. Noise amplitude distribution was evaluated in the three experimental conditions described above.

No relevant noise pickup was observed in the raw nerve signals (top plots of Fig. 13) recorded during platform movement or when the force control was engaged, as an effect of the selected linear power drivers for the actuators instead of switching ones. Fig. 11 depicts neural data from a SAI unit of the test subject in the three MS-mode, CL-mode and OL-mode experimental conditions detailed above. Neural spikes are identified in MS-mode and marked with dots, corresponding to the phases during which the finger of the test subject was manually probed. The spike template applied for spike sorting in MS-mode was then used to evaluate whether or not neural spikes were elicited under the two other stimulation conditions due to electromagnetic interference by the platform (since the fingertip of the test subject was not mechanically stimulated in CL-mode and OL-mode, and a SAI unit is expected to be silent in that condition). Noticeably, no spikes could be identified in both the CL-mode and OL-mode, confirming that the platform did not induce vibrations resulting in spurious neural firing. As one could expect, the mechatronic platform had an effect in the background neural noise, confirmed by the higher amplitude of the CL-mode and OL-mode traces if compared to the spike-free regions of the MS-mode one. However, the overlap of the traces shows that the increase in noise was not enough to mask the spikes occurring while manually probing (MS-mode) the fingertip of the test subject.

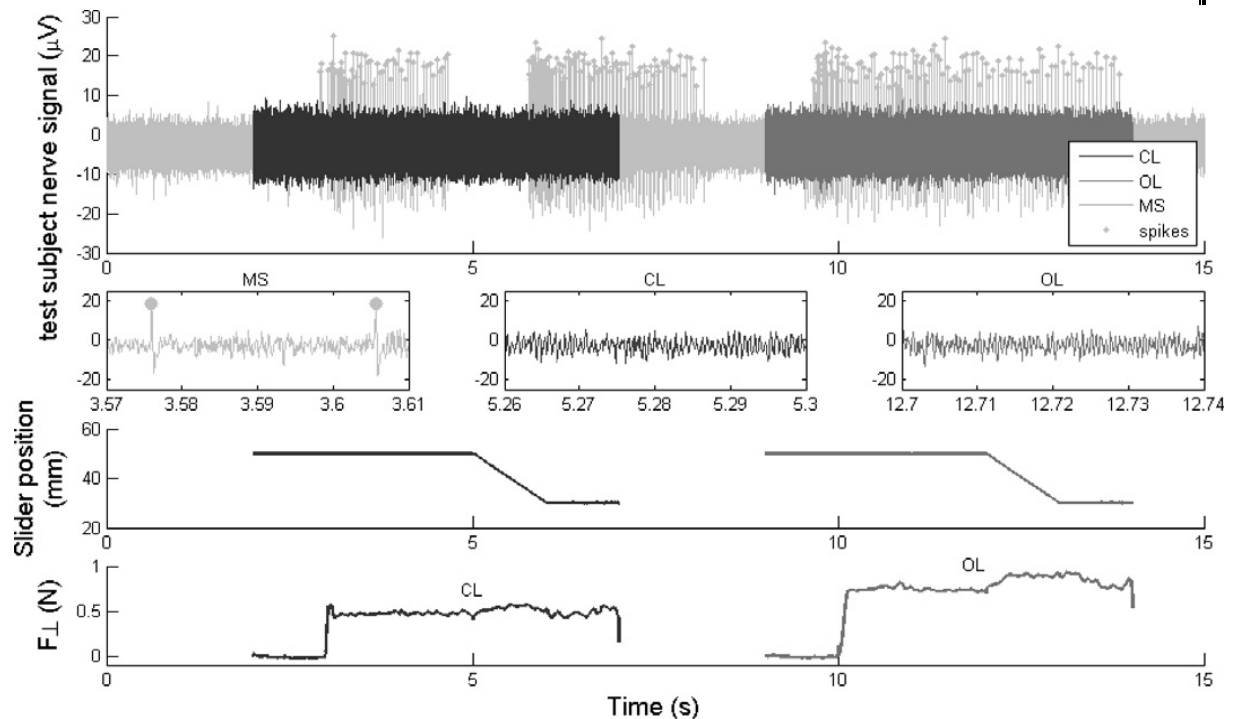


**Fig. 11.** From Oddo et al. (Mechatronics 2011). Neural recordings under the three MS-mode, CL-mode and OL-mode experimental conditions, described in Section 3.2, are depicted in the top plot for assessment of platform electromagnetic compatibility with the microneurographic technique. Left to right, the insets in the second row from the top show zooms on neural data recorded from the test subject with MS-mode, CL-mode and OL-mode. The position of the translational slider and the normal component of the indentation force are shown as well under both the CL-mode and OL-mode experiments.

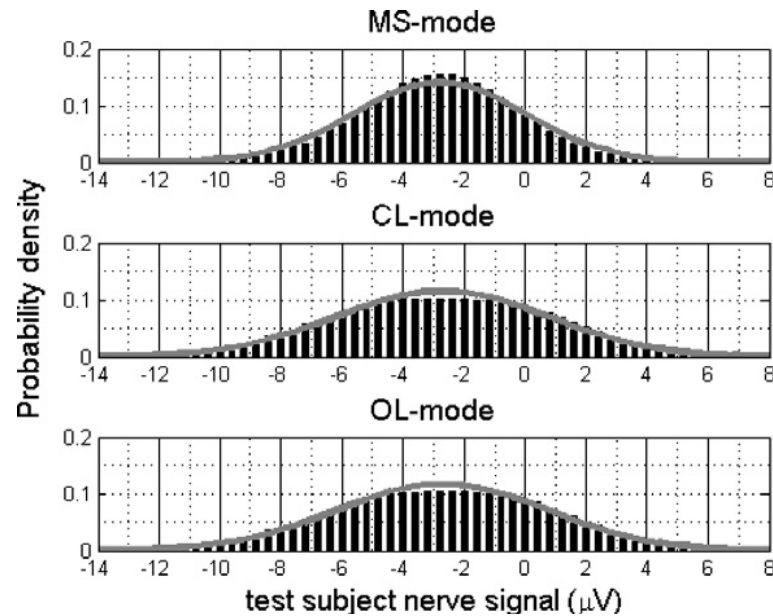


**Fig. 12.** From Oddo et al. (Mechatronics 2011). Statistical neural noise analysis for each of the three MS-mode, CL-mode and OL-mode stimulation conditions. The probability that the neural signal belongs to a bin (width set to 0.4  $\mu\text{V}$ ) is evaluated based on amplitude levels experimentally occurring in 38 s of data at 12.8 kHz. The solid line shows Gaussian fitting of noise probability density.

A statistical noise analysis is presented in Fig. 12 for each of the three MS, CL and OL stimulation conditions, where the probability that the neural signal belongs to a bin (width set to  $0.4 \mu\text{V}$ ) is evaluated based on amplitude levels experimentally occurring in 38 s of data at 12.8 kHz. A Gaussian fitting is shown as well in Fig. 12: platform activation causes a non relevant increase in noise standard deviation from  $2.82 \mu\text{V}$  (MS-mode) to  $3.43 \mu\text{V}$  (OL-mode) and  $3.48 \mu\text{V}$  (MS-mode), and had almost no effect in its mean value.

To directly assess the presence of biologically significant vibrations introduced by the platform, the spectra resulting from the point processes of identified neural spikes was calculated considering the firing of RA units during indentation and sliding motion of a smooth polypropylene plastic surface, in comparison to that occurring with periodic gratings having spatial period between  $280 \mu\text{m}$  and  $1920 \mu\text{m}$ .

As shown in Fig. 13b depicting a single RA afferent, after the expected short burst of impulses at the start of motion, this unit fired only sporadic impulses. The spectra of the firing for all the data from the same RA unit is shown in Fig. 13c for  $1600 \mu\text{m}$  spatial period grating, meaningfully depicting the modulation of firing at the expected fundamental frequency (i.e. the ratio between the sliding velocity and the spatial period of the presented surface; further related details are provided in Section 3) of 12.5 Hz at a sliding velocity of 20 mm/s, as well as significant modulation at harmonics up to 200 Hz. Therefore, the spatial period of the grating was revealed as a modulation of firing frequency as the ridges of the surface were sliding across the receptive field of the RA unit, confirming the high sensitivity in encoding the mechanical characteristics of the stimulating surface in this unit. This frequency locking experimental outcome will be discussed more in details in the next section with a dedicated focus on artificial touch and on the ongoing parallel human touch investigation. In the frequency domain, the spectrum for all the data from stimulation with a smooth plastic surface in the same unit reveals no periodic firing or pickup of vibrations (Fig. 13d). To succeed in this objective, a relevant design choice was the introduction of custom dead bands (Fig. 9b and c) which allowed errors lower than specific thresholds to occur, thus avoiding vibrations produced by continuous sub-threshold error-correction control actions.

Human microneurography recordings also confirmed excellent repeatability (Fig. 13a), being mainly a consequence of the intrinsically reduced jitter in the scheduling of periodic control tasks by the implemented hierarchical control architecture (particularly, the hardware programmable FPGA logics for the embedded controller). Similar results were obtained in all recorded afferents.

The dedicated design of the platform allowed to implement a wide variety of passive- (Oddo et al., Sensors 2009; Oddo et al., IEEE RoBio 2009; Oddo et al., Sensors 2009; Muhammad et al., MNE 2011; Oddo et al., IEEE TRo 2011) and active- (Beccai et al., 2009; Oddo et al., IEEE TRo 2011) protocols in artificial touch studies, also supported by parallel human touch outcomes via the microneurographic technique (Oddo et al., Sensors 2011), as it is detailed in Section 3.

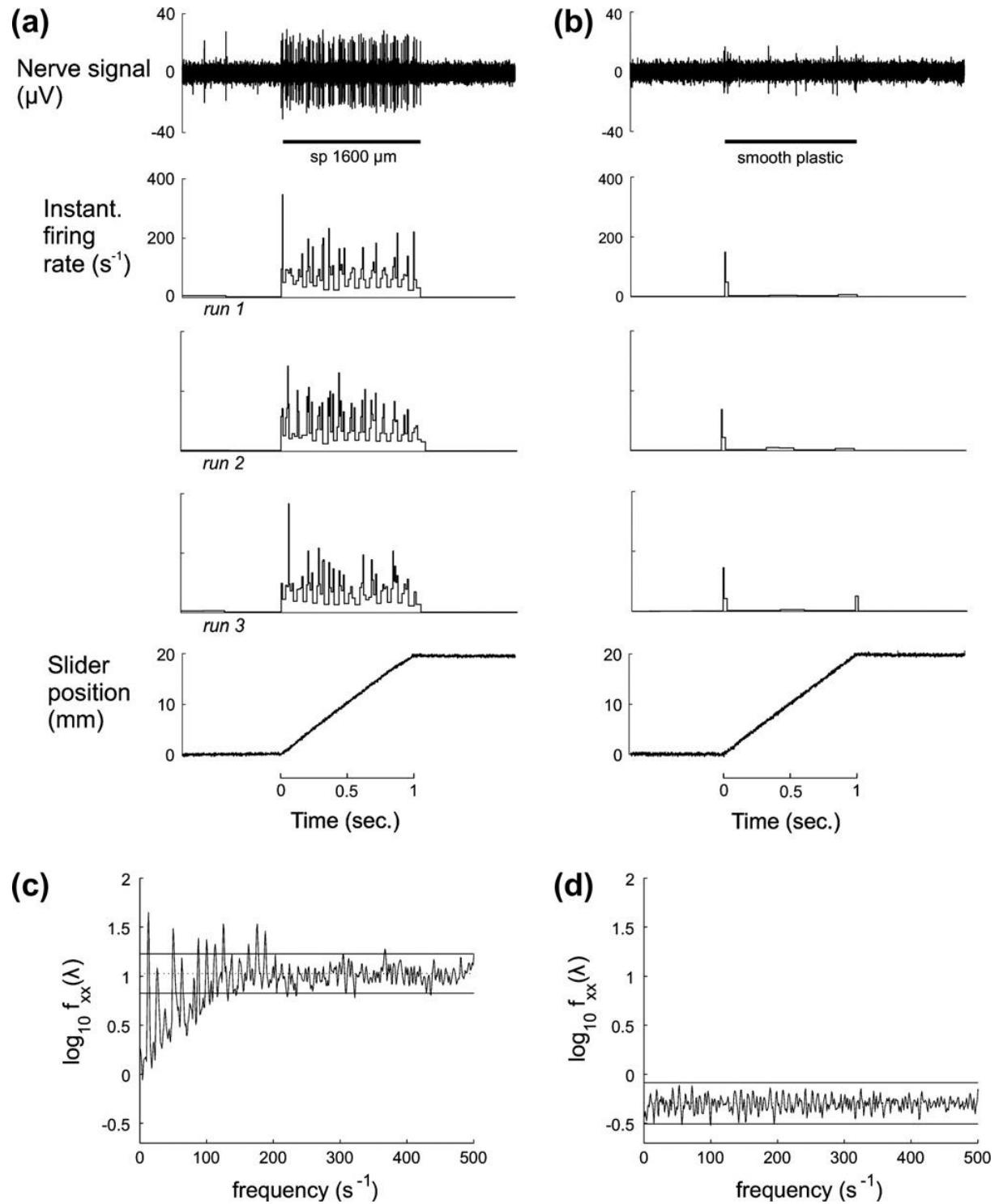


**Fig. 13.** From Oddo et al. (Mechatronics 2011). Microneurographic recording from a RA (Meissner) tactile afferent unit. (a) Stimulation with a ridged grating. Records from top, recorded nerve signal, instantaneous rate of nerve discharges during three repeated runs of the same stimulus, slider position. (b) Stimulation with a smooth plastic surface on the same unit, records as in A. (c) Spectrum of nerve discharge during ridged grating stimulation. Solid lines show  $p < 0.01$  confidence limits. (d) Spectrum for a smooth surface as in C.

### 3. Passive- and active- artificial discrimination of textures

Finite element analyses modeling the fingerpad during dynamic touch tasks showed that temporal frequency changes at the position of receptors encode information on spatial coarseness of the tactile stimuli (Konyo et al., Eurohaptics 2005). As for human touch studies, periodic ridged tactile stimuli (gratings) can provide significant information in the experimental evaluation of artificial tactile systems, also because they are standardized test surfaces which can be used as a kernel to decompose and represent more general polyharmonic surfaces (Bensmaïa & Hollins, 2005; De Boissieu et al., 2009) encountered in everyday life exploratory tasks.

Some studies showed that the spatial period  $\Delta p_S$  of a grating is in inversely proportional relationship with the principal frequency  $f_{princ}(t)$  of the mechanical vibration elicited when a motion occurs at finger-stimulus interface with  $v(t)$  relative velocity (Konyo et al., IEEE IROS 2005), such that:

$$f_{princ}(t) = \frac{v(t)}{\Delta p_S} \quad (1)$$

Therefore, the frequency-locking behavior introduced by Equation (1) consists in a decreasing value of the frequency of the vibration while increasing the stimulus spatial period, and in a frequency value increasing together with the stimulus sliding velocity. Such relationship is motivated by considering that during a stimulus-fingerpad relative motion characterized by constant velocity  $v$ , two adjacent ridges of the grating get into contact with the same region of the fingertip after a time lag equal to  $\Delta p_S/v$ , thus eliciting a repetitive and stationary mechanical wave. The inverse of such time lag is the vibratory frequency in Equation (1), which is time dependent in case of sliding velocity being non-constant with time.

Provided that it is possible to estimate somehow the relative instant velocity  $v(t)$ , or in the simpler case that velocity is constant or a priori known, Equation (1) represents an effective encoding of roughness (i.e., spatial coarseness  $\Delta p_S$ ), which may be useful for discrimination of surfaces.

Also, electrophysiological results showed modulation of the firing patterns by mechanoreceptors in the fingerpad being coherent with Equation (1), both in monkey (Darian-Smith & Oke, 1980) and in human subjects (Oddo et al., Mechatronics 2011, Oddo et al., Sensors 2011). In artificial touch, successful encoding based on Equation (1) is in the capability to elicit such vibrations by stimulus-skin interface, by motion dynamics and by contact mechanics, and to gather them via the sensing units integrated in the finger. It is remarkable to point out that the particular amount of contact force at tactile stimulus-fingertip interface has no effect in modulating the value of the principal frequency, provided that the applied load is in the adequate range for eliciting the mechanical vibration and for allowing such periodic wave to be gathered by the sensing units (Oddo et al., IEEE RoBio 2009).

Several tactile sensing technologies have been investigated and were reported in comprehensive reviews on the topic (Lee & Nicholls, 1999; Maheshwari & Saraf, 2008; Dahiya et al., 2010; Yousef et al., 2011). Most of studies for artificial roughness encoding showed experimental results under passive-touch protocols with precise control and knowledge of the relative sliding velocity  $v(t)$ , i.e. surfaces were presented to a still sensorized fingertip which was not integrated into an actuated finger, or without relative movements of finger phalanxes (mechanical linkages) in case of integration. Therefore, while aiming at discrimination of textures, the non-realistic (i.e., appropriate for a controlled environment only such as in laboratory investigation, in application-specific industrial contexts, etc.) but informative passive-touch condition allowed for normalization of Equation (1) with respect to sliding velocity  $v$ , guaranteeing a frequency encoding being a function of spatial coarseness  $\Delta p_s$  only (Mukaibo et al., 2005; Okamoto et al., 2006; Edwards et al., 2008; Oddo et al., Sensors 2009; Oddo et al., IEEE RoBio 2009; Muhammad et al., MNE 2011; Oddo et al., Sensors 2011).

Looking at the background of previous studies referring to Equation (1) as a potential method for roughness encoding, an approach was to develop a finger-like multilayered texture sensor integrating five strain gauges (Fig. 14a) mimicking Meissner corpuscles (RA). Such artificial tactile system was shown to be appropriate for identifying the difference in roughness, softness and frictional properties of various materials (Mukaibo et al., 2005; Zhang et al., 2006). Textural information was quantitatively retrieved by estimating the vibrational frequency excited while indenting and sliding a periodic stimulus with spatial wavelength in the millimeters range (Okamoto et al., 2006), showing significant results down to 0.6 mm (Mukaibo et al., 2005). Roughness encoding as in Equation (1) was achieved for 200  $\mu\text{m}$  wavelengths as well, but the results were not fully significant possibly due to the size of the artificial tactile system (Fig. 14b), being it three times higher than that of the human finger. This is confirmed by the improved performance shown by Hidaka et al. (2009) with a modified design mimicking the actual dimensions of the human finger. Remarkably, the value of the fundamental frequency (Equation 1) was not affected by a change in the indentation depth (Fig. 14c), which modulated its absolute amplitude without any practical effect on its relative appearance with respect to the other spectral components (Mukaibo et al., 2005).

The same approach based on Equation (1) was previously shown in dynamic- passive-touch by Scheibert et al. (2004) for a pair of very fine surfaces, having spatial periods set to 60  $\mu\text{m}$  and 140  $\mu\text{m}$  (Fig. 15), which were encoded by means of MEMS technology embedded into a polymeric packaging material. However, in such work the contact force was considerably high (7 N) with respect to the typical values used by humans in texture discrimination activities.

A fingertip shape tactile sensor integrating a microphone, referring to the Pacinian system as a source of bioinspired design, has also been investigated to quantify textural features (Edwards et al., 2008) presented by medium-coarse stimuli producing a square wave 1 mm in height, varying in wavelength from 1 to 4 mm in 0.5 mm increments (Fig. 16).

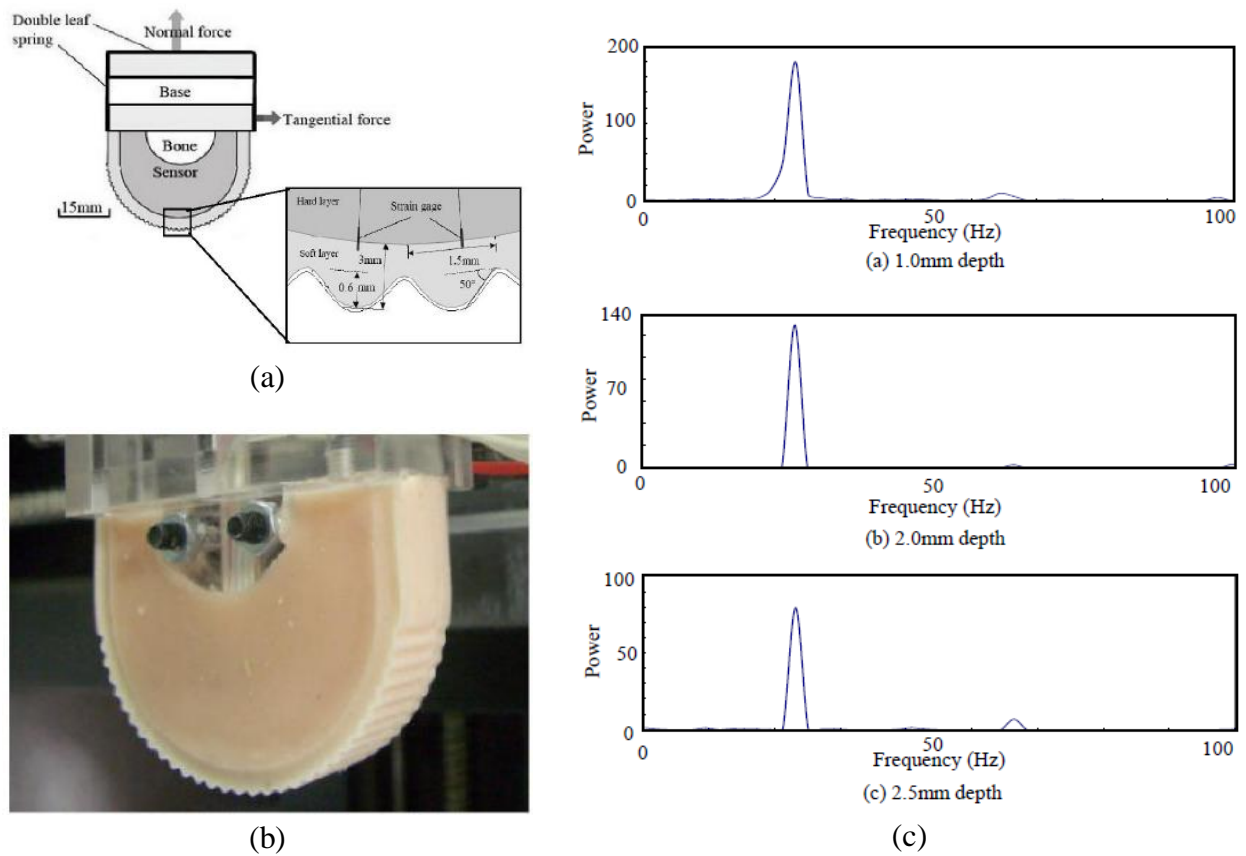


**Fig. 14.** From Mukaibo et al. (2005) and Zhang et al. (2006). a) Schematic structure of the tactile sensor; b) fabricated tactile sensor; c) spectral analysis with a periodic grating, showing coherence with Equation (1) at three indentation levels.

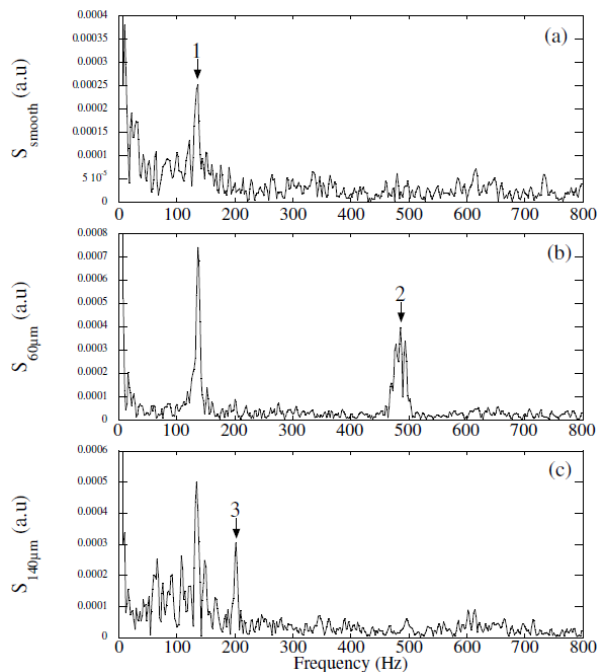


**Fig. 15.** From Scheibert et al. (2004). Spectra of the tangential contact force measured while sliding three tactile stimuli at constant sliding velocity (30 mm/s) and high contact force (7 N), showing coherence with Equation (1). a) smooth stimulus; b) stimulus with 60  $\mu\text{m}$  periodic patterning; c) stimulus with 140  $\mu\text{m}$  periodic patterning.

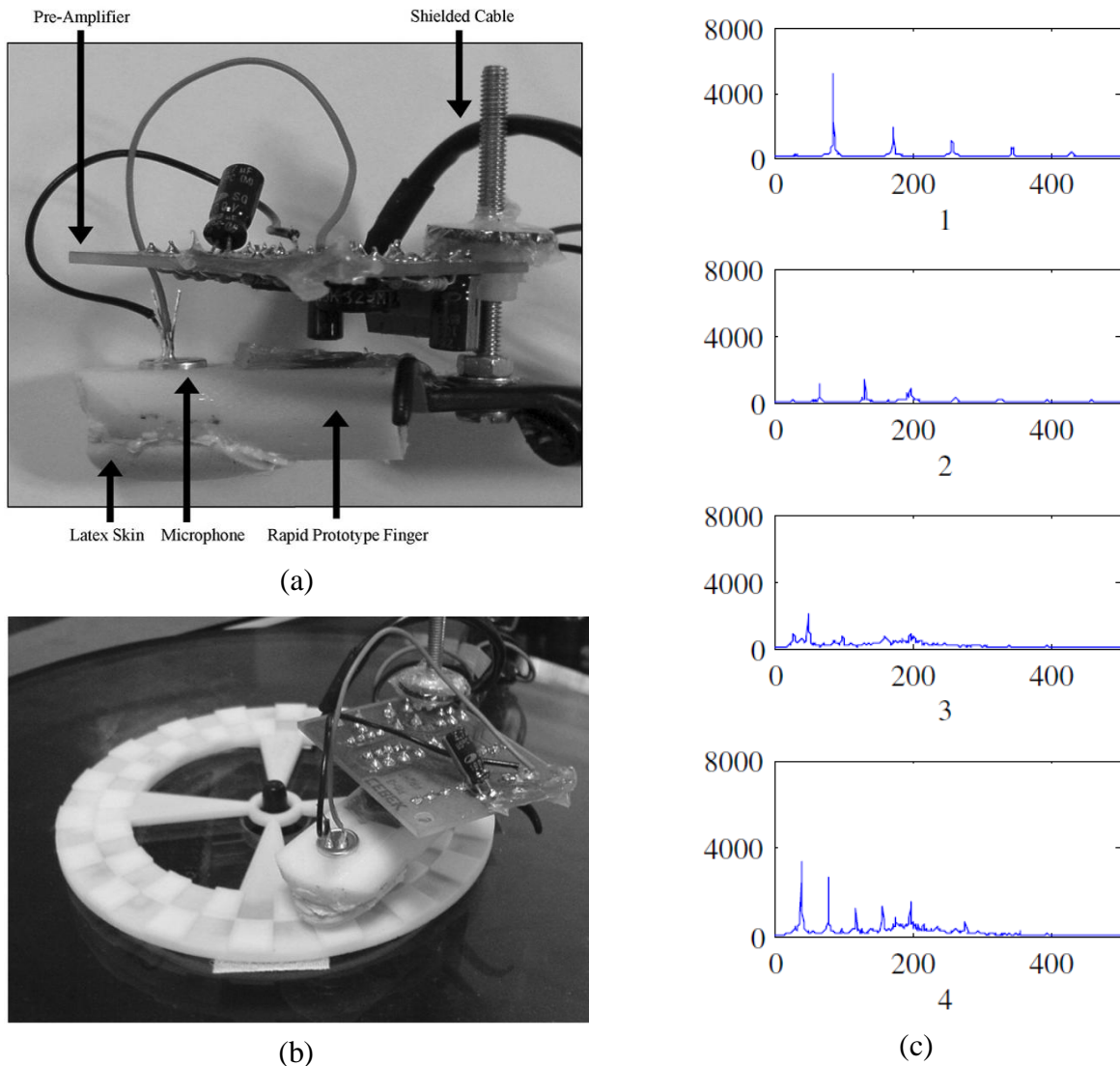


**Fig. 16.** From Edwards et al. (2008). a) Artificial finger with microphone as a sensing element; b) Experimental setup for passive-touch evaluation of patterned disks; c) experimental spectral (power in dB vs. frequency in Hz) signatures of disks presenting a ridged patterning.

Wettels et al. (2008) developed a tactile sensor array consisting of a rigid core surrounded by a weakly conductive fluid contained within an elastomeric skin. The sensor uses the deformable properties of the fingerpad and tactile information relative to the contact force is retrieved from impedance measurements via embedded electrodes (Wettels et al., 2008; Lin et al., 2009). Feasibility of dynamic roughness encoding was stated via time-frequency inspection in the work by Fishel et al. (2008) by means of a pressure sensor located away from the skin and functioning as a hydrophone in an fluid. However, the experimental outcomes shown in such work by Fishel and colleagues went in an opposite direction with respect to the ones discussed above, since a lack of a velocity induced modulation effect was shown (Fig. 17). Therefore, the spectral patterns elicited in the output of the remote pressure sensor did not follow the frequency-locked behavior stated by Equation (1), and the vibrational signatures were associated by the authors to the occurrence of slip regardless of the actual instant sliding velocity.

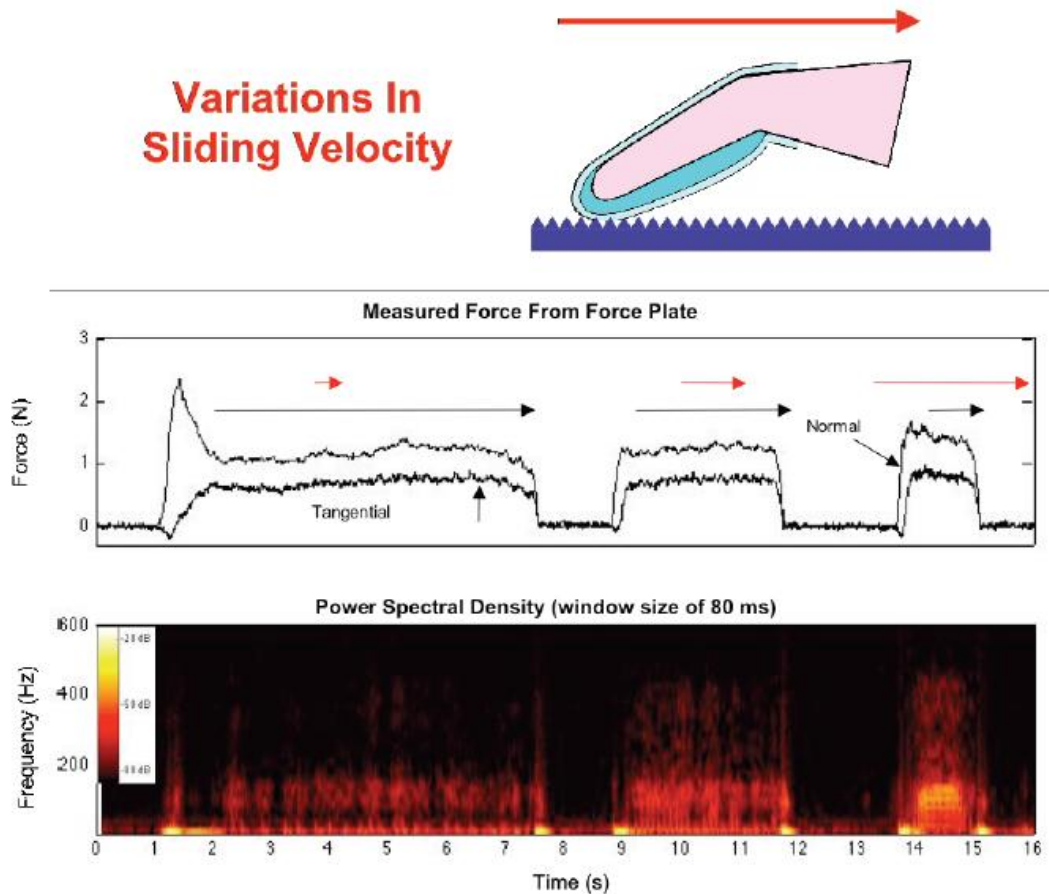


**Fig. 17.** Experimental results by Fishel et al. (2008) contrasting with Equation (1).

Most probably, such phenomenon was due to the particular design of the artificial finger, since the sensing element was at considerable distance from the location of contact with the surface. Moreover, rather than under automatic control, the artificial finger was manually moved by the operator over specimens, confirming the importance of the availability of a mechatronic platform (as discussed in Section 2) to evaluate artificial tactile systems under precise experimental conditions guaranteeing significance of experimental data.

State of the art cross shape 3D MEMS sensors (Beccai et al., 2005) were integrated with polymeric packaging in a compliant 2x2 tactile array which was developed and evaluated for roughness encoding (Oddo et al., Sensors 2009). As previously demonstrated, the used microsensor (Fig. 18b) is appropriate for integration into a packaging architecture resulting in a robust and compliant tactile system for application within artificial hands (Beccai et al, 2008). Such integration can thus yield to a robust yet highly sensitive device offering the possibility to provide information about static contact forces and dynamic events with one tactile element.

In the bare configuration of the sensor, the cylindrical mesa, located at the center of the cross-shape structure, transmits an externally applied force to the sensor inducing stresses in the four tethers where four p-type piezoresistors are implanted. The fractional change in resistance  $\Delta R/R$  of each piezoresistor of the microsensor is proportional to the longitudinal and the transversal stress components, while the design of the sensor is such that the transversal stress component in

the implanted piezoresistors is negligible with respect to the longitudinal one (Oddo et al., 2007). In a packaged configuration, each single sensor of the array provides local information on the contact interaction at its interface with the surrounding polymeric material, with the advantages of distributed tactile sensing (as discussed by Hosoda et al., 2006); in addition, the used tactile sensors also provide directional information by means of the output readings from the four piezoresistors.

Although the MEMS sensor is suitable, both bare (Beccai et al., 2005) or packaged (Beccai et al., 2008), for solving the contact force, the raw voltage readings were used in all the studies for artificial roughness encoding integrating the device (Oddo et al., Sensors 2009; Oddo et al., IEEE RoBio 2009; Beccai et al., 2009; Oddo et al., Sensors 2011; Oddo et al., IEEE TRO 2011). As stated by the authors, such choice represents an added value of the system, not only because the contact force was not addressed in the studies discussed in the following, but mainly because it turns out into a technique being more robust and less-time consuming for the operator. This also avoided the need for smart techniques guaranteeing fast and accurate calibration (as well as periodic re-calibration operations) of each MEMS before packaging, as done with this device by Oddo and colleagues (2007), or after packaging as for example performed by Vásárhelyi et al. (2007) with another but similar sensor together with the introduction of an analytical model for point contact loads.

In the research study by Oddo and colleagues (Sensors 2009) four microsensors were integrated into a 2x2 array, with a pitch of 2.3 mm (indicated by  $\Delta X$  in Fig. 18), via flip-chip bonding on a silicon carrier chip connecting the 9 NiAu pads of each microsensor. The silicon carrier chip was wire bonded by means of 25  $\mu\text{m}$  Al wires to a Printed Circuit Board (PCB) in order to connect the array to the external readout instrumentation (detailed in Oddo et al., 2009). The developed system had in total 16 sensitive elements to external mechanical stimuli in an area of about 21  $\text{mm}^2$  (i.e., 0.76 channels/ $\text{mm}^2$ ), similarly to the density of SAI mechanoreceptors in humans (70 units/ $\text{cm}^2$ ; Johansson & Vallbo, 1979; Vallbo & Johansson, 1984).

The packaging of the array of silicon sensors was developed so that the resulting artificial tactile system could present a selection of characteristics inspired to those of the human fingerpad. The round shape of the packaging of the array was chosen based on the anthropomorphic features of the distal phalanx of the cybernetic hand CyberHand (Carrozza et al., 2006; Beccai et al., 2007; Beccai et al., 2008). The curved geometry was also identified in order to increase the portion of load gathered by the sensors in case of contact with a planar textured surface (according to Vásárhelyi et al., 2006). As shown in Fig. 18, the dimensioning parameters for the packaging where  $r_0$  and  $d$ , which were set to 8 mm and 1.3 mm, respectively, for obtaining adequate sensitivity as well as partially overlapping sensing ranges between *nearest-neighbour* MEMS units and acceptable low-pass spatial filtering effect (cf. a related significant study by Shimojo et al., 1997) with respect to the used stimuli. The packaging material was polyurethane (Poly 74-40, PolyTek, USA), protected by an outer thin protective layer of polyimide having thickness of 0.05 mm and shore A 82 hardness (ST1882, Stevens Urethanes, USA) in order to prevent wear.

The experimental analysis of the tactile sensor array was performed by using medium-coarse regular gratings, with spatial periods from 2.6 mm to 4.1 mm. The contact force was set within the range used by humans in the discrimination of fine forms during active dynamic touch experience (Lederman, 1974) and the sliding velocities matched the range commonly used in related neurophysiologic studies (Darian-Smith & Oke, 1980): by means of the mechatronic platform discussed in Section 2 (Oddo et al., Mechatronics 2011), the tactile stimuli were indented with regulated 1N normal force and stroked at constant sliding velocity from 15 mm/s to 48 mm/s (TABLE I; Fig. 18d).

The tactile sensor array demonstrated repeatable contact imaging during the static stimulus indentation phases of the experimental protocol (Oddo et al., Sensors 2009). To provide an example of the consistency between the surface geometry and the static artificial touch representation, it is remarkable to observe the output signals variations relatively to the steps between phases A (starting of data acquisition) and B (sensor loading) and between phases D (steady state after stimulus sliding) and E (sensor unloading) in Fig. 19, which points out that the step heights varied between different experimental runs depending on the used grating (but not on the velocity, as it is detailed in Oddo et al., Sensors 2009). This property was welcome and was due to the fact that, meanwhile in such phases the mechatronic platform kept unchanged the horizontal position of the tactile stimulus, a variation of the grating periodicity modified the portion of the ridge under each MEMS unit.

However, as is also the case in human touch studies (discussed in Section 4.0), static imaging is a limiting approach since it would require a high density of sensing elements to reliably discriminate fine textures (Kim et al., 2005). Conversely, in case that the relative sliding velocity is known or measured somehow, the application of a tangential sliding motion allows to overcome such limitation taking advantage of the elicited vibrational cues, as from Equation (1).

In the dynamic passive-touch experimental work by Oddo et al. (Sensors 2009) this resulted in a repeatable (as confirmed from analysis of average Pearson cross-correlation coefficients, all being close to 1) and expected (TABLE I) frequency shift of sensor outputs depending on the applied stimulus and on its scanning velocity.



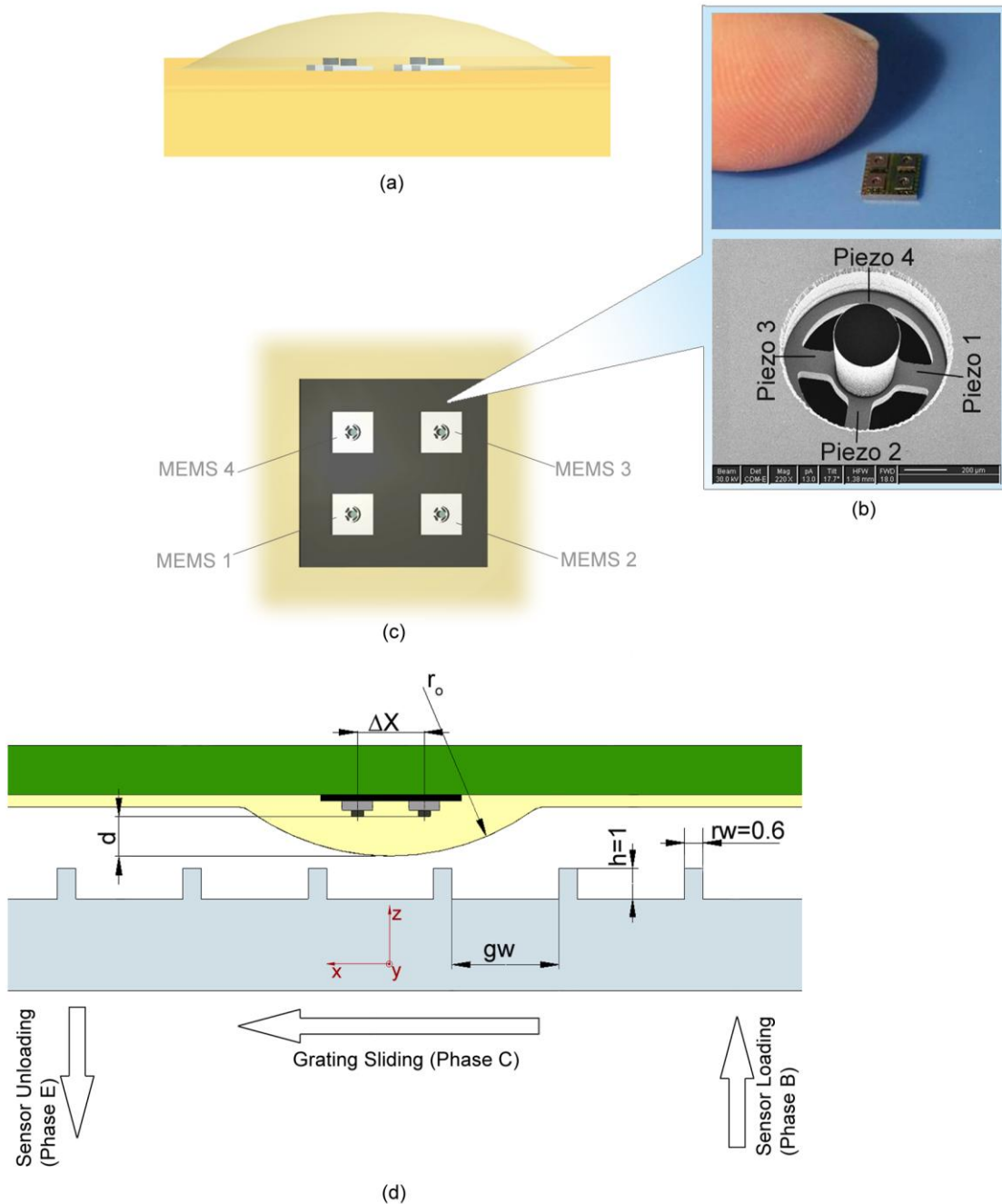


**Fig. 18.** From Oddo et al. (Sensors 2009). (a) 3D design of the tactile sensor array. (b) Top: The 2x2 MEMS array compared with human finger; bottom: a FIB image of the MEMS sensor. (c) Top view of the sensor array. (d) Schematic representation of a cross section of the packaged tactile array and grating dimensions. Groove width  $gw$  ranged from 2.0 mm to 3.5 mm, resulting in  $\Delta p_s$  values reported in TABLE I, while ridge height  $h$  and ridge width  $rw$  had fixed values indicated (in mm) in figure. The key phases of the experimental protocol are indicated in the figure.

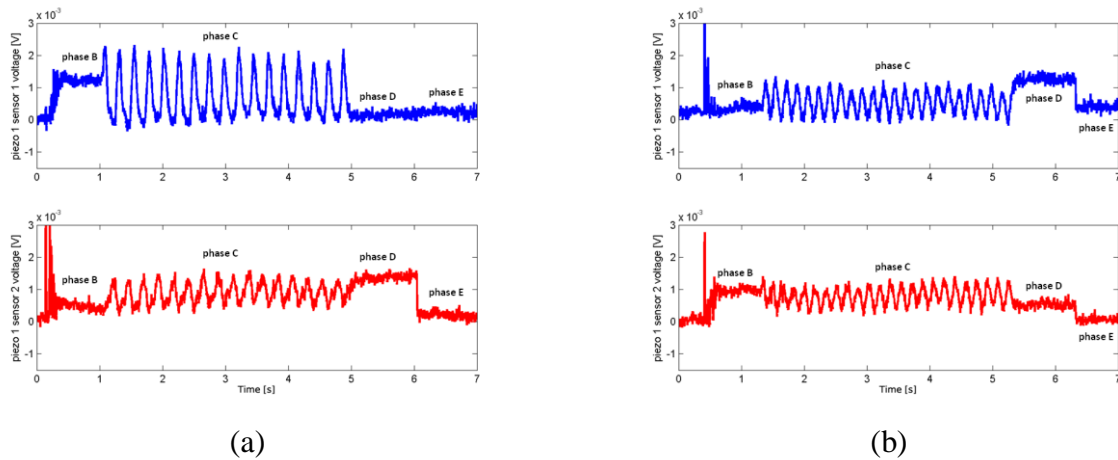


**Fig. 19.** From Oddo et al. (Sensors 2009). Time plot of the readings from piezoresistor 1 of MEMS sensors 1 and 2 of the array. Gratings having 3.6 mm (a) and 2.6 mm (b) spatial periods were applied with translational speed set to 15 mm/s (TABLE I). The frequency modulation due to the variation of the stimulus can be appreciated via cursory inspection of the plots. The steps corresponding to the loading and unloading of the stimulus (phases A-B and D-E) may be more or less evident in a specific unit of the array depending on whether the ridge of the grating falls under a sensor unit or not (static imaging by the tactile sensor array).

To identify the principal frequency (Equation 1), the results of the study by Oddo et al. (Sensors 2009) demonstrated the better processing quality guaranteed by using structured information from different units of a tactile sensor array, fitting pairs of sensor outputs over sinusoidal waveforms having the same frequency (Fig. 20) instead of applying a naïve Fourier analysis separately on each channel.

This processing choice allowed to overcome frequency discretization limitations which could be encountered with FFT while considering narrow observation windows. The technological approach together with the proposed frequency estimation method guaranteed an error from 1.7% down to 0.5% over the range (between 3.7 Hz and 18.5 Hz, reported in TABLE I) of principal frequencies associated to the spatial coarseness of the experimented tactile stimuli. Therefore, the experimental results for dynamic artificial touch with medium-coarse periodic gratings demonstrated remarkable coherence between the principal frequency commonly revealed by the packaged MEMS sensor units and the expected one. Moreover, the data analysis procedure was potentially suitable for most near real-time settings, guaranteeing outstanding performance down to observation windows having 0.4 s duration. The fitting procedure also revealed to be robust tough, in addition to the observable principal frequency shift associated to the combination of the used grating and stimulus sliding velocity, the signal power had overtones (the first three or four harmonics of the fundamental frequency) introduced by both the non-linear packaging material and the sharp edges of the periodic ridged surfaces.

Therefore, the technological and the signal processing outcomes of the work by Oddo et al. (Sensors 2009) were a successful preliminary attempt to artificially achieve roughness encoding in case of medium-coarse patterning, i.e. a deterministic link was obtained between the spatial coarseness of the presented stimuli and the features extracted from the outputs of the spatially-located sensors.

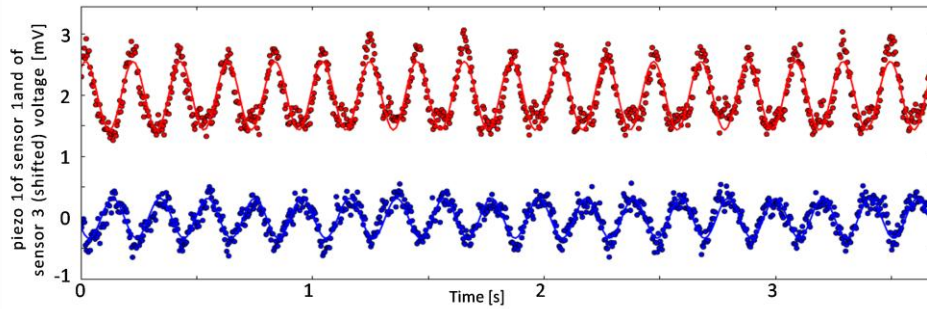


**Fig. 20.** From Oddo et al. (Sensors 2009). Fitting of a sine wave, over a pair of outputs from the tactile array, to identify the principal frequency according to Equation (1). The plot refers to experimental data resulting from the sliding motion ( $v=15$  mm/s) of a grating with spatial period  $\Delta p_S=3.1$  mm.

A similar investigation was in parallel carried out (in collaboration with the Micro Engineering Research Centre of University of Birmingham) by means of a purposely developed capacitive technology (Muhammad et al., SNA 2011), which was experimented for roughness encoding in passive-touch (Muhammad et al., MNE 2011). The finger mock-up was obtained by means of sensing elements consisting of an upper  $2\ \mu\text{m}$  highly doped single crystal silicon diaphragm, a  $2\ \mu\text{m}$  air cavity formed by sacrificial layer releasing and a lower electrode consisting of highly doped silicon. The edges of the sensing diaphragm were fixed by supporting oxide structures. A cross sectional schematic diagram of a single tactile unit is shown in Fig. 21a. The diaphragm dimensions were  $500\ \mu\text{m} \times 400\ \mu\text{m}$ . Each tactile unit was  $150\ \mu\text{m}$  apart, allowing for high density of sensing structures within a given area (Fig. 21b). The array which was fabricated and tested in the studies by Muhammad and colleagues (SNA 2011; MNE 2011) had 4 individual microfabricated capacitors as sensing elements (Fig. 21b).

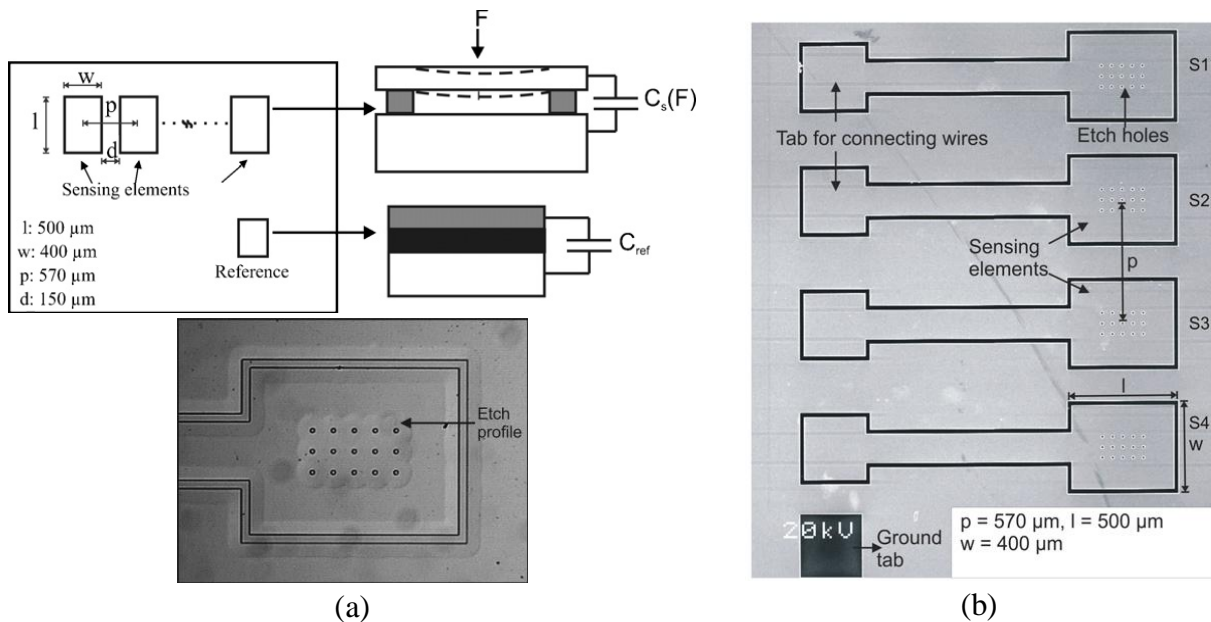


**Fig. 21.** From Muhammad et al. (SNA 2011; MNE 2011). (a) Top: schematic representation of the tactile sensor array showing geometrical dimensions of devices and cross sections of sensors and reference devices. Bottom: optical image showing the profile of the sensing membrane. (b) SEM image of  $1 \times 4$  linear tactile sensor array showing geometrical dimensions of device.

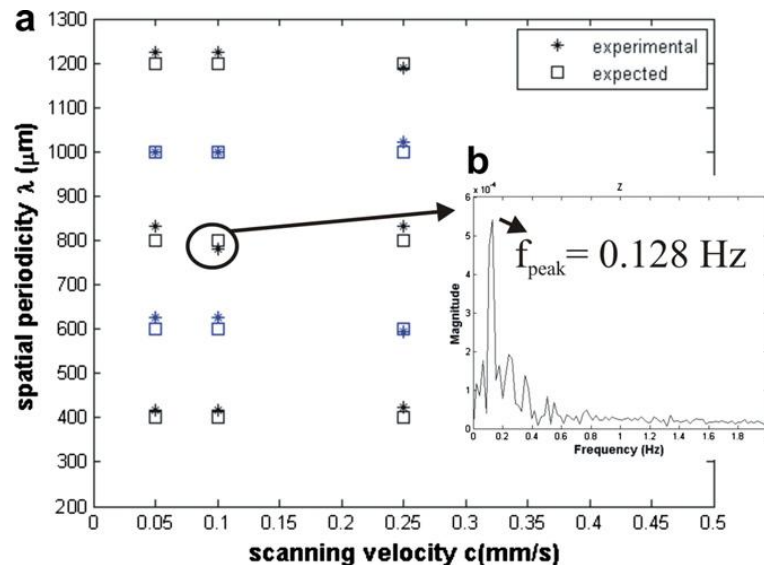


**Fig. 22.** From Muhammad et al. (MNE 2011). (a) Expected and experimentally determined, based on Equation (1), grating spatial periods at three different scan velocities and (b) FFT spectrum for single measurement depicting the experimental peak frequency  $f_{\text{peak}}$ , showing meaningful coherence with the expected principal frequency  $f_{\text{princ}}$  (TABLE I).

The array of capacitive sensors was packaged with a 200  $\mu\text{m}$  thin layer of PDMS (Sylgard 184) to protect the chip from damage and to provide a skin-like covering for transmitting applied loads to the sensing diaphragm.

Experimental results under a dynamic passive-touch protocol at very low sliding velocities (TABLE I) and contact forces (10 mN) consisted in the quantitative evaluation of the capacitive sensing technology via five gratings varying in spatial periodicity from 400  $\mu\text{m}$  to 1200  $\mu\text{m}$  with a 200  $\mu\text{m}$  step, and qualitative assessment of discrimination suitability with fabrics.

Remarkably, in the evaluation with gratings a significant coherence of the experimental peak frequency  $f_{\text{peak}}$  with the expected principal frequency  $f_{\text{princ}}$  was observed according to the values predicted by Equation (1). The presented experimental results have a particular relevance especially considering that very low contact forces and sliding velocities were evaluated (Muhammad et al., MNE 2011), much lower than the other values used in the parallel studies (TABLE I). Therefore, Equation (1) was further validated as a common law underlying the physical phenomena of dynamic touch sensing, regardless of the particular sensing technology (piezoresistive or capacitive) and without too limiting constraints on the boundary conditions of the tactile stimulation procedure.

As a further step towards integration of the artificial touch system into robotic hands (Carrozza et al., 2006; Controzzi et al., 2008; Beccai et al., 2008.; Cipriani et al., 2009; Cipriani et al., 2010), an improved version of the MEMS sensor by Beccai et al. (2005) was employed to overcome previous limitations which allowed to develop a finger mock-up only (Oddo et al., Sensors 2009) rather than a fingertip mimicking human anthropometry (Oddo et al., IEEE RoBio 2009; Beccai et al., 2009; Oddo et al., Sensors 2011; Oddo et al., IEEE TRo 2011).

In those subsequent works the array was built by connecting four microsensors via flip-chip bonding directly on a rigid-flex board which was concurrently designed with the distal phalanx of an artificial finger in order to achieve the following outcomes:

- ✓ a 2x2 array of 4 microsensors integrated in an artificial fingertip with robust (both mechanical and electrical) connection and with all the conditioning electronics fully integrated on board;
- ✓ a 2x2 sensing array that could be suitably packaged with skin-like materials without affecting the tactile array itself nor compromising the integration in the artificial fingertip;
- ✓ suitability for integration into articulated fingers to be applied in anthropomorphic robotic hands.

The bare sensor array, depicted in Fig. 23, had 16 channels as total tactile sensor outputs for transducing the mechanical interaction with external tactile stimuli, and it had a pitch of 2.36 mm, therefore achieving a density of 0.72 channels/mm<sup>2</sup> (16 channels / 22.28 mm<sup>2</sup>). This was similar to the innervation density of SAI (Merkel) mechanoreceptors in humans (70 units/cm<sup>2</sup>; Johansson & Vallbo, 1979; Vallbo & Johansson, 1984), which have been considered as a mean for roughness encoding in studies with monkeys (Yoshioka et al., 2001).

The sensors of the array are labeled as S1, S2, S3 and S4 (according to Fig. 27A and Fig. 37A), while the outputs of each sensor are labeled as P1, P2, P3 and P4 (as shown in Fig. 27B and Fig. 37B). P1 and P3 are related to piezoresistors implanted on the cross shape structure on tethers oriented across the finger axis, while P2 and P4 are on tethers oriented along the finger.

Unlike the previous approach (Oddo et al., Sensors 2009), the wire bonding could be avoided in the new design because of the rigid-flex board solution. Also, with respect to the previous study a new version of the electronics was used; the number of discrete components was reduced because of the improved design of the MEMS sensor, enabling the full integration in the distal phalanx of a robotic finger. Each piezoresistor-resistor arm was supplied by means of a 5V DC regulated voltage, and the node between each piezoresistor and the completing integrated resistor was directly acquired without pre-amplification by means of a 16-channel 24-bit Analog to Digital Converter (ADS1258, Texas Instruments) with tunable sampling frequency. Depending on the application, different sampling frequencies were possible (values typically used were in the range between 250 Hz and 400 Hz) by: i) modulating the overall conversion rate (this operation affects the signal to noise ratio S/N) of the ADC lodged onto the fingertip, or ii) selecting the number of converted channels (this operation does not affect S/N) without changing the overall conversion rate of the ADC.

Fig. 24 shows a diagram of the experimental set-up used in all the passive-touch studies following the full integration of sensor array and electronics into the distal phalanx (Oddo et al., IEEE RoBio 2009; Oddo et al., Sensors 2011), prior to full evaluation in active-touch (Beccai et al., 2009; Beccai et al., 2011; Oddo et al., IEEE TRO 2011). The experimental procedures were similar to that of the previous study (Oddo et al., Sensors 2009).

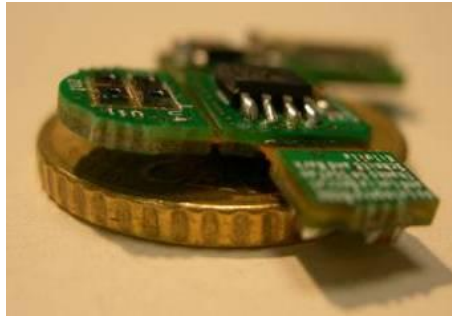


**Fig. 23.** From Oddo et al. (IEEE RoBio 2009). The developed rigid-flex board integrating the 2x2 array of MEMS sensors.

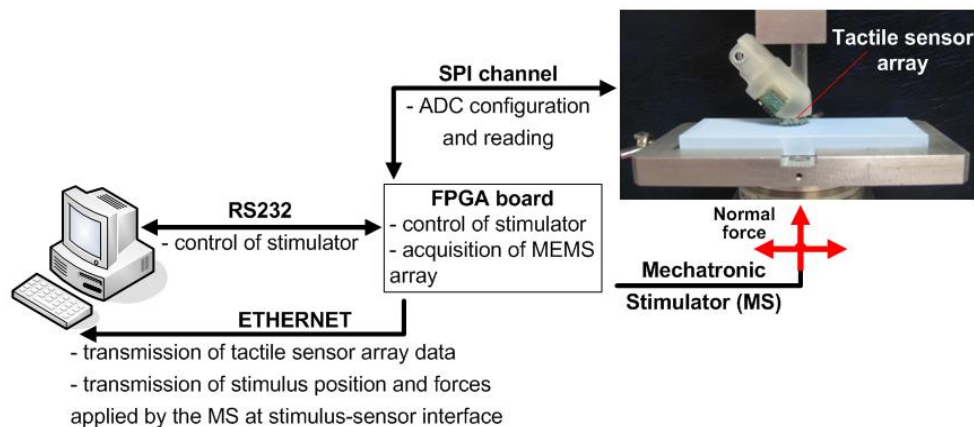


**Fig. 24.** From Oddo et al. (IEEE RoBio 2009). Block diagram and picture of the experimental setup implementing the control of the tactile stimulator together with the acquisition of data from the MEMS sensor array in passive-touch protocols.

Fingerprints, varying in coarseness and shape, were embossed onto the surface of the packaging material encapsulating the MEMS sensors in all the research works (Oddo et al., RoBio 2009; Beccai et al., 2009; Beccai et al., 2011; Oddo et al., Sensors 2011; Oddo et al., IEEE TRO 2011) which used the array depicted in Fig. 23. This design choice followed the significant contributions by Maeno and colleagues in the simulative analysis (Maeno et al., 1998; Yamada et al., 2002) and artificial emulation (Yamada et al., 2002; Hidaka et al., 2009) of fingerprints, showing that their structure increases the sensitivity in tactile activities with a major effect on surface-located type I receptors.

In a preliminary study (Oddo et al., IEEE RoBio 2009), biomimetism was pursued by designing a bi-layer packaging with increasing hardness going from the inner layer to the external surface, by introducing fingerprints, by mimicking the positioning of surface-located type I human mechanoreceptors and by allowing the design to be compatible with a thin protective layer mimicking stratum corneum of the human skin.

Fig. 25 shows a model of the packaged sensor array and the fabricated prototype having concentric medium-coarse ridges with groove width set to 0.7 mm and ridge width to 0.5 mm (hence being scaled-up, about three times, with respect to human fingerprints) and curvature radius between 9.75 mm and 15.75 mm. PDMS (Sylgard 184, Dow Corning, USA) was used as an external layer, stacked over an inner film of Dragon Skin (Smooth-On, USA). The result of the integration of the packaged tactile sensor array in the artificial fingertip is shown in Fig. 26.

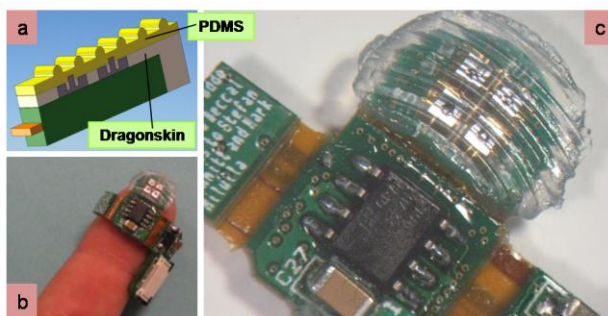


**Fig. 25.** From Oddo et al. (IEEE RoBio 2009). a) Cross-section of the sensor array showing the sensors positioning and the packaging structure; b) rigid-flex board with sensor array and packaging wrapped around a human index-finger distal-phalanx; c) close-up view of a fabricated prototype with bi-layer packaging and ridges.

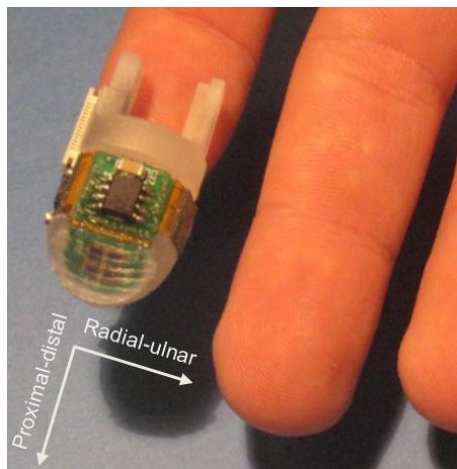


**Fig. 26.** From Oddo et al. (IEEE RoBio 2009). Integration of the fabricated prototype in the distal phalanx of the robotic fingertip; the proximal-distal and radial-ulnar directions are shown.

Though the assessment was preliminary in the work by Oddo et al. (RoBio 2009), specific foundations were posed to go towards a final fingertip design (Oddo et al., Sensors 2011) and to implement the subsequent experimental protocols in active touch (Beccai et al., 2009; Beccai et al., 2011; Oddo et al., IEEE TRO 2011). In such preliminary passive-touch dynamic experiments (Oddo et al., IEEE RoBio 2009, summarized in TABLE I) under regulated normal contact forces (between 100 mN and 400 mN), the frequency shift of the principal spectral component was observed in sensor outputs coherently with Equation (1), as a function of the spatial periodicity (from 400  $\mu\text{m}$  to 1900  $\mu\text{m}$ ) of the gratings and their sliding velocity (from 5 mm/s to 40 mm/s).

Moreover, in its preliminary experimental evaluation (Oddo et al., IEEE RoBio 2009), the fingertip integrating the tactile sensor array was oriented to provide stimulus motion selectively along the proximal-distal direction or along the radial-ulnar direction (Fig. 26). Remarkable encoding of roughness was revealed with fine gratings particularly when the stimulation was operated along the proximal-distal direction of the finger, showing a more consistent frequency-locked (Equation 1) behavior if compared to the radial-ulnar stimulation. This phenomenon was evident in the form of appreciable time-domain vibrations during proximal to distal stimulus sliding motion, or in the form of a principal tone coherent with the expected one in the frequency domain. As a matter of fact, due to the value of the curvature radius of the artificial ridges of the fingertip, in the proximal to distal stimulation condition the sliding motion of the ridges of the grating was mainly across the fingerprints, while in the radial to ulnar the sliding motion of the ridges of the grating was mainly along the fingerprints. This is the reason why the ridges embossed onto the packaging material particularly behaved as vibration promoters under the proximal-to-distal motion condition, enhancing the artificial roughness encoding capabilities of the artificial finger. The vibrations arose in the radial-ulnar direction for coarse stimuli only, and always showed lower amplitude than under the distal-proximal stimulation condition.

Such preliminary experimental findings were further examined under a dedicated research activity (Oddo et al., Sensors 2011). In such subsequent study, the influence of fingerprints and their curvature in tactile sensing performance was investigated by comparative analysis of different design parameters of an artificial fingertip inspired to the biological model, having straight or curved fingerprints, while leaving unchanged the other design features (Fig. 27): the morphology of the packaging encapsulating the sensor array (i.e. the curvature of fingerprints, as depicted in Fig. 27A-B) was selectively varied, and the consequences on directional isotropy were evaluated by means of dynamic- passive- experiments varying the reciprocal orientation between the artificial fingertip and the gratings (Fig. 27C and Fig. 30). Such analysis was inspired to previous observations with monkey subjects, providing evidence that gratings locally oriented parallel to the finger ridges elicit stronger response than tactile stimuli oriented along the orthogonal direction (Wheat & Goodwin, 2000).

In order to support the significance of the artificial touch results, in parallel (Fig. 29) electrophysiological studies were carried out (Oddo et al., Sensors 2011) by means of microneurographic recordings of the activity of single, identified afferent units in the fingertips of healthy human volunteers (Vallbo et al., 2004).

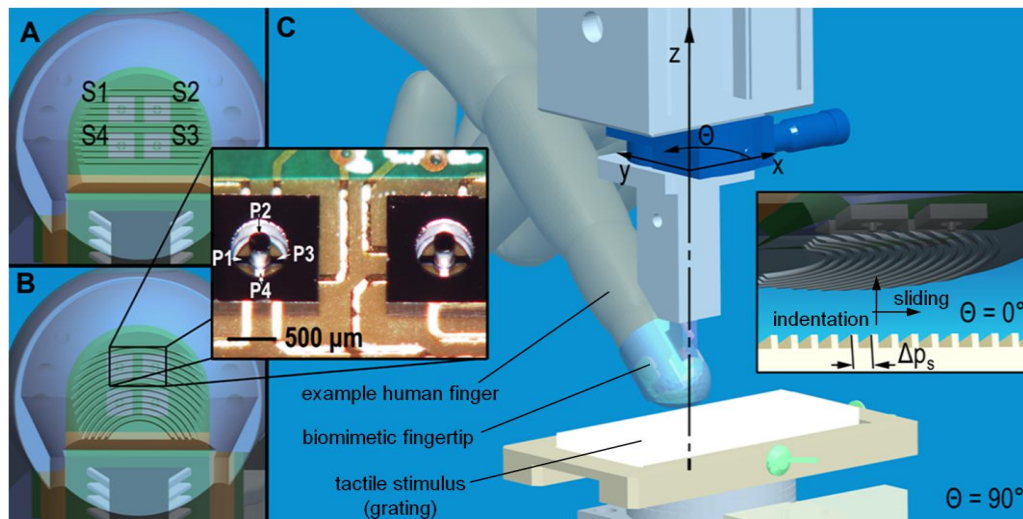


**Fig. 27.** From Oddo et al. (Sensors 2011). Design of the biomimetic fingertip integrating the rigid-flex board with 2x2 MEMS sensor array and readout electronics. Fingerprints embossed in the polymeric packaging had two curvatures. **Panel A** shows fingertip *a* design with straight fingerprints. **Panel B** shows fingertip *b* design with curved fingerprints. The inset shows two elements of the array of MEMS sensors. The piezoresistors (P1...P4) and the sensors (S1...S4) of the array are labeled according to the convention used in the text. **Panel C** shows a drawing of the experimental setup for indenting and sliding tactile stimuli in dynamic passive-touch experiments. An example human finger model is overlapped as a comparison to the developed biomimetic fingertip. The finger is rotated in steps of  $10^\circ$  along the  $z$ -axis (stimulus sliding across the distal phalanx in the depicted configuration, i.e.  $\theta=90^\circ$ ). The inset provides a close-up view of stimulus-artificial finger interface (stimulus sliding along the distal phalanx in the depicted configuration, i.e.  $\theta=0^\circ$ ).

Recently it has been asserted that human fingerprints contribute to the encoding of fine textures as they may perform spectral selection and amplification of tactile information in the frequency band, centered at about 250 Hz, of optimal sensitivity of Pacinian afferents (Scheibert et al, 2009). However, in such work Scheibert and colleagues, by experimenting an artificial tactile sensing technology, showed a principal frequency differing from Equation (1), since the spatial period  $\Delta p_f$  of fingerprints appeared (instead of  $\Delta p_s$ ) in the dominant vibrations gathered by the tactile sensor, resulting in  $f_{princ} = v/\Delta p_f$ . This means that the encoding of relative sliding velocity only, without any modulating effect due to roughness of the tactile stimulus, was achieved via the dominant frequency (while textural information was stated to be coded in the sidebands of the principal frequency). Such principal frequency encoding being a function of velocity only is confirmed in the study by Damian et al. (2010), applying the principle for slippage speed detection. Similar considerations apply to the same kind of vibrations dominated by the structure of fingerprints, reported as a potential way to encode roughness in the study by Wettels and colleagues (2008). Most probably, in the work by Scheibert et al. (2009) the dominance of finger skin geometry ( $\Delta p_f$ ) on stimulus surface features ( $\Delta p_s$ ) in the retrieved principal spectral component was: i) activated by the used stimulus, whose edges were positioned randomly (white-noise 1D patterning, i.e. extremely polyharmonic), and ii) gathered thanks to the quite wide receptive field of the sensor due to the relatively thick 2 mm packaging layer (a relevant related analysis is provided by Vásárhelyi et al., 2006) mimicking the positioning of deeply located (i.e. type II) Pacinian mechanoreceptors.

Conversely, in the dedicated experimental analysis on the role and contribution of fingerprints in artificial roughness encoding (Oddo et al., Sensors 2011), a different kind of biomimetism was sought in the packaging design. A fine skin-like layer was fabricated above the MEMS sensors, as for the positioning of slowly adapting type I (SAI; Merkel) and rapidly adapting (RA; Meissner) units: the artificial epidermal ridge had a height  $h_1$  of 170  $\mu\text{m}$ , while the thickness  $h_2$  of the homogeneous packaging layer covering the sensor array was 600  $\mu\text{m}$  (Fig. 28); The coarseness of human fingerprints (between-ridge distance typically comprised within 0.3 mm and 0.5 mm; Peters et al., 2009) was also mimicked: in finger *a* (Fig. 27A), fingerprints were embossed with straight parallel ridges having between-ridge distance  $\Delta p_f$  set to 400  $\mu\text{m}$ , while finger *b* (Fig. 27B) had concentric fingerprints with groove and ridge widths as for prototype *a*, and the fingerprint passing from the center of the sensor array had curvature radius of 4.8 mm. The encapsulation was performed by means of soft polymeric packaging (Dragon Skin, Smooth-On, USA), having shore A 10 hardness and recovering its original form after a mechanical stimulation.

To make a comparative analysis (Oddo et al., Sensors 2011) between the human subject and the artificial system, the same class of ridged tactile stimuli was presented to both the biomimetic fingertip (Fig. 29B) and to human subjects (Fig. 29A) via dynamic passive-touch protocols implemented through the same core mechatronic platform (Oddo et al., Mechatronics 2011, discussed here in Section 2) that can indent the stimuli to the fingertip and slide them in a smooth tangential fashion (Fig. 27C).

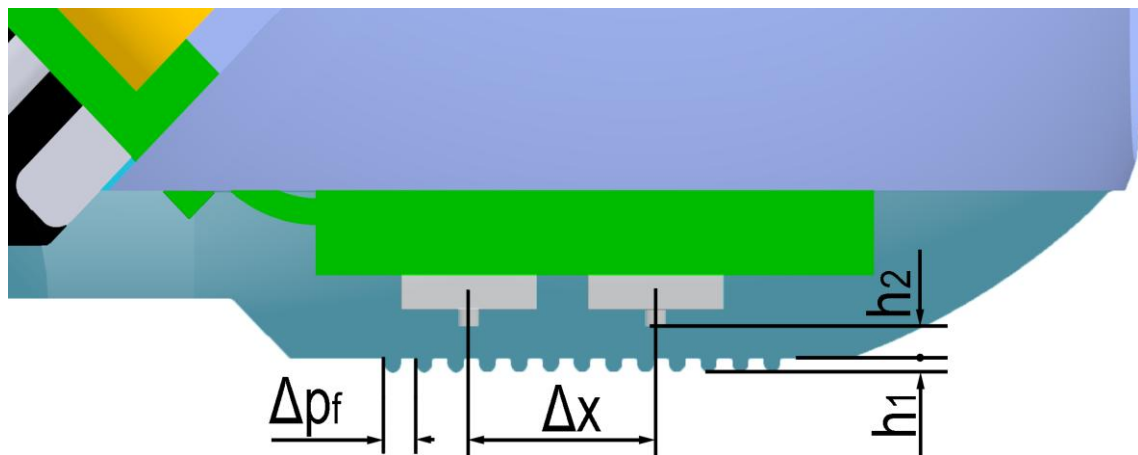


**Fig. 28.** From Oddo et al. (Sensors 2011). Cross section of the biomimetic fingertip, showing two sensors of the array and the structure and dimensions of fingerprints. The array pitch  $\Delta X$  is 2.36 mm, the fingerprints have between-ridge distance  $\Delta p_f$  set to 400  $\mu\text{m}$ , while their thickness  $h_1$  is 170  $\mu\text{m}$ . The thickness  $h_2$  of the homogeneous packaging layer covering the sensor array is 600  $\mu\text{m}$ .

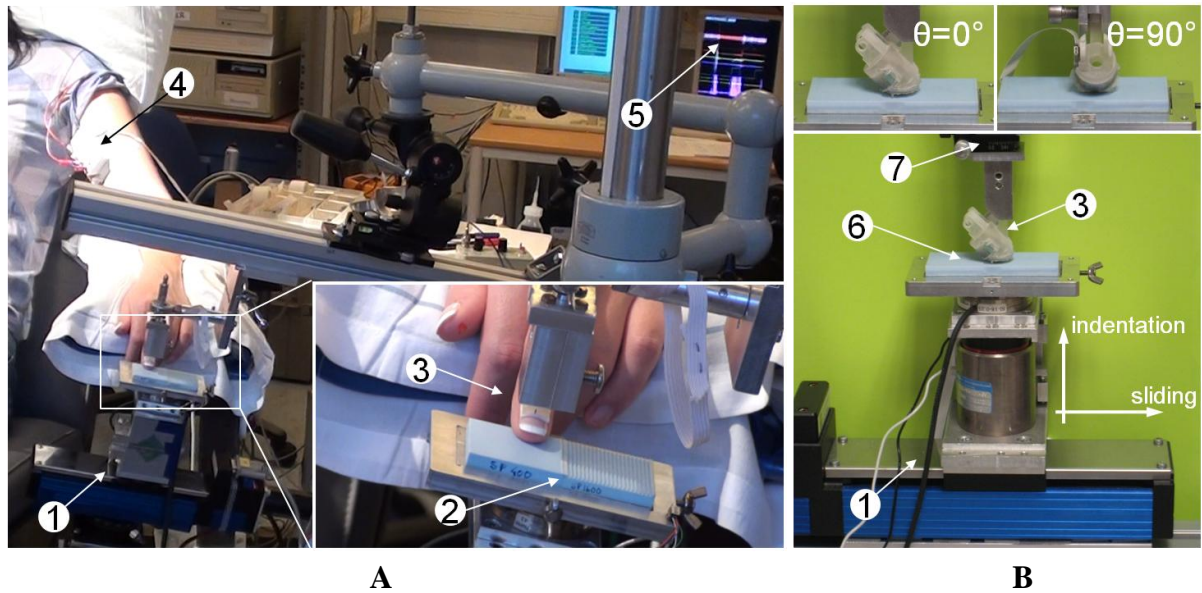


**Fig. 29.** From Oddo et al. (Sensors 2011). Experimental set-up in human (**Panel A**) and artificial (**Panel B**) touch experiments. 1: core mechatronic tactile stimulation platform; 2: pair of half-gratings; 3: human and biomimetic finger support; 4: first stage of microneurography electronics; 5: display with neural data for experiment monitoring; 6: single full-grating; 7: rotational stage with goniometer.

With such parallel investigation, evidences of a modulation mechanism according to Equation (1) were provided with RA human mechanoreceptors for fine and coarse gratings and with SAI for coarse gratings only (both RA and SAI are type I mechanoreceptors; Fig. 1), as it is detailed in the following.

Fig. 31 shows sample nerve recordings, gathered from the median nerve above the elbow using the microneurographic technique (Vallbo et al., 2004), from a human RA receptor during stimulus sliding motion across the distal phalanx (i.e.  $\theta=90^\circ$ ). The subject's fingerprint at the location of the depicted RA unit has a tangent oriented at approximately  $46^\circ$  from the direction parallel to the ridges of the gratings (=  $44^\circ$  degrees from the direction of the sliding motion). Spectral analysis of the nerve discharge patterns (Rosenberg et al., 1998) showed significant modulation at the frequency determined by the stimulus spatial period  $\Delta p_s$ , according to Equation (1). A similar relationship depending on the stimulus spatial period was observed in the activity of single human mechanoreceptors with receptive fields in the finger tips of the second and third fingers. Particularly, for the tested gratings in the 280-520  $\mu\text{m}$  spatial period range, this frequency-locked modulation was for 8 of 9 RA afferents units where this was tested, but not in any of the SAI units ( $n=5$ ). For gratings in the 1600-1920  $\mu\text{m}$  spatial period range, the modulation was observed in all of the tested RA and SAI units ( $n=7$  and 5, respectively; 10-20 mm/s sliding velocity). Moreover, it should be noted that the average discharge rates of single tactile afferents never directly reflected the spatial periods of the stimuli. As an example, average discharge rate was 40 Hz for the unit in Fig. 31A, and 55.5 Hz for the unit in Fig. 31B. Thus, there was no 1:1 (or higher order) locking of the nerve discharges, but the spatial periodicity were reflected as a frequency modulation (Equation 1) of the discharge patterns.

In the artificial touch study on fingerprints (Oddo et al., Sensors 2011), the indentation force was 200 mN, which is one of the values used in the parallel human touch study and is within the range used by humans during tactile exploratory tasks (Jones & Lederman, 2006); the force level was not varied since the previous related artificial touch studies (Oddo et al., Sensors 2009; Oddo et al., IEEE RoBio 2009) showed that a modulation of the contact force in the 100 mN – 1 N range resulted in a principal frequency being coherent with Equation (1). The velocity was 10 mm/s, which is the lower boundary of the range of exploratory velocities typically used by humans (Lederman, 1983), and was not varied in this work since previous studies (Oddo et al., Sensors 2009; Oddo et al., IEEE RoBio 2009; Oddo et al., IEEE TRo 2011) showed (up to 48 mm/s, in Oddo et al., Sensors 2009, as reported in TABLE I) that a change in velocity coherently modulates the principal frequency according to Equation (1).

According to the experimental protocol, the two artificial fingertip prototypes *a* (straight fingerprints, Fig. 30-top) and *b* (curved fingerprints, Fig. 30-bottom) were evaluated by rotating them from  $\theta=0^\circ$  (stimulus sliding along the distal phalanx, Fig. 30-left) to  $\theta=90^\circ$  (stimulus sliding across the distal phalanx, Fig. 30-right) in steps of  $10^\circ$ , thus indenting and sliding the ridged stimuli with ten different fingertip orientations.

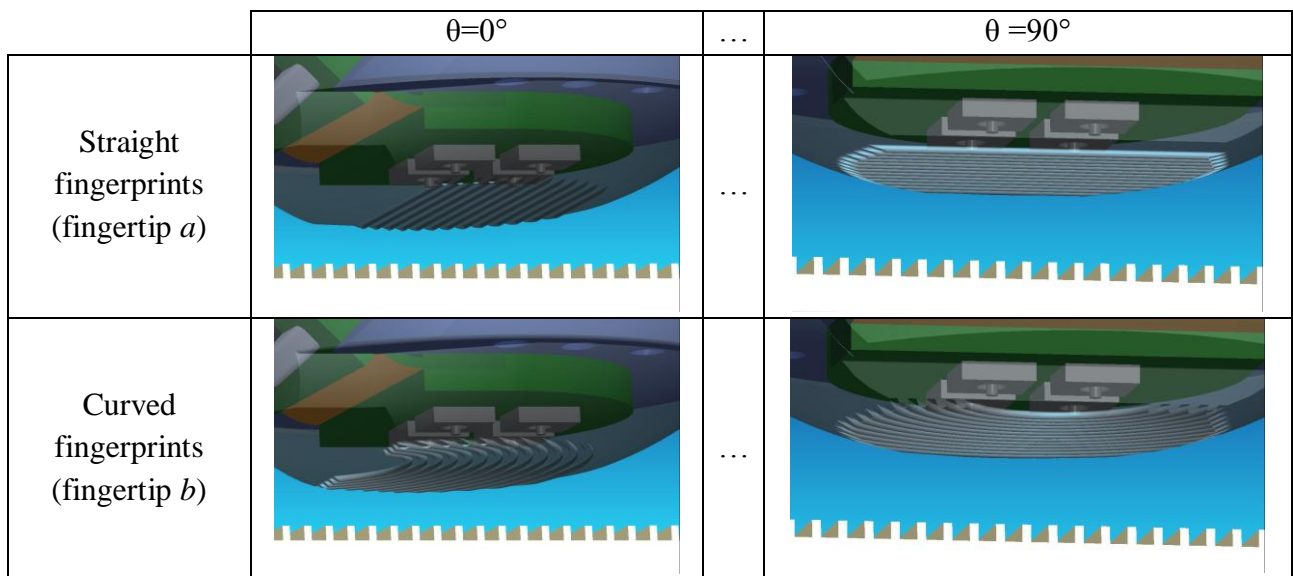


**Fig. 30.** From Oddo et al. (Sensors 2011). Protocol for the artificial touch experiments: the two biomimetic fingertip prototypes, differing in the curvature of fingerprints, were rotated in steps of  $10^\circ$  from  $\theta=0^\circ$  (stimulus sliding along the distal phalanx) to  $\theta=90^\circ$  (stimulus sliding across the distal phalanx).

Importantly, the BioRobotic investigation in artificial touch (Oddo et al., Sensors 2011) showed that the structure of fingerprints affects the directional isotropy in the encoding of the principal spatiotemporal frequency of stimuli (Equation 1): curved fingerprints guaranteed higher directional isotropy than straight fingerprints, as it is detailed in the following. Moreover, such experimental results were coherent with those shown by Chen and colleagues (2006) by means of carbon microcoils embedded into an elastic polysilicone matrix, mimicking Meissner (RA) corpuscles.

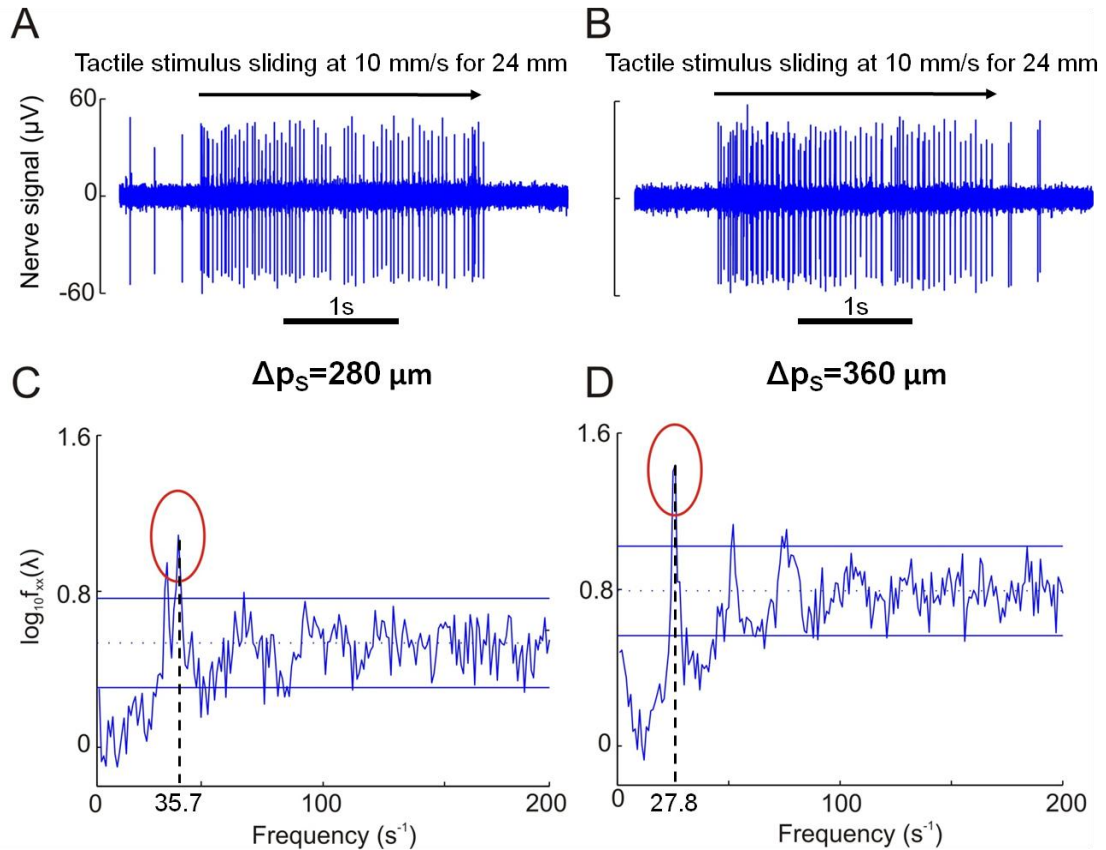


**Fig. 31.** From Oddo et al. (Sensors 2011). **Panels A** and **B** show microneurographic recordings from human single tactile RA afferents in the fingertips during stimulation as in Fig. 27C and Fig. 29A; a 10 mm/s sliding motion was applied across the distal phalanx. **Panels C** and **D** show spectral analysis of the nerve discharge trains from 12 repeated stimulus runs for the units shown in **A** and **B**. Grating spatial periodicity  $\Delta p_s$  is 280  $\mu m$  in **A** and **C**, 360  $\mu m$  in **B** and **D**. Principal frequencies resulting from Equation (1) according to the specific combination of grating spatial periodicity  $\Delta p_s$  and sliding velocity  $v$  are 35.7 and 27.8 Hz for **Panels C** and **D**, respectively, with meaningful coherence with the depicted experimental results. Horizontal lines in **C** and **D** show  $p < 0.01$  confidence limits for

**Fig. 32.** significant frequency modulation.

In Fig. 33 and in Fig. 34 time domain data from single channels (Piezoresistor 2 of Sensor 1 and Piezoresistor 4 of Sensor 4, respectively) of the experimented biomimetic fingertip designs is plotted above the related Short Time Fourier Transform (STFT). The insets on the right of the STFT plots show the spectra obtained by applying a Fast Fourier Transform (FFT) to the single channel data highlighted in red in the time domain plots. Particularly, Fig. 33A-B shows time domain traces from Piezoresistor 2 of Sensor 1 in fingertip *b* (see Fig. 27 for the labeling of sensors of the tactile array) during stimulation with 360  $\mu m$  and 440  $\mu m$  regular gratings rotated at an angle  $\theta = 10^\circ$ . The periodic patterns at 27.8 Hz (360  $\mu m$  grating) and at 22.7 Hz (440  $\mu m$  grating) associated to the spatial periodicity of tactile stimuli are clearly visible either in time (vibrational component), in frequency (dominant peak in the FFT, marked with a dotted line) and in time-frequency (red region, marked with a dotted line in the STFT) domains. Since the sliding velocity remains constant in the performed experiments, the dominant frequency of the vibrations elicited by the tactile stimulus is proportional to the inverse of the spatial period of the grating

(Equation 1), while the intensity of the vibrations increases with the spatial period. Both these effects appear to be coherent with the study by Bensmaïa and Hollins (2003), where the mechanical vibrations recorded in the fingertip of human subjects are shown to scale down in peak frequency and to increase in peak-to-peak amplitude while increasing the spatial period.

The relevance of the dynamic stimulation phase (i.e. the dataset corresponding to surface-fingertip tangential relative motion) to extract vibrational patterns which are correlated to the stimulus surface features is confirmed by the STFT spectrograms depicted below the time domain plots, which show a sudden frequency step at the onset of the stimulus sliding-motion. The spectral pattern remains stable while the periodic grating is stroked at constant velocity. More importantly, as confirmed by the FFT spectra, the frequency peak corresponds to the expected value depending on the applied stimulus according to Equation (1), i.e. 27.8 Hz for the 360  $\mu\text{m}$  surface and 22.7 Hz for the 440  $\mu\text{m}$  one. As previously anticipated, this artificial vibrational roughness encoding is meaningfully coherent with the parallel microneurography results in humans, and with previous studies with monkeys (Darian-Smith & Oke, 1980).

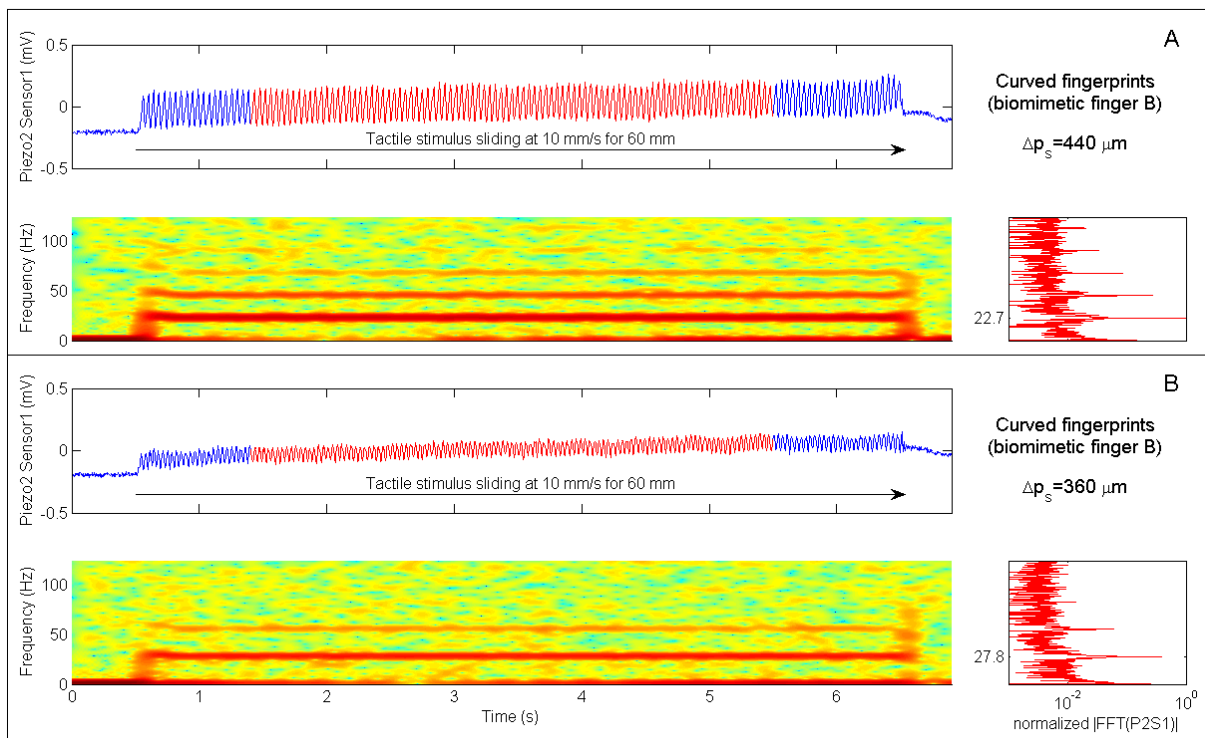


**Fig. 33.** From Oddo et al. (Sensors 2011). Encoding of stimulus spatial period  $\Delta p_s$  in either time, frequency and time-frequency domains. Data belongs to Piezoresistor 2 of Sensor 1 of the biomimetic fingertip and was acquired while sliding at 10mm/s (200mN indentation force) the 440  $\mu\text{m}$  (**Panel A**) and 360  $\mu\text{m}$  (**Panel B**) periodic stimuli over the biomimetic fingertip with curved fingerprints (shown in Fig. 27B). According to Equation 1, the expected principal frequency was 22.7 Hz (**A**) or 27.8 Hz (**B**). The rotation of the fingertip was  $10^\circ$  with respect to the stimulus sliding direction (reference frame shown in Fig. 27C).

A comparison between the A-D and the E-H panels in Fig. 34 shows the effect of the curvature of fingerprints in the encoding of stimulus spatial features in relation to the rotation of the biomimetic fingertip. The four rows show results for  $\theta = 10^\circ$ ,  $\theta = 20^\circ$ ,  $\theta = 40^\circ$  and  $\theta = 90^\circ$ . There is higher isotropy with the curved fingerprints than with the straight ones, which have a strongly preferred direction when the sliding is closer to the direction along the distal phalanx (i.e. across the fingerprints). As shown in Fig. 34A, with straight fingerprints the vibratory patterns are noticeable either in time and frequency domains for  $\theta = 10^\circ$ , while those patterns are considerably reduced and masked by the other spectral components when the fingertip is rotated (Fig. 34B-D) so to have a sliding oriented closer to the direction across the distal phalanx (i.e. along the fingerprints).

Extended analysis of the spectrum of readings from both the biomimetic finger designs as a function of the rotation angle  $\theta$  brings evidence of the higher anisotropy anticipated above for straight fingerprints (Fig. 35A compared to Fig. 35B). Within the plots shown in Fig. 35, the expected (Equation 1) principal frequency is represented by a straight red line, while for output  $PiSj$  ( $i^{th}$  piezoresistor of  $j^{th}$  sensor, according to Fig. 27A-B) the correctly identified dominant peaks (arising for frequencies higher than a 2.5 Hz threshold) are marked with red circles in the figures.

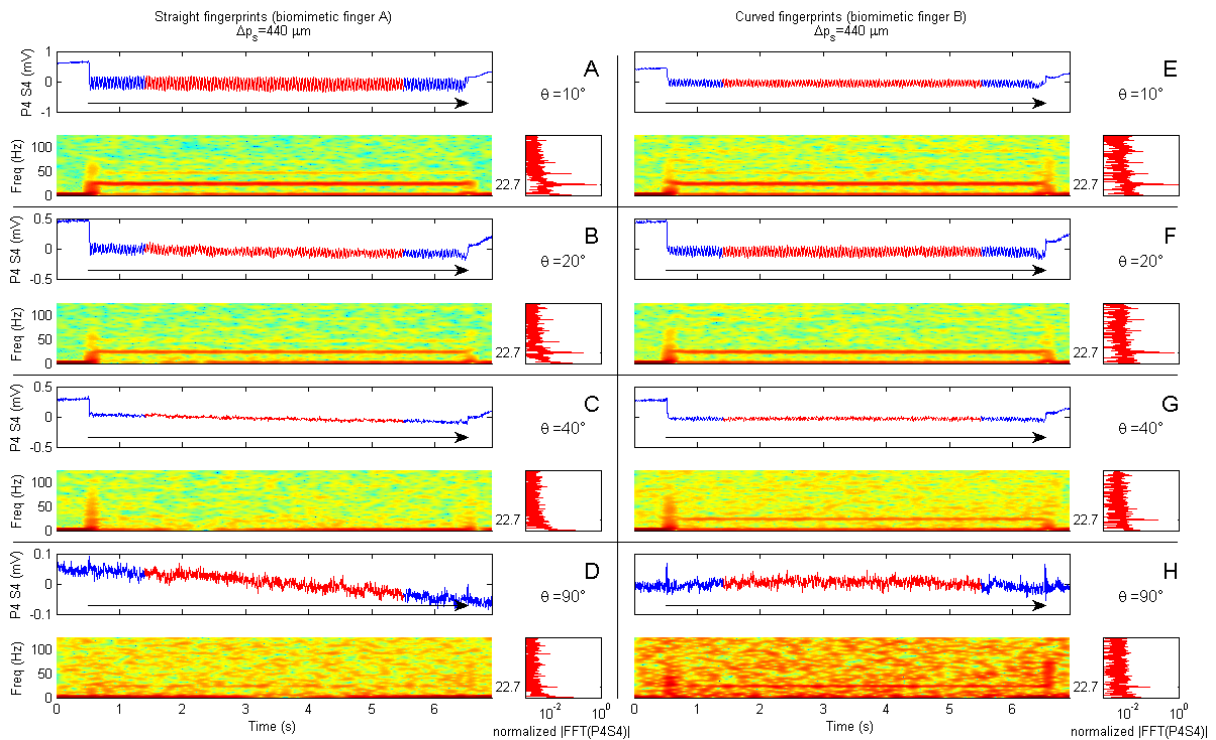


**Fig. 34.** From Oddo et al. (Sensors 2011). Encoding of stimulus spatial period  $\Delta p_s$  as a function of fingertip rotation  $\theta$  for both the prototypes with straight and curved fingerprints. Data belongs to Piezoresistor 4 of Sensor 4 and was acquired while sliding at 10 mm/s (200 mN indentation force) the 440  $\mu\text{m}$  periodic stimulus over the biomimetic finger with straight fingerprints (**Panels A to D**) and with curved fingerprints (**Panels E to H**). According to Equation 1, the expected principal frequency was 22.7 Hz. A description of each row of the subplots is provided within Fig. 33. The plotted results are obtained by rotating the finger of an angle  $\theta$  set to  $10^\circ$  (**A, E**),  $20^\circ$  (**B, F**),  $40^\circ$  (**C, G**) and  $90^\circ$  (**D, H**) with respect to the stimulus sliding direction.

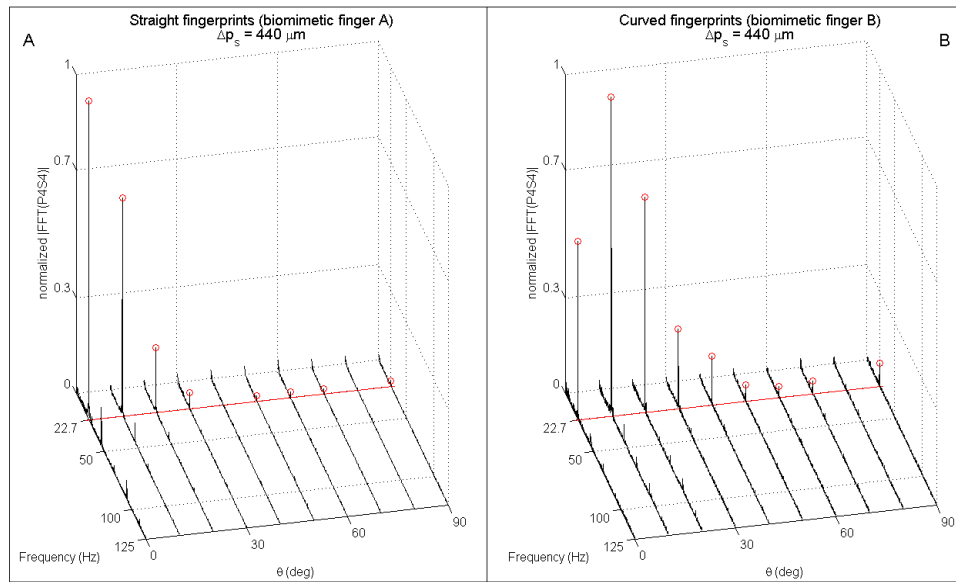


**Fig. 35.** From Oddo et al. (Sensors 2011). Single-sided normalized amplitude spectra as a function of the rotation of the biomimetic fingertip with straight (**Panel A**) and curved (**Panel B**) fingerprints. Data is related to 4.096s subsets gathered from Piezoresistor 4 of Sensor 4 (P4S4) while the stimulus was indented and rubbed tangentially to the finger. Normal stimulus-fingertip contact force was set to 200mN, while the sliding velocity was 10mm/s. According to Equation 1, the expected principal frequency (marked with a red straight line) was 22.7 Hz. The red circles highlight the correctly identified (by applying Equation 2) peak frequency per each stimulation combination. Higher isotropy as a function of the rotation angle is appreciated with the fingertip having curved fingerprints.

It is significant to point out that, differing from Fig. 35A (straight fingerprints), in Fig. 35B (curved fingerprints) the peak is not at  $\theta=0^\circ$  but at  $\theta=10^\circ$ . This is a consequence of the curvature of fingerprints, which affects the sensitivity of the packaged system in tradeoff with the preferred direction of Piezoresistor P4, hence widening the region of effective roughness encoding as a function of the finger rotation angle  $\theta$ : the tangent to the curved fingerprints at the location of Sensor S4 is orthogonal to the  $x$  axis sliding motion direction (and contemporarily parallel to ridges of the grating) when  $\theta=17.4^\circ$  (i.e.,  $>10^\circ$ ), while piezoresistor P4 shows its maximum sensitivity (Beccai et al., 2005; Oddo et al., 2007) to tangential loads (reaching the sensor through the packaging material) being oriented along the direction of its tether, which is aligned with the  $x$  axis when  $\theta=0^\circ$  (i.e.,  $<10^\circ$ ).

Remarkably, the observed peak frequency values were at the expected values depending on the tested stimulus spatial period and constant sliding velocity (Equation 1): the shape of the fingerprints was shown to have an effect on the possibility to promote and sense such vibrations (therefore modulating, up to masking, their amplitude), not in shifting the peak values on the frequency axis. Such results presented with simple gratings appear to go in the direction of those with more complex surfaces presented by Bensmaïa & Hollins (2005), since in such work the mechanical vibrations were found to have spectra repeatably related to the surfaces which were experimented with different subjects (therefore, having different fingerprints one to the other) at constant finger-stimulus relative velocity.

The experimental analysis of the artificial fingertip suggests that the structural anisotropy of fingerprints, due to their shape, has a major role in determining the level of anisotropy in the encoding of tactile stimuli spatial features. The sensory systems with straight fingerprints embedded in the skin-like packaging had noticeably higher directional preference, while higher isotropy was observed with curved ones. As from the quotations reported in Section 10, Bensmaïa and colleagues (2006) raised the open question whether the anisotropy observed in humans is related to the structural anisotropy of the skin or to afferent branching at neural level. In the work by Oddo and colleagues (Sensors 2011), the experimented biomimetic artificial fingertips differed in the packaging skin-like layer design only; moreover, the anisotropy was observed on a channel by channel basis, not only as an aggregated effect among different outputs of the array. Therefore, from a robotic point of view the presented results agree with the hypothesis according to which the directional anisotropy is affected by the structure of fingerprints. Starting from these initial results, further investigations are needed to evaluate a potential concurrent role of afferent branching at neural level.

Definitively, the obtained results (Oddo et al., Sensors 2011) provide inputs for the design of artificial sensory systems to best encode textural features in case that the target active-touch application has or has not a preferred direction for the finger-stimulus relative motion.

In the literature, a significant study for the artificial active-touch discrimination of textures was presented by Hosoda and colleagues (2006), by means of a soft fingertip with a smooth surface embedding in a random manner strain gauges and PVDF films at different depths of the rubber layers, allowing for active discrimination of five different types of materials based on the analysis of variance of the dynamic sensor outputs (Fig. 36); however, a closed modeling of the relationship between sensor outputs and the spatial coarseness (i.e., the physical quantity related to roughness) of tactile stimuli was not provided.

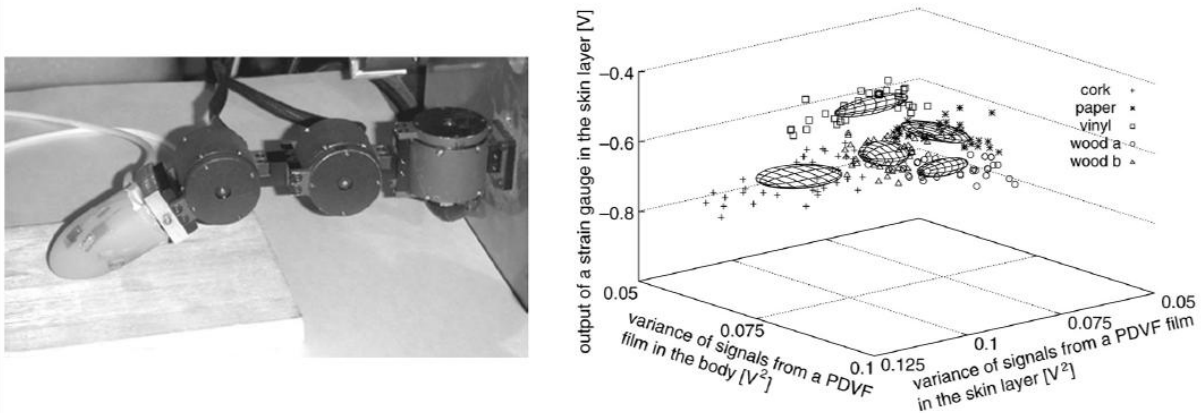


**Fig. 36.** Left: multi layered fingertip with randomly distributed strain gauges and PVDF film sensors, integrated in an exploratory robotic finger for active discrimination of tactile surfaces. Right: discrimination of five materials based on readings from a strain gauge and variance of signals from a pair of PVDF films located in different layers of the finger (Hosoda et al., 2006).

Some other works presented the integration of tactile sensing in actuated robotic fingers, but the focus has been mainly on grasp stabilization rather than on the encoding of spatial coarseness. Examples are the Gifu III Robotic Hand (Mouri et al., 2002) and the DLR II Hand (Huang et al., 2006) with embedded 6-axis force sensors.

In a recent work (Oddo et al., IEEE TRo 2011) the *passive* roughness-encoding studies discussed above were extended to the application with an *active* robotic finger (Fig. 37) to emulate the possible behavior of a robotic or prosthetic hand in exploring objects. The objective was to develop an exploratory artificial finger equipped with tactile microsensors at its fingertip and a method for robust discrimination of surfaces based on roughness encoding during stereotyped movements. Such a system may be exploited in future next generation hand prostheses (Carrozza et al., 2006; Cipriani et al., 2010) with the aim of providing non-invasive or invasive afferent sensory feedback.

The robotic finger (Fig. 37d) was human sized (Buchholz et al., 1992), tendon driven (Carrozza et al., 2006; Cipriani et al., 2009; Cipriani et al., 2010) and underactuated (Birglen & Gosselin, 2004; Luo et al., 2004), i.e. with more DoFs than actuators, as Hirose's soft finger (1985). The array of MEMS sensors and the design of the packaging layer were the same as for fingertip *b* with curved fingerprints (Fig. 27B and Fig. 28) discussed above (and detailed in Oddo et al., Sensors 2011).

With the robotic finger, the coherence between the theoretical (Equation 1) and the experimental fundamental frequency was initially demonstrated, as a control condition, in passive-touch (TABLE I). The passive-touch study was intended to show and evaluate the encoding principle (Equation 1) with the complete articulated finger (rather than with the fingertip as discussed above), under a protocol allowing to directly decouple the contribution of velocity  $v(t)$  from stimulus spatial coarseness  $\Delta p_s$ . After a first active contact by the finger, gratings having very close spatial periods (400, 440 and 480  $\mu\text{m}$ ) were stroked at controlled known velocity by a simplified version of the mechatronic tactile stimulation platform discussed in Section 2 (Oddo et al., Mechatronics 2011).

In the core set of experiments, as experimental condition, the approach was evaluated under a full active-touch protocol with the robotic finger mimicking via a pre-programmed trajectory the natural exploratory movement by the hand, and without measuring the actual instant sliding velocity (to establish a technique avoiding the need for proprioceptive kinesthetic information). Active-touch experiments were implemented by contacting the tactile stimulus controlling the MCP joint (phases 1-2 of Fig. 37d), and subsequently flexing the PIP and DIP joints (phase 3b of Fig. 37d) so to perform a smooth human-like exploratory task lasting 2s. The contact forces at finger-stimulus interface, recorded by a load cell, were comprised within 100 and 300 mN and therefore belonged to the range used in human exploratory tasks (Jones & Lederman, 2006).

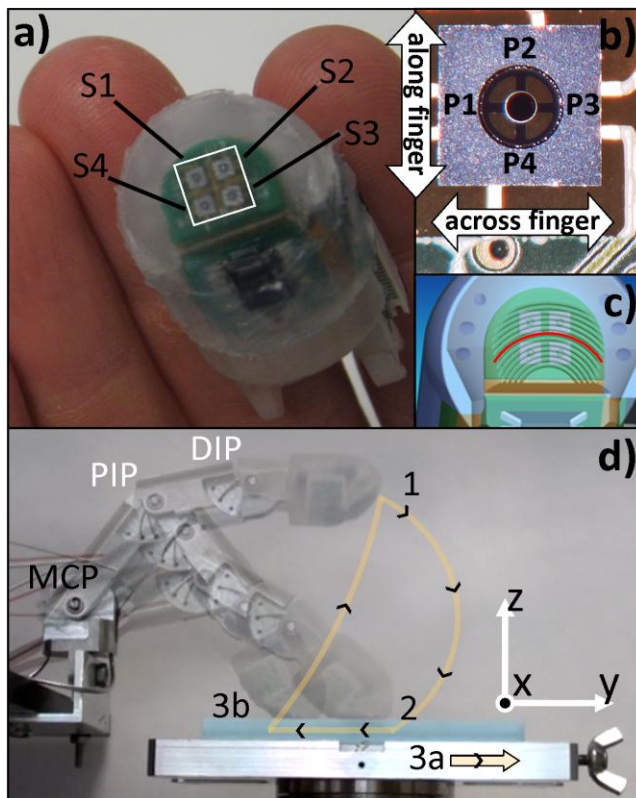


**Fig. 37.** From Oddo et al. (IEEE TRo 2011). a) Distal phalanx of the robotic finger, in comparison to human hand, integrating the  $2 \times 2$  sensor array (S1 to S4), electronics and polymeric packaging with fingerprints; the square with white borders highlights the  $22.3 \text{ mm}^2$  area of the array, where a  $72 \text{ units/cm}^2$  density is reached. b) Close up view of sensor S4 of the array. The four outputs of the sensor are marked at the roots of the tethers of the cross-shape structure. For all the sensors of the array, P1 and P3 are on tethers oriented across the finger, while P2 and P4 are on tethers oriented along the finger. c) Design of the sensor array showing the fingerprints, having  $400 \mu\text{m}$  ridge to ridge distance; the curvature radius of the fingerprint highlighted in red is  $4.8 \text{ mm}$ . d) Setup, reference frame and phases of the protocol for the passive-touch (1, 2 and 3a) and active-touch (1, 2 and 3b) experiments. The 2 degrees of actuation (DoA) are obtained via independent control of MCP joint and underactuated coupling between the PIP and DIP joints.

The core active-touch results with gratings as tactile stimuli (Oddo et al., IEEE TRo 2011) demonstrated a surface identification approach based on (i) the implementation of a stereotyped feedforward exploratory trajectory: this is bioinspired to sensorimotor control models (Scott et al., 2004) since it is based on planned motion trajectory rather than continuous feedback from dedicated proprioceptive sensors; (ii) time-frequency analysis via wavelet transform on the outputs of the tactile sensors, showing a clustering of the fundamental frequency as a function of the tactile stimulus; (iii) k-NN (k nearest neighbors) discrimination based on extracted fundamental frequency from the sensor array, without requiring dedicated proprioceptive sensors for the time-varying end-effector velocity, yielding 97.6% worst case discrimination accuracy in active-touch conditions (while in the control passive-touch study 100% accuracy was achieved by means of a look up table).

In the process towards discrimination of surfaces via roughness encoding, a wavelet analysis technique (Grinsted et al., 2004) was introduced to take into account that the end-effector velocity could be time variant in active-touch experiments. As a consequence, the fundamental frequency (Equation 1) would dynamically modulate within each exploratory session while rubbing the surface. To allow retrieving such dynamic frequency-modulation, the continuous Wavelet Transform (WT) was used, expanding into a time-frequency space the output signals from the sensor array. More reliably than the single-channel WT, the Cross Wavelet Transform (XWT) was applied to identify time-frequency regions with high common power between outputs from different sensors of the array, hence establishing a robust elaboration method based on combined processing of pairs of sensor outputs.

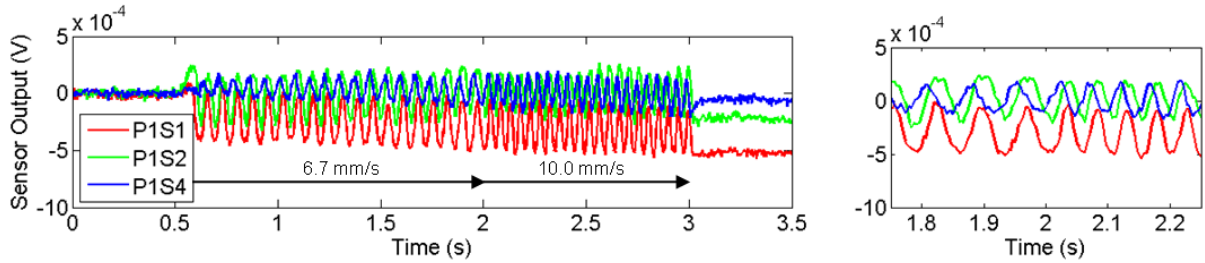


**Fig. 38.** From Oddo et al. (IEEE TRo 2011). Time domain plots under a passive-touch run with the  $480\ \mu\text{m}$  grating (P1S1, P1S2 and P1S4, according to the labeling of Fig. 37b-c, are shown). The stimulus sliding motion starts at  $t_1=0.5\ \text{s}$  with a  $6.7\ \text{mm/s}$  velocity up to  $t_2=2.0\ \text{s}$ , when the velocity is raised to  $10\ \text{mm/s}$ . The sliding motion stops at  $t_3=3.0\ \text{s}$ . Vibrational encoding of stimulus spatial period is appreciated between  $t_1=0.5\ \text{s}$  and  $t_3=3.0\ \text{s}$ . The plots on the right show a zoom on the encoding of stimulus controlled velocity step at  $t_2=2\ \text{s}$ . Sensors S1 and S2 are on the distal part of the fingerpad in symmetrical positions with respect to the axis of the finger, and thus the related P1S1 and P1S2 signals are in-phase during the stimulus sliding motion. Sensor S4 is more proximal on the fingerpad and so P1S4 shows a phase difference with respect to P1S1 and P1S2. The phase difference between S4 and S1/S2 outputs is not affected by the varying velocity (Equation 2).

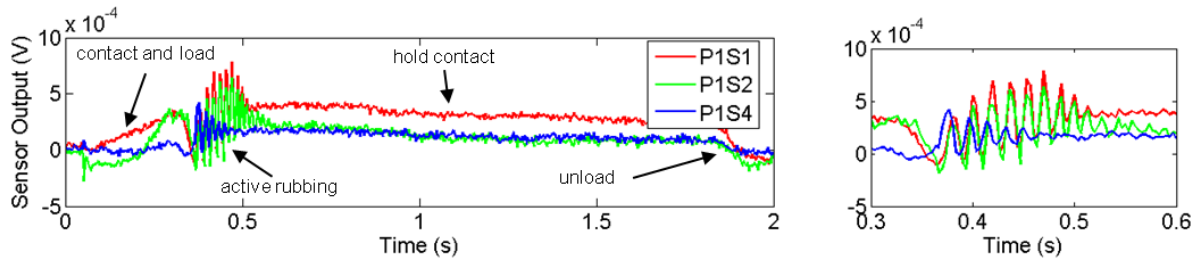


**Fig. 39.** From Oddo et al. (IEEE TRo 2011). Time domain plots under an active-touch experiment with the ridged tactile stimulus having spatial period  $\Delta p=480\ \mu\text{m}$  (P1S1, P1S2 and P1S4, according to the labeling of Fig. 37b-c). The graphs show experimental data comprising the load, rubbing and unload phases of the active-touch exploratory task. The plot on the right focus on the active rubbing of the ridged stimulus, showing vibrational encoding of roughness. Similarly to the passive-touch experiment shown in Fig. 45, the signal from P1S1 is in phase with P1S2 and shows a phase difference with P1S4, as expected from Equation (2).

The application of the  $WT$  and of the  $XWT$  is graphically represented with colors mapping the normalized power in time-frequency space, where the 5% significance level is highlighted as a thick contour. In addition, the  $XWT$  provides information about the local relative phase differences between sensor outputs. Phase information obtained via  $XWT(O1, O2)$  is also graphically represented, by arrows pointing right or left if the signals are in-phase or in anti-phase, pointing down if sensor output  $O1$  leads  $O2$  of  $\pi/2$  and pointing up if  $O2$  leads  $O1$ .

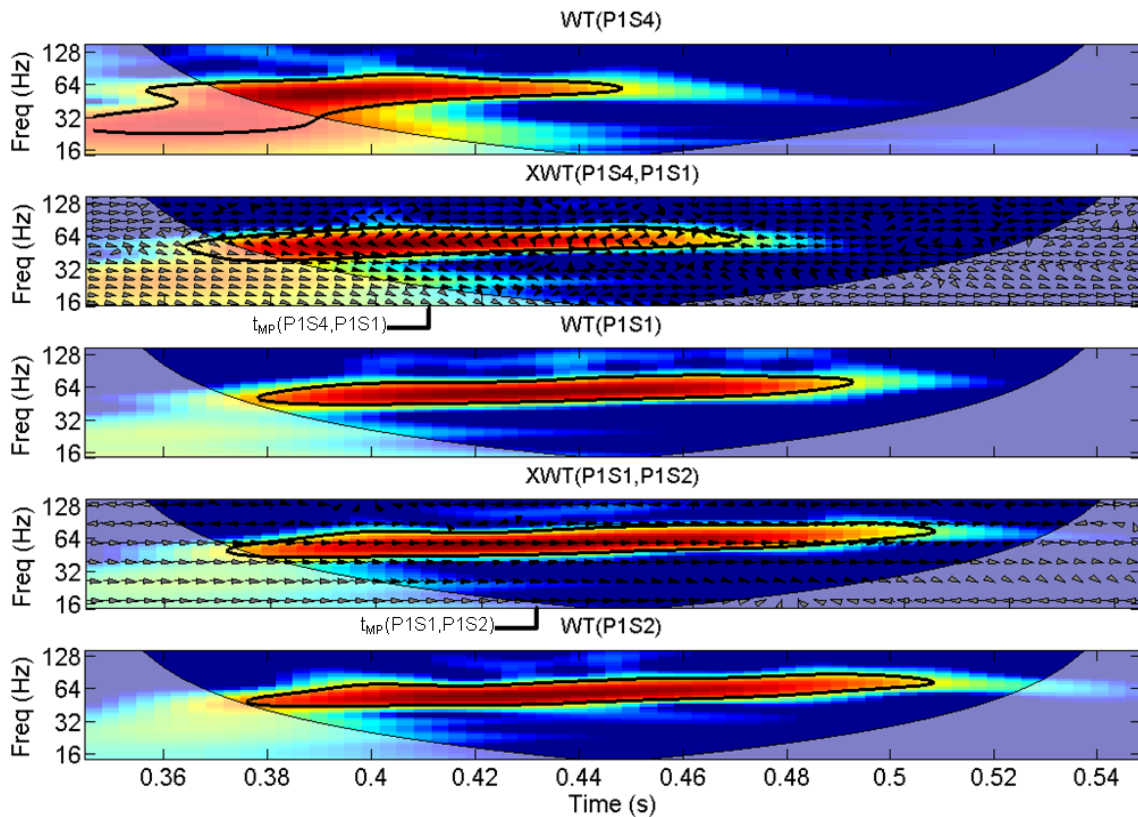


**Fig. 40.** From Oddo et al. (IEEE TRo 2011). *WT* on single channels (P1S4, P1S1 and P1S2) of the array and *XWT* on channel pairs P1S4-P1S1 and P1S1-P1S2. The plots focus on the active-touch exploration of the 480  $\mu\text{m}$  stimulus by the robotic finger, showing the frequency encoding during the rubbing phase of stimulus spatial period and of the time variant velocity according to Equation (1). The shifting of the high-power red zone towards higher frequencies reveals that the end-effector velocity varied (increasing) with time while rubbing the sample. High-power regions in time-frequency space are colored in red and maximum cross-power intents  $t_{MP}$  are indicated for both the channel pairs. The thick contour surrounding the red region identifies the 5% significant level. The arrows in the *XWT* plots are a graphical representation of the phase difference between the pairs of channels (pointing right: in-phase; left: anti-phase; down: series1 leading series2 by  $90^\circ$ ).

As depicted in Fig. 38, in passive-touch the vibrational roughness encoding lasted steadily (1.6% maximum standard deviation with respect to the expected principal frequency) for all the sliding motion of the stimulus; conversely, in active-touch each unit of the array best encoded the tactile stimulus in a subset only of the exploratory task. This phenomenon was due to the varying inclination of the fingertip in active-touch, which resulted in a shift of the center of pressure on the fingerpad. As a consequence, the active stereotyped exploratory task presented a subset lasting about 150 ms during which the spatial coarseness of the tactile stimuli was encoded with vibrational cues by at least one unit of the array (cf. Fig. 39). An overlap of about 80 ms was observed (Fig. 39-right and Fig. 41) for the combined vibrational activation of distal sensor units (S1 and S2) and proximal sensor ones (S3 and S4, the former not shown for the sake of graphical clearness).

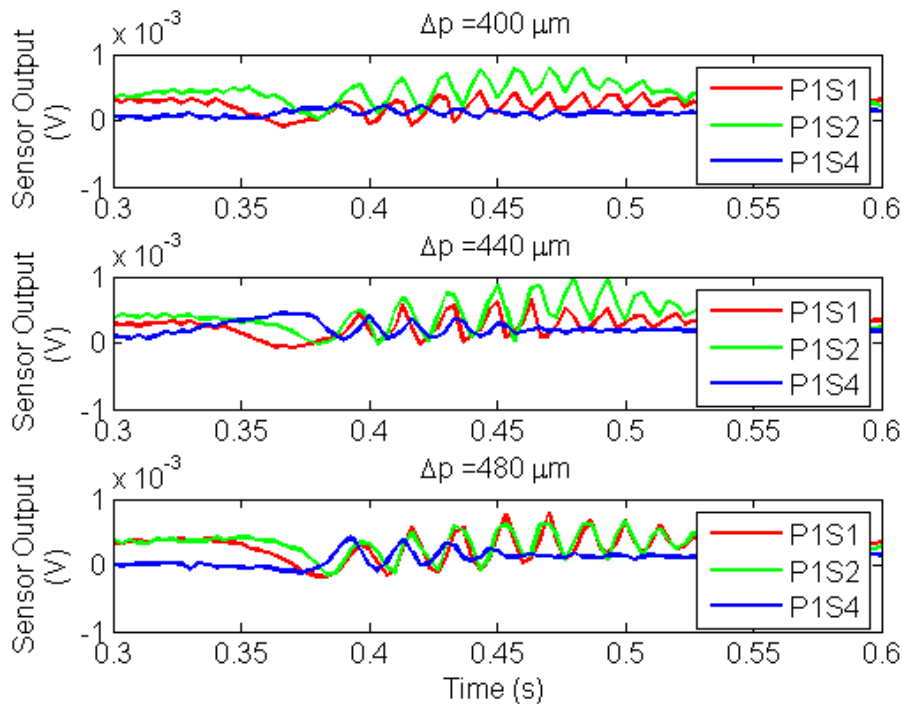


**Fig. 41.** From Oddo et al. (IEEE TRo 2011). Active-touch vibrational frequency encoding in time domain of the grating spatial period, by sensor outputs P1S1, P1S2 and P1S4. Moreover, P1S1 and P1S2 were always in-phase, while the phase difference with P1S4 varied depending on the surface, coherently with Equation (2). In the depicted figure, this is confirmed by the horizontal shift of the blue trace with respect to the red and green ones while comparing the plots for the three different gratings.

The data analysis technique identified the significant regions resulting, in time-frequency space, in maximum cross-power between adjacent units of the array. Even in the condition of non-constant end-effector velocity (Fig. 40) while actively exploring surfaces, due to the execution of movements being stereotyped across the runs, the so identified principal frequency values showed a clustering (Fig. 42) as a function of spatial coarseness of tactile stimuli, confirming a roughness encoding being applicable to machine learning classifiers for discrimination of textures (Oddo et al., IEEE TRo 2011). It is significant to point out that, coherently with the physical model underlying Equation (1), finer grating spatial periods  $\Delta p$  resulted in higher frequencies in both the axes of Fig. 42.

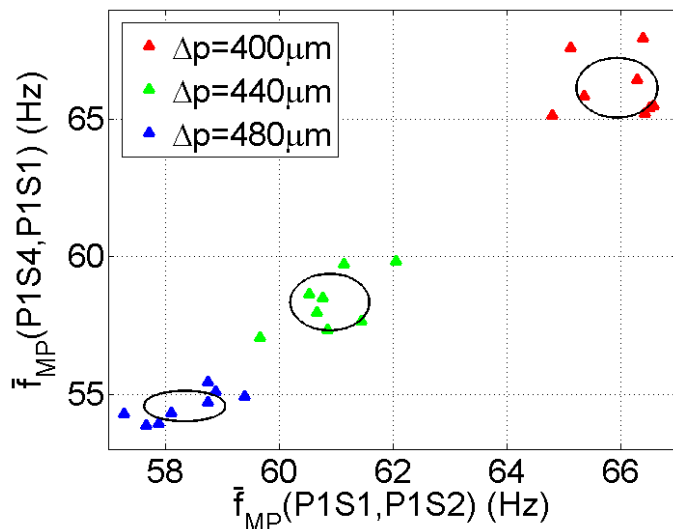


**Fig. 42.** From Oddo et al. (IEEE TRo 2011). Scatter plot of the run-by-run mean values of the fundamental frequencies identified by two pairs of sensor outputs under the active-touch protocol. A clear clustering is shown depending on the explored surface, and coherent frequency increase while decreasing the spatial period  $\Delta p$  of the grating. The ellipses depict low dispersion of data within each cluster, as a result of significant repeatability. These are centered on the centroid of each cluster, and have axes lengths set to twice the standard deviation of experimental principal frequency values belonging to each cluster.

To quantitatively assess discrimination accuracy in active-touch, the training and test operation of the k-NN classifier was performed 10000 times, by using a *leave-M-out* validation for evaluation of discrimination performance:  $M$  experimental runs out of the 24 active-touch ones were randomly selected as a test set, while the others were used to train the *nearest neighbor* classifier, provided that each of the three stimuli appeared with the same number of occurrences, i.e.  $(24-M)/3$ , in every training set. Therefore, for each train and test operation,  $M=3$  results in a classifier being trained over 7 random runs out of the 8 repeated ones per stimulus, down to a single random training run per stimulus with  $M=21$ . The latter condition is a worst case evaluation because a training set based on a single experimental observation would be more sensitive to the potential occurrence of outliers. Due to high repeatability, a k-NN classification applied to data of Fig. 42 guaranteed excellent discrimination performance: a 97.6% identification accuracy (i.e., much higher than the 1/3 performance in case of random choice) was obtained in the worst case training based on a single run per stimulus and the other runs used as validation set (leave-21-out); the accuracy raised to 100% with all the gratings by using at least 4 runs per stimulus as a training set (leave-12-out).

Therefore, surfaces differing down to 40  $\mu\text{m}$  were identified in active-touch by both hardware and processing method based on exteroceptive tactile information (Oddo et al., IEEE TRo 2011). As a consequence of high accuracy, the 40  $\mu\text{m}$  threshold underestimates the potential performance and the developed technology could ensure better results while tested with finer stimuli.

In addition, preliminary active-touch experimental results with five textiles (differing in texture or orientation) were also shown as a proof of discrimination feasibility in a more realistic tactile stimulation scenario (in comparison to gratings) with everyday life surfaces (Oddo et al., IEEE TRo 2011).

In the active-touch study by Oddo and colleagues (IEEE TRo, 2011), the five surfaces were a fine denim cut along two different orientations (Fig. 43a-b), a coarse denim cut along two different orientations (Fig. 43c-d) and a nap textile (Fig. 43e). For all the runs and textiles, here the  $XWT$  was calculated on channel pairs to inspect data. Fig. 43 depicts one  $XWT(PIS1, PIS2)$  example for each textile.

Remarkably, each textile showed a repeatable *specific pattern* in time-frequency space in all the experimental runs (Oddo et al., IEEE TRo 2011).

Such repeatability was confirmed calculating the correlation indexes for each time-domain raw single sensor output over all the combinations of pairs of repeated runs with the same textile. As an example, average correlation coefficients for channel PIS1 over repeated runs are  $0.96 \pm 0.01$  for textiles A and E,  $0.97 \pm 0.01$  for textiles B and C and  $0.98 \pm 0.01$  for textile D. All the

coefficients are very close to one with significant confidence interval, demonstrating high repeatability. Moreover, average correlation coefficients lower in a range between 0.78 and 0.90, with significant confidence as well, while considering combinations of runs related to pairs of different stimuli, thus confirming the suitability for the discrimination of realistic surfaces. However, textiles present a surface structure being more complex and realistic with respect to gratings. Therefore, a number of spectral components rather than a single fundamental frequency should be taken into account in order to yield high classification performance (up to the full time-varying spectrum, to succeed in the discrimination of unspecified tactile stimuli having a very complex surface structure).

Remarkable achievements were presented in the literature in the passive-touch identification of general surfaces, showing that significant information could be extracted in the frequency domain from information gathered via tactile sensors (Mayol-Cuevas et al., 1998; Tanaka, 2001; Mukaibo et al., 2005; de Boissieu et al., 2009). Considering that a complex texture can be intended as a combination of gratings with appropriate spatial periods, such studies and the active-touch work by Oddo and colleagues (IEEE TRo, 2011) confirm the significance of the previous principal frequency approach while dealing with simplified but standardized surfaces such as gratings.

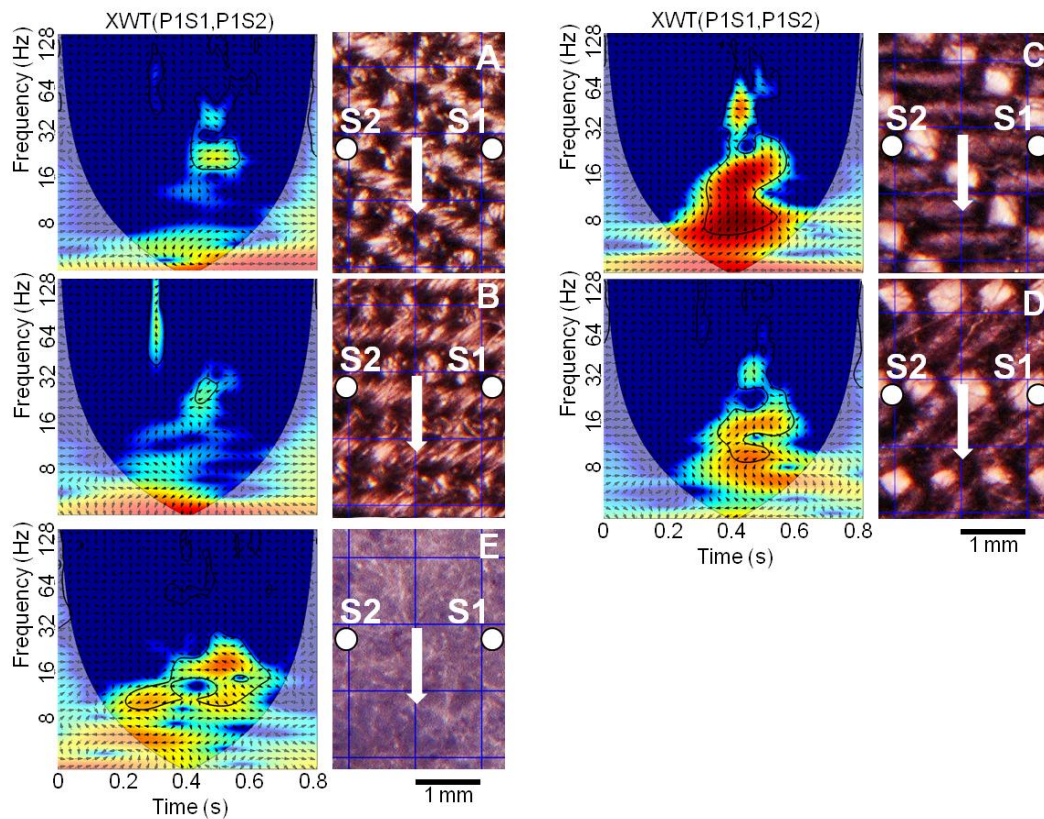


**Fig. 43.** From Oddo et al. (IEEE TRo 2011). The left plots show the XWT on channel pair P1S1-P1S2 during active rubbing of five textiles. The textured structure of each specimen is shown on the right by means of optical microscopy (Hirox KH-7700 digital microscope). The relative positioning of sensors S1 and S2 is marked on the right images, together with an arrow representing the active rubbing direction.

In all the passive-touch experiments discussed above, velocity was constant and known (TABLE I), while in active-touch it was not directly measured. However, as a final evaluation of tested velocity range in comparison to typical human exploratory tasks, this information can be reconstructed by inverting Equation (1) via the knowledge of tested stimuli and measured maximum (75.9 Hz) and minimum (49.8 Hz) principal frequencies recorded during the active-rub operations (Oddo et al., IEEE TRo 2011). This resulted in active-touch velocities monotonically increasing approximately from 22 mm/s to 31 mm/s within the significant time-frequency region of each run. Thus, the tested velocities belong to the wide range (from a few mm/s up to more than a hundred of mm/s) used by humans during active exploratory tasks (Jones & Lederman, 2006).

Moving from the observation that humans appear to be able to discriminate tactile stimuli in such wide velocity range without any significant velocity induced effect on perceived roughness (Lederman 1983, Meftah 2000), one may observe that an encoding of roughness solely based on Equation (1) might be affected by a perceptual inversion in case that coarser tactile stimuli are rubbed at higher velocity than that of finer ones. In the research works discussed above, this was avoided in passive-touch by precise knowledge and control of the sliding velocity, while in active-touch the potential inconvenience was overcome by means of a stereotyped exploratory motion. However, in real robotic applications, as well as in human exploratory tasks, the velocity is neither constant nor the trajectory is exactly the same among different tactile experiences. A possible hypothesis in human touch, as well as a feasible option in robotics would be to deal on proprioceptive information to measure such velocity, and then normalize Equation (1). However, this approach would be compromised by a motion occurring to the tactile surface while actively exploring it. Moreover, as discussed in Section 4.0, the contribution of kinesthetic afferents was excluded by a study by Lederman (1981) with respect to roughness perception in humans.

Therefore, it would be welcome for an artificial tactile sensing system to smartly unravel the velocity dependence of Equation (1), without the need for proprioceptive kinesthetic information, under unconstrained exploratory tasks. The availability of distributed tactile sensors (as the tactile sensing system in the human hand is distributed) gives the opportunity to address this objective, as it is detailed in the following.

A smart solution was proposed by Shinoda and Ando (1999), via a vertical sampling principle implemented by means of a pair of separated pressure probes, to determine a single dominant spatial frequency of the tactile stimulus and the full spatial spectrum of an arbitrary surface (Fig. 44). In their work, the discrimination operation did not require a priori knowledge of the relative sliding velocity, because the dependence of the spectra on the velocity was normalized by using observers being spatially located vertically at different depths of the tactile sensor, which could measure the lag for the mechanical wave produced by the sliding stimulus to propagate from the top layer to the deeper one.

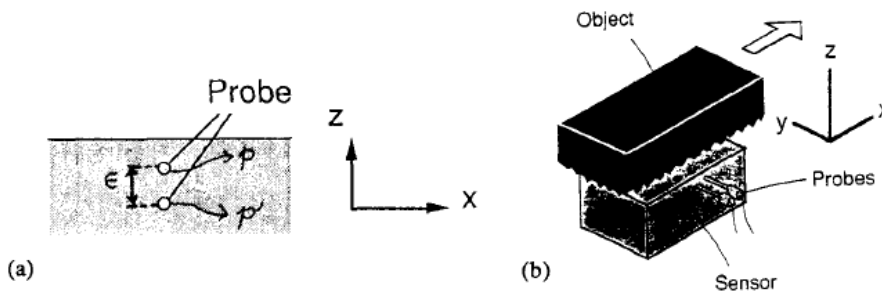


**Fig. 44.** Positioning (a) of the pressure sensing units in the tactile system based on vertical sampling (Shinoda & Ando, 1992), and passive touch experimental setup (b).

Differently from the approach by Shinoda and Ando, horizontal sampling was proposed in the active-touch study by Oddo and colleagues (IEEE TRo 2011). Phase information between neighboring sensors was taken into account as a further feature in addition to the fundamental frequency useful for discriminating among surfaces.

Considering piezoresistors belonging to sensor tethers which are oriented along the same direction, the gathered output signals are expected to show vibrational components having a phase difference  $\Delta\varphi_{i,j}$  being not dependent on the sliding velocity of the stimulus:

$$\Delta\varphi_{i,j} = 2\pi \frac{\Delta y_{j,i}}{\Delta p_s} \quad (2)$$

Where  $\Delta y_{j,i} = y_i - y_j$  is the difference of the  $y$  coordinates of Sensor  $S_i$  and Sensor  $S_j$  (while considering sensors aligned along the finger axis, i.e. S1-S4 and S2-S3,  $\Delta y_{j,i}$  corresponds to the 2.36 mm pitch of the array in case that the plane of the sensors is parallel to the stimulus), according to the labeling introduced in Fig. 37a. This results in signals always in-phase if considering the couple S1-S2 or the couple S3-S4, and with phase differences depending on the tactile stimulus for the other combinations.

In passive-touch, during finger-stimulus contact, sensors S1 and S2 of the array on the distal part of the phalanx were simultaneously aligned under the same ridge of each grating (same  $y$  coordinate, i.e.  $\Delta y_{1,2}=0$ , according to the reference frame in Fig. 37d). Therefore, coherently with Equation (2), the outputs from piezoresistors belonging to sensor tethers which are oriented along the same direction (e.g. P1S1 and P1S2) were in-phase for all the runs regardless of the grating spatial period. This is also confirmed in time domain by Fig. 38 (in-phase P1S1 and P1S2 signals) and depicted by the horizontal arrows in time-frequency space of the  $XWT(P1S1, P1S2)$  plots in Fig. 45. Conversely, a phase difference was observed from sensor units lodged at different positions along the axis of the finger (e.g. P1S1 and P1S4, represented with red and blue traces in Fig. 38 and with arrows in the second subplot of Fig. 45). Velocity had no effect on the phase relationships, as shown by the arrows before and after the velocity variation at  $t_2=2.0s$  in Fig. 45. This property of *phase locking* is coherent with Equation (2) (since no velocity appears in the equation) and can be applied to remove the velocity dependence of Equation (1).

However, a problem occurs with respect to Equation (2): phase differences can be experimentally measured only in a  $2\pi$  range, introducing limiting conditions for inverting Equation (2) (i.e.:  $\Delta p > 2\Delta y_{pitch}=4.72$  mm or  $\Delta p > \Delta y_{pitch}=2.36$  mm depending on the actual knowledge of the sign of the relative finger-stimulus velocity). This means that, by just considering two spatially located sensors of a regular array, phase differences can be analytically reconstructed only in case that two sensors are encountered along the rubbing direction within a half or full spatial wavelength of the tactile stimulus. Such limiting conditions for spatially distributed sampling are equivalent to the Nyquist theorem for time domain sampling.

Gratings with different spatial period  $\Delta p_S$  caused a modulation in the relative phase between units lodged along the direction of the finger axis (e.g. S4 with respect to S1 and S2) in active-touch as well (Oddo et al., IEEE TRo 2011). Consistently with Equation (2), the phase difference between units aligned across the finger axis (e.g. S1-S2, with  $\Delta y_{1,2}=0$ mm) did not modulate. As an example from two couples of outputs from the array in both time (inspecting the relative timing between vibratory peaks in Fig. 39) and time-frequency (inspecting the arrows in Fig. 40) domains, the signals from P1S1 and P1S2 were in-phase, while a phase difference was observed between P1S4 and P1S1. The same behavior is shown in Fig. 41 for all the three used gratings (varying in  $\Delta p$ ), as confirmed by the horizontal shift of the blue trace with respect to the red and green ones (Oddo et al., IEEE TRo 2011).

It is relevant to point out that the phase relationships around the red high power time-frequency regions (i.e. around  $t_{MP}$  time instants indicated in the plots) depicted for active-touch in Fig. 40 were consistent with the passive-touch ones (cf. Fig. 45). This is observable by comparing the arrows (equal down-right pointing) in the significant regions of the two figures.

Related future directions, also considering recent human touch hypotheses (Johansson & Flanagan, 2009) as a potential source of bioinspired design and data analysis, are discussed in Section 4.

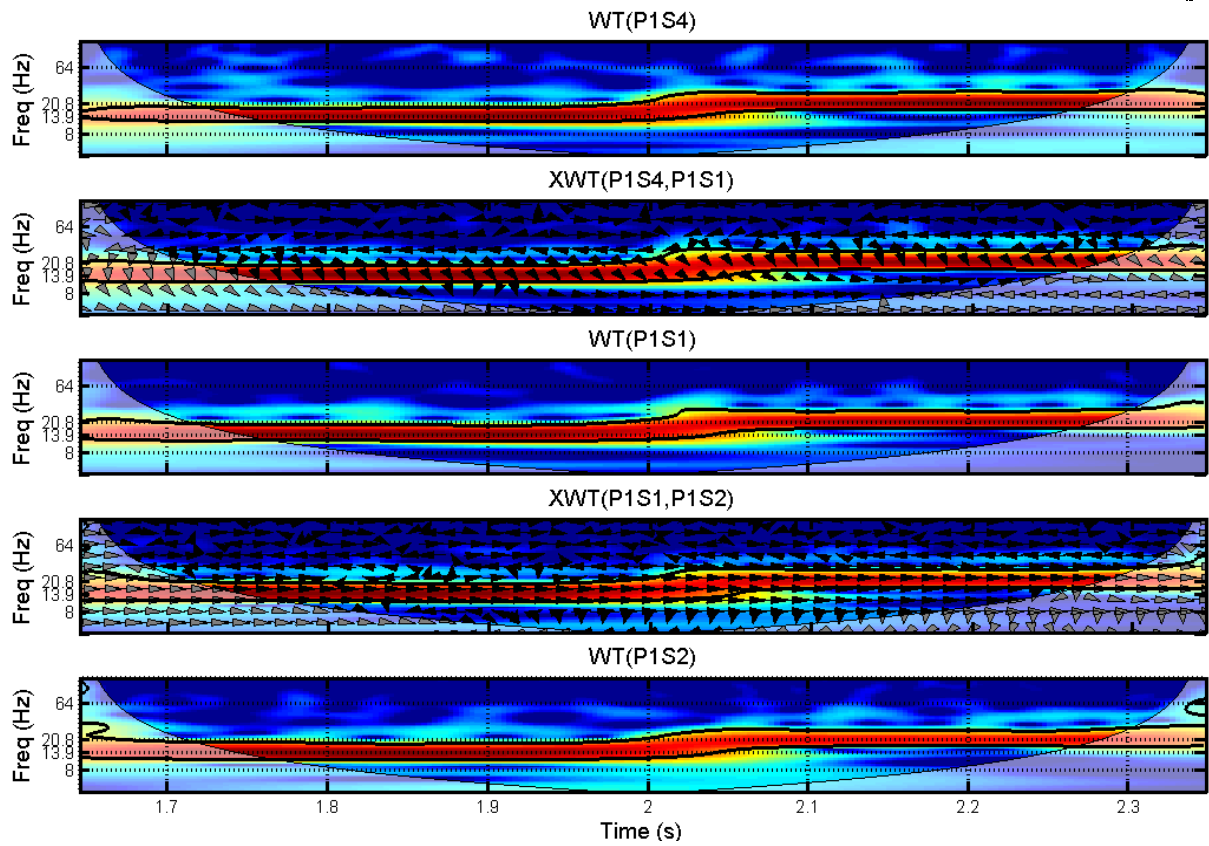


**Fig. 45.** From Oddo et al. (IEEE TRo 2011). *WT* on single channels (P1S4, P1S1 and P1S2) of the array and *XWT* on channel pairs P1S4-P1S1 and P1S1-P1S2. The plots focus on the velocity step during the passive-touch presentation of the 480  $\mu\text{m}$  stimulus to the robotic finger.

## 4. Conclusions and future research directions

The research activities on artificial tactile sensing focused on the discrimination of textures with specific reference to the roughness dimension. Three main objectives were concurrently addressed under a biorobotic approach, resulting in the specific technological and scientific outcomes summarized below.

1) Investigation of the experimental methods, findings and debate with respect to the human sense of touch, with particular reference to:

a) the classes of mechanoreceptors and strategies involved in the neural coding and perception of textures in comparison to the particular structure of the human hand and of the afferent neural pathways, as a source of bioinspired design in the biorobotic study;

b) the techniques (such as microneurography) and tactile stimulation procedures (mainly passive- and active- protocols) which are typically used in (dynamic) touch studies to characterize the biological system and to assess electrophysiological and psychophysical models, as a source of bioinspired experimental evaluation in the biorobotic study;

c) the methodological approaches undertaken in the assessment of models and theories, as a source of bioinspired critical analysis of (experimental versus expected) results in the biorobotic study.

2) Design, development and assessment of a custom mechatronic platform (Oddo et al., Mechatronics 2011) for tactile-stimulation under passive-touch protocols, to foster the parallel studies on the human sense of touch and on its artificial mimicry:

a) particular requirements were addressed due to the exacting demands of electrophysiological methods (microneurography and EEG), and dedicated design choices were operated to deal with the particular tactile stimulation conditions and protocols targeted in human and artificial touch studies;

b) the system was conceived to enable parametric, precise, repeatable and smooth stimulus indentation and tangential sliding over the (human/artificial) fingerpad, under standardized conditions, no induced vibrations, no significant electromagnetic interference, and simple programming by the experimenter;

c) an original methodological contribution was provided in the experimental assessment of the appropriate design of the platform. This was achieved by merging the evaluation of traditional quantitative error indexes (to evaluate the performance in tracking reference trajectories) together with a validation using the human mechanoreceptors as instrumental sensors in order to assess the compatibility of the platform with the exacting demands of electrophysiological methods (particularly, the lack of significant electromagnetic interference and absence of spurious vibrations);

d) the availability of the mechatronic tactile stimulation platform enabled the passive-touch biorobotic studies on artificial tactile sensing, as an investigation parallel to the experimental analysis of the human sense of touch (Oddo et al., Sensors 2009; Oddo et al., IEEE RoBio 2009; Beccai et al., 2009; Beccai et al., 2011; Oddo et al., IEEE TRo 2011; Oddo et al., Sensors 2011);

e) the dedicated design and architecture of the platform enables electrophysiological and psychophysical systematic studies on the human sense of touch.

3) Design, development and assessment of artificial tactile systems, integrating arrays of MEMS sensors (Oddo et al., Sensors 2009; Oddo et al., IEEE RoBio 2009; Beccai et al., 2009; Muhammad et al., SNA 2011; Muhammad et al., MNE 2011; Beccai et al., 2011; Oddo et al., Sensors 2011; Oddo et al., IEEE TRo 2011):

a) mimicking particular structural features of the biological system, with particular reference to human type I mechanoreceptors and fingerprints (Oddo et al., Sensors 2011; Oddo et al., IEEE TRo 2011);

b) evaluation under experimental protocols (passive- and active-) inspired to electrophysiological and psychophysical human touch studies;

c) evaluation with contact forces and velocities in the range used by humans during tactile exploratory tasks;

d) addressing open scientific topics (mechanoreceptors being more informative with respect to texture, coding strategies, role of fingerprints) on the human sense of touch and on its bioinspired mimicry (positioning of sensing units, processing algorithms, packaging design);

e) integration (in the final design of the fingertip: Oddo et al., IEEE TRo 2011) into an articulated robotic finger mimicking human anthropometry and flexion-extension degrees of freedom;

f) using periodic gratings (with spatial periods comprised between 320  $\mu\text{m}$  and 4.1 mm) as tactile stimuli, experimental validation of a frequency-locking mechanism in both passive- (with constant and known sliding velocity: Oddo et al., Sensors 2009; Oddo et al., IEEE RoBio 2009; Beccai et al., 2009; Muhammad et al., SNA 2011; Muhammad et al., MNE 2011; Oddo et al., Sensors 2011; Oddo et al., IEEE TRo 2011) and active- (with non-constant and unknown velocity, but stereotyped exploratory motion: Oddo et al., IEEE TRo 2011) artificial touch: the outputs of the MEMS sensors showed spectra with a principal frequency being directly proportional to the instant relative velocity between the artificial finger and the specimen and inversely proportional to the spatial period of the grating (Equation 1), therefore operating an encoding of roughness;

- g) showing the substantial processing advantage in using more than one output of the array for finding out the common principal frequency produced during dynamic presentation (passive-touch) or exploration (active-touch) of periodic gratings;
- h) under passive-touch stimulation with constant sliding-velocity, exact coherence between the frequency-locking artificial coding and the spectra resulting from the analysis of the neural firing by human mechanoreceptors. In human touch this phenomenon was observed for all the (fine and coarse) tested gratings in a large proportion of recorded RA human mechanoreceptor afferents; the same applies to the recorded SAI units in case of coarse stimuli only;
- i) excellent accuracy in the passive- and active- artificial tactile discrimination of gratings by means of the frequency-locking mechanism;
- j) in the stereotyped active-touch experiments with gratings, tactile information was enough for the successful discrimination of surfaces via the frequency-locking mechanism, without the need to integrate information from dedicated sensors for end-effector velocity;
- k) suitability of the developed artificial touch technologies for discrimination of realistic specimens (Oddo et al., MNE 2011; Oddo et al., IEEE TRo 2011), such as textiles, via a spectral analysis on sensor outputs, therefore extending the frequency-locking mechanism to polyharmonic surfaces;
- l) showing that the structure of fingerprints affects the directional isotropy in the encoding of the principal spatiotemporal frequency of stimuli: under a dedicated differential passive-touch study with gratings, curved fingerprints guaranteed higher directional isotropy than straight fingerprints (Oddo et al., Sensors 2011);
- m) experimental evidences of a phase-locking mechanism (Equation 2) stating that the variations in the phase differences between sensor outputs are directly proportional to the distance between the tactile units (which is known by design) and inversely proportional to the spatial coarseness (i.e., the physical quantity associated to perceived roughness) of the tactile stimulus (Oddo et al., IEEE TRo 2011); therefore, such experimental results support the possibility to include phase differences from adjacent sensor outputs as a further discrimination feature additional to the spectral signature of tactile stimuli (cf. frequency-locking);
- n) ready for integration into mechatronic hands of humanoid robots (Oddo et al., IEEE TRo 2011);
- o) ready for integration into robotic hands for prosthetic applications aiming at providing sensory feedback with bioinspired coding of tactile information (Oddo et al., IEEE TRo 2011).

In both humanoid robotics and prosthetics, an artificial tactile system would take benefit from the feasibility of hard real-time discrimination under unconstrained non-constant exploratory velocities by the mechatronic hand. According to the results presented in this research study, the combination of frequency-locking and phase-locking, together with a smart irregular physical-positioning of sensor units (getting design inputs from the biological model), could enable such desired features. This is briefly introduced in the following to provide a few hints on the possible future research directions.

Irregular physical-positioning could allow to obtain a system of multiple and independent phase relationships (Equation 2) overcoming the Nyquist-like aliasing effect discussed in Section 3 with respect to space-domain sampling via the distributed array. Therefore with such an approach, similar to the human tactile system (Yoshioka et al., 2001), spatial features finer than the nearest neighbor spacing of tactile units could be discriminated under general unconstrained trajectories by the finger, overcoming the limiting condition of stereotypization for the exploratory motion (Oddo et al., IEEE TRo 2011).

To smoothly merge the frequency- and phase- locking mechanisms, the hypothetical human model based on coincidence detection of neural spikes (Fig. 3, discussed in Section 4.0) proposes a relevant source of bioinspiration (Johansson & Flanagan, 2009). This results into the biorobotic model depicted in Fig. 46, which proposes an integrated spatio-temporal discrimination approach, rather than spatial (i.e. taking into account static stimulus representation by distributed sensor units) or temporal (i.e. taking into account the vibrational stimulus representation by single sensor units) only. Such biorobotic model follows the research direction suggested by Shimojo and Ishikawa (1993), since they proposed a spatial filter function adaptively tuning to the sensor-stimulus relative motion parameters, therefore pointing out the centrality of a spatio-temporal approach in tactile sensing.

Under the proposed biorobotic model (Fig. 46): i) the sensor outputs would be converted into neural-like spikes; ii) their phase differences would select, via the compensating effect introduced by the pipeline of delay blocks, the instant pattern of activation in the mesh of second-order artificial neurons; iii) the frequency of the recorded mechanical vibrations would modulate the rate of activation; iv) machine learning techniques would associate the dynamic pattern of activated second-order artificial neurons to the explored textured surface.

Purposely, the proposed model (Fig. 46) does not include a dedicated proprioceptive sensory system for kinesthetic information (e.g., end-effector velocity): this choice could open a dedicated biorobotic investigation on the possible self-sufficiency of the tactile system for discrimination of surfaces under general non-stereotyped active exploratory tasks (as discussed in Section 4.0 with respect to passive- vs. active- touch in the study by Lederman, 1981), in order to go towards a common theory for human and robot mediated coding and perception of texture. Importantly, this could also open various possibilities while pursuing the integration of artificial touch technology into an upper limb prosthesis, via non-invasive (e.g. vibrating tactors, Kaczmarek et al., 2001) or invasive (e.g. direct peripheral neural feedback, Dhillon & Horch, 2005; Rossini et al., 2010) interfaces.

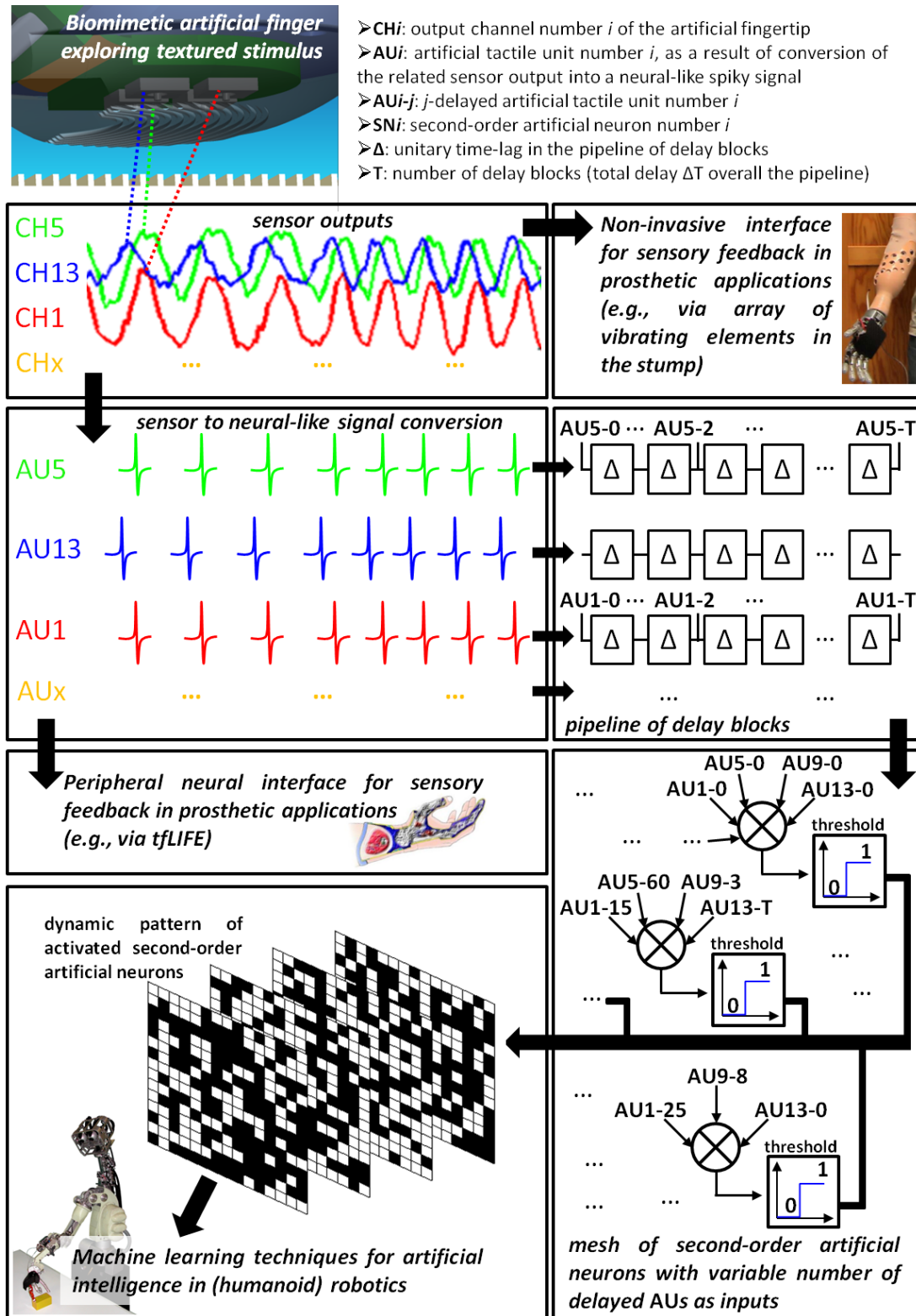


**Fig. 46.** Future directions towards spatiotemporal processing of textural information in artificial touch. Application scenarios (non invasive and invasive sensory feedback in prosthetic applications, and humanoid robotics) are associated to each module of the proposed model.

## BIBLIOGRAPHY

- Astarloa A, Lazaro J, Bidarte U, Jimenez J, Zuloaga A. FPGA technology for multiaxis control systems. *Mechatronics* 2009;19(2):258–68.
- Beccai L, Oddo CM, Cipriani C, Carrozza MC. A biorobotic approach for artificial touch: from the development of a MEMS sensor to the tactile array integration into an actuated finger. In: *Proc. of the humanoid 09 workshop on tactile sensing in humanoid – tactile sensors and beyond*, December 7, 2009, Paris, France, pp. 38–41.
- Beccai L, Oddo CM, Controzzi M, Cipriani C, Carrozza MC. Roughness discrimination of surfaces in artificial active touch. In: *Proc. of the Theo Murphy Meeting on Active touch sensing*, The Royal Society, January 31–February 2, 2011, Chicheley Hall, UK.
- Beccai L, Roccella S, Arena A, Valvo F, Valdastrì P, Menciassi A, Carrozza MC, Dario P. Design and fabrication of a hybrid silicon three-axial force sensor for biomechanical applications. *Sens. Actuator A-Phys.* 2005;120:370–82.
- Beccai L, Roccella S, Ascari L, Valdastrì P, Sieber A, Carrozza MC, Dario P. Development and Experimental Analysis of a Soft Compliant Tactile Microsensor for Anthropomorphic Artificial Hand. *IEEE-ASME Trans. Mechatron.* 2008;13(2):158–68.
- Beccai L, Roccella S, Oddo CM, Carrozza MC. Sensing fingertip for bio-inspired tactile encoding. In *Proceedings of the First Italian Conference on Bioengineering*; Burattini, R., Contro, R., Dario, P., Landini, L., Eds.; Pàtron editore: Bologna, Italy, 2008; pp. 787.
- Beckmann S, Bjrnsson M, Backlund-Wasling H, Wessberg J. Brain decoding of texture processing using independent component analysis and support vector machines. In: *Proc. 2009 IEEE international symposium on intelligent signal processing*, August 26–28, 2009, Budapest, Hungary, pp. 287–92.
- Bensmaïa SJ, Craig JC, Yoshioka T, Johnson KO. SA1 and RA Afferent Responses to Static and Vibrating Gratings. *J. Neurophysiol.* 2006;95(3):1771–82.
- Bensmaïa SJ, Hollins, M. The vibrations of texture. *Somatosens. Mot. Res.* 2003;20(1):33–43.
- Bensmaïa SJ, Hollins, M. Pacinian representations of fine surface texture. *Percept. Psychophys.* 2005;67(5):842–54.
- Bicchi A. Hands for dextrous manipulation and powerful grasping: A difficult road towards simplicity. *IEEE Trans. Robot. Autom.* 2000; 16(6):652–62.
- Biddiss E, Beaton D, Chau T. Consumer design priorities for upper limb prosthetics. *Disability and Rehabilitation: Assistive Technology* 2007;2(6):346–357.

- Birglen L, Gosselin CM. Kinetostatic Analysis of Underactuated Fingers. *IEEE Trans. on Robotics and Automation* 2004;20(2).
- Birznieks I, Jenmalm P, Goodwin AW, Johansson RS. Encoding of direction of fingertip forces by human tactile afferents. *J Neurosci* 2001;21:8222–37.
- Blake DT, Hsiao SS, Johnson KO. Neural Coding Mechanisms in Tactile Pattern Recognition: The Relative Contributions of Slowly and Rapidly Adapting Mechanoreceptors to Perceived Roughness. *J. Neurosci.* 1997;17(19):7480–89.
- Bliss JC, Katcher H, Rogers CH, Shepard RP. Optical-to-Tactile Image Conversion for the Blind. *IEEE Transactions on Man-Machine Systems* 1970;11:58-65.
- Buchholz B, Armstrong TJ, Goldstein SA. Anthropometric data for describing the kinematics of the human hand. *Ergonomics* 1992;35(3):261-273.
- Byrne J. A feedback controlled stimulator that delivers controlled displacements or forces to cutaneous mechanoreceptors. *IEEE Trans Biomed Eng* 1975;22:66–9.
- Carrozza MC, Cappiello G, Micera S, Edin BB, Beccai L, Cipriani C. Design of a cybernetic hand for perception and action. *Biol. Cybern.* 2006;95(6):629-44.
- Chambers MR, Andres KH, Von Duering M, Iggo A. The structure and function of the slowly adapting type II mechanoreceptor in hairy skin. *Quart J Exp Physiol* 1972;57:417–45.
- Chen X, Sakai J, Yang S, Motojima S. Biomimetic Tactile Sensors with Fingerprint-Type Surface Made of Carbon Microcoils/Polysilicone. *Jpn. J. Appl. Phys.* 2006;45:L1019–L1021.
- Cipriani C, Antfolk C, Balkenius C, Rosén B, Lundborg G, Carrozza MC, Sebelius F. A Novel Concept for a Prosthetic Hand with a Bidirectional Interface: a Feasibility Study. *IEEE Trans. Biomedical Engineering* 2009;56(11) part 2:2739-43.
- Cipriani C, Controzzi M, Carrozza MC. Objectives, Criteria and Methods for the Design of the SmartHand Transradial Prosthesis. *Robotica* 2010;28(6)919-927.
- Connor CE, Hsiao SS, Phillips JR, Johnson KO Tactile roughness: neural codes that account for psychophysical magnitude estimates. *J. Neurosci.* 1990;10(12):3823–36.
- Connor CE, Johnson KO. Neural coding of tactile texture: comparison of spatial and temporal mechanisms for roughness perception. *J Neurosci* 1992;12(9):3414–26.
- Controzzi M, Cipriani C, Carrozza MC. Mechatronic Design of a Transradial Cybernetic Hand. In *Proc. of the IEEE/RSJ Int. Conf. on Intelligent Robots and Systems IROS*, Nice, 2008.
- Dahiya RS, Metta G, Valle M, Sandini G. Tactile Sensing—From Humans to Humanoids. *IEEE Trans Robot* 2010;26(1):1-20.

- Damian DD, Martinez H, Dermitzakis K, Hernandez-Arieta A, Pfeifer R. Artificial Ridged Skin for Slippage Speed Detection in Prosthetic Hand Applications. In Proc. of the IEEE/RSJ International Conference on Intelligent Robots and Systems IROS, October 18-22, 2010, Taipei, Taiwan, pp. 904-909.
- Darian-Smith I, Oke LE. Peripheral neural representation of the spatial frequency of a grating moving across the monkey's finger pad. *J Physiol* 1980;309:117-33.
- Dario P. Tactile sensing-technology and applications. *Sens. Actuators A: Phys.* 1991;26:251-61.
- Dario P, Hannaford B, Takanishi A. Guest Editorial Special Issue on Biorobotics. *IEEE Trans Robot* 2008;24(1):3-4.
- De Boissieu F, Godin C, Guilhamat B, David D, Serviere C, Baudois D. Tactile texture recognition with a 3-axial force MEMS integrated artificial finger. In *Proceedings of Robotics: Science and Systems (RSS) 2009*, 49-56.
- Dhillon G, Horch K. Direct neural sensory feedback and control of a prosthetic arm. *IEEE Trans. Neural Syst. Rehabil. Eng.* 2005;13(4):468-472.
- Edwards J, Lawry J, Rossiter J, Melhuish C. Extracting Textural Features from Tactile Sensors. *J. Bioinspiration Biomimetics* 2008;3:1-12.
- Fishel JA, Santos VJ, Loeb GE. A robust micro-vibration sensor for biomimetic fingertips. In *Proc. 2nd IEEE/RAS-EMBS Int. Conf. Biomed. Robot. Biomechatron.*, Oct. 19-22, 2008, Scottsdale, AZ, pp. 659-663.
- Gardner EP, Palmer CI. Simulation of motion of the skin. I. Receptive fields and temporal frequency coding by cutaneous mechanoreceptors of OPTACON pulses delivered to the hand. *J Neurophysiol* 1989;62:1410-436.
- Gerling GJ, Thomas GW. The effect of fingertip microstructures on tactile edge perception. In *Proc. of the First Joint Eurohaptics Conference, 2005 and Symposium on Haptic Interfaces for Virtual Environment and Teleoperator Systems, 2005. World Haptics 2005*, Mar. 18-20, 2005, Pisa, Italy, pp. 63-72.
- Gerling GJ, Thomas GW. Fingerprint lines may not directly affect SA-I mechanoreceptor response. *Somatosens. Mot. Res.* 2008;25(1):61-76.
- Goodwin AW, Morley JW, Clarke C, Lumaksana B, Darian-Smith I. A stimulator for moving textured surfaces sinusoidally across the skin. *J Neurosci Methods* 1985;14:121-5.
- Goodwin A, Morley J. Sinusoidal movement of a grating across the monkey's fingerpad: representation of grating and movement features in afferent fiber responses. *J Neurosci* 1987;7:2168-80.

Grave de Peralta R, Gonzalez S, Lantz G, Michel CM, Landis T. Noninvasive localization of electromagnetic epileptic activity I. Method descriptions and simulations. *Brain Topogr* 2001;14:131–7.

Grinsted A, Moore JC, Jevrejeva S. Application of the cross wavelet transform and wavelet coherence to geophysical time series. *Nonlinear Processes in Geophysics* 2004;11:561–566.

Hidaka Y, Shiokawa Y, Tashiro K, Maeno T, Konyo M, Yamauchi T. Development of an Elastic Tactile Sensor Emulating Human Fingers for Tele-Presentation Systems. In *Proceedings of the IEEE SENSORS 2009 Conference 2009*, 1919-1922.

Hirose S. Connected differential mechanism and its applications. In *Proc. Int. Conf. on Advanced Robotics*, pp. 319-326, 1985.

Hollins M, Bensmaïa SJ, Washburn S. Vibrotactile adaptation impairs discrimination of fine, but not coarse, textures. *Somatosens. Mot. Res.* 2001;18(4):253–262.

Hollins M, Faldowski R, Rao S, Young F. Perceptual dimensions of tactile surface texture: A multidimensional scaling analysis. *Percept. Psychophys.* 1993; 54(6):697–705.

Hollins M, Risner SR. Evidence for the duplex theory of tactile texture perception. *Percept Psychophys* 2000;62:695–705.

Hosoda K, Tada Y, Asada M. Anthropomorphic robotic soft fingertip with randomly distributed receptors. *Robot. Auton. Syst.* 2006;54(2):104–9.

Howe RD. Tactile sensing and control of robotic manipulation. *Adv. Robotics* 1994; 8(3):245–61.

Huang H, Jiang L, Liu Y, Hou L, Cai H, Liu H. The mechanical design and experiments of HIT/DLR prosthetic hand. In *Proc. IEEE Int. Conf. Robot. Biomimetics*, Dec. 17–20 2006, pp. 896–901.

Iskakov R, Albu-Schaeffer A, Schedl M, Hirzinger G, Lopota V. Influence of sensor quantization on the control performance of robotics actuators. In: *Proc. 2007 IEEE/RSJ international conference on intelligent robots and systems*, October 29–November 2, 2007, San Diego, CA, USA. pp. 1085–92.

Johansson RS, Birznieks I. First spikes in ensembles of human tactile afferents code complex spatial fingertip events. *Nature Neuroscience* 2004;7(2):170-177.

Johansson RS, Flanagan JR. Coding and use of tactile signals from the fingertips in object manipulation tasks. *Nature Rev. Neurosci.* 2009;10:345-59.

Johansson RS, Vallbo ÅB. Tactile sensibility in the human hand: relative and absolute densities of four types of mechanoreceptive units in glabrous skin. *J. Physiol. (Lond.)* 1979;286:283-300.

- Johnson KO, Lamb GD. Neural mechanisms of spatial tactile discrimination: Neural patterns evoked by Braille-like dot patterns in the monkey. *J. Physiol* 1981;310:117-144.
- Johnson KO, Phillips JR. A rotating drum stimulator for scanning embossed patterns and textures across the skin. *J Neurosci Methods* 1988;22:221–31.
- Johnson KO, Yoshioka T. Neural mechanisms of tactile form and texture perception. In: Nelson RJ, editor. *The somatosensory system: deciphering the brain's own body image*. Boca Raton, FL (USA): CRC Press LLC; 2001. pp. 73–101.
- Jones LA, Lederman SJ. Tactile sensing. In: Jones LA, Lederman SJ, editors. *Human hand function*. New York, NY (USA): Oxford University Press; 2006. pp. 44–74.
- Kaczmarek KA, Webster JG, Bach-y-Rita P, Tompkins WJ. Electrotactile and vibrotactile displays for sensory substitution systems. *IEEE Trans. Biomed. Eng.* 1991;38(1):1–16.
- Killebrew JH, Bensmaia SJ, Dammann JF, Denchev P, Hsiao SS, Craig JC, Johnson KO. A dense array stimulator to generate arbitrary spatio-temporal tactile stimuli. *J Neurosci Methods* 2007;161:62-74.
- Kim SH, Engel J, Liu C, Jones DL. Texture classification using a polymer-based MEMS tactile sensor. *J. Micromech. Microeng.* 2005;15:912–20.
- Kinoshita H, Backstrom L, Flanagan JR, Johansson RS. Tangential torque effects on the control of grip forces when holding objects with precision grip. *J. Neurophys.* 1997;78(3):1619-1630.
- Klatzky RL, Lederman SJ, Hamilton C, Grindley M, Swendsen RH. Feeling textures through a probe: Effects of probe and surface geometry and exploratory factors. *Percept. Psychophys.* 2003;65:613-31.
- Konyo M, Maeno T, Yoshida A, Tadokoro S. Roughness sense display representing temporal frequency changes of tactile information in response to hand movements. In *Proceedings of the First Joint Eurohaptics Conference and Symposium on Haptic Interface for Virtual Environment and Teleoperator Systems 2005*, 609-10.
- Konyo M, Yoshida A, Tadokoro S, Saiwaki N. A tactile synthesis method using multiple frequency vibrations for representing virtual touch. In *Proceedings of the IEEE/RSJ International Conference on Intelligent Robots and Systems 2005*, 3965-71.
- Kyung KU, Ahn M, Kwon DS, Srinivasan MA. A compact planar distributed tactile display and effects of frequency on texture judgment. *Advanced Robotics* 2006;20:563-80.
- LaMotte RH, Friedman RM, Lu C, Khalsa PS, Srinivasan MA. Raised object on a planar surface stroked across the fingerpad: responses of cutaneous mechanoreceptors to shape and orientation. *J Neurophysiol* 1998;80:2446–66.

- LaMotte RH, Srinivasan MA. Surface microgeometry: Neural encoding and perception. *Information Processing in the Somatosensory System*. In Wenner-Gren Intl. Symposium Series; Franzen, O., Westman, J. Eds.; Macmillan Press: New York, NY, USA, 1991; pp. 49-58.
- LaMotte RH, Whitehouse GM, Robinson CJ, Davis F. A tactile stimulator for controlled movements of textured surfaces across the skin. *J Electrophysiol Tech* 1983;10:1-17.
- Lawrence MA, Kitada R, Klatzky RL, Lederman SJ. Haptic roughness perception of linear gratings via bare finger or rigid probe. *Perception* 2007;36:547-57.
- Lederman SJ. Tactile roughness of grooved surfaces: the touching process and effects of macro- and microsurface structure. *Percept. Psychophys.* 1974;16(2):385-95.
- Lederman SJ. The perception of surface roughness by active and passive touch. *Bulletin of the Psychonomic Society* 1981;18(5):253-255.
- Lederman SJ. Tactual Roughness Perception: Spatial and Temporal Determinants. *Canadian Journal of Psychology* 1983;37(4):498-511.
- Lee MH, Nicholls HR. Tactile sensing for mechatronics: A state of the art survey. *Mechatronics* 1999;9:1-31.
- Libouton X, Barbier O, Plaghki L, Thonnard J-L. Tactile roughness discrimination threshold is unrelated to tactile spatial acuity. *Behav Brain Res* 2010;208(2):473-8.
- Lin CH, Erickson TW, Fishel JA, Wettels N, Loeb GE. Signal processing and fabrication of a biomimetic tactile sensor array with thermal, force and microvibration modalities. In *Proc. IEEE Int. Conf. Robot. Biomimetics*, Dec. 19-23, 2009, Guilin, China, pp. 129-134.
- Looft FJ, Williams WJ. On-line receptive field mapping of cutaneous receptors. *IEEE Trans Biomed Eng* 1979;26:350-6.
- Luo M, Mei T, Wang X, Yu Y. Grasp Characteristics of An Underactuated Robot Hand. In *Proc. 2004 IEEE Int. Conf. on Robotics and Automation*, pp. 2236-41.
- Maeno T, Kobayashi K, Yamazaki N. Relationship Between Structure of Finger Tissue and Location of Tactile Receptors, *JSME International Journal* 1998;41(1):94-100.
- Maheshwari V, Saraf RF. High-resolution thin-film device to sense texture by touch. *Science* 2006; 312:1501-4.
- Maheshwari V, Saraf RF. Tactile devices to sense touch on a par with a human finger. *Angew Chem. Int. Edit.* 2008;47(41):7808-26.
- Mayol-Cuevas WW, Juárez-Guerrero J, Muñoz-Gutiérrez S. A First Approach to Tactile Texture Recognition. In: *Proc. IEEE Int. Conf. on Systems, Man, and Cybernetics*, Oct. 11-14, 1998, San Diego, CA, USA, vol. 5, pp. 4246-50.

Meftah EM, Belingard L, Chapman CE. Relative effects of the spatial and temporal characteristics of scanned surfaces on human perception of tactile roughness using passive touch. *Exp. Brain. Res.* 2000;132:351-61.

Morley JW, Goodwin AW, Darian-Smith I. Tactile Discrimination Of Gratings. *Exp. Brain Res.* 1983;49(2):291-9.

Mouri T, Kawasaki H, Yoshikawa K, Takai J, Ito S. Anthropomorphic robot hand: Gifu hand III. Presented at ICCAS, Oct. 16-19, 2002, Jeonbuk, Korea.

Muhammad HB, Oddo CM, Beccai L, Recchiuto C, Anthony CJ, Adams MJ, Carrozza MC, Hukins DWL, Ward MCL. Development of a bioinspired MEMS based capacitive tactile sensor for a robotic finger. *Sensors and Actuators A Physical* 2011;165:221-9.

Muhammad HB, Recchiuto C, Oddo CM, Beccai L, Anthony CJ, Adams MJ, Carrozza MC, Ward MCL. A capacitive tactile sensor array for surface texture discrimination. *Microelectron Eng* 2011, in press, doi:10.1016/j.mee.2011.01.045.

Mukaibo Y, Shirado H, Konyo M, Maeno T. Development of a texture sensor emulating the tissue structure and perceptual mechanism of human fingers. In *Proceedings of the IEEE International Conference on Robotics and Automation 2005*, 2565-70.

Nakazawa N, Ikeura R, Inooka H. Characteristics of human fingertips in the shearing direction. *Biol Cybern* 2000;82(3):207-14.

Oddo CM, Beccai L, Felder M, Giovacchini F, Carrozza MC. Artificial roughness encoding with a bio-inspired MEMS-based tactile sensor array. *Sensors* 2009;9:3161-83.

Oddo CM, Beccai L, Muscolo GG, Carrozza MC. A biomimetic MEMS-based tactile sensor array with fingerprints integrated in a robotic fingertip for artificial roughness encoding. In: *Proc. 2009 IEEE conference on robotics and biomimetics*, December 19-23, 2009, Guilin, China. pp. 894-900.

Oddo CM, Beccai L, Vitiello N, Backlund Wasling H, Wessberg J, Carrozza MC. A Mechatronic Platform for Human Touch Studies. *Mechatronics* 2011;21:604-13.

Oddo CM, Beccai L, Wessberg J, Backlund Wasling H, Mattioli F, Carrozza MC. Roughness encoding in human and biomimetic artificial touch: spatiotemporal frequency modulation and structural anisotropy of fingerprints. *Sensors* 2011:in press.

Oddo CM, Controzzi M, Beccai L, Cipriani C, Carrozza MC. Roughness Encoding for Discrimination of Surfaces in Artificial Active Touch. *IEEE Trans Robot* 2011;99:in press.

Oddo CM, Valdastrì P, Beccai L, Roccella S, Carrozza MC, Dario P. Investigation on calibration methods for multi-axis, linear and redundant force sensors. *Meas. Sci. Technol.* 2007;18(3):623-31.

- Okamoto S, Konyo M, Mukaibo Y, Maeno T, Tadokoro S. Real-time estimation of touch feeling factors using human finger mimetic tactile sensors. In Proceedings of the IEEE/RSJ International Conference on Intelligent Robots and Systems 2006, 3581-86.
- Pasquero J, Luk J, Lévesque V, Wang Q, Hayward V, MacLean KE. Haptically enabled handheld information display with distributed tactile transducer. *IEEE Trans Multimedia* 2007;9(4):746-53.
- Pawluk DTV, Howe RD. Dynamic lumped element response of the human fingerpad. *J Biomech Eng* 1999;121:178-83.
- Peters RM, Hackeman E, Goldreich D. Diminutive Digits Discern Delicate Details: Fingertip Size and the Sex Difference in Tactile Spatial Acuity. *J. Neurosci.* 2009;29(50):15756-15761.
- Prescott T. Vibrissal behaviour in rodents and marsupials. Lecture at the Theo Murphy meeting on Active Touch Sensing. Jan, 31st 2011. Chicheley Hall, Buckinghamshire, UK.
- Prevost A, Scheibert J, Debréguas G. Effect of fingerprints orientation on skin vibrations during tactile exploration of textured surfaces. *Communicative & Integrative Biology* Sept.-Oct. 2009;2:1-3.
- Radwin R, Jeng O, Giske E. A new automated tactility test instrument for evaluating hand sensory function. *IEEE Transactions on Rehabilitation Engineering* 1993;1:220-5.
- Romo R, Ruiz S, Crespo P, Hsiao SS. A tactile stimulator for studying motion processing in the somatic sensory system of primates. *J Neurosci Methods* 1993;46:139-46.
- Rosenberg JR, Halliday DM, Breeze P, Conway BA. Identification of patterns of neuronal connectivity – partial spectra, partial coherence, and neuronal interactions. *J. Neurosci. Meth.* 1998;83:57-72.
- Rossini PM, Micera S, Benvenuto A, Carpaneto J, Cavallo G, Citi L, Cipriani C, Denaro L, Denaro V, Di Pino G, Ferreri F, Guglielmelli E, Hoffmann KP, Raspopovic S, Rigosa J, Rossini L, Tombini M, Dario P. Double nerve intraneural interface implant on a human amputee for robotic hand control. *Clin. Neurophysiol* 2010;121(5):777-83.
- Scheibert J, Leurent S, Prevost A, Debréguas G. The role of fingerprints in the coding of tactile information probed with a biomimetic sensor. *Science* 2009;323:1503-6.
- Scheibert J, Prevost A, Debréguas G, Rousier R, Rey P. A Novel Biomimetic Haptic Sensor to study the Physics of Touch. In Proceedings of Méchanotransduction 2004.
- Schneider W, Slugg RM, Turnquist BP, Meyer RA, Campbell JN. An electromechanical stimulator system for neurophysiological and psychophysical studies of pain. *J Neurosci Methods* 1995;60:61-8.

- Scott SH. Optimal feedback control and the neural basis of volitional motor control. *Nature Reviews Neuroscience* 2004;5:532-46.
- Serina ER, Mote CD, Rempel D. Force response of the fingertip pulp to repeated compression – effects of loading rate, loading angle and anthropometry. *J Biomech* 1997;30(10):1035–40.
- Shinoda H, Ando S. A tactile sensing algorithm based on elastic transfer function of surface deformation. In *Proceedings of the IEEE International Conference on Acoustics, Speech, and Signal Processing 1992, ICASSP-92*;3:589-92.
- Shimojo M, Ishikawa M. An active touch sensing method using a spatial filtering tactile sensor. In *Proceedings of the IEEE International Conference on Robotics and Automation 1993*, 948-954.
- Shimojo M. Mechanical filtering effect of elastic cover for tactile sensor. *IEEE Trans. Rob. Autom.* 1997;13(1):128-32.
- Smith AM, Chapman CE, Deslandes M, Langlais J-S, Thibodeau M-P. Role of friction and tangential force variation in the subjective scaling of tactile roughness. *Exp Brain Res* 2002;144:211–23.
- Soneda T, Nakano K. Investigation of vibrotactile sensation of human fingerpads by observation of contact zones. *Tribol. Intl.* 2010;43:210–217.
- Srinivasan MA, Whitehouse JM, LaMotte RH. Tactile detection of slip: Surface microgeometry and peripheral neural codes. *J. Neurophysiol.* 1990;63:1323–32.
- Summers IR, Chanter CM. A broadband tactile array on the fingertip. *J Acoust Soc Am* 2002;112:2118-26.
- Tanaka M. Development of tactile sensor for monitoring skin conditions. *Journal of Materials Processing Technology* 2001;108:253-6.
- Vallbo AB, Hagbarth KE, Wallin BG. Microneurography: how the technique developed and its role in the investigation of the sympathetic nervous system. *J Appl Physiol* 2004;96:1262–9.
- Vallbo AB, Johansson RS. Properties of cutaneous mechanoreceptors in the human hand related to touch sensation. *Human Neurobiol* 1984;3:3–14.
- Vásárhelyi G, Ádám M, Vázsonyi É, Bársony I, Dücso C. Effects of the elastic cover on tactile sensor arrays. *Sens. Actuator A-Phys.* 2006;132:245-51.
- Vásárhelyi G, Fodor B, Roska T. Tactile sensing-processing: interface-cover geometry and the inverse-elastic problem. *Sens. Actuator A-Phys.* 2007;140:8-18.
- Vidal-Verdú F, Hafez M. Graphical tactile displays for visually-impaired people. *IEEE Transactions on Neural Systems and Rehabilitation Engineering* 2007;15:119-130.

- Wagner CR, Lederman SJ, Howe RD. A tactile shape display using RC Servomotors. In: Proc. 2002 IEEE symposium on haptic interfaces for virtual environment and teleoperator systems, March 24–25, 2002, Orlando, USA. pp. 354–5.
- Wettels N, Santos VJ, Johansson RS, Loeb GE. Biomimetic tactile sensor array. *Adv. Robot.* 2008;22:829–849.
- Wheat HE, Goodwin AW. Tactile Discrimination of Gaps by Slowly Adapting Afferents: Effects of Population Parameters and Anisotropy in the Fingerpad. *J. Neurophysiol.* 2000;84(3):1430–44.
- Wheat HE, Salo LM, Goodwin AW. Human ability to scale and discriminate forces typical of those occurring during grasp and manipulation. *J Neurosci* 2004;24:3394-3401.
- Yamada D, Maeno T, Yamada Y. Artificial Finger Skin having Ridges and Distributed Tactile Sensors used for Grasp Force Control. *Journal of Robotics and Mechatronics* 2002;14(2):140–6.
- Yoshioka T, Bensmaïa SJ, Craig JC, Hsiao SS. Texture perception through direct and indirect touch: An analysis of perceptual space for tactile textures in two modes of exploration. *Somatosens. Mot. Res.* 2007;24(1):53–70.
- Yoshioka T, Gibb B, Dorsch AK, Hsiao SS, Johnson KO. Neural coding mechanisms underlying perceived roughness of finely textured surfaces. *J Neurosci* 2001;21:6905–16.
- Yoshioka T, Zhou J. Factors involved in tactile texture perception through probes. *Adv. Robotics* 2009; 23:747–66.
- Yousef H, Boukallel M, Althoefer K. Tactile sensing for dexterous in-hand manipulation in robotics—A review. *Sensors and Actuators A: physical* 2011;in press.
- Zhang Y, Mukaibo Y, Maeno T. A multi-purpose tactile sensor inspired by human finger for texture and tissue stiffness detection. *Proceedings of the IEEE International Conference on Robotics and Biomimetics* 2006, 159–164.
- Zhang Y. Sensitivity enhancement of a micro-scale biomimetic tactile sensor with epidermal ridges. *J. Micromech. Microeng.* 2010;20(8):1-7.

## PUBLICATIONS LIST

### *Published papers*

#### 1. ISI journals

1. **C.M. Oddo**, L. Beccai, J. Wessberg, H. Backlund Wasling, F. Mattioli, M.C. Carrozza. *Roughness encoding in human and biomimetic artificial touch: spatiotemporal frequency modulation and structural anisotropy of fingerprints*. Sensors 2011, in press (special issue “Bioinspired Sensor Systems”).
2. **C.M. Oddo**, M. Controzzi, L. Beccai, C. Cipriani, M.C. Carrozza. *Roughness Encoding for Discrimination of Surfaces in Artificial Active Touch*. IEEE Transactions on Robotics, 2011, 99, in press (special issue “Robotic Sense of Touch”).
3. **C.M. Oddo**, L. Beccai, N. Vitiello, H. Backlund Wasling, J. Wessberg, M.C. Carrozza. *A Mechatronic Platform for Human Touch Studies*. Mechatronics, 2011, 21, pp. 604-613.
4. H.B. Muhammad, C. Recchiuto, **C.M. Oddo**, L. Beccai, C.J. Anthony, M.J. Adams, M.C. Carrozza, M.C.L. Ward. *A capacitive tactile sensor array for surface texture discrimination*. Microelectronic Engineering, In Press, corrected Proof, Available online 22 January 2011.
5. H.B. Muhammad, **C.M. Oddo**, L. Beccai, C. Recchiuto, C.J. Anthony, M.J. Adams, M.C. Carrozza, D.W.L. Hukins, M.C.L. Ward. Development of a bioinspired MEMS based capacitive tactile sensor for a robotic finger. Sensors and Actuators A: Physical, 2011, 165, pp. 221-229.
6. **C.M. Oddo**, L. Beccai, M. Felder, F. Giovacchini, M.C. Carrozza. *Artificial roughness encoding with a bio-inspired MEMS based tactile sensor array*. Sensors, 2009, 9(5), pp. 3161-3183.
7. **C.M. Oddo**, P. Valdastri, L. Beccai, S. Roccella, M. C. Carrozza, P. Dario. *Investigation on calibration methods for multi-axis, linear and redundant force sensors*. Meas. Sci. Technol., 2007, 18(3), pp. 623-631 (before starting the PhD programme).

#### 2. Journals

8. H.B. Muhammad, **C.M. Oddo**, L. Beccai, M.J. Adams, M.C. Carrozza, D.W. Hukins, M.C.L. Ward. Design of a Biomimetic MEMS based Capacitive Tactile Sensor. Procedia Chemistry (Proceedings of the 23<sup>rd</sup> Eurosensors Conference) 1, 2009, pp. 124-127.
9. N. Vitiello, **C.M. Oddo**, S. Roccella, S. Micera, M.C. Carrozza. *Digitus: towards a platform for the characterization of the finger biomechanics in fine manipulation*. Gerontechnology 2008; 7(2):232 (extended abstract).

#### 3. Book chapters

10. H.F. Kwok, K. Darkins, **C.M. Oddo**, L. Beccai, A. Wing. *Contact Force and Duration Effects on Static and Dynamic Tactile Texture Discrimination*. Haptics: Generating and Perceiving Tangible Sensations. Lecture Notes in Computer Science, vol. 6192/2010, pp. 9-16. Springer Berlin / Heidelberg 2010.

#### 4. International Conferences

11. L. Beccai, **C.M. Oddo**, M. Controzzi, C. Cipriani, M.C. Carrozza. *Roughness discrimination of surfaces in artificial active touch*. In proceedings of the Theo Murphy Meeting on Active touch sensing, The Royal Society, January 31-February 2, 2011, Chicheley Hall, UK (extended abstract).
12. H.K. Backlund, **C.M. Oddo**, L. Beccai, M.C. Carrozza, J. Wessberg. *Human single afferent response to tactile stimuli with varying roughness: a population-level description in the time- and frequency-domains*. In 40th Annual meeting of the Society for Neuroscience, November 13-17, 2010, San Diego, CA, USA (extended abstract).
13. H.B. Muhammad, C. T. Recchiuto, **C.M. Oddo**, L. Beccai, M.J. Adams, M.C. Carrozza, M. Ward, *A MEMS tactile sensor array for texture recognition*. In 36th International Conference on Micro & Nano Engineering, Genova, Italy, 19-22 September 2010.
14. H.B. Muhammad, N.C. Hunt, R.M. Shelton, L.M. Grover, M.C.L. Ward, **C.M. Oddo**, C.T. Recchiuto, L. Beccai. *Incorporation of novel MEMS tactile sensors into tissue engineered skin*. In Proceedings of the iCBBE 2010 IEEE 4th International Conference on Bioinformatics and Biomedical Engineering, 2010, pp. 1-4.
15. **C.M. Oddo**, L. Beccai, G.G. Muscolo, M.C. Carrozza. *A Biomimetic MEMS-based Tactile Sensor Array with Fingerprints integrated in a Robotic Fingertip for Artificial Roughness Encoding*. In Proceedings of the RoBio09 IEEE 2009 Conference on Robotics and Biomimetics, Guilin, China, December 2009, pp. 894-900. **Finalist for best student paper award**.
16. L. Beccai, **C.M. Oddo**, C. Cipriani, M.C. Carrozza. *A biorobotic approach for artificial touch: from the development of a MEMS sensor to the tactile array integration into an actuated finger*. Workshop on Tactile Sensing in Humanoids – Tactile Sensors & Beyond, in the Humanoids 09 9th IEEE-RAS International Conference on Humanoid Robotics, pp. 38-41, 2009.14.
17. M. Björnsdotter Åberg, S. Beckmann, H. Backlund-Wasling, L. Beccai, **C.M. Oddo**, N. Vitiello, J. Wessberg. *Decoding human EEG dynamics due to tactile texture processing using independent component analysis and support vector machines*. In 39th Annual meeting of the Society for Neuroscience, October 17-21, 2009, Chicago, IL, USA (extended abstract).
18. **C.M. Oddo**, N. Vitiello, S. Roccella, S. Micera, R. Saletti, M.C. CARROZZA. *Digitus: towards a platform for the characterization of finger biomechanics in fine manipulation*. In Proceedings of the 6th International Conference of the International Society for Gerontechnology, Pisa, Italy 2008, pp. 1-4.
19. N. Vitiello, U. Olcese, **C.M. Oddo**, J. Carpaneto, S. Micera, M. C. Carrozza, P. Dario, *A simple highly efficient non invasive EMG-based HMI*. In Proceedings of the 28th IEEE EMBS Annual International Conference, New York, USA, Aug 30-Sept 3, 2006, pp. 3403-3406 (before starting the PhD programme).

#### 5. National Conferences

20. **C.M. Oddo**, N. Vitiello, Stefano Marco Maria De Rossi, Marco Cempini, Roberto Farolfi, Alessandro Pignotti, Jacopo Corbetta, Massimo Grava, Jacopo Rigosa, Stefano Mintchev, Gerardo De Pasquale, Luca Ceccanti, Dario Cazzaro, Luca Invernizzi, Maria Chiara Carrozza, Paolo Dario, Stefano Roccella. *The pESApod hexapod robot*. In Workshop Agenzia Spaziale Italiana su Robotica mobile per esplorazione lunare Unmanned. Roma, 1-2 Luglio 2009, pp. 1-12.

21. **C.M. Oddo**, N. Vitiello, S. Roccella, S. Micera, R. Saletti, M.C. Carrozza. Development of a FPGA-based digital control platform for the biomechatronic interface DIGITUS. In Congresso nazionale di bioingegneria 2008. Atti. Pisa, 3-5 Luglio 2008, BOLOGNA: Patron editore, ISBN/ISSN: 8855529838 (extended abstract).
22. L. Beccai, S. Roccella, **C.M. Oddo**, M.C. Carrozza. Sensing fingertip for bio-inspired tactile encoding. In Congresso nazionale di bioingegneria 2008. Atti. Pisa, 3-5 Luglio 2008, BOLOGNA: Patron editore, p. 787, ISBN/ISSN: 8855529838 (extended abstract).

**APPENDIX: COPY OF SIGNIFICANT PAPERS PUBLISHED  
DURING THE PHD PROGRAMME**



## A mechatronic platform for human touch studies

Calogero Maria Oddo<sup>a</sup>, Lucia Beccai<sup>b</sup>, Nicola Vitiello<sup>a,\*</sup>, Helena Backlund Wasling<sup>c</sup>, Johan Wessberg<sup>c</sup>, Maria Chiara Carrozza<sup>a</sup>

<sup>a</sup>The BioRobotics Institute, Scuola Superiore Sant'Anna, viale Rinaldo Piaggio 34, I-56025 Pontedera, Pisa, Italy

<sup>b</sup>Center for Micro-BioRobotics@SSSA, Istituto Italiano di Tecnologia (IIT), viale Rinaldo Piaggio 34, I-56025 Pontedera, Pisa, Italy

<sup>c</sup>Department of Physiology, University of Gothenburg, Medicinaregatan 11, SE-40530 Goteborg, Sweden

### ARTICLE INFO

#### Article history:

Received 10 April 2010

Accepted 27 February 2011

Available online 23 March 2011

#### Keywords:

Mechatronic tactile stimulator  
Electrophysiological measurements  
Fingertip mechanoreceptors  
Microneurography  
Tactile stimuli encoding  
Biorobotics

### ABSTRACT

The development of a mechatronic tactile stimulation platform for touch studies is presented. The platform was developed for stimulation of the fingertip using textured surfaces, providing repeatable tangential sliding motion of stimuli with controlled indentation force. Particular requirements were addressed to make the platform suitable for neurophysiological studies in humans with particular reference to electrophysiological measurements, but allowing a variety of other studies too, such as psychophysical, tribological and artificial touch ones. The design of the mechatronic tactile stimulator is detailed, as well as the performance in tracking reference trajectories. Using microneurography, we recorded from human tactile afferents and validated the platform compatibility with the exacting demands of electrophysiological methods, comprising the absence of spurious vibrations and the lack of relevant electromagnetic interference.

© 2011 Elsevier Ltd. All rights reserved.

### 1. Introduction

To study neuronal mechanisms of the sense of touch in the human hand, active or passive protocols are used. In active touch the subjects are asked to explore tactile stimuli [1], while in passive studies tactile stimuli are presented to the fingertip, which is kept still [2]. The exploration or presentation of stimuli should be replicated several times in the same conditions to infer models based on statistical analysis of acquired data [3]. To achieve standardization and repeatability, the passive touch approach requires a robotic stimulator that enables detailed analyses of receptor response or Central Nervous System (CNS) processing through controlled variation of stimulation parameters, of stimulus materials, spatial coarseness and tribological properties, to make comparisons between sessions or participants, or to average over a large number of replications. As regards the neurophysiologic experimental paradigms, in the periphery the activity of single afferents in the skin can be recorded using the microneurography technique [4]; CNS activity can be probed using electroencephalography (EEG) to reconstruct cortical sources [5], while sensory thresholds and percepts can be assessed using psychophysical methods [6].

This study presents the development of a 2 DoFs mechatronic system that could indent and slide textured stimuli to the fingerpad with feedback-controlled normal contact force and parametric sliding trajectories while recording the normal and tangential forces at finger-stimulus interface. The robotic system has been devised with an open design approach since it is simple to command via a graphical user interface, is upgradable thanks to the FPGA control electronics, and can be used to perform neurophysiological studies in humans with techniques such as microneurography and EEG [7] even in combination with psychophysical experimental paradigms. Also, it is suitable for tribological and artificial touch studies as well and it allows to implement a wide variety of protocols for active [8] and passive studies [9].

There are a number of particular requirements in the design of such a robotic device. First, to allow repeatable experiments with standardized conditions, accuracy and precision in the control of stimulation parameters, such as the contact force and the sliding velocity profile, is required. Second, the device must guarantee a range of forces and movement velocities covering those that would be used by humans in the exploration of textures, while both normal and tangential forces need to be recorded as they are fundamental for human touch investigation. Studies on discriminative touch [10,11] suggested: for the indentation force a range of at least 100 mN–5 N, with a control accuracy of about 5% of the reference force and sensing resolution within a few mN; 100 mm of stroke along the sliding direction and velocities up to 150 mm/s with  $\mu\text{m}$  position sensing resolution and steady state control accu-

\* Corresponding author. Tel.: +39 050 883 472; fax: +39 050 883 101/497.

E-mail addresses: [oddoc@sssup.it](mailto:oddoc@sssup.it) (C.M. Oddo), [lucia.beccai@iit.it](mailto:lucia.beccai@iit.it) (L. Beccai), [n.vitiello@sssup.it](mailto:n.vitiello@sssup.it) (N. Vitiello), [helena.backlund@physiol.gu.se](mailto:helena.backlund@physiol.gu.se) (H.B. Wasling), [wessberg@physiol.gu.se](mailto:wessberg@physiol.gu.se) (J. Wessberg), [chiara.carrozza@sssup.it](mailto:chiara.carrozza@sssup.it) (M.C. Carrozza).

racy. The third challenging requirement, given that some classes of tactile receptors are highly sensitive to vibration up to 400 Hz or more [12], is in developing a stimulator that could get into contact with the human finger free from any spurious vibration that could interfere with the encoding of tactile stimuli. Fourth, electrophysiological methods such as microneurography and EEG involve recording of signals in the  $\mu\text{V}$  range, and electromagnetic interference from the robotic system has to be minimized. Fifth, these experiments can require the participant to sit in a natural position and to remain relaxed for hours. Hence, the subject's comfort puts stringent demands on the mounting of the device and on the control laws of each DoF so that it can be adapted in 3D space to the position of the subject's arm, hand and finger [13].

Finally, the programming operation by the experimenter to implement the targeted protocols has to be simple and flexible, and upgradeability of the platform should be possible.

All these requirements and specifications have hitherto not been addressed by a single device in the scientific literature. LaMotte and colleagues presented an advanced stimulator [14], which was too bulky to be easily oriented in 3D space and which relied on the early digital electronics available at the time; the scotch yolk stimulator [15] used a complex mechanism resulting in a lack of flexibility of the experimental protocol; the rotating drum stimulators [16,17] regulated the indentation force in open loop, and thus could not reject external disturbances. Finally, with respect to studies on encoding of texture and its related dimensions (e.g. roughness), most platforms were developed for experiments in monkeys [18] rather than humans, then presenting less demanding requirements since higher level of invasiveness is tolerated in animal model studies.

Here, we outline the development of a platform that fulfils all these requirements for tactile stimulation in human studies, and that was replicated in five exemplars with customizations for electrophysiological, psychophysical, and artificial touch studies and for tribological experiments on different tactile surfaces as well. A typical passive touch sequence, with stimulus indentation and sliding is presented and quantitative indexes are calculated for assessing over repeated runs the performances of the controllers of the 2 DoFs. Using microneurography, we recorded from human tactile afferents under passive touch stimulation and showed that the platform is compatible with the exacting demands of electro-

physiological methods, specifically the absence of spurious vibrations and lack of electromagnetic interference.

## 2. Materials

### 2.1. Mechanism and actuation

The core system had two orthogonal DoFs (Fig. 1) to indent and slide the tactile stimulus tangentially to the fingerpad. A voice-coil actuator (NCC05-18-060-2X, H2W Tech.) applied the indentation force with a 12.7 mm stroke. A linear guide (LTP 60.180.0804-02, SKF Multitec) driven by a DC motor (RE35, Maxon Motors) applied the sliding motion through a 4 mm pitch ball bearing screw, allowing a maximum velocity of 300 mm/s and a stroke of 110 mm. The propagation of the small vibrations produced by the screw was filtered by applying four vibration isolation mounts (520053, Radiaflex) at the corners of the interface between the voice-coil actuator and the linear guide. Each of the used vibration isolation mounts had an axial stiffness (indentation direction) of 133.3 N/mm and a radial stiffness (sliding direction) of 16.7 N/mm. Considering the parallel of the four elements, the resulting axial stiffness was 533.3 N/mm and the radial stiffness was 66.7 N/mm. This means that, by applying a 500 mN indentation force (i.e. a typical value in the targeted experimental protocols) a maximum deformation of 1  $\mu\text{m}$  will occur. Moreover, in the developed platform the axial deformation is not subjected to very limiting constraints since, as detailed in the following, the indentation axis is under force control. Oppositely, the resulting stiffness along the sliding direction needs attention since such axis is under position control. In this case, a tangential force component of 500 mN (i.e. a typical experimental value) will cause a deformation of 7.5  $\mu\text{m}$  along the sliding direction (resulting from equilibrium of forces) and an acceptable (lower than  $0.02^\circ$ , resulting from equilibrium of torques) misalignment between the sliding direction and the tactile stimulus on top the voice-coil actuator, complying with the design constraints. Linear Current Amplifier Modules (LCAM, Quanser), guaranteeing very low electromagnetic interference, were chosen for driving the actuators. Switching power devices were avoided since the typical (10–50 kHz) range for PWM carrier frequency is higher than half the microneurography sampling rate, but just outside the cutoff

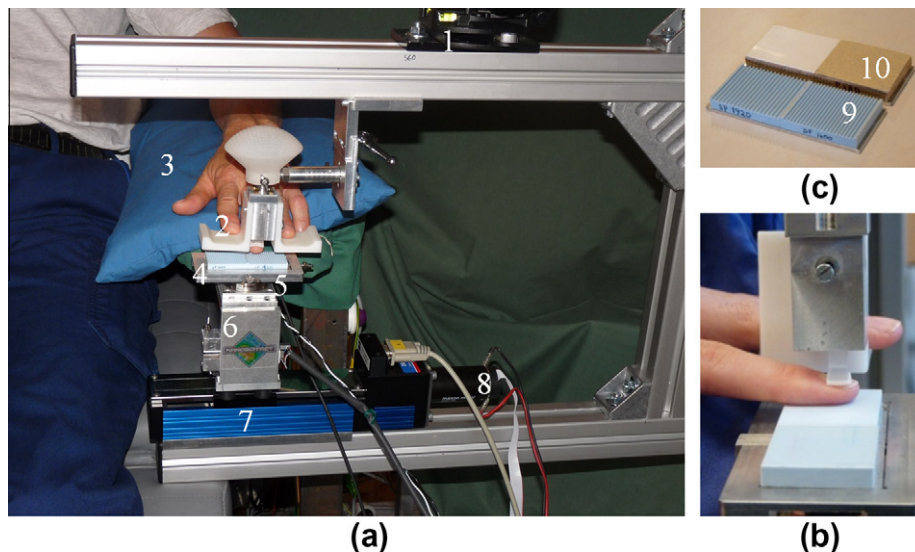


**Fig. 1.** (a) Experimental set-up during microneurography: frame hold by spherical joint (1), hand-finger support system (2), vacuum cast for arm support (3), carrier for stimuli (4), load cell (5), voice-coil actuator assembly for indentation of stimuli (6), linear guide for tangential sliding of stimuli (7), DC motor with encoder (8). (b) Fingerpad-stimulus interface with finger fixation system and free fingers support. (c) Examples of the used stimuli glued to a changeable aluminum plate: a couple of ridged stimuli (9), smooth plastic and rough sandpaper (10).

frequency of the bandpass filter preceding the sampling block (further details in Section 3.1). Hence, even introducing shielding techniques, a residual slight coupling between the PWM carrier frequency and  $\mu\text{V}$  range microneurography data could have been aliased at significant low frequencies, affecting the band of interest.

## 2.2. Stimuli and fingertip-hand support and mechanical assembly

An aluminum carrier for the stimuli was integrated above the voice coil (Fig. 1). The carrier could house sequences of textured stimuli on a 77 mm  $\times$  32 mm changeable plate.

The finger fixation system allowed a stable positioning while the stimuli were applied to the central part of the fingertip, and contemporarily could be disentangled operating on a screw to alternate passive and active touch protocols (Fig. 1b). This paper presents passive touch protocols only: artificial active touch was preliminarily tested with a robotic actuated finger [9], while human active touch will be investigated in future works.

The subject's nail could be fixed with superglue or adhesive medical tape to a plastic resin curved support which was then secured to a custom passive 3D joint with solid angle protractor for fine positioning. The other fingers of the hand could be either positioned on a flat ergonomic support or left free depending on what the subject felt was most comfortable.

The two DoFs actuation, sensors and mechanical components integrating stimuli and fingertip-hand supports were lodged in an aluminum frame (Fig. 1a). Since microneurography relies on the experience of the investigator and it is very complex to arbitrarily and precisely choose a specific single afferent unit to record from, platform adaptation in 3D space was fundamental to access large portions of fingerpad. Moreover, the subject cannot move after that the tactile unit has been identified. Hence, at the top, the mechanical structure was interfaced with a spherical joint (808RC4, Manfrotto) to a multi-DoFs passive-joint mechanical support grounded on the floor (Fig. 1a). The overall system could be swiveled towards and from the hand in simple manner and dexterously oriented, with 3D rotations up to about 30°, to fit the fingerpad recorded unit and the particular position of the subject during the experiments. To the authors' knowledge, in literature it has not been yet reported a tactile stimulation platform allowing such a high adaptability in 3D space for studies on texture dynamic encoding. The two DoFs control laws were designed to cope with this required 3D adaptation, as it is detailed in Section 2.4.

## 2.3. Sensors

The targeted experimentations required the measurement of either the normal and the tangential components of finger-stimulus contact force, as these are relevant information to be investigated in correlation with texture encoding in humans [19,20]. Moreover, the force measurement was required to implement feedback force control along the indentation axis, in order to prevent deviations from nominal conditions to have major effects (most of all the variable inclination of the platform to fit the particular position of the subject's finger), as in a model based design would occur. A load cell (Nano43, ATI IA) was used for this purpose. The transducer was located as much distal as possible, close to the end effector just under the carrier, to limit the inertial effects on the load cell measurements (e.g.: since the mass of the current carrier is 80 g, a relatively high acceleration of 250 mm/s<sup>2</sup> affects the force reading along the direction of motion with a 20 mN inertial component), while contemporarily allowing to change the tactile stimuli. A battery operated PCB, with low-noise bipolar instrumentation amplifiers (INA128, TI) and 16 bit multi-channel A/D converter (ADS8345, TI), was designed to interface the load cell with the control electronics achieving a RMS noise level of 2.1 mN. A

4096 levels per turn incremental optical encoder (MR Type L-1024, Maxon) measured the displacement of the linear guide with a resolution of 0.98  $\mu\text{m}$  and two magnetic limit switches were integrated at the extremities of the linear ball screw guide for delimitating the workspace.

## 2.4. Hierarchical control

A multi-layered hierarchical control architecture was implemented, partitioning the tasks between a general purpose PC and an embedded hardware-programmable logics (Fig. 2a).

The HIGH-level layer ran a GUI (Labview, NI) to generate, save, load or execute buffers of HIGH-level commands and for displaying the received platform data. The implemented curves for the linear guide position were a ramp, a sine wave and a polynomial fifth order wave, which had settable parameters and could be interlaced obtaining almost arbitrary motion profiles. The indentation force reference was modulated by the experimenter via sequences of commands. The set of commands for both the DoFs could be extended by modifying the software libraries.

MID- and LOW-level control layers were embedded in a Field Programmable Gate Array (EP2C35 FPGA, Altera) with a 100 MHz principal clock, partitioning [21] the control and communication tasks between custom hardware logic modules and a soft-core processor (Nios II/f) running C/C++ software routines. This design choice represented an advancement with respect to state of the art systems coherently with the trend showed in the literature of mechatronic tactile stimulators, which used digital controllers [22] for avoiding to integrate complex mechanisms such as in the *scotch yolk stimulator* [15] and reducing as much as possible the analog circuitry, [14,22–24]. Despite this design solution is promising, only a few mechatronic tactile stimulators were based on FPGA control electronics [25,26]. For the platform presented here, this choice was operated for two main reasons: (1) to allow future upgradeability of the architecture of control electronics (e.g. by instantiating on the same FPGA a number of additional parallel soft-core processors, peripherals, custom digital hardware modules, etc., as partially shown here in Section 3.2); (2) to achieve, via hardware-software codesign, parallel scheduling of periodic routines implementing the motion control laws and of interruptions managing the communication (commands and platform data, at high rate in the upgraded architecture with Ethernet mentioned in Section 3.2) functions. The MID-level layer was in charge of interpreting HIGH-level commands received through RS232, of point-to-point trajectory generation for the linear guide LOW-level controller, and of force target generation for the voice coil LOW-level controller. The RS232 was also used for transmitting the platform variables to the GUI for display purposes. The more relevant variables (three contact force components at finger-stimulus interface, target normal contact force component  $F_{\perp}(t)_{des}$ , actual linear guide position and its target position  $x(t)_{des}$ , an on-off trigger signal switching each time that a new command was executed) were converted to an analog output at 1 kHz over 16 bit (DAC8581, TI) for flexible integration and synchronization with analog signal acquisition systems, for example during microneurography.

LOW-level logic modules, designed in HDL, were instantiated onboard the FPGA to interface with the incremental optical encoder of the translational stage and to enhance safety by asynchronously deactivating the power drivers in case of unplanned workspace violations indicated by the limit switches. Data from the ADC of load cell electronics was acquired by means of dedicated FPGA custom hardware modules as well, implementing circular reading of the six load cell channels via SPI and a digital filter (16 kHz : 1 kHz oversampling-averaging-desampling per channel) to reduce the noise level by a factor of  $1/\sqrt{16}$ . This oper-

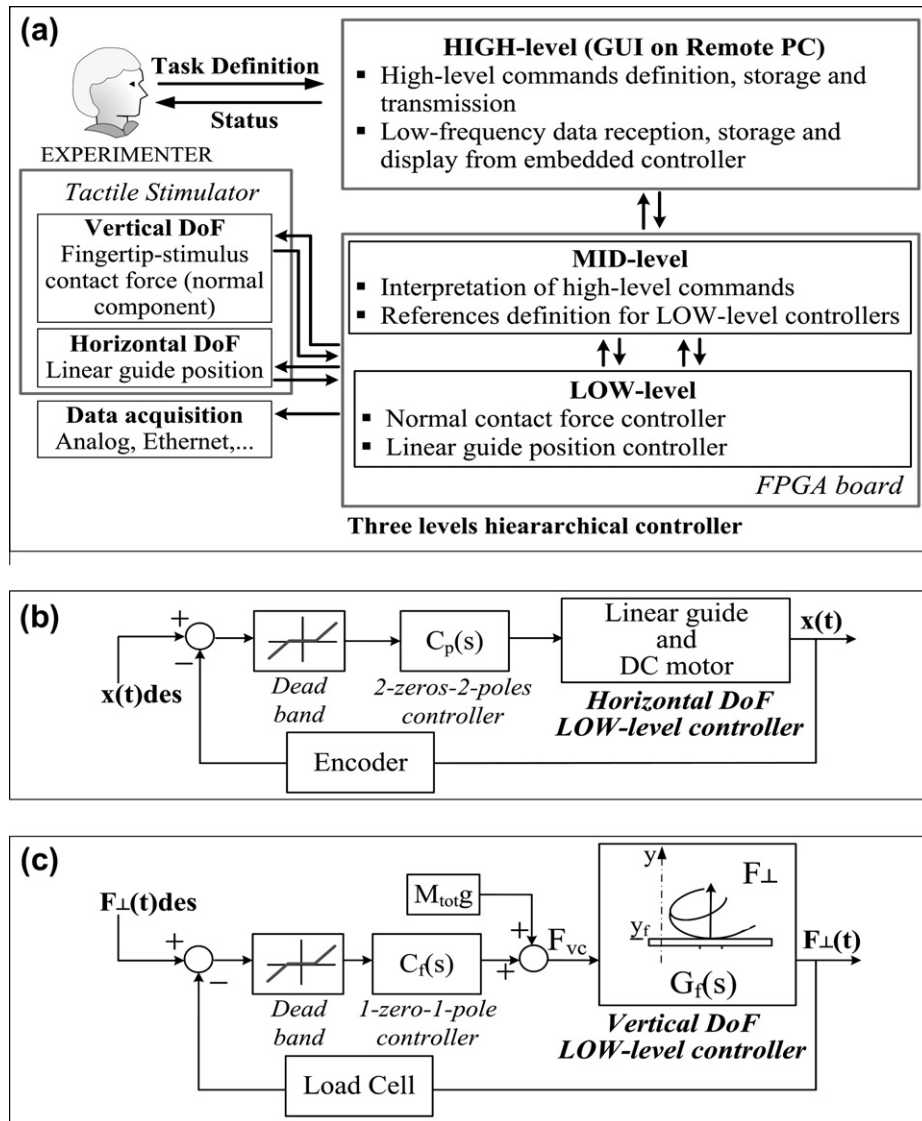


**Fig. 2.** (a) Overview of the Dynamic Platform hierarchical controller. (b) Block diagram of the LOW-level closed-loop position controller along the sliding direction. (c) Block diagram of the LOW-level closed-loop force controller along the indentation direction.

ation was relevant to meet the targeted performance for both force sensing and control. The parallel hardware implementation in FPGA logics avoided to load the processor with such operations, while an instruction based software approach could have been affected by jitter while scheduling load cell ADC high-rate interrupts. The LOW-level controller was interfaced to the power drivers through a dual 12 bit DAC (TLV5618, TI) and implemented (zero-order-hold digitalization at 1 kHz) the 2 DoFs control laws, which were in closed loop with integrator to reject disturbances (e.g. variable friction) or modifications of the boundary conditions (e.g. the inclination of the platform in 3D space for adapting it to the position of the subject during microneurography).

In the Laplace domain, the linear guide position controller  $C_p(s)$  had 2-zeros-2-poles and an *ad hoc* dead band (Fig. 2b) of  $\pm 2$  encoder counts, to prevent any steady state vibration [27]. Due to the quasi non backdrivability of the screw mechanism, the dynamics along the sliding direction was modeled without considering the interaction with the finger and the controller was dimensioned to have closed loop stability, at least 6 dB of amplitude margin and  $45^\circ$  of phase margin, zero error at steady state and reference trajectory tracking error in the order of tens of  $\mu\text{m}$ .

The normal component of the stimulus-fingertip contact force was regulated with a 1-zero-1-pole  $C_f(s)$  closed loop controller and an *ad hoc* dead band (Fig. 2c), set to  $\pm 6.3$  mN (i.e. three times the measurement standard deviation reported in Section 2.3), to avoid steady state vibrations.

As shown in Eq. (1), both the controllers had an integrator, to reject any steady state error apart for the tolerance admitted by the dead bands to avoid vibrations.

$$C_p(s) = k_p \frac{(s + s_{p1})(s + s_{p2})}{s(s + s_{p3})} \quad (1a)$$

$$C_f(s) = k_f \frac{(s + s_{f1})}{s} \quad (1b)$$

In order to define the  $C_f(s)$  coefficients, the stimulus-fingertip contact mechanics was modeled along the normal direction to the separation surface.

Naming  $y$  the position of the end effector along the indentation direction and  $y_f$  the position of first contact with the fingerpad (Fig. 1c), the vertical DoF dynamics is described by:

$$M_{tot}\ddot{y}(t) + f_v\dot{y}(t) + f_c\text{sign}(\dot{y}(t)) + M_{tot}g + K_{nl}(y(t) - y_f) = F_{vc}(t) \quad (2a)$$

if  $y(t) \geq y_f$

$$M_{tot}\ddot{y}(t) + f_c \text{sign}(\dot{y}(t)) + M_{tot}g = F_{VC}(t) \quad \text{if } y(t) < y_f \quad (2b)$$

where  $M_{tot}$  is the total mass moving vertically,  $g$  is the gravitational acceleration,  $f_c$  is the dynamic friction force along the vertical DoF,  $F_{VC}$  is the force provided by the voice coil,  $f_v$  (2.5 Ns/mm) and  $K_{nl}$  take into account the mechanical characteristics of the fingertip [28–30], i.e. the viscosity and the non-linear elasticity, respectively. Given that  $C_f(s)$  has to control the normal component of the contact force, the dynamics for  $y(t) \geq y_f$  was considered for fitting the compensator. Eq. (2a) was linearized for dimensioning the closed loop controller: the dynamic friction was neglected as the vertical motion is supported by low friction miniaturized linear motion rolling guides;  $M_{tot}g$  was neglected because it does not affect system dynamics being an additive constant contribution; the non-linear coefficient  $K_{nl}$  was changed in the linear coefficient  $K_l$  (3.5 N/mm), providing an estimation of human finger stiffness up to 1000 mN.

Considering the previous simplifications, Eq. (1a) resulted in:

$$M_{tot}\ddot{y}(t) + f_v\dot{y}(t) + K_l(y(t) - y_f) = F_{VC}(t) \quad (3)$$

To obtain the transfer function  $G_f = F_{Cont}^n(s)/F_{VC}(s)$ , the  $\tilde{y} = y - y_f$  ( $\dot{\tilde{y}} = \dot{y}$  and  $\ddot{\tilde{y}} = \ddot{y}$ ) coordinate change was applied to Eq. (3). In the Laplace domain this resulted in:

$$(M_{tot}s^2 + f_v s + K_l)\tilde{y}(s) = F_{VC}(s) \quad (4)$$

The normal contact force  $F_{Cont}^n$  was measured by the load cell and defined as:

$$F_{Cont}^n(t) = f_v\dot{\tilde{y}} + K_l\tilde{y} \quad (5)$$

In the Laplace domain:

$$F_{Cont}^n(s) = (f_v s + K_l)\tilde{y}(s) \quad (6)$$

So that:

$$G_f(s) = \frac{F_{Cont}^n(s)}{F_{VC}(s)} = \frac{f_v s + K_l}{M_{tot}s^2 + f_v s + K_l} \quad (7)$$

Starting from (7), the  $C_f(s)$  coefficients were set in order to satisfy the following requirements: closed loop stability, at least 6 dB of amplitude margin and 45° of phase margin, zero error at steady state and indentation force tracking error in the order of tens of mN.

### 3. Methods

#### 3.1. Microneurography

Impulses of single tactile afferents in the left index and middle fingers were recorded using the microneurographic technique in 16 human healthy volunteers [4]. The experiments presented in this work were carried out at the Department of Physiology of University of Gothenburg and were approved by the ethics board of the University of Gothenburg. The subjects seated comfortably in a dentist's chair, the left arm resting in a vacuum cast for stabilization and maximum comfort. Tungsten needle electrodes were inserted in the left median nerve, 8 cm above the elbow. The nerve signal was band-pass filtered at 200–4000 Hz, sampled at 12.8 kHz together with analog data from the platform, and stored on a PC using the ZOOM/SC system developed at the Department of Physiology, Umeå University, Sweden. Recorded nerve impulses were inspected off-line on an expanded time scale using in-house software implemented in MATLAB (The Mathworks) and were accepted for subsequent analyses only if they could be validated as originating from a single afferent. The units' responses and receptive fields were explored using calibrated nylon filaments (von Frey hairs) and were classified as SAI, SAII, RAI, or PC according

to the adaptation of the response to sustained stimulation and size of the receptive field [31,32].

#### 3.2. Experimental protocol

Sliding motions of a smooth aluminum stimulus (Fig. 1c) were applied with different indentation force levels to the index finger of a human subject to show sample protocols allowed by the open platform. To point out the flexibility in the upgrading of the chosen architecture, thanks to the used hardware-programmable logics, platform variables were transmitted to a PC via Ethernet at 5 kHz (significantly higher rates were possible) by a second parallel processor instantiated onboard the FPGA, similarly to [8]. Dynamic performance indexes, calculated on repeated runs of the same buffer of commands, are defined and provided in Section 4.

To assess the repeatability of reiterated stimulus presentations during electrophysiological measurements, periodic ridged stimuli were fabricated from TUFSET Rigid Polyurethane thermosetting plastics material, measuring 32 mm × 35 mm and mounted in pairs on changeable plates (Fig. 1c). While gathering neural data via microneurography from 12 RA, 7 SAI, 3 SAII and 2 Pc single afferent units in the fingerpad, the platform applied sliding motions, repeated in runs of 12, across the distal phalanx using stimuli with spatial period between 280 μm and 1920 μm, with normal contact force set to 100 mN, 200 mN or 400 mN, sliding distance of 24 mm and velocity from 5 mm/s up to 40 mm/s. To directly assess the presence of biologically significant vibrations introduced by the platform, 2 RA units were in addition similarly stimulated using a smooth polypropylene plastic surface as well. The spectra resulting from the point processes of identified neural spikes were calculated.

The lack of significant electromagnetic interference coupling with the electrode for microneurography due to the platform was investigated by means of analysis of neural recordings from a SAI unit (left index finger), under three experimental conditions: (1) Manual Stimulation (MS)-mode: while the platform was not actuated, the experimenter manually stimulated the finger of the subject (test subject) from which neural data was recorded; (2) Closed Loop (CL)-mode: a 1600 μm periodic ridged stimulus was indented and scanned across the fingertip of a second subject (control subject), in close proximity to the fingertip of the test subject (from which neural data was recorded), with 500 mN feedback controlled contact force, sliding distance of 20 mm and velocity set to 20 mm/s; (3) Open Loop (OL)-mode: to double check whether or not the time varying driving current (related to the indentation DoF actuator in feedback force control) affected the microneurography results, the same protocol of point 2 was operated apart for the fact that the indentation was in open loop by supplying a constant current to the voice-coil actuator, resulting in a normal contact force of about 750 mN before the onset of stimulus sliding motion. Noise amplitude distribution was evaluated in the three experimental conditions described above.

### 4. Results and discussion

#### 4.1. Dynamic performance evaluation

Fig. 3 shows some sequences of commands implemented by the developed tactile stimulator. Error parameters were defined to quantitatively assess the dynamic performances of the mechatronic platform while indenting and sliding tactile stimuli on a human finger, as detailed in the following:

$$RMSE_{pos\_ctrl}(t_a, t_b)_i = \sqrt{\frac{1}{|t_b - t_a|} \int_{t_a}^{t_b} (x(t)des_i - x(t)_i)^2 dt} \quad (8)$$

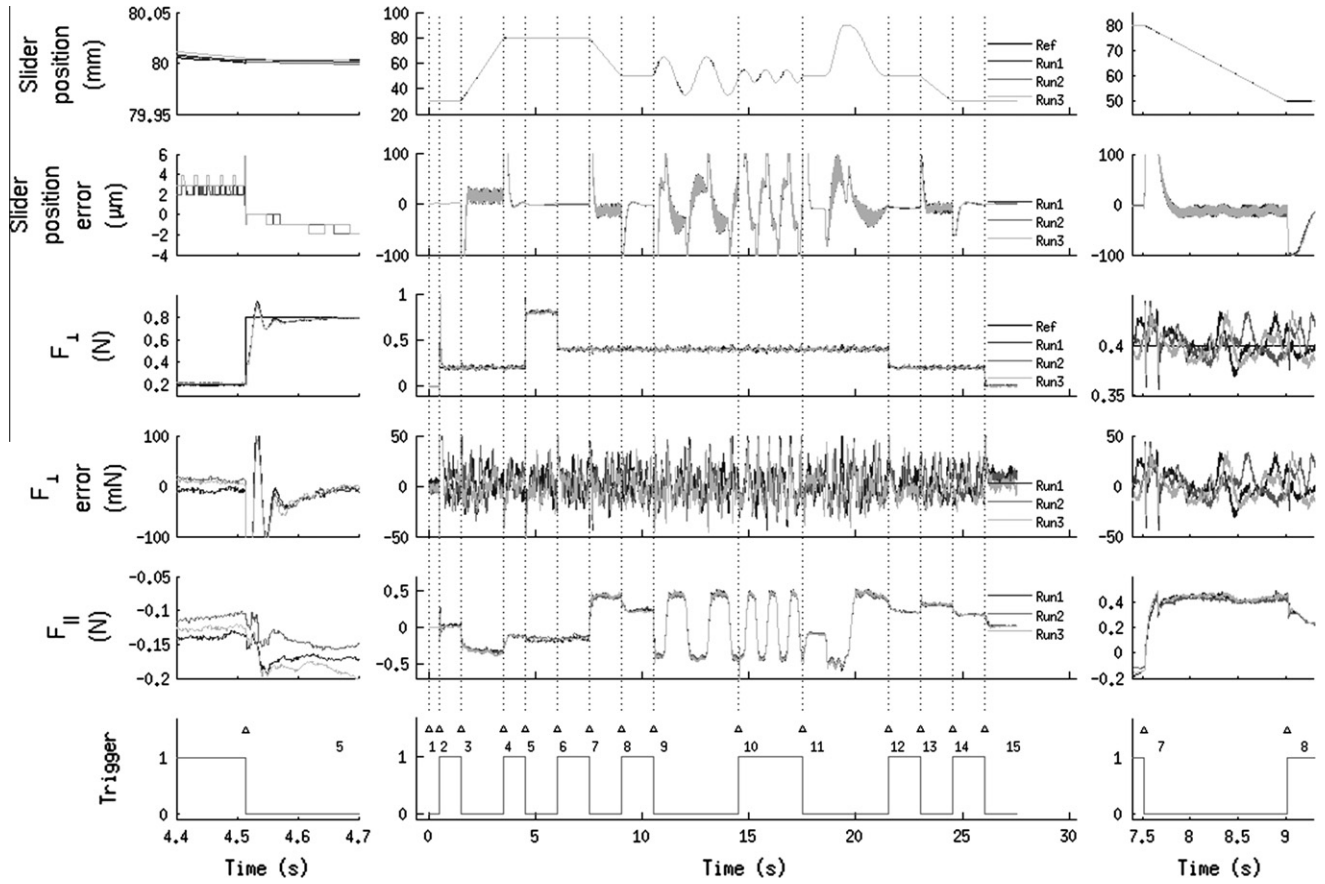


**Fig. 3.** Sample protocols that can be implemented with the mechatronic platform. Three runs, from the 10 repetitions acquired at 5 kHz through Ethernet digital transmission, of the same sequence of commands are superimposed to show high repeatability. The plots represent, from the top: position of the translational slider (target and actual), error in tracking the reference slider position, indentation force at finger-stimulus interface (target and actual), error in tracking the reference indentation force, tangential force component along the direction of the sliding motion, Boolean channel switching each time a new high-level command is executed. Phases 2 and 15, at the beginning and at the end of the protocol, are the loading and unloading of the smooth aluminum stimulus to the finger. In phase 3 the stimulus is stroked for 50 mm at 25 mm/s and normal contact force at 200 mN; phases 5 and 6 are normal contact force steps from 200 mN to 800 mN and then to 400 mN; from phase 7 to phase 11 the normal contact force is held at 400 mN, while the stimulus is stroked for 30 mm at constant speed of 20 mm/s (phase 7), while two (phase 9, 15 mm amplitude at 0.5 Hz) or three (phase 10, 5 mm amplitude at 1 Hz) sine waves are executed, or while a fifth order polynomial trajectory is followed (phase 11). Phase 13 is a position ramp from 50 mm to 30 mm in 1.5 s and normal contact force set to 200 mN. The left inset shows a zoom on the transitory between phase 4 and phase 5. The right inset shows a zoom on dynamic phase 7.

$$RMSE_{force\_ctrl}(t_a, t_b)_i = \sqrt{\frac{1}{t_b - t_a} \int_{t_a}^{t_b} (F_{\perp}(t) des_i - F_{\perp}(t)_i)^2 dt} \quad (9)$$

where RMSE is the Root Mean Square Error (related to the sliding position or to the indentation force) in the  $[t_a, t_b]$  time interval of the  $i$ th run of the considered reference trajectory. Actually, the continuum time integrals in Eqs. (8) and (9) are computed by means of a discrete summation, since the system is discrete time, with 5 kHz packet transmission frequency via Ethernet.

Among  $N$  repetitions, the Tracking Error ( $TE$ ) is defined as the mean value of the calculated RMS Error for each run, with a confidence interval  $\Delta TE$  associated to the standard deviation of the RMS Error parameters:

$$TE_{pos\_ctrl}(t_a, t_b) = \frac{1}{N} \sum_{i=1}^N RMSE_{pos\_ctrl}(t_a, t_b)_i \quad (10)$$

$$TE_{force\_ctrl}(t_a, t_b) = \frac{1}{N} \sum_{i=1}^N RMSE_{force\_ctrl}(t_a, t_b)_i \quad (11)$$

$$\Delta TE_{pos\_ctrl}(t_a, t_b) = \sqrt{\frac{1}{N} \sum_{i=1}^N (RMSE_{pos\_ctrl}(t_a, t_b)_i - TE_{pos\_ctrl}(t_a, t_b))^2} \quad (12)$$

$$\Delta TE_{force\_ctrl}(t_a, t_b) = \sqrt{\frac{1}{N} \sum_{i=1}^N (RMSE_{force\_ctrl}(t_a, t_b)_i - TE_{force\_ctrl}(t_a, t_b))^2} \quad (13)$$

The tracking error parameters, calculated over  $N = 10$  runs of the protocol shown in Fig. 3, are summarized in Table 1, confirming adequate control performances. Table 2 summarizes the Tracking Error along the indentation axis, with normalization to the normal contact force reference.

The error parameters are calculated for each phase of the protocol shown in Fig. 3, where the interval  $[t_{i-1}, t_i]$  is related to the  $i$ th phase. The results provided within Table 1 considered subsets of each stimulation phase too, obtained discarding the first 150 ms of data at the onset of each motion. This operation was performed to assess the tracking performances more fairly, since the reference trajectories or their first derivatives had discontinuities, thus affecting the tracking error at the transition between two subsequent phases of the protocol. The error parameters summarized in Table 1 point out that the reference slider position is tracked with an error lower than 28  $\mu\text{m}$  for ramps (phases 3, 7 and 13), that reference sine waves (phases 9 and 10) having peak velocities up to 47.1 mm/s are followed with error lower than 68  $\mu\text{m}$ , and that the tested 5th order polynomial trajectory (phase 11) presents a Tracking Error lower than 43  $\mu\text{m}$ . As regards the regulation of the inden-

**Table 1**  
Position and force control tracking error parameters, calculated for each stimulation phase depicted in Fig. 3.

Phase	$t_a$	$t_b$	$TE_{pos\_ctrl}(t_a, t_b)$ [ $\mu\text{m}$ ]	$\Delta TE_{pos\_ctrl}(t_a, t_b)$ [ $\mu\text{m}$ ]	$TE_{force\_ctrl}(t_a, t_b)$ [mN]	$\Delta TE_{force\_ctrl}(t_a, t_b)$ [mN]
1	$t_0$	$t_1$	1.5	0.0	2.3	0.9
	$t_0 + 150$ ms	$t_1$	1.7	0.0	2.4	1.0
2	$t_1$	$t_2$	1.5	0.0	126.1	3.2
	$t_1 + 150$ ms	$t_2$	1.6	0.0	13.2	1.5
3	$t_2$	$t_3$	89.3	0.7	13.3	1.9
	$t_2 + 150$ ms	$t_3$	27.9	0.3	12.8	1.9
4	$t_3$	$t_4$	87.6	3.3	11.6	1.5
	$t_3 + 150$ ms	$t_4$	37.0	1.1	10.2	1.5
5	$t_4$	$t_5$	2.8	0.5	38.8	0.9
	$t_4 + 150$ ms	$t_5$	2.9	0.5	13.0	3.4
6	$t_5$	$t_6$	0.5	0.9	24.5	1.8
	$t_5 + 150$ ms	$t_6$	0.5	0.9	10.9	2.7
7	$t_6$	$t_7$	60.7	0.2	13.2	0.8
	$t_6 + 150$ ms	$t_7$	19.5	0.2	11.6	1.1
8	$t_7$	$t_8$	32.9	1.3	11.4	1.1
	$t_7 + 150$ ms	$t_8$	14.9	1.4	11.3	1.0
9	$t_8$	$t_9$	161.0	1.2	15.4	0.9
	$t_8 + 150$ ms	$t_9$	58.8	0.3	14.7	0.7
10	$t_9$	$t_{10}$	125.4	1.7	19.1	1.6
	$t_9 + 150$ ms	$t_{10}$	67.4	0.3	19.1	1.6
11	$t_{10}$	$t_{11}$	87.1	1.5	14.0	1.3
	$t_{10} + 150$ ms	$t_{11}$	42.6	0.3	13.6	1.3
12	$t_{11}$	$t_{12}$	7.6	0.3	17.9	0.9
	$t_{11} + 150$ ms	$t_{12}$	7.8	0.5	9.6	1.2
13	$t_{12}$	$t_{13}$	21.4	1.3	10.8	1.7
	$t_{12} + 150$ ms	$t_{13}$	9.7	0.3	10.4	1.9
14	$t_{13}$	$t_{14}$	23.2	0.3	10.2	1.3
	$t_{13} + 150$ ms	$t_{14}$	13.6	0.8	9.9	1.3
15	$t_{14}$	$t_{15}$	1.4	0.7	16.3	1.6
	$t_{14} + 150$ ms	$t_{15}$	1.4	0.8	5.9	2.5

tation force, all the calculated parameters showed (Table 1) absolute Tracking Error lower than 20 mN, while the normalized error was comprised between 1.6% and 6.6% (force reference is at 0 N in phases 1 and 15 and the normalization thus results in a Not a Number). The high value appearing for  $TE_{force\_ctrl}(t_1, t_2)$  (both absolute in Table 1 and normalized in Table 2) is misleading, since phase 2 included a free flight motion of the stimulus before contacting the finger. By discarding the first part of data, the  $TE_{force\_ctrl}(t_1 + 150 \text{ ms}, t_2)$  index calculated in phase 2 becomes comparable to the other phases, as shown in Table 1 and in Table 2.

As a further relevant result, the extremely reduced values of the confidence intervals  $\Delta TE$  summarized in Tables 1 and 2, and the overlapping curves within different runs of Fig. 3 confirm that the developed mechatronic platform guarantees excellent repeatability in the presentation of tactile stimuli. This achievement is fundamental in touch studies: even if the tracking of the reference curves may get relatively worse in certain conditions, the actual trajectories under feedback control are almost coincident among different runs.

#### 4.2. Microneurography validation experiments

The excellent repeatability, being mainly a consequence of the intrinsically reduced jitter in the scheduling of periodic control tasks by the implemented hierarchical control architecture (particularly, the hardware programmable FPGA logics for the embedded controller), is confirmed by human microneurography recordings too, which showed very strong similarity over repeated runs using periodic ridged stimuli. An example from a RA (Meissner) afferent unit is shown in Fig. 4a, where the instantaneous rate plots from different runs highlight the repeatability of the stimuli delivered by the platform, and the stability of the mounting of the finger. Here, the 1600  $\mu\text{m}$  spatial period of the TUFSET surface is revealed as a modulation of firing frequency as the ridges of the surface were sliding across the receptive field of the RA unit. Similar re-

sults were obtained in all other recorded afferents. With respect to repeatability, the availability of the switching trigger shown in Fig. 3 (both as a bit in the digital Ethernet stream and as a physical

**Table 2**  
Tracking error parameters for force feedback control along the indentation axis, normalized to the normal contact force reference, calculated for each stimulation phase depicted in Fig. 3.

Phase	$t_a$	$t_b$	$\%TE_{force\_ctrl}(t_a, t_b)$	$\%\Delta TE_{force\_ctrl}(t_a, t_b)$
1	$t_0$	$t_1$	NaN	NaN
	$t_0 + 150$ ms	$t_1$	NaN	NaN
2	$t_1$	$t_2$	63.0	1.6
	$t_1 + 150$ ms	$t_2$	6.6	0.7
3	$t_2$	$t_3$	6.6	0.9
	$t_2 + 150$ ms	$t_3$	6.4	0.9
4	$t_3$	$t_4$	5.8	0.7
	$t_3 + 150$ ms	$t_4$	5.1	0.8
5	$t_4$	$t_5$	4.8	0.1
	$t_4 + 150$ ms	$t_5$	1.6	0.4
6	$t_5$	$t_6$	6.1	0.5
	$t_5 + 150$ ms	$t_6$	2.7	0.7
7	$t_6$	$t_7$	3.3	0.2
	$t_6 + 150$ ms	$t_7$	2.9	0.3
8	$t_7$	$t_8$	2.9	0.3
	$t_7 + 150$ ms	$t_8$	2.8	0.2
9	$t_8$	$t_9$	3.9	0.2
	$t_8 + 150$ ms	$t_9$	3.7	0.2
10	$t_9$	$t_{10}$	4.8	0.4
	$t_9 + 150$ ms	$t_{10}$	4.8	0.4
11	$t_{10}$	$t_{11}$	3.5	0.3
	$t_{10} + 150$ ms	$t_{11}$	3.4	0.3
12	$t_{11}$	$t_{12}$	9.0	0.4
	$t_{11} + 150$ ms	$t_{12}$	4.8	0.6
13	$t_{12}$	$t_{13}$	5.4	0.8
	$t_{12} + 150$ ms	$t_{13}$	5.2	1.0
14	$t_{13}$	$t_{14}$	5.1	0.6
	$t_{13} + 150$ ms	$t_{14}$	5.0	0.6
15	$t_{14}$	$t_{15}$	NaN	NaN
	$t_{14} + 150$ ms	$t_{15}$	NaN	NaN

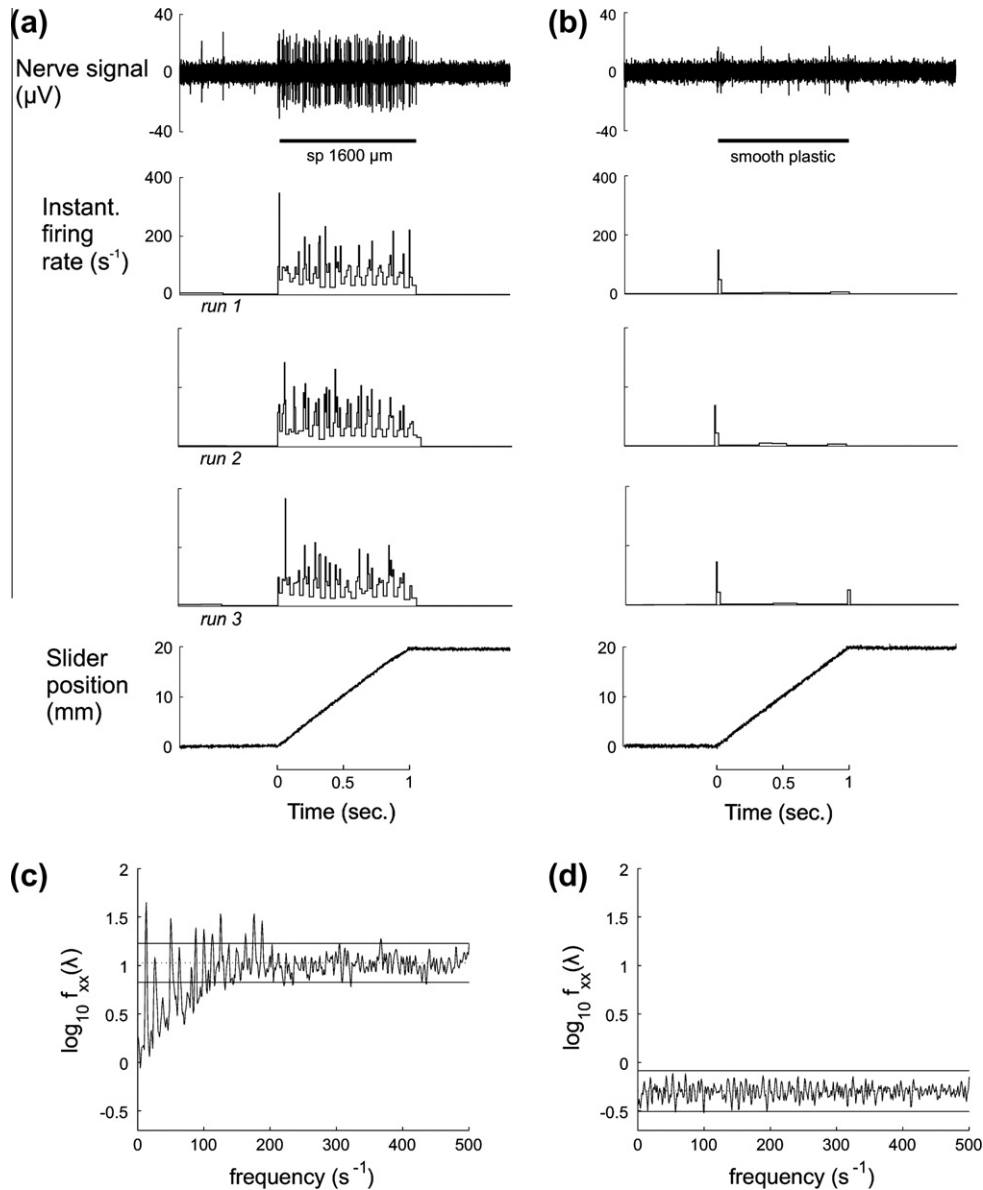


**Fig. 4.** Microneurographic recording from a RA (Meissner) tactile afferent unit. (a) Stimulation with a ridged grating. Records from top, recorded nerve signal, instantaneous rate of nerve discharges during three repeated runs of the same stimulus, slider position. (b) Stimulation with a smooth plastic surface on the same unit, records as in A. (c) Spectrum of nerve discharge during ridged grating stimulation. Solid lines show  $p < 0.01$  confidence limits. (d) Spectrum for a smooth surface as in C.

channel for interfacing with the analog instrumentation for electrophysiological measurements) allows to precisely synchronize multiple runs of the same protocol, thus enabling in future studies the quantitative investigation of the biological system through statistical analysis on huge datasets.

In the time domain, the immunity from spurious vibrations was confirmed by microneurography recording from RA units using a smooth plastic surface, shown in Fig. 4b. After the expected short burst of impulses at the start of motion, this unit fired only sporadic impulses. The spectra of the firing for all the data from the same RA unit is shown in Fig. 4c for 1600  $\mu\text{m}$  spatial period grating, meaningfully depicting the modulation of firing at the expected fundamental frequency (i.e. the ratio between the sliding velocity and the spatial period of the presented surface) of 12.5 Hz at a sliding velocity of 20 mm/s, as well as significant modulation at harmonics up to 200 Hz, thus revealing the high sensitivity in encoding the mechanical characteristics of the stimulating surface in this unit. In the frequency domain, the spectrum for all the data from stimulation with a smooth plastic surface in the same unit re-

veals no periodic firing or pickup of vibrations (Fig. 4d). To succeed in this objective, a relevant design choice was the introduction of custom dead bands (Fig. 2b and c) which allowed errors lower than specific thresholds to occur, thus avoiding vibrations produced by continuous sub-threshold error-correction control actions.

#### 4.3. Electromagnetic noise assessment

No relevant noise pickup was observed in the raw nerve signals (top plots of Fig. 4) recorded during platform movement or when the force control was engaged, as an effect of the selected linear power drivers for the actuators instead of switching ones. Platform electromagnetic compatibility with the microneurography technique was quantitatively assessed, as presented in the following. Fig. 5 depicts neural data from a SAI unit of the test subject in the three MS-mode, CL-mode and OL-mode experimental conditions detailed in Section 3.2. Neural spikes are identified in MS-mode and marked with dots, corresponding to the phases during which the finger of the test subject was manually probed. The spike

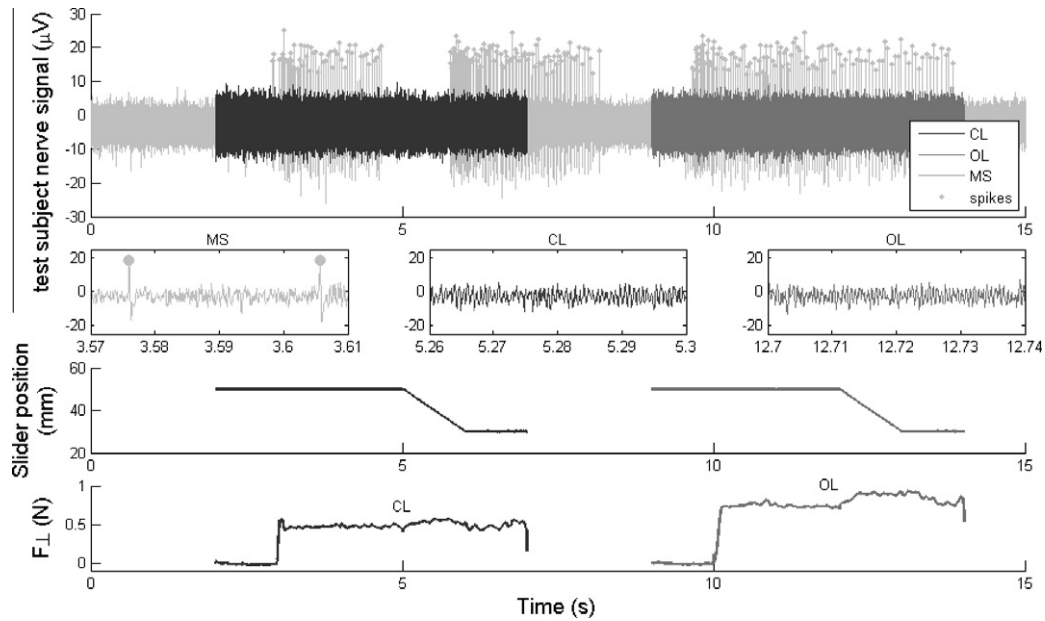


**Fig. 5.** Neural recordings under the three MS-mode, CL-mode and OL-mode experimental conditions, described in Section 3.2, are depicted in the top plot for assessment of platform electromagnetic compatibility with microneurography technique. Left to right, the insets in the second row from the top show zooms on neural data recorded from the test subject with MS-mode, CL-mode and OL-mode. The position of the translational slider and the normal component of the indentation force are shown as well under both the CL-mode and OL-mode experiments.

template applied for spike sorting in MS-mode was then used to evaluate whether or not neural spikes were elicited under the two other stimulation conditions due to electromagnetic interference by the platform (since test subject fingertip was not mechanically stimulated in CL-mode and OL-mode, and a SAI unit is expected to be silent in that condition). Noticeably, no spikes could be identified in both the CL-mode and OL-mode, confirming that the platform did not induce neural firing and hence validating the results presented above, since the spectra of Fig. 4 were related to the identified neural spikes (i.e. a point process). As one could expect, the mechatronic platform had an effect in the background neural noise, confirmed by the higher amplitude of the CL-mode and OL-mode traces if compared to the spike-free regions of the MS-mode one. However, the overlap of the traces shows that the increase in noise was not enough to mask the spikes occurring while manually probing (MS-mode) the fingertip of the test sub-

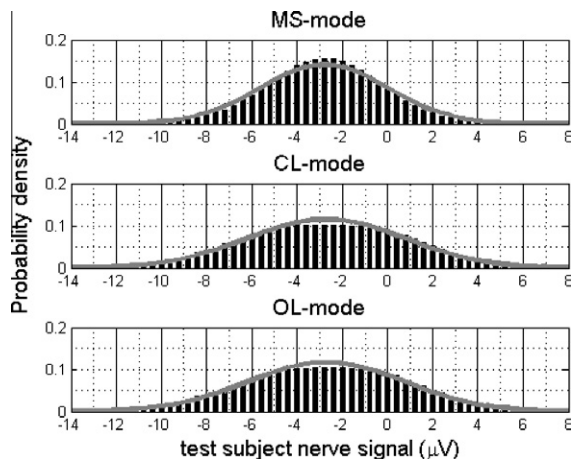


**Fig. 6.** Statistical neural noise analysis for each of the three MS-mode, CL-mode and OL-mode stimulation conditions, described in Section 3.2. The probability that the neural signal belongs to a bin (width set to  $0.4 \mu\text{V}$ ) is evaluated based on amplitude levels experimentally occurring in 38 s of data at 12.8 kHz. The solid line shows Gaussian fitting of noise probability density.

**Table 3**

Gaussian distribution neural signal background noise fitting parameters (mean MN and standard deviation  $\Delta N$ ) and related confidence intervals for evaluating platform electromagnetic compatibility under the three MS-mode, CL-mode and OL-mode tactile stimulation conditions described in Section 3.2.

Stimulation condition	MN ( $\mu\text{V}$ )	$\Delta N$ ( $\mu\text{V}$ )
MS-mode	$-2.81 \pm 0.01$	$2.82 \pm 0.01$
CL-mode	$-2.72 \pm 0.02$	$3.48 \pm 0.01$
OL-mode	$-2.72 \pm 0.02$	$3.44 \pm 0.01$

ject. Despite the main message conveyed by Fig. 5 is related to platform electromagnetic noise assessment, a compared visual inspection of the CL-mode and OL-mode force traces points out as well the stabilizing effect of closed loop indentation force control with respect to constant current open loop one, particularly from the onset of the sliding motion. A statistical noise analysis is presented in Fig. 6 for each of the three MS, CL and OL stimulation conditions, where the probability that the neural signal belongs to a bin (width set to  $0.4 \mu\text{V}$ ) is evaluated based on amplitude levels experimentally occurring in 38 s of data at 12.8 kHz. A Gaussian fitting is shown as well in Fig. 6, and the related parameters are summarized in Table 3, showing significant fitting confidence. Platform activation causes a non relevant increase in noise standard deviation  $\Delta N$  from  $2.82 \mu\text{V}$  (MS-mode) to  $3.43 \mu\text{V}$  (OL-mode) and  $3.48 \mu\text{V}$  (MS-mode), and had almost no effect in its mean value MN. Hence, no relevant difference was observed between closed loop and constant current open loop modalities, confirming that the spectra extracted (Fig. 4) from the point processes of identified spike trains were not electromagnetically induced by the specific indentation force controller.

## 5. Conclusions

The design and experimental validation of a mechatronic tactile stimulator was presented in this work as a new tool for the investigation of human touch. The system was conceived to enable parametric, precise, repeatable and smooth stimulus presentation with

standardized conditions, no vibrations and simple programming for indenting and sliding the surfaces on the fingerpad. Moreover, the chosen FPGA solution guaranteed to the platform adequate throughput together with design upgradeability [8,33], which was not typical of tactile stimulation systems previously reported in the literature [22,14,34].

Future works will present results of ongoing studies on the measurement of peripheral neural firing and brain responses by means of microneurography and EEG, and of (even combined) psychophysical experiments on human touch. In parallel, the same system is enabling studies on artificial tactile sensors in robotics [8,33] and future investigations will focus on artificial touch evaluation of a variety of tactile surfaces, such as textiles.

## Acknowledgment

This work was supported in part by the EU under the NANOBIO-TACT (FP6-NMP-033287) and NANBIOTOUCH (FP7-NMP-228844) projects. The authors thank: Stefano Roccella and Marco Donati for meaningful discussions and contribution in the design phase at ARTS Lab of Scuola Superiore Sant'Anna; Riccardo Di Leonardo of Scuola Superiore Sant'Anna and Karin Göthner of University of Gothenburg for technical assistance; Simon Johnson and Bill Ranken from Unilever R&D for providing the ridged stimuli used in the current experiments.

## References

- [1] Lawrence MA, Kitada R, Klatzky RL, Lederman SJ. Haptic roughness perception of linear gratings via bare finger or rigid probe. *Perception* 2007;36:547–57.
- [2] Yoshioka T, Gibb B, Dorsch AK, Hsiao SS, Johnson KO. Neural coding mechanisms underlying perceived roughness of finely textured surfaces. *J Neurosci* 2001;21:6905–16.
- [3] Johansson RS, Birznieks I. First spikes in ensembles of human tactile afferents code complex spatial fingertip events. *Nat Neurosci* 2004;7:97–8.
- [4] Vallbo AB, Hagbarth KE, Wallin BG. Microneurography: how the technique developed and its role in the investigation of the sympathetic nervous system. *J Appl Physiol* 2004;96:1262–9.
- [5] Grave de Peralta R, Gonzalez S, Lantz G, Michel CM, Landis T. Noninvasive localization of electromagnetic epileptic activity I. Method descriptions and simulations. *Brain Topogr* 2001;14:131–7.
- [6] Hollins M, Risner SR. Evidence for the duplex theory of tactile texture perception. *Percept Psychophys* 2000;62:695–705.
- [7] Beckmann S, Bjrnstodter M, Backlund-Wasling H, Wessberg J. Brain decoding of texture processing using independent component analysis and support vector machines. In: Proc. 2009 IEEE international symposium on intelligent signal processing, August 26–28, 2009, Budapest, Hungary. p. 287–92.
- [8] Oddo C.M., Beccai L, Muscolo GG, Carrozza MC. A biomimetic MEMS-based tactile sensor array with fingerprints integrated in a robotic fingertip for artificial roughness encoding. In: Proc. 2009 IEEE conference on robotics and biomimetics, December 19–23, 2009, Guilin, China. p. 894–900.
- [9] Beccai L, Oddo CM, Cipriani C, Carrozza MC. A biorobotic approach for artificial touch: from the development of a MEMS sensor to the tactile array integration into an actuated finger. In: Proc. of the humanoid 09 workshop on tactile sensing in humanoids – tactile sensors and beyond, December 7, 2009, Paris, France, p. 38–41.
- [10] Johnson KO, Yoshioka T. Neural mechanisms of tactile form and texture perception. In: Nelson RJ, editor. *The somatosensory system: deciphering the brain's own body image*. Boca Raton, FL (USA): CRC Press LLC; 2001. p. 73–101.
- [11] Jones LA, Lederman SJ. Tactile sensing. In: Jones LA, Lederman SJ, editors. *Human hand function*. New York, NY (USA): Oxford University Press; 2006. p. 44–74.
- [12] Connor CE, Johnson KO. Neural coding of tactile texture: comparison of spatial and temporal mechanisms for roughness perception. *J Neurosci* 1992;12(9):3414–26.
- [13] Birznieks I, Jenmalm P, Goodwin AW, Johansson RS. Encoding of direction of fingertip forces by human tactile afferents. *J Neurosci* 2001;21:8222–37.
- [14] LaMotte RH, Whitehouse GM, Robinson CJ, Davis F. A tactile stimulator for controlled movements of textured surfaces across the skin. *J Electrophysiol Tech* 1983;10:1–17.
- [15] Goodwin AW, Morley JW, Clarke C, Lumaksana B, Darian-Smith I. A stimulator for moving textured surfaces sinusoidally across the skin. *J Neurosci Methods* 1985;14:121–5.
- [16] Darian-Smith I, Oke LE. Peripheral neural representation of the spatial frequency of a grating moving across the monkey's finger pad. *J Physiol* 1980;309:117–33.
- [17] Johnson KO, Phillips JR. A rotating drum stimulator for scanning embossed patterns and textures across the skin. *J Neurosci Methods* 1988;22:221–31.
- [18] LaMotte RH, Friedman RM, Lu C, Khalsa PS, Srinivasan MA. Raised object on a planar surface stroked across the fingerpad: responses of cutaneous mechanoreceptors to shape and orientation. *J Neurophysiol* 1998;80:2446–66.
- [19] Smith AM, Chapman CE, Deslandes M, Langlais J-S, Thibodeau M-P. Role of friction and tangential force variation in the subjective scaling of tactile roughness. *Exp Brain Res* 2002;144:211–23.
- [20] Libouton X, Barbier O, Plaghki L, Thonnard J-L. Tactile roughness discrimination threshold is unrelated to tactile spatial acuity. *Behav Brain Res* 2010;208(2):473–8.
- [21] Astarloa A, Lazaro J, Bidarte U, Jimenez J, Zuloaga A. FPGA technology for multi-axis control systems. *Mechatronics* 2009;19(2):258–68.
- [22] Looft FJ, Williams WJ. On-line receptive field mapping of cutaneous receptors. *IEEE Trans Biomed Eng* 1979;26:350–6.
- [23] Byrne J. A feedback controlled stimulator that delivers controlled displacements or forces to cutaneous mechanoreceptors. *IEEE Trans Biomed Eng* 1975;22:66–9.
- [24] Schneider W, Slugg RM, Turnquist BP, Meyer RA, Campbell JN. An electromechanical stimulator system for neurophysiological and psychophysical studies of pain. *J Neurosci Methods* 1995;60:61–8.
- [25] Wagner CR, Lederman SJ, Howe RD. A tactile shape display using RC Servomotors. In: Proc. 2002 IEEE symposium on haptic interfaces for virtual environment and teleoperator systems, March 24–25, 2002, Orlando, USA. p. 354–5.
- [26] Pasquero J, Luk J, Lévesque V, Wang Q, Hayward V, MacLean KE. Haptically enabled handheld information display with distributed tactile transducer. *IEEE Trans Multimedia* 2007;9(4):746–53.
- [27] Iskakova R, Albu-Schaeffer A, Schedl M, Hirzinger G, Lopota V. Influence of sensor quantization on the control performance of robotics actuators. In: Proc. 2007 IEEE/RSJ international conference on intelligent robots and systems, October 29–November 2, 2007, San Diego, CA, USA. p. 1085–92.
- [28] Serina ER, Mote CD, Rempel D. Force response of the fingertip pulp to repeated compression – effects of loading rate, loading angle and anthropometry. *J Biomech* 1997;30(10):1035–40.
- [29] Pawluk DTV, Howe RD. Dynamic lumped element response of the human fingerpad. *J Biomech Eng* 1999;121:178–83.
- [30] Nakazawa N, Ikeura R, Inooka H. Characteristics of human fingertips in the shearing direction. *Biol Cybern* 2000;82(3):207–14.
- [31] Vallbo AB, Johansson RS. Properties of cutaneous mechanoreceptors in the human hand related to touch sensation. *Human Neurobiol* 1984;3:3–14.
- [32] Chambers MR, Andres KH, Von Duering M, Iggo A. The structure and function of the slowly adapting type II mechanoreceptor in hairy skin. *Quart J Exp Physiol* 1972;57:417–45.
- [33] Oddo CM, Beccai L, Felder M, Giovacchini F, Carrozza MC. Artificial roughness encoding with a bio-inspired MEMS-based tactile sensor array. *Sensors* 2009;9:3161–83.
- [34] Romo R, Ruiz S, Crespo P, Hsiao SS. A tactile stimulator for studying motion processing in the somatic sensory system of primates. *J Neurosci Methods* 1993;46:139–46.

Article

## Artificial Roughness Encoding with a Bio-inspired MEMS-based Tactile Sensor Array

Calogero Maria Oddo <sup>1</sup>, Lucia Beccai <sup>1,\*</sup>, Martin Felder <sup>2</sup>, Francesco Giovacchini <sup>1</sup> and Maria Chiara Carrozza <sup>1</sup>

<sup>1</sup> ARTS Lab - Advanced Robotics Technology and Systems Laboratory, Scuola Superiore Sant'Anna, Polo Sant'Anna Valdera / Viale Rinaldo Piaggio 34, 56025 Pontedera, PI, Italy; E-Mails: oddoc@sssup.it (C.M. O.); f.giovacchini@arts.sssup.it (F. G.); carrozza@sssup.it (M.C. C.)

<sup>2</sup> Informatics - Robotics & Embedded Systems, Technical University of Munich / 85748 Garching b. Muenchen, Germany; E-mail: felder@in.tum.de (M. F.)

\* Author to whom correspondence should be addressed; E-Mails: l.beccai@sssup.it; Tel.: +3-905-088 3064; Fax: +3-905-088-3101/497

Received: 3 March 2009; in revised form: 22 April 2009 / Accepted: 24 April 2009 /

Published: 27 April 2009

---

**Abstract:** A compliant 2x2 tactile sensor array was developed and investigated for roughness encoding. State of the art cross shape 3D MEMS sensors were integrated with polymeric packaging providing in total 16 sensitive elements to external mechanical stimuli in an area of about 20 mm<sup>2</sup>, similarly to the SA1 innervation density in humans. Experimental analysis of the bio-inspired tactile sensor array was performed by using ridged surfaces, with spatial periods from 2.6 mm to 4.1 mm, which were indented with regulated 1N normal force and stroked at constant sliding velocity from 15 mm/s to 48 mm/s. A repeatable and expected frequency shift of the sensor outputs depending on the applied stimulus and on its scanning velocity was observed between 3.66 Hz and 18.46 Hz with an overall maximum error of 1.7%. The tactile sensor could also perform contact imaging during static stimulus indentation. The experiments demonstrated the suitability of this approach for the design of a roughness encoding tactile sensor for an artificial fingerpad.

**Keywords:** MEMS tactile sensor array; bio-inspired sensor; roughness encoding; dynamic touch; static contact imaging.

---

## 1. Introduction

Artificial tactile sensors which aim to mimic human discrimination capabilities should encode information correlated with the stimulus spatial features, with its motion dynamics as well as with contact mechanics. Roughness is a fundamental feature for texture perception [1,2,3], which has been associated with the spatial modulation of the used stimuli (i.e. “surface coarseness”) [4]. In experiments on human perception of tactile roughness the type of used surfaces often have patterns (gratings or rising dots) with features that can be independently varied in size and spacing [5,6]. This way, unlike for natural surfaces in which the spatial pattern features vary randomly, the physical characteristics of the explored surface, on which roughness perception is based, can be studied and identified.

The physical determinant of perceived roughness is not yet fully understood [2,4] and there is a varied set of spatial features that should be taken into account for studies on roughness perception (e.g., using ridged stimuli: groove width, ridge width, ridge orientation, ridge height, material compliance, surface lubrication and fine finishing, etc.). In human psychophysical experiments, for example, some groups highlighted the presence of a relatively narrow region where the sense of roughness increases together with the groove width of ridged stimuli, followed by a flattened perception in case of very coarse gratings (up to 8.5 mm of groove width) [7]. In parallel to this, using embossed dots, some researchers presented monotonic functions of roughness and dots spacing [5], while an inverse “U” shape was shown in [8].

Considering dynamic exploration of extremely fine textures, various researchers showed that humans can detect even up to microtextures [9], highlighting the role of fingerprint ridges as vibration promoters [10] and considering the Pacinian Corpuscles as vibration detectors [11]. Some groups joined the Katz’s *duplex theory* considering vibrations useful for revealing fine forms, and a spatial mechanism (i.e. the static image of the contact between the texture and the finger) as the basis for coarse surfaces roughness perception [12]. Importantly, in the last decade, other groups proposed and gave evidence to a unified peripheral neural mechanism highlighting the role of SA1 afferents with respect to the other mechanoreceptors [13,1].

The understanding of the neural mechanisms underlying roughness encoding is in progress, however evidence was given to the fact that temporal frequency changes of tactile information play a major role in roughness perception in humans [5]. Finite element analyses using human finger model during dynamic touch showed that spatial information of the textured surface are related to temporal frequency changes at the position of tactile receptors [14]. In touch activities, if humans have the ability to estimate somehow the relative hand velocity  $v$  between the textured surface and the exploring finger, the spatial period  $\Delta p$  of the surface can be perceived by detecting the temporal frequency of the vibration [15], such that:

$$f = \frac{v}{\Delta p} \quad (1)$$

The findings and debate of researchers on human touch are directly linked with the development of artificial tactile sensors, which is one of the chief challenges in robotics. Many technologies have been investigated and can be analysed in comprehensive reviews on the topic [16,17]. For the above

reasons, with regards to the many reported efforts to reproduce human capability to detect texture, the developed sensors were mainly based on the analysis of the vibration gathered during dynamic exploration or on the contact imaging [18] by means of static indentation. An approach was to develop a finger-like multilayered texture sensor integrating five strain gauges for identifying the difference in roughness, softness and frictional properties of various materials [19]. Employing such device, the texture information of a surface was quantitatively detected by estimating the vibrational frequency excited by indenting and sliding a periodic stimulus with spatial wavelength in the millimeters range [20]. A similar method was previously shown in [21] for finer surfaces. Another noticeable solution was presented in [22], where a spatial filter function was used adaptively depending on sensor-stimulus relative motion parameters, thus pointing out the centrality of a spatio-temporal approach in tactile sensing. Hosoda and colleagues developed a soft fingertip with randomly distributed strain gauges and PVDF films at different depths [23], allowing for discrimination of five different types of materials. Other recent biomimetic fingertips focused on the transduction properties, which could be either acoustic [24] or electrical [25], of the packaging materials for converting the surface features of the explored textures into recorded vibrations. Finally, one of the most recent developments is represented by a high-resolution thin film sensor built by Maheshwari and Saraf [26] by means of a layer-by-layer self-assembly technique, that responds to an applied force either with electroluminescent emissions or with a change in current density. A charge-coupled device (CCD) camera was used to capture the electroluminescent emissions from the sensor providing imaging stress distribution with spatial resolution of about 40  $\mu\text{m}$ .

In this work, the investigated artificial tactile sensor integrates a MEMS array having a number of sensing elements (16 channels in about 20  $\text{mm}^2$ , i.e. 0.8 channels/ $\text{mm}^2$ ) similar to the innervation density of *Slowly Adapting type 1* (SA1) mechanoreceptors in the hand (about 1 unit/ $\text{mm}^2$ ) [27]. The technological approach is based on a 3D MEMS core unit [28] with a soft and compliant packaging. As previously demonstrated, the microsensor can be integrated with a packaging architecture resulting in a robust and compliant tactile sensor for application in artificial hands, while sensitive enough to detect slip events, showing that silicon based tactile sensors can go beyond laboratory practice [29].

In the long term, the presented artificial approach aims, on one side, at developing a device capable of mimicking the texture discrimination properties of the human hand and which can be integrated in an anthropomorphic artificial hand, while on the other it is intended as an artificial model to be used as a test bench for neuroscientific hypotheses describing the mechanisms of roughness perception. This long term objective gets inspiration from the above mentioned work of Yoshioka and colleagues [13], in which it was shown that spatial variation in the firing rates of SA1 units-only can account for roughness perception even when the explored texture is finer than the SA1 innervation density.

In order to go in such direction, the specific objective of the current work was to gather the vibrations which are supposed to be the basis for the encoding of roughness in dynamic touch, as well as to perform static imaging of the contact with the same array of tactile sensors. The present experimental analysis evaluates whether there is a substantial processing advantage in using more than one output of the array for finding out the common principal frequency produced during dynamic stimulus presentation. This way, by merging the estimation of the common frequency detected by more than one sensor unit together with the knowledge of the sliding velocity of the applied stimulus, texture related features could be extracted. The suitability of the sensor for both static contact imaging

and vibration detection was evaluated by means of an experimental protocol containing both motionless and dynamic contact phases involving forces and velocities in the range of those used by humans in discriminative touch.

The paper is organized as follows. In Section 2 the design of the sensor array is shown, describing the elementary MEMS unit, the packaging and the readout electronics. In Section 3 the experimental protocol and the used data analysis methods are presented. Section 4 shows the experimentation with the array prototype, which has been carried out with ridged stimuli sliding at constant velocity and regulated normal force after and before a static indentation phase. Finally, results are discussed in Section 5 and future work insights are given in the Conclusions.

## 2. Materials

### 2.1. MEMS Sensor Array

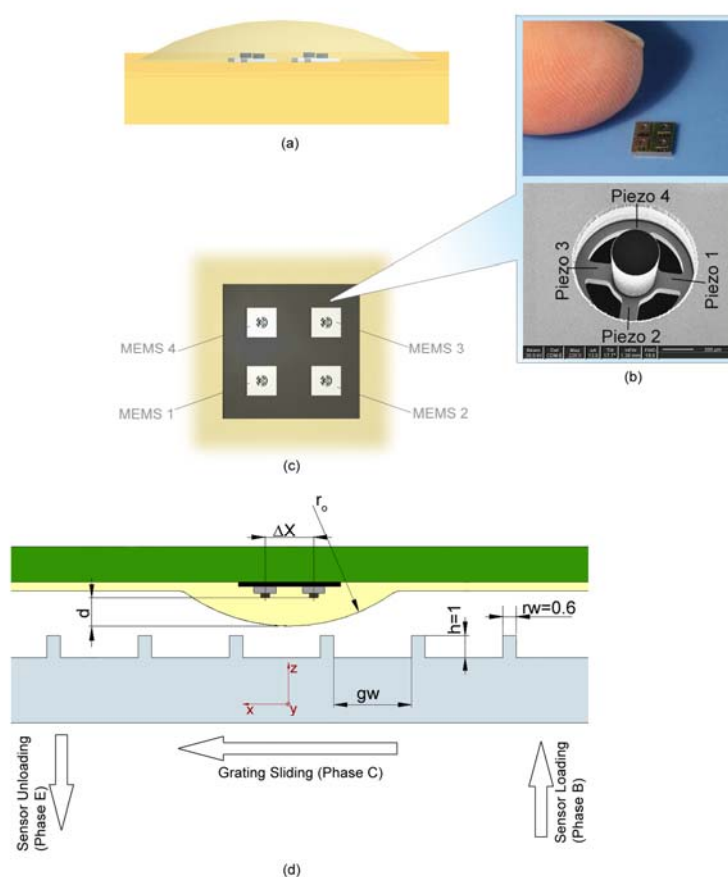
The elementary cell of the array was the 3D MEMS sensor described in [28], shown in Figure 1, which has a high aspect ratio 3D structure ( $1.5\text{ mm}\times 1.5\text{ mm}\times 625\text{ }\mu\text{m}$ ). In the bare configuration of the sensor, the cylindrical mesa, located at the center of the cross-shape tethers, transmits an externally applied force to the sensor inducing stresses in the four tethers where four p-type piezoresistors are implanted. The fractional change in resistance  $\Delta R/R$  of each piezoresistor of the microsensor is proportional to the longitudinal and the transversal stress components, while the design of the sensor is such that the transversal stress component in the implanted piezoresistors is neglectable with respect to the longitudinal one. In the current experimentation four microsensors were bonded on a silicon carrier chip connecting the 9 NiAu pads of each microsensor by means of a micro-soldering paste by using flip-chip bonding method. As stated in the Introduction in this study attention was paid in developing an array with a density of sensing elements that could be compared to the innervation density of Slowly Adapting type 1 (SA1) mechanoreceptors in the hand ( $\approx 1\text{ unit}/\text{mm}^2$ ) [27]. The tactile sensor array, depicted in Figure 1, had 16 channels as total tactile sensor outputs. It had a pitch of 2.3 mm (indicated by  $\Delta X$  in Figure 1) for technological reasons, i.e. mainly because of the operation room needed for the flip-chip bonding method and layout of the carrier chip. The resulting area of the sensing array was of  $21.16\text{ mm}^2$  inscribing each MEMS unit inside a square of area  $5.29\text{ mm}^2$ . The silicon carrier chip was wire bonded by means of  $25\text{ }\mu\text{m}$  Al wires to a Printed Circuit Board (PCB) in order to connect the array to the external instrumentation. The perimeter of the array was secured with a two component epoxy glue in order to protect the wire bonding and to improve the stability of the silicon carrier chip.

The MEMS tactile array was packaged with a synthetic material (as explained in the next section) that mechanically filters the external applied load and creates a distribution of stresses in the new configuration of microsensor and packaging, with respect to the externally applied stimulus. For the investigation reported in the present work, the outputs of the piezoresistors (i.e. the sensing elements) have been analyzed directly for their dynamic behaviour, whilst they have not been used to extract the three components of an applied force. This avoided to address the calibration of each MEMS before packaging, as done with this device in [30], or after packaging as for example performed in [31] with a different sensor together with the introduction of an analytical model for point contact loads.

## 2.2. Packaging

The packaging of the bare silicon sensors array was developed so that the resulting tactile sensor could have compliance and softness characteristics inspired to those of the human fingerpad. Previous investigations for the application in an anthropomorphic artificial hand were considered, in which it was demonstrated that it is possible to integrate the silicon microsensor in a soft and compliant, but robust packaging [29]. In particular, the round shape of the packaging of the array was chosen based on the anthropomorphic features of the distal phalanx of the cybernetic hand CyberHand [32,33]. In parallel, a suitable curved geometry was identified in order to increase the portion of load gathered by the sensors in case of contact with a planar textured surface, as pointed out in [34]. As shown in Figure 1, the dimensioning parameters for the packaging where  $r_0$  and  $d$ , which were set to 8 mm and 1.3 mm, respectively, for obtaining adequate sensitivity as well as partially overlapping sensing ranges between *nearest-neighbour* MEMS units and acceptable low-pass spatial filtering effect [35] with respect to the used stimuli.

**Figure 1.** (a) 3D design of the tactile sensor array. (b) Top: The 2×2 MEMS array compared with human finger; bottom: a FIB image of the MEMS sensor. (c) Top view of the sensor array. (d) Schematic showing a cross section of packaging design and grating dimensions. Groove width  $g_w$  ranged from 2.0 mm to 3.5 mm (see Table1), while ridge height  $h$  and ridge width  $r_w$  had fixed values indicated (in mm) in figure. The phases of the experimental protocol are also indicated.



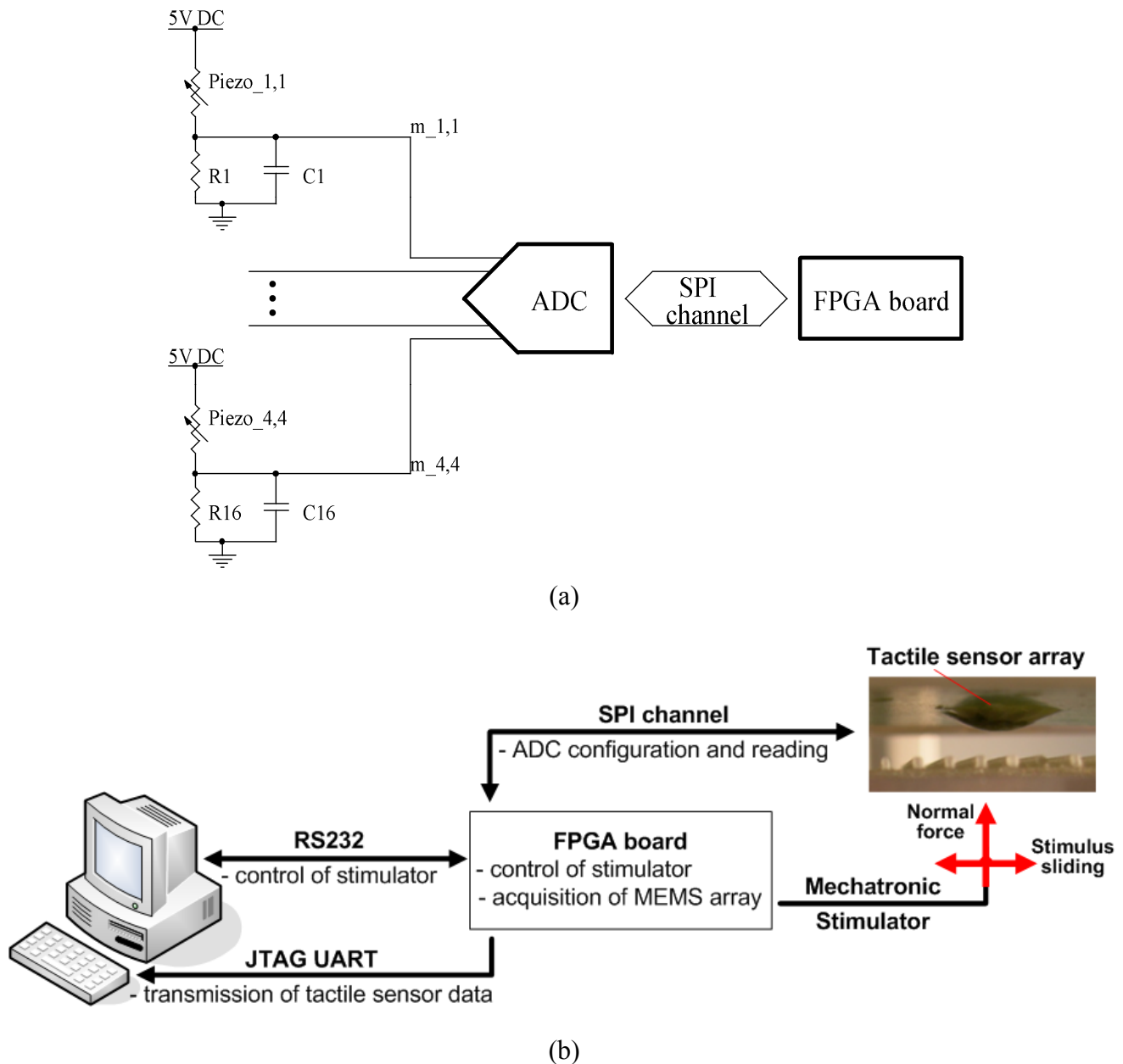
The 2×2 array was packaged with polyurethane (Poly 74-40, PolyTek, USA) and an outer thin protective layer of polyimide having thickness of 0.05 mm and shore A 82 hardness (ST1882, Stevens Urethanes, USA) in order to prevent the inner packaging from wearing. In fact, preliminary trials demonstrated that the ridged stimuli can damage the packaging of the array. In the present study, a type of polyurethane with shore A 40 hardness (instead of the previous shore A 45 [29]) was used attempting a step forward in human finger mimicry. Moulds hosting the array were built with rapid prototyping resin using a 3D printer, and the liquid part A and part B were poured immediately after being mixed and degassed. The polyimide layer was applied after polyurethane curing and showed excellent adhesion provided that the air between the cover and the thin sheet was removed. Moreover, the protective layer was secured by means of a frame also built in rapid prototyping resin.

### 2.3. Readout Electronics

Each piezoresistor was connected in series to a surface mount resistor (R1 ... R16) located on the designed PCB, as shown in Figure 2(a). The values of R1 ... R16 were all set to 820 Ω, which is close to the mean resistance of the piezoresistors of the 2×2 array, thus almost achieving sensitivity maximization from the quarter bridge voltage divider. The used quarter bridge topology produces a variation of the acquired voltage proportional to the fractional change in resistance of each piezoresistor. Capacitors (C1 ... C16, all having capacitance of 1 μF) were placed in parallel to each completing resistor, resulting in a low-pass single pole filter at about 390 Hz (i.e.  $\frac{1}{2\pi(R_{piezo} // R)C} \approx \frac{1}{\pi R_{piezo} C}$ ) for reducing the noise level at frequencies outside the band of interest.

The piezoresistor-resistor arms were supplied by means of a 5V DC regulated voltage, and the node between each piezoresistor and the completing resistor was directly acquired without pre-amplification by means of a 16-channel 24-bit Analog to Digital Converter (ADS1258, Texas Instruments). Each channel was sampled at a frequency of 241 Hz, which could be varied via software up to 24.7 kHz selecting a subset of channels and changing the conversion options of the used ADC. Considering the chosen sampling frequency and the cut-off of the RC low-pass filter, the fulfillment of the Nyquist theorem for aliasing avoidance mainly relied on the expected baseband properties of the gathered signals (refer to Figures 4 and 5 in the following for a qualitative validation of such assumption). Digital data transfer between the ADC and the acquisition system was performed by means of SPI protocol. The data acquisition system was based on Field Programmable Gate Array (FPGA) technology (CycloneII, Altera) and had a 64 bit hardware timer running at 50 MHz, so that the acquisition of each channel had a time reference with resolution of 20 ns and practically unlimited length. Acquired data was buffered by a soft-core processor (NiosII, Altera) instantiated onboard the FPGA and transmitted at the end of each session to a Personal Computer with JTAG UART protocol, as shown in Figure 2(b). The storage of data was allowed within the Nios II Integrated Development Environment by enabling the option “Filing System to open files on the PC” in the Altera Host Based File System.

**Figure 2.** Schematic view of the readout electronics (a). Block diagram of the overall experimental setup (b).



### 3. Methods

#### 3.1. Experimental Protocol

The packaged array was mounted on a mechatronic tactile stimulator capable of indenting the sensor with force feedback control and stroking a stimulus over it with precise position control. The configuration of the array/stimulus interface and the experimental protocol are reported in Figure 1(d) while Figure 2(b) shows a diagram of the overall experimental set-up.

Four types of stimuli were built with rapid prototyping resin material, with spatial periods  $\Delta p$  varying from a minimum of 2.6 mm to a maximum of 4.1 mm, as detailed in Table 1.

In order to evaluate whether the sensor outputs could be processed for automatically recognizing the instant of contact, data acquisition started prior to the phase during which the stimulus contacted the sensor array (phase A). In a second phase of the experiment, the stimulator was commanded to contact the tactile sensor (phase B). The sensor array was loaded setting at 1 N the reference of the normal force feedback controller given that such value is in the middle of the force range used by humans in fine forms discrimination during active dynamic touch experience [36].

The loading resulted in a contact spike in the signals gathered from the MEMS array. The target force level was held for 1 s. After that, the sliding of stimulus started (phase C) along the  $x$ -axis [piezo1-piezo3 direction of Figure 1(b)] while maintaining enabled the force feedback controller, thus obtaining a stimulation with normal force held at 1 N and tangential force depending on the contact mechanics and on the motion dynamics.

Three different translational velocities (15 mm/s, 30 mm/s and 48 mm/s) of the stimulus were chosen for overlapping with the range commonly used in related neurophysiologic studies [37]. The direction of motion (along the  $x$ -axis as shown in Figure 1) was always the same, as well as the sign of velocity and the starting absolute position. The sliding was applied for 60 mm, providing dynamic stimulations of 4 s, 2 s or 1.25 s depending on the applied velocity. At the end of the sliding motion there was a steady state of 1 s at 1 N (phase D) and, finally, the tactile sensor array was unloaded (phase E). The initial and final static phases of the protocol were performed with repeatable conditions in order to enable analyses on static imaging capabilities of the sensor in addition to the dynamic behaviour investigation.

### 3.2. Common Frequency Detection

#### Preprocessing

During the sliding of the periodic ridged stimulus over the packaged sensor array (phase C; see Figure 1), the output signal  $m_{i,j}$  from the  $i$ -th piezoresistor of the  $j$ -th MEMS unit of the  $2 \times 2$  array clearly showed a principal frequency component  $f$ , while the contact and the unloading operations could be revealed by the first spike and the last step in the outputs, as shown in Figure 3.

Defining as  $v$  the sliding velocity of the grating, the relationship reported in Equation (1) is expected for  $f$ .

Referring to Figure 1 (d) and Table 1, the spatial period  $\Delta p_k$  of the of the  $k$ -th grating is given by the sum of the groove width and of the ridge width, thus:  $\Delta p_k = gw_k + rw_k$ .

**Table 1.** Grating groove width ( $gw$ ) and spatial period ( $\Delta p$ ) with respect to the sample type. Ridge width ( $rw$ ) was fixed to 0.6 mm for all types.

Grating number	1	2	3	4
gw (mm)	2.0	2.5	3.0	3.5
$\Delta p$ (mm)	2.6	3.1	3.6	4.1

In order to be able to detect the common frequency between all the fitting curves of the output signals, attention was paid in respecting the Nyquist condition for the sampling frequency ( $f < \frac{f_c}{2}$ )

with a safety factor, such that at least 13 samples per period were guaranteed even in the worst case stimulation conditions (i.e. minimum grating periodicity  $\Delta p_k$  and maximum speed of the stimulus, as shown in Table 2).

**Table 2.** Expected principal frequency from sensor outputs depending on the spatial periodicity ( $\Delta p$ ) and on the sliding velocity ( $v$ ) of the applied grating.

Expected frequency vs. $\Delta p$ and $v$	$\Delta p = 4.1$ mm	$\Delta p = 3.6$ mm	$\Delta p = 3.1$ mm	$\Delta p = 2.6$ mm
$v = 15$ mm/s	3.66 Hz	4.17 Hz	4.84 Hz	5.77 Hz
$v = 30$ mm/s	7.32 Hz	8.33 Hz	9.68 Hz	11.54 Hz
$v = 48$ mm/s	11.71 Hz (not tested)	13.33 Hz (not tested)	15.48 Hz	18.46 Hz

To ensure data quality, a simple procedure was implemented to remove prior to processing data that was not useful for the dynamic analysis of the recorded signals. The redundancy in the system was used by jointly observing the outputs of two piezoresistors from different MEMS sensors. Since the contact spike mentioned in Section 3.1 was less pronounced for some piezoresistors than for others, the best defined spike was extracted from either one of the two time series.

To this end:

$$s = \arg \max_j (\max(m_{i,j}(t \leq t_{init})) - \text{median}(m_{i,j}(t \leq t_{init}))) \quad (2)$$

selects the sensor  $s$  whose data was used for initial spike detection. Here,  $t_{init} = 0.8$ s is a time threshold before which the spike is expected to appear. The location of the spike  $t_{spike}$  is then detected by:

$$t_{spike} = \arg \max_t (m_{i,s}(t)) \quad (3)$$

and used for both time series. According to the measurement protocol, the movement starts at  $t = 1.0$ s after the spike, and ends after 60mm of stimulus have been traversed. The effective sample length was set to  $L_{eff} = 55$ mm for pre-processing operations, in order to avoid introducing invalid data in case of inherent timing variations. The start and the end of the valid range thus were:

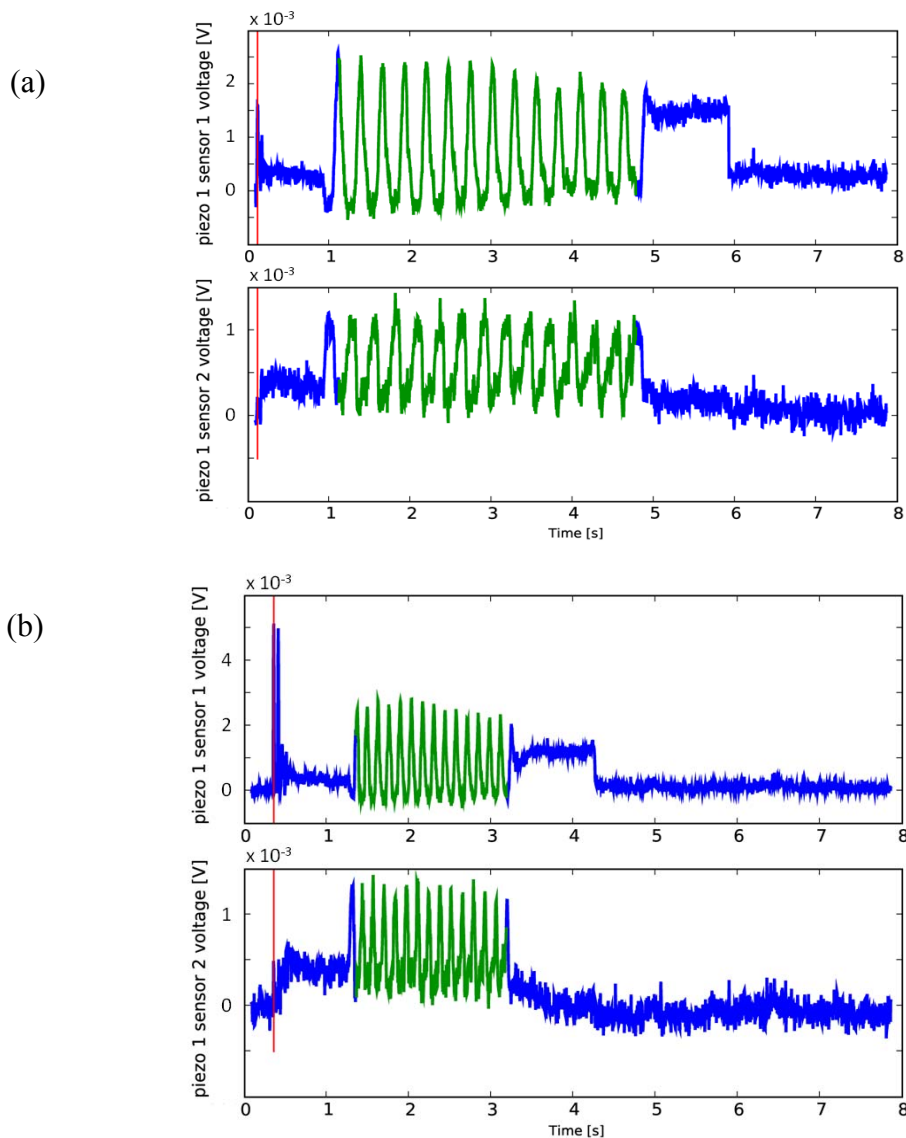
$$t_{start} = t_{spike} + \Delta t \quad (4)$$

$$t_{end} = t_{start} + \frac{L_{eff}}{v} \quad (5)$$

with  $v$  denoting the sliding velocity of the grating.

Ten different combinations of sliding velocity and grating periodicity were formed, as detailed in Section 4, Table 3. Four measurement runs of the sensor array were carried out for each combination, yielding a total of 40 runs. In the following, these data series are referred by number, with run 1 to 4 belonging to combination one, run 5 to 8 to combination 2 and so forth. Figure 3 shows typical outputs of the procedure, which performed flawlessly on all 40 data sets.

**Figure 3.** Automatic contact detection applying Equations (2) and (3) and selection of the stimulus sliding phase (phase C, indicated in green in the plots) by means of Equations (4) and (5) using piezoresistor 1 of MEMS sensors 1 and 2 of the array. The plots refer to data series 12 (a) and 16 (b), where a grating of 4.1 mm spatial periodicity was applied with translational speeds of 15 mm/s and 30 mm/s, respectively, according to Tables 2 and 3. The red line marks the detected spike, blue data are cropped for common frequency analysis.



An optional pre-processing step consisted in chopping the time series into time windows of size  $w$ . In most practical applications with gradually or abruptly changing surface characteristics, a trade-off will have to be found between the response delay given by the finite window size, and the accuracy of retrieval. Here this is investigated with non-overlapping windows to minimize redundancy, while in practice one could probably use strongly overlapping windows and thus higher update rates, if enough computation power is available.

## Fast Fourier Transform

The most important prerequisite for advanced use of the developed sensor array was to establish a robust retrieval procedure for the fundamental spatio-temporal frequency of the system. As a first step, the two selected piezoresistors voltage time series underwent a Fast Fourier Transform (FFT) separately, to find a first guess for the fundamental frequency  $f$ , namely at the maximum of the periodogram. Note that by selecting the maximum peak as the fundamental frequency using naïve Fourier analysis, a discretization error of up to:

$$\frac{1}{2} \Delta f = \frac{1}{2} \frac{f_C}{N} = \frac{1}{2w} \quad (6)$$

occurred, where  $f_C = 241$  Hz was the channel sampling frequency and  $N$  the number of data points in the time window. The first guess magnitude of the fundamental oscillation was also difficult to read from the spectrum, because it would have to include contributions from the slopes surrounding the central peak. The solutions implemented in the following overcame this inconvenience. While it would certainly improve accuracy to average the contributions surrounding the fundamental frequency peak and/or to take into account overtones that often can be seen in the spectra, this procedure would involve several heuristic decisions about thresholds and boundaries.

## Least squares fitting

In order to overcome to the discretization problem mentioned above, during dynamic stimulation each sensor output was fitted with a sine wave by using Equation (7):

$$m_{i,j} \approx B_{i,j} + A_{i,j} \cdot \sin(2\pi f(t - t_{i,j})) \quad (7)$$

where:

- $m_{i,j}$  is the signal obtained from the  $i$ -th piezoresistor of the  $j$ -th MEMS unit of the  $2 \times 2$  array;
- $B_{i,j}$  and  $A_{i,j}$  are the offset and the amplitude of the sine waves used for fitting each  $m_{i,j}$ ;
- $t_{i,j}$  is an offset time which well fits the sine waves with data acquired during the exploration phase;
- $f$  is the common principal frequency coming out from the output signals using the analysis described below; observe that  $f$  is expected to be the same for all the outputs of the sensor array.

Therefore, a simpler second step was chosen, where a function of the form:

$$h(t, f, A_{i,j}, B_{i,j}, t_{i,j}) = B_{i,j} + A_{i,j} \sin(2\pi f(t - t_{i,j})) \quad (8)$$

was defined to be fitted to each channel's time domain data (see also Equation (7)). This was done by performing a gradient descent on the error function (considering piezoresistor 1 of MEMS sensors 1 and 2) overall the runs of a same combination of grating and velocity:

$$E = \sum_k \left( \left( h(t_k, f, A_{1,1}, B_{1,1}, t_{1,1}) - m_{1,1}(t_k) \right)^2 + \left( h(t_k, f, A_{1,2}, B_{1,2}, t_{1,2}) - m_{1,2}(t_k) \right)^2 \right) \quad (9)$$

with  $k$  running over all data points in the chosen time window,  $t_k$  the sampling instants and  $m_{i,j}(t_k)$  the signal obtained from piezoresistor  $i$  of unit  $j$  of the array. Thus there were seven fitting parameters:

$A_{1,1}$ ,  $A_{1,2}$ ,  $B_{1,1}$ ,  $B_{1,2}$ ,  $t_{1,1}$ ,  $t_{1,2}$ , and  $f$ . The purpose of this procedure was to both remove the discretization errors of the FFT, and introduce a priori information, because all the sensors were dragged over the same physical surface at the same speed, and then the same fundamental frequency was expected. It is possible to extend this method to include all valid piezoresistor readings from all sensors, if additional accuracy is required. To test this retrieval procedure, data from all measurement series was processed, averaging over the four measurements of each configuration of grating width and velocity. The data window width  $w$  was varied from 0.2 s to 1.0 s. For each  $w$ , the start of the time window was stepped through from  $t_{start}$  to  $t_{end-w}$  in steps of 50 ms.

### 3.3. Error Parameters and Repeatability

The RMS error between the estimated frequency and the nominal one was used as a quality index for comparing the FFT results with the fitting procedure described above, i.e.:

$$\varepsilon_{method}(C, w) = \sqrt{\frac{1}{n \cdot q} \sum_{n,q} (f_{estimated}(n, q) - f_{nominal}(C))^2} \quad (10)$$

where the subscript *method* may be FFT or LSq depending on the usage of Naïve Fourier analysis or time domain least squares fit, respectively, for estimating the principal frequency. Moreover,  $n$  loops over all time windows in a measurement run, and  $q$  over all four runs belonging to parameter combination  $C$  and window size  $w$ . Also, a relative error parameter was used by dividing the RMS error of Equation (10) by the nominal frequency  $f_{nominal}(C)$  and expressing the result as a percentage.

Repeatability was checked by pairwise cross-correlation of the measurement timeseries of piezoresistor  $i$  of MEMS unit  $j$  during the stimulus sliding phase (cf. Figure 3) of the four runs sharing one parameter combination  $C$ , and averaging the results. Hence, with  $l$  and  $p$  denoting two of those four runs:

$$r_{i,j}(C) = \frac{1}{12} \sum_{l \neq p} \left( \frac{1}{k-1} \sum_{t=t_a}^{t_{a+k}} \left( \frac{m_{i,j,l}(t) - \bar{m}_{i,j,l}}{\sigma_{i,j,l}} \frac{m_{i,j,p}(t) - \bar{m}_{i,j,p}}{\sigma_{i,j,p}} \right) \right) \quad (11)$$

is the average Pearson cross-correlation coefficient. Measurements  $m$  had to be shifted by up to half a cycle relative to each other to account for phase differences due to the lack of synchronization between the starting of data saving and the starting of stimulation between different runs. Therefore, the inner sum runs over the remaining overlap region  $t_a$  to  $t_{a+k}$ , for which the mean signal  $\bar{m}$  and the standard deviation  $\sigma$  are calculated.

## 4. Experimental Results

This Section reports the experimental results obtained indenting and sliding the used ridged stimuli according to the parameters given in Table 2. The first part reports the preliminary naïve Fourier analysis which was performed in the process for establishing a robust retrieval procedure for the principal frequency induced by the grating spatial periodicity and sliding speed. Those preliminary results, as expected, were affected by considerable and oscillatory discretization errors depending on the chosen observation window. The second part shows the results with the proposed least squares

fitting procedure, which guaranteed very high accuracy and quite fast error convergence increasing the observation window. Furthermore, the results with the least squares fitting are compared with the Fast Fourier Transform ones. Qualitative and quantitative evidence of data repeatability is given in the third part. Finally, the last subsection concerns results on the static imaging capabilities as another major feature of the designed sensor.

### Fast Fourier Transform

The preliminary naïve Fourier analysis showed a considerable discretization error, according to Equation (6). This error can be quite significant for small windows, since the fundamental frequencies considered lie in the order of 1 to 10 Hz in this experiment. Figure 4 shows a typical Fourier analysis covering the full range of a sliding measurement (phase C, depicted in Figure 1). As a rather extreme example, the results using FFT with a 0.35 s time window analysis can be seen in Figure 5.

**Figure 4.** Naïve Fourier analysis (lower plot) over the full length of a typical dataset considering a single channel of a sensor unit of the array (upper plot). The maximum Fourier peak is selected as a frequency estimate, which leads to a discretization error of up to half a bar width (cf. Equation (6)) if the true frequency happens to lie in between two bars.

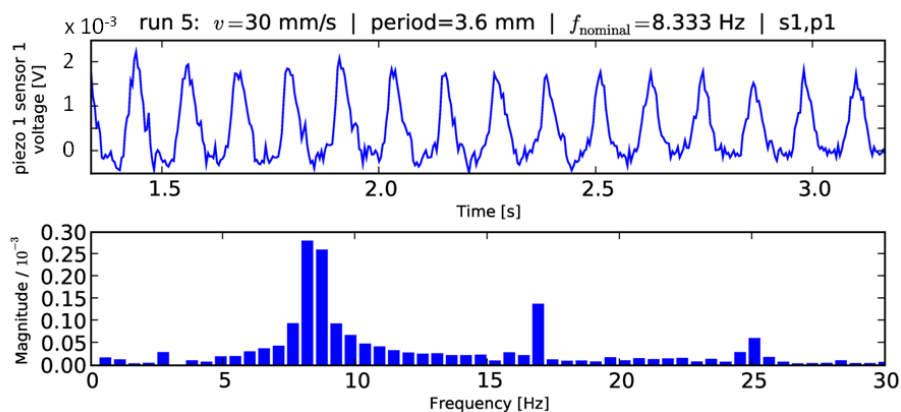
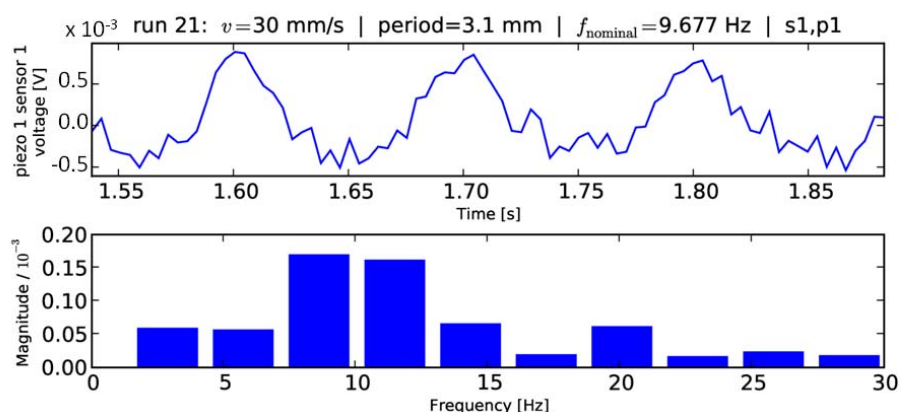


**Figure 5.** As Figure 4, but for a different data series and a narrower window of 0.35 s, showing higher discretization error with naïve Fourier analysis.



## Least Squares Fitting

Figure 6 shows a graphical representation of the fitting procedure using the maximum allowed time window for the considered run. Such figure clearly shows the retrieval of the principal frequency coming out from the used combination of stimulation parameters. The frequency estimate errors, defined in Section 3.3 for comparing the FFT results with the fitting procedure described at the end of Section 3.2, are shown in Figure 7 and Table 3. Results from all windows and experiments were averaged for each point in the graphs.

**Figure 6.** Result of the least squares fitting procedure considering piezoresistor 1 of MEMS sensor 1 (blue line) and piezoresistor 1 of MEMS sensor 2 (red line, shifted for easing the graphical representation) with a maximum width time window. The plot refers to data series 20, where a grating of 3.1 mm spatial periodicity was applied with translational speed of 15 mm/s, according to Tables 2 and 3.

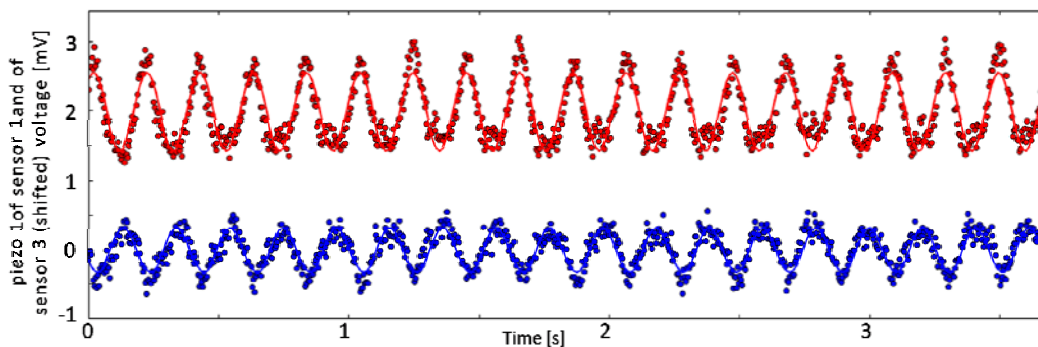


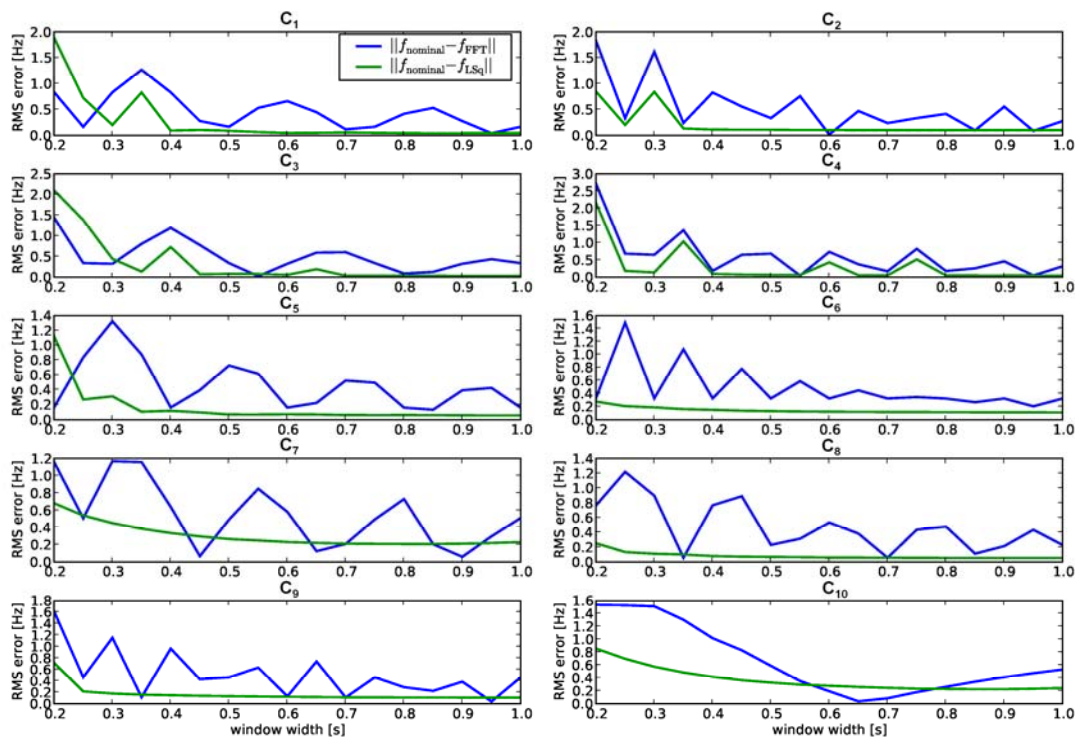
**Table 3.** Average RMS errors obtained by FFT ( $\epsilon_{\text{FFT}}$ ) and least square fit estimation ( $\epsilon_{\text{LSq}}$ ) using the full data range. The top row indicates the expected frequency,  $f_{\text{nominal}}$ , depending on the measurement run. The combination  $C$  of spatial period  $\Delta p$  and velocity  $v$  associated to each measurement run is also indicated.

	Measurement run									
	1-4	5-8	9-12	13-16	17-20	21-24	25-28	29-32	33-36	37-40
$f_{\text{nominal}}$ [Hz]	4.17	8.33	3.66	7.32	4.84	9.68	15.48	5.77	11.54	18.46
$C$	$C_1$	$C_2$	$C_3$	$C_4$	$C_5$	$C_6$	$C_7$	$C_8$	$C_9$	$C_{10}$
$\Delta p$ [mm]	3.6	3.6	4.1	4.1	3.1	3.1	3.1	2.6	2.6	2.6
$v$ [mm/s]	15	30	15	30	15	30	48	15	30	48
	piezo <sub>1,1</sub> vs. piezo <sub>2,1</sub>									
$\epsilon_{\text{FFT}}$	0.072	0.135	0.113	0.182	0.078	0.168	0.286	0.033	0.053	0.063
[%]	1.72	1.62	3.1	2.49	1.62	1.73	1.85	0.57	0.46	0.34
$\epsilon_{\text{LSq}}$	0.038	0.105	0.027	0.058	0.052	0.123	0.257	0.053	0.124	0.272
[%]	0.91	1.26	0.73	0.79	1.08	1.27	1.66	0.93	1.07	1.47

Table 3. Cont.

piezo <sub>4,1</sub> vs. piezo <sub>2,1</sub>										
$\epsilon_{\text{FFT}}$	0.072	0.135	0.1	0.152	0.075	0.165	0.257	0.036	0.059	0.189
[%]	1.72	1.61	2.74	2.08	1.56	1.7	1.66	0.62	0.52	1.03
$\epsilon_{\text{LSq}}$	0.04	0.127	0.029	0.063	0.06	0.126	0.262	0.055	0.123	0.266
[%]	0.97	1.52	0.78	0.87	1.24	1.31	1.69	0.95	1.07	1.44

**Figure 7.** Frequency estimation errors per combination of grating and velocity, averaged over all experiments and window positions, versus the width of the observation window. Errors for  $f_{\text{FFT}}$  (blue line) refer to the initial guess obtained through naïve Fourier analysis, while the ones for  $f_{\text{LSq}}$  (green line) are related to the estimates gained by the minimization of Equation (9).

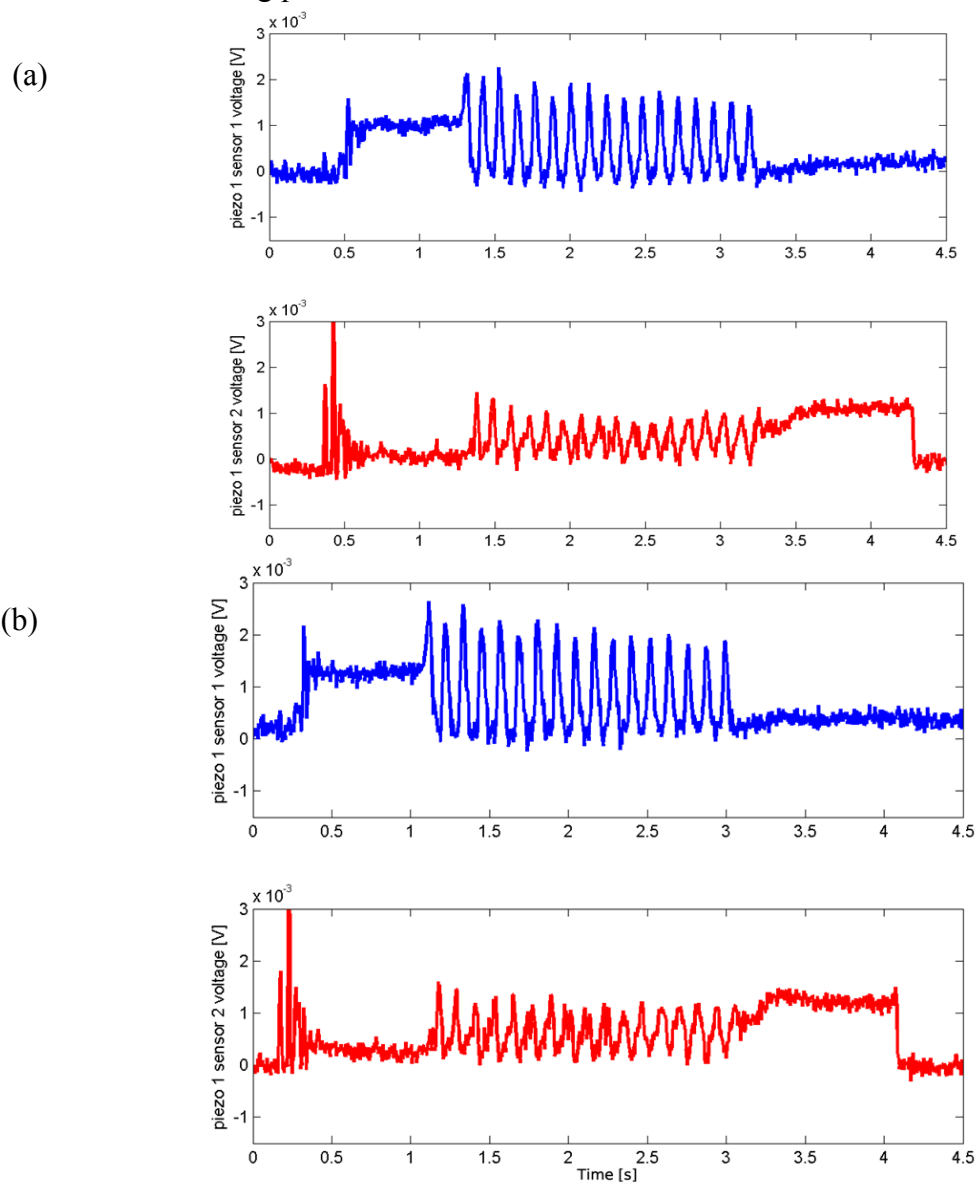


As expected, errors in the initial guess  $f_{\text{FFT}}$  ranged from about  $\frac{1}{2w}$  to almost zero, as the pattern of FFT-frequencies moved over the nominal frequency for each setup. However, the second estimation step using the least squares fit was very stable and converged for almost all windows larger than 0.4s. Using the entire available time series for each experiment, about 1.5s to 5s, led to the average errors shown in Table 3. To check consistency, results using piezoresistor 1 from MEMS sensors 1 and 2 in Equation (9) were compared to those using piezoresistor 1 from MEMS sensors 2 and 4. The errors obtained seem to agree very well, as shown in Table 3.

## Repeatability

Figure 8 shows plots of the same channels within different runs having the same experimental conditions. Moreover, the cross-correlation coefficients defined in Section 3.3 confirmed a high degree of repeatability within one set of parameters  $C$ .

**Figure 8.** Time plot of the readings from piezoresistor 1 of MEMS sensors 1 and 2 of the array. The plots refer to data series 6 (a) and 7 (b), where a grating of 3.6 mm spatial periodicity was applied with translational speed of 30 mm/s, according to Tables 2 and 3. It is noticeable to observe the high repeatability, as well as the similarity with Figure 9(a), which only differs for the stimulus translational speed and thus results in an expansion of the time scale during phase C.

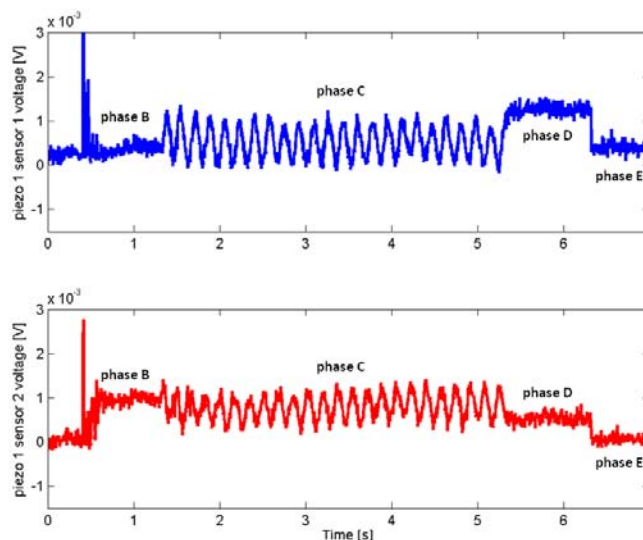


As an example, for piezoresistor 1 of MEMS sensor 1 the average Pearson correlation coefficients ranged from 0.87 to 0.97, while for piezoresistor 1 of MEMS sensor 2 their values went from 0.80 to 0.89 depending on the chosen parameters combination  $C$ . Moreover, all the coefficients for the

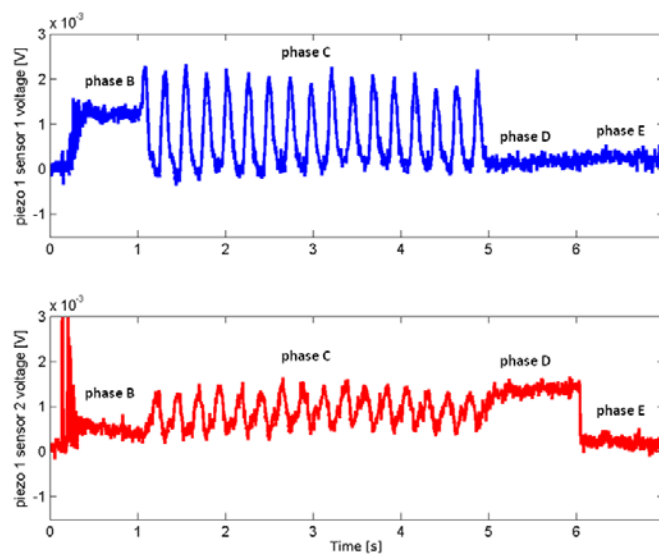
channels close to the leading edge (e.g. MEMS sensor 1) of the stimulus during the sliding motion (phase C) were always higher than the ones for the channels at the falling edge (e.g. MEMS sensor 2) of the stimulus; this phenomenon is discussed in Section 5. The frequency modulation due to the variation of the stimulus can be appreciated in Figure 9, while a comparison between Figure 8 and Figure 9(a) points out the effect of stimulus velocity variation.

**Figure 9.** Time plot of the readings from piezoresistor 1 of MEMS sensors 1 and 2 of the array. The plots refer to data series 1 (a) and 31 (b), where gratings of 3.6 mm and 2.6 mm spatial periodicity were applied with translational speed of 15 mm/s, respectively, according to Tables 2 and 3. The frequency modulation due to the variation of the stimulus can be easily appreciated. The steps corresponding to the loading and unloading of the stimulus (phases A-B and D-E) may be more or less evident in a specific unit of the array depending on whether the ridge of the stimulus falls under a sensor unit or not, showing the static imaging potentiality of the tactile sensor array.

(a)



(b)



## Static Imaging

In parallel to the analysis of the frequency shift due to the variation of dynamic stimulation conditions, another major experimental result concerned the static imaging capabilities of the developed tactile sensor array. This further outcome was possible by choosing a proper experimental protocol, which included static phases in the initial and final parts of stimulation with repeatable conditions overall the runs. Figures 3, 8 and 9 show such results.

## 5. Discussion

The experimental results shown for dynamic artificial touch with medium-coarse periodic gratings demonstrated the perfect coherence between the principal frequency commonly revealed by the packaged MEMS sensor units and the expected one, as shown in Table 3 and Figure 7, as well as the consistency between the surface geometry and the static image of the stimulus-sensor interface.

Looking at the background of neurophysiological and psychophysical touch studies briefly reported in the Introduction, the technological and the signal processing outcomes of this work may be classified as a successful preliminary attempt to artificially achieve roughness encoding in case of medium-coarse patterning, i.e. a deterministic link (see Table 3) was obtained between the “spatial coarseness” of the presented stimuli and the features extracted from the sensor outputs.

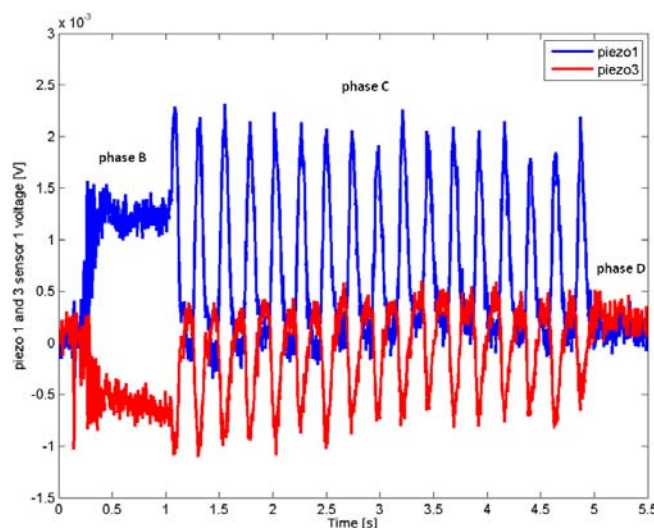
These results pointed out the better processing quality guaranteed by using structured information from different units of a tactile sensor array instead of naïve Fourier analysis separately on each channel, overcoming frequency discretization limitations. These limitations are shown in Figures 4 and 5, which differ both in the time window length used for FFT and in the grating periodicity. The latter is the reason for the 1.4 Hz difference between the nominal frequencies, which could not be detected with FFT due to the low resolution of the FFT in the relevant frequency range (width of bars ~0.5 Hz in Figure 4 vs. ~2.5 Hz in Figure 5). As a consequence, using the naïve FFT approach to retrieve the frequency in a 0.35 s time window for both data series, would result in the two gratings being not distinguished, as shown in the respective plots of Figure 7. On the contrary, with the least squares fitting procedure the separation was well feasible, and the common frequency expected when indenting and sliding at constant speed periodic ridged surfaces across an array of sensors was accurately estimated. The technological approach together with the proposed frequency estimation method guaranteed an error from 1.7% down to 0.5% over the range of spatial frequencies considered, independently of the combination of MEMS sensor units used (see Table 3). Moreover, as shown in Figure 7, limiting the evaluation to fixed size time windows reduced the accuracy somewhat, but the method stayed stable down to 0.4 s window size, making it potentially suitable for most near real-time settings. The applied method revealed to be robust even if, in addition to the observable principal frequency shift associated to the combination of the used grating and stimulus sliding velocity, the signal power had overtones (the first three or four harmonics of the fundamental frequency) introduced by both the non-linear packaging and the sharp edges of the periodic ridged surfaces. On the contrary, the fitting based on Fourier analysis resulted in an oscillatory behavior of the error respect to the observation window length. Further stability and precision with the gradient descent fitting method

could be gained by taking into account all four MEMS sensors and tuning the sampling rate according to the target application.

As depicted in Figure 8 and confirmed by the calculated average Pearson cross-correlation coefficients, the gathered data had high repeatability across different runs of the same experimental conditions. Furthermore, as seen in Figure 8 already, MEMS sensor 1 produced higher voltage amplitudes, leading to a better Signal-to-Noise (S/N) ratio, which in turn caused the higher correlation between runs with respect to MEMS sensor 2. This effect may be associated to the shape of the compliant packaging, which could induce higher stresses in piezoresistors of the sensor unit located at the leading edge. Reversing the scan direction (not shown) exchanged the roles of MEMS sensors 1 and 2 in this regard. Moreover, it is noticeable to observe the excellent similarity between the plots shown in Figure 8 and the plot of Figure 9 (a). These graphs only differ for the stimulus translational speed and thus result in a compression in the time scale during phase C.

The modulation of the principal frequency due to the variation of the stimulus can be appreciated in the time domain plots of Figure 9. Moreover, as detailed in Figure 10, couples of piezoresistors of a sensor unit which are located one in front to the other along the direction of motion [piezoresistors 1 and 3 in Figure 1(b)] responded with opposite sign to the stimulus. Therefore, even with packaged silicon sensors and dynamic stimulations, the symmetries of the static calibration matrix observed in [30] for the bare MEMS sensor were still present in this work.

**Figure 10.** Time plot showing the opposite sign of the variation of the readings from piezoresistors 1 and 3 of MEMS 1 during sliding. The plot refers to data series 1, where a grating of 3.6 mm spatial periodicity was applied with translational speed of 15 mm/s, according to Tables 2 and 3.



Finally, as regards the consistency between the surface geometry and the static artificial touch representation, it is remarkable to observe the output signals variations relatively to the steps between phases A (starting of data acquisition) and B (sensor loading) and between phases D (steady state after stimulus sliding) and E (sensor unloading). Figures 3, 8 and 9 point out that the step heights varied between different runs depending on the used grating (but not on the velocity). This was due to the fact

that a variation of the grating periodicity modified the portion of the ridge under each MEMS unit, being the initial and final position of the stimulus carrier always the same for all runs during phase C.

## 6. Conclusions and Future Work

The experimental analyses performed in this work demonstrated the suitability of the developed tactile sensor for revealing medium-coarse spatial features of the explored surface, both with dynamic and static stimulation. Future work will focus on performing similar experiments incorporating the developed technology in a bio-inspired mechatronic finger. Given that the feasibility of using a polyimide thin protective layer has been shown in this investigation, the actuated finger may use a polyimide glove (mimicking the human stratum corneum) for preventing the sensor to be worn or damaged by water or grit. Moreover, because of the possibility to integrate the readings from the array with proprioception information during active touch tasks, the combination of information regarding the estimated common frequency and the velocity of the finger could solve Equation (1) and provide quantitative measurements revealing texture properties of the explored stimuli. Investigations will also be performed in implementing processing strategies to separate the velocity and periodicity information contained in Equation (1) directly from the measurements of the array, thus avoiding the need to use the knowledge of the stimulus sliding velocity (in case of passive touch experiments) or proprioception information from an actuated finger (in case of active touch ones). Experiments will be performed with other stimuli, addressing not only a medium-coarse spatial periodic patterning, but also more general fine textures (e.g. sandpapers, gratings with oblique or aperiodic ridges or 2D patterning, ...) and the frequency content due to the kind of material. In that case, the focus could move from principal frequency analysis to spectral analysis over the full frequency range, or to wavelet transform if the frequency content is supposed to change with respect to time and/or stimulus-sensor relative positioning. Moreover, the fact that the MEMS sensor is triaxial may be exploited in future work with stimuli having 2D patterning: in this paper, the raw sensor outputs were directly analyzed guaranteeing great accuracy in principal frequency retrieval without encoding the force vector at MEMS-packaging interface or at packaging-stimulus interface.

These planned experiments will require some modifications to the packaging design (e.g. lower thickness, material with different hardness or viscosity, introduction of fingerprints, etc.) in order to achieve even a higher sensitivity and selectivity for each MEMS unit [31,34] and a reduction of the low-pass spatial filtering effect introduced by the materials embedding the sensor [35] while still providing robustness for application in artificial hands dexterously interacting with the environment [29,32].

Finally, future investigations will experiment with artificial tactile sensors the unified paradigm proposed by Yoshioka and colleagues [13] for the perception of fine and coarse textured surfaces, in order to go towards a common theory for human and robot mediated coding and decoding of tactile stimuli.

## Acknowledgements

This study was funded by the NANOBIOACT project (EU-FP6-NMP-033287). The authors would like to thank Nicola Vitiello from Scuola Superiore Sant'Anna (Pisa, Italy) for his collaboration

in the development of the mechatronic stimulator, Mark Mitulla and Stefan Schmitt from the IMM (Institute of Microtechnology of Mainz, Germany) for their collaboration in the sensor fabrication. Finally, the authors express their thanks to the anonymous reviewers for the precious suggestions.

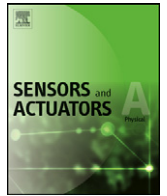
## References and Notes

1. Johnson, K.O.; Yoshioka, T. Neural mechanisms of tactile form and texture perception. In *The Somatosensory System: Deciphering the Brain's Own Body Image*; Nelson, R.J., Ed.; CRC Press LLC: Boca Raton, FL, USA, 2001; pp. 73-101.
2. Jones, L.A.; Lederman, S.J. Tactile Sensing. In *Human Hand Function*; Jones, L.A., Lederman, S.J., Eds.; Oxford University Press: New York, NY, USA, 2006; pp. 44-74.
3. Hollins, M.; Faldowski, R.; Rao, S.; Young, F. Perceptual dimensions of tactile surface texture: a multidimensional scaling analysis. *Percept. Psychophys.* **1993**, *54*, 697–705.
4. Yoshioka, T.; Bensmaïa, S.J.; Craig, J.C.; Hsiao, S.S. Texture perception through direct and indirect touch: An analysis of perceptual space for tactile textures in two modes of exploration. *Somatos. Mot. Res.* **2007**, *24*, 53-70.
5. Meftah, E.M.; Belingard, L.; Chapman, C.E. Relative effects of the spatial and temporal characteristics of scanned surfaces on human perception of tactile roughness using passive touch. *Exp. Brain. Res.* **2000**, *132*, 351-361.
6. Smith, M.; Chapman, C.E.; Deslandes, M.; Langlais, J.S.; Thibodeau, M.P. Role of Friction and Tangential Force Variation in Subjective Scaling of Tactile Roughness, *Exp. Brain. Res.* **2002**, *144*, 211-223.
7. Lawrence, M.A.; Kitada, R.; Klatzky, R.L.; Lederman, S.J. Haptic roughness perception of linear gratings via bare finger or rigid probe. *Perception* **2007**, *36*, 547-557.
8. Klatzky, R.L.; Lederman, S.J.; Hamilton, C.; Grindley, M.; Swendsen, R.H. Feeling textures through a probe: Effects of probe and surface geometry and exploratory factors. *Percept. Psychophys.* **2003**, *65*, 613–631.
9. LaMotte, R.H.; Srinivasan, M.A. Surface microgeometry: Neural encoding and perception. Information Processing in the Somatosensory System. In *Wenner-Gren Intl. Symposium Series*; Franzen, O., Westman, J. Eds.; Macmillan Press: New York, NY, USA, 1991; pp. 49-58.
10. Scheibert, J.; Leurent, S.; Prevost, A.; Debrégas, G. The role of fingerprints in the coding of tactile information probed with a biomimetic sensor. *Science* **2009**, *323*, 1503-1506.
11. Srinivasan, M.A.; Whitehouse J.M.; LaMotte R.H. Tactile detection of slip: Surface microgeometry and peripheral neural codes. *J. Neurophysiol.* **1990**, *63*, 1323-1332.
12. Hollins, M.; Risner, S.R. Evidence for the duplex theory of tactile texture perception. *Percept. Psychophys.* **2000**, *62*, 695-705.
13. Yoshioka, T.; Gibb, B.; Dorsch, A.K.; Hsiao, S.S.; Johnson, K.O. Neural coding mechanisms underlying perceived roughness of finely textured surfaces. *J. Neurosci.* **2001**, *21*, 6905-6916.
14. Konyo, M.; Maeno, T.; Yoshida, A.; Tadokoro, S. Roughness sense display representing temporal frequency changes of tactile information in response to hand movements. In *Proceedings of the First Joint Eurohaptics Conference and Symposium on Haptic Interface for Virtual Environment and Teleoperator Systems*, 2005; pp. 609-610.

15. Konyo, M.; Yoshida, A.; Tadokoro, S.; Saiwaki, N. A tactile synthesis method using multiple frequency vibrations for representing virtual touch. In *Proceedings of the IEEE/RSJ International Conference on Intelligent Robots and Systems 2005*, Edmonton, Canada, 2-6 August, 2005; pp. 3965-3971.
16. Lee, M.H.; Nicholls, H.R. Tactile sensing for mechatronics: A state of the art survey. *Mechatronics* **1999**, *9*, 1–31.
17. Maheshwari, V.; Saraf, R.F. Tactile devices to sense touch on a par with a human finger. *Angew Chem. Int. Edit.* **2008**, *47*, 7808–7826.
18. Kim, S.H.; Engel, J.; Liu, C.; Jones, D.L. Texture classification using a polymer-based MEMS tactile sensor. *J. Micromech. Microeng.* **2005**, *15*, 912-920.
19. Mukaibo, Y.; Shirado, H.; Konyo M.; Maeno T. Development of a texture sensor emulating the tissue structure and perceptual mechanism of human fingers. In *Proceedings of the IEEE International Conference on Robotics and Automation 2005*, Barcelona, Spain, 18-22 April 2005; pp. 2565-2570.
20. Okamoto, S.; Konyo, M.; Mukaibo, Y.; Maeno, T.; Tadokoro, S. Real-time estimation of touch feeling factors using human finger mimetic tactile sensors. In *Proceedings of the IEEE/RSJ International Conference on Intelligent Robots and Systems 2006*, Beijing, China, October 2006; pp. 3581-3586.
21. Scheibert, J.; Prevost, A.; Debrégas, G.; Rousier, R.; Rey, P. In *A Novel Biomimetic Haptic Sensor to study the Physics of Touch*, Proceedings of Méchanotransduction 2004.
22. Shimojo, M.; Ishikawa, M. An active touch sensing method using a spatial filtering tactile sensor. In *Proceedings of the IEEE International Conference on Robotics and Automation 1993*, Seoul, Korea, May 1993; pp. 948-954.
23. Hosoda, K.; Tada, Y.; Asada, M. Anthropomorphic robotic soft fingertip with randomly distributed receptors. *Robot. Auton. Systems* **2006**, *54*, 104–109.
24. Fishel, J.A.; Santos, V.J.; Loeb, G.E. A Robust Micro-Vibration Sensor for Biomimetic Fingertips. In *Proceedings of the IEEE 2nd Biennial IEEE/RAS-EMBS International Conference on Biomedical Robotics and Biomechatronics 2008*, Scottsdale, AZ, USA, 19-22 October, 2008; pp. 659-663.
25. Wettels, N.; Santos, V.J.; Johansson, R.S.; Loeb, G.E. Biomimetic Tactile Sensor Array. *Adv. Robot.* **2008**, *22*, 829–849.
26. Maheshwari, V.; Saraf, R.F. High-resolution thin-film device to sense texture by touch. *Science* **2006**, *312*, 1501-1504.
27. Johansson, R.S.; Vallbo, Å.B. Tactile sensibility in the human hand: relative and absolute densities of four types of mechanoreceptive units in glabrous skin. *J. Physiol. (Lond.)* **1979**, *286*, 283-300.
28. Beccai, L.; Roccella, S.; Arena, A.; Valvo, F.; Valdastrì, P.; Menciassi, A.; Carrozza, M.C. Design and fabrication of a hybrid silicon three-axial force sensor for biomechanical applications. *Sens. Actuator A-Phys.* **2005**, *120*, 370-382.
29. Beccai, L.; Roccella, S.; Ascari, L.; Valdastrì, P.; Sieber, A.; Carrozza, M.C.; Dario, P. Development and Experimental Analysis of a Soft Compliant Tactile Microsensor for Anthropomorphic Artificial Hand. *IEEE-ASME Trans. Mechatron.* **2008**, *13*, 158-168.

30. Oddo, C.M.; Valdastri, P.; Beccai, L.; Roccella, S.; Carrozza, M.C.; Dario, P. Investigation on calibration methods for multi-axis, linear and redundant force sensors. *Meas. Sci. Technol.* **2007**, *18*, 623-631.
31. Vásárhelyi, G.; Fodor, B.; Roska, T. Tactile sensing-processing: interface-cover geometry and the inverse-elastic problem. *Sens. Actuat. A-Phys.* **2007**, *140*, 8-18.
32. Carrozza, M.C.; Cappiello, G.; Micera, S.; Edin, B.B.; Beccai, L.; Cipriani, C. Design of a cybernetic hand for perception and action. *Biol. Cybern.* **2006**, *95*, 629-644.
33. Beccai, L.; Roccella, S.; Oddo, C.; Carrozza, M.C. Sensing fingertip for bio-inspired tactile encoding. In *Proceedings of the First Italian Conference on Bioengineering*; Burattini, R., Contro, R., Dario, P., Landini, L., Eds.; Pàtron editore: Bologna, Italy, 2008; p. 787.
34. Vásárhelyi, G.; Ádám, M.; Vázsonyi, É.; Bársony, I.; Dücső, C. Effects of the elastic cover on tactile sensor arrays. *Sens. Actuat. A-Phys.* **2006**, *132*, 245-251.
35. Shimojo, M. Mechanical filtering effect of elastic cover for tactile sensor. *IEEE Trans. Rob. Autom.* **1997**, *13*, 128-132.
36. Lederman, S.J. Tactile roughness of grooved surfaces: the touching process and effects of macro- and microsurface structure. *Percept. Psychophys.* **1974**, *16*, 385-395.
37. Darian-Smith, I.; Oke, L.E. Peripheral neural representation of the spatial frequency of a grating moving across the monkey's finger pad. *J. Physiol.-London* **1980**, *309*, 117-133.

© 2009 by the authors; licensee Molecular Diversity Preservation International, Basel, Switzerland. This article is an open-access article distributed under the terms and conditions of the Creative Commons Attribution license (<http://creativecommons.org/licenses/by/3.0/>).



## Development of a bioinspired MEMS based capacitive tactile sensor for a robotic finger

H.B. Muhammad<sup>a,\*</sup>, C.M. Oddo<sup>b</sup>, L. Beccai<sup>c</sup>, C. Recchiuto<sup>b</sup>, C.J. Anthony<sup>a</sup>, M.J. Adams<sup>a</sup>,  
M.C. Carrozza<sup>b</sup>, D.W.L. Hukins<sup>a</sup>, M.C.L. Ward<sup>a</sup>

<sup>a</sup> Bio-medical and Micro Engineering Research Centre, School of Mechanical Engineering, University of Birmingham, Edgbaston, Birmingham, B15 2TT, United Kingdom

<sup>b</sup> Advanced Robotics Technology and Systems Laboratory, Polo Sant'Anna Valdera – Scuola Superiore Sant'Anna, Viale Rinaldo Piaggio 34, 56025 Pontedera (Pisa), Italy

<sup>c</sup> Center for MicroBioRobotics IIT@SSSA, viale Rinaldo Piaggio 34, 56025 Pontedera (Pisa), Italy

### ARTICLE INFO

#### Article history:

Received 6 September 2010

Received in revised form 27 October 2010

Accepted 31 October 2010

Available online 9 November 2010

#### Keywords:

MEMS

Tactile sensor

Biomimetic

Capacitive sensor

### ABSTRACT

This paper presents the development of a MEMS based capacitive tactile sensor intended to be incorporated into a tactile array as the core element of a biomimetic fingerpad. The use of standard microfabrication technologies in realising the device allowed a cost efficient fabrication involving only a few process steps. A low noise readout electronics system was developed for measuring the sensor response. The performance of both bare and packaged sensors was evaluated by direct probing of individual capacitive sensor units and characterising their response to load–unload indentation cycles.

© 2010 Elsevier B.V. All rights reserved.

### 1. Introduction

There is a growing need for reliable, low cost tactile sensing devices for applications in areas such as robotics, minimal invasive surgery and automation of industrial manufacturing processes [1]. The last thirty years has seen tremendous progress in research on the design and development of tactile sensors. While earlier studies explored various transduction principles and sensor requirements, recent work in the field has involved the development of sensor prototypes that are tailored for specific applications. Biological tactile receptors in the human fingertips, also known as mechanoreceptors, serve as an inspiration for the development of robotic tactile sensors [2–6]. The biological tactile system offers a sophisticated mechanism through which subtle variations in texture can be perceived and this provides a standard for the performance of artificial tactile devices.

When developing sensors for incorporation into a robotic finger, the main challenges arise from the required high spatial and force resolution, and sufficiently small dimensions that allow integration within the space constraints of a finger. For robotic applications, the two main research areas on tactile sensor development are: sensors for enabling the robot to effectively perform lifting and grasping tasks and sensors for giving robots the ability to characterise differ-

ent surface textures [7,8]. Texture is implemented as protrusions or undulations on the surface of a material that manifests as changes in forces when a sensor is moved across a surface. A brief overview of tactile sensors that have been reported to date for robotic applications and the technologies employed in each case are given in Table 1. Piezoelectric and piezoresistive principles have most commonly been used for the sensing elements. Preceding devices are generally larger than the mechanoreceptors in the human finger pad and lack the spatial resolution of the human finger (approximately 1 mm) [9] and its ability to provide the rich data set of information on spatial distribution of contact forces. To overcome these limitations, a highly dense array of micro tactile elements is needed.

The main objective of this work was to develop and characterise highly sensitive Micro Electro Mechanical Systems (MEMS) based tactile sensors for implementation into a robust microscale sensing array. The elementary sensor units should be individually addressable and provide information on spatial features of contacting stimuli. This would eventually allow for surface characterisation of various textures with the added feature of human finger pad like spatial resolution. In order to facilitate potential incorporation of the device into a robotic finger, it requires compatibility with integration of a layer of elastomeric skin-like material on the surface, mimicking the compliance and conformance of human skin. Thus the system would be able to come into contact with textured stimuli in a biomimetic manner and also be sufficiently sensitive to encode features of texture related attributes such as roughness.

\* Corresponding author. Tel.: +44 0121 4144217; fax: +44 0121 4143958.

E-mail address: [hbm768@bham.ac.uk](mailto:hbm768@bham.ac.uk) (H.B. Muhammad).

**Table 1**  
Overview of tactile sensing devices developed to date for robotic applications.

Author (year)	Sensing technology/description	Application	No. of elements	Sensing element size	Array pitch	Force range	Sensitivity
Dario et al. [10]	Piezoelectric polymer: Multilayer structure including an epidermal PVDF layer, a conductive rubber intermediary layer and bottom PVDF dermal layer	Detection of contact pressure, hardness and surface texture	128	–	–	–	740 mV/N
Howe et al. [7]	Accelerometer: Conventional quartz crystal embedded in polyurethane foam and attached to outer 2 mm silicone rubber skin	Slip and texture perception	–	25 mm diameter	–	–	–
Omata et al. [11]	Piezoelectric ceramic: PZT element surrounded by 3 mm diameter hemisphere of silicone	Hardness, softness detection	–	15 mm × 65 mm	–	–	–
Yeung et al. [12]	Piezoresistive polymer: Matrix of Force Sensing Resistors with elastic overlay	Object recognition	16 × 16	–	1.58 mm	–	–
Beebe et al. [13]	MEMS piezoresistive: Silicon sensing diaphragm with load transmitting torlon dome Spatial resolution: 2–4 mm	Force sensing	1	2 mm radius	–	0–100 N	1.4 mV/N
Chu et al. [14]	MEMS capacitive: Silicon diaphragm, glass + polymer substrate, elastomer coating Spatial resolution: 2.2 mm	Robot fingers	3 × 3	0.450 mm radius	–	0–1 g	0.13 pF/g in z, 0.32 pF/g in x and y
Maeno et al. [15]	Strain gauge: 15 phosphor bronze plates embedding strain gauges (thickness 0.1 mm) are incorporated within a silicone rubber body	Detection of slip	15	–	–	–	–
Dargahi et al. [16]	Piezoelectric polymer: PVDF film	Force sensing	3	–	–	0–2 N	57.5 V/N
Mei et al. [17]	MEMS piezoresistive: Square silicon membrane and outer silicone rubber layer	Grip force control, object recognition	4 × 8	4 mm × 4 mm	–	0–50 N	13 mV/N
Leineweber et al. [18]	MEMS capacitive: Polysilicon membrane	Micromanipulation	8	0.24 mm × 0.24 mm	0.240 mm	0–3 bar	1.35 V/bar
Beccai et al. [19]	MEMS piezoresistive: Silicon based flexible sensing structure with four tethers in a cross-shape and centrally integrated force transmitting mesa. 4 piezoresistors implanted in tethers	Biomechanical applications	1	1.5 mm × 1.5 mm × 0.625 mm	–	3 N for normal force 0.5 N for tangential force	0.026 N <sup>-1</sup> in z, 0.054 N <sup>-1</sup> in x and y
Hosoda et al. [20]	Randomly distributed strain gauges and PVDF film embedded within an anthropomorphic soft fingertip	Robotic fingers – texture discrimination	24	–	–	–	0.1 V/N
Wettels et al. [3]	Impedance based: Fingertip shaped with rigid central core surrounded by weakly conductive fluid and covered by a silicone elastomeric skin. Spatial resolution: 2 mm	Robotic, prosthetic	–	–	–	–	33.3 kΩ/N
Scheibert et al. [21]	MEMS based piezoresistive device embedded in elastomer film. Cylindrical post attached to a suspended circular Silicon membrane (with 4 embedded piezoresistive gauges)	Fingertip like biomimetic tactile sensor	1	1 mm radius, 0.1 mm thick	–	–	–

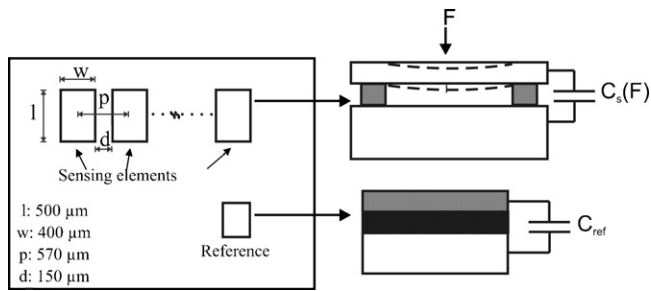


**Fig. 1.** Schematic of tactile sensor array showing geometrical dimensions of devices and cross sections of sensors and reference devices.

For the individual sensing elements a capacitive sensing principle is chosen. This offers advantages over commonly employed piezoresistive, strain gauge and piezoelectric sensing principles in terms of increased sensitivity, long term drift stability, lower temperature sensitivity and power consumption [22,23]. The devices are fabricated using well established microfabrication technologies, allowing for a high density of sensing devices within a given area and thus mimicking the distributed sensory arrangement in the human skin. The devices are silicon based and can easily be incorporated within silicone rubber artificial skin like coating materials [24].

In the next section, the design, simulation and fabrication process of the sensor are presented; Section 3 details the readout electronics; Section 4 the experimental setup, methodologies and results; Finally, experimental results are discussed.

## 2. Sensor description

### 2.1. Design and operating principle

An individual sensing element consists of an upper  $2\ \mu\text{m}$  highly doped single crystal silicon diaphragm, a  $2\ \mu\text{m}$  air cavity formed by sacrificial layer releasing and a lower electrode consisting of highly doped silicon. The edges of the sensing diaphragm are fixed by supporting oxide structures. A cross sectional schematic diagram of a single tactile unit is shown in Fig. 1. The diaphragm dimensions are  $500\ \mu\text{m} \times 400\ \mu\text{m}$ . Each tactile unit is  $150\ \mu\text{m}$  apart which allows for high density of sensing structures within a given area. The array fabricated and tested in this work has 4 individual sensing elements. As shown in Fig. 1, reference capacitors ( $C_{\text{ref}}$ ) were also included in close proximity to each individual sensor and designed to be insensitive to applied pressure. They consist of two silicon plates that are separated by oxide dielectric. The dimensions of these devices were calculated such that their capacitance would equal that of the corresponding sensor at zero applied pressure. The presence of reference capacitors allows the measurement of a differential response and therefore eliminating the effects of parasitic capacitance.

**Table 2**

Summary of FEA simulation results for case of uniformly distributed pressure of 115 kPa applied to the sensor diaphragm.

Maximum stress at maximum deflection	0.468 GPa
Resonant frequency	587 kHz
Maximum change in capacitance	500 fF

The capacitance  $C_s$  of the sensing unit can be expressed as:

$$C_s(F) = \frac{A\varepsilon}{d} \quad (1)$$

where  $C_s(F)$  is the capacitance of the sensing region, which is a function of the applied force  $F$ ,  $\varepsilon$  is the permittivity of air,  $A$  is the area of the silicon diaphragm and  $d$  is the gap between the two silicon plates.

When a pressure is applied to the surface of the sensor, the deflection of the sensing membrane will create a change in capacitance of the device. The capacitance of the sensor as a function of applied force can be expressed as:

$$C_s(F) = \int_{x=0}^a \int_{y=0}^b \frac{\varepsilon}{d_0 - w(x, y)} dx dy \quad (2)$$

where  $w(x, y)$  is the diaphragm deflection as a function of  $x$  and  $y$  coordinates and  $a$  and  $b$  are the dimensions of the sensing area. The deflection is dependent on the applied force and dimensions of the diaphragm. Detailed analyses of the deflection of clamped sensing diaphragms have been carried out elsewhere and are not discussed in this paper [25]. Instead, Finite Element Analysis (FEA) is used to model diaphragm deflection under applied loads (Section 2.2). The sensor capacitance is a non-linear function of the applied force. Thus the sensitivity of the device is a function of the geometrical dimensions of the sensing diaphragm and the zero pressure electrode separation  $d_0$ . A greater sensitivity can be attained by increasing the length of the sensing membrane and decreasing the thickness and initial electrode separation distance. The working range of the device is determined by the initial plate distance  $d_0$ . Thus there exists an inherent trade off between increased sensitivity and device range.

### 2.2. Simulation

FEA was used to assess the electromechanical behaviour of sensing diaphragms as more accurate results are obtained compared to analytical solutions, especially for large deflections [26]. Using Comsol Multiphysics® the performance of the sensor was simulated assuming the case of a uniformly distributed pressure on the surface of the sensing membrane. The model assumes the contact area of stimulus is in the order of dimensions as the sensor. The results from the simulation are presented in Table 2 and Fig. 2. A capacitance change of 500 fF was predicted for the applied pressure range 0–120 kPa (corresponding to forces of 0–24 mN).

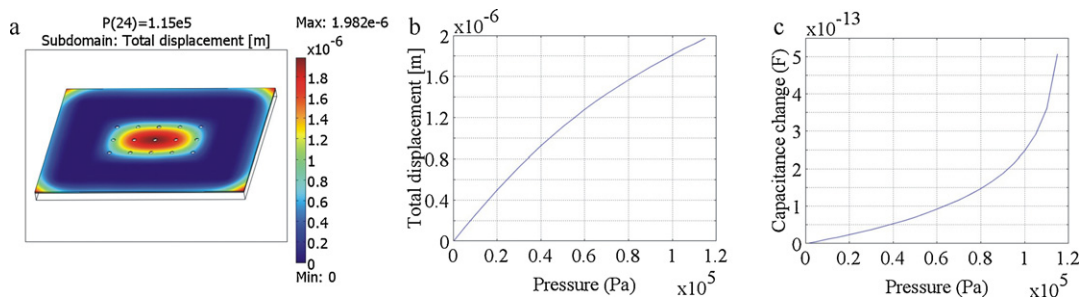


**Fig. 2.** (a) FEA results showing displacement of sensor diaphragm in response to uniformly distributed pressure varying from 0 to 115 kPa, (b) Plot of maximum diaphragm displacement with pressure, (c) Expected change in capacitance with uniform applied pressure on the sensor diaphragm.

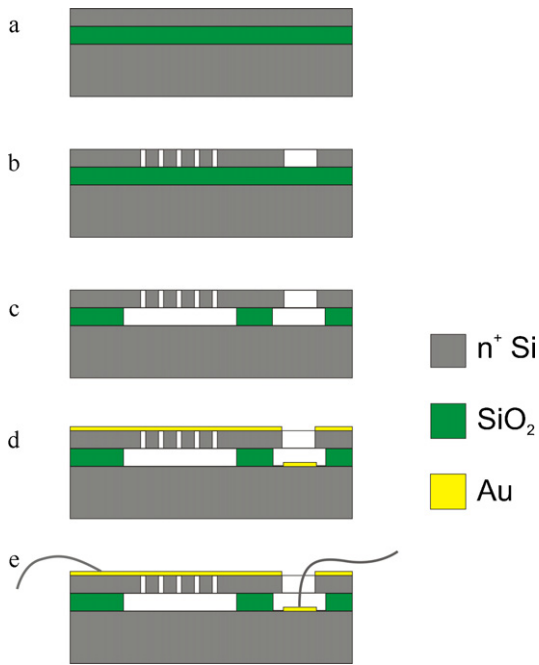


Fig. 3. Process flow for device fabrication.

This provides a basis for developing the signal acquisition electronics. The maximum stress in the sensing diaphragm found from the simulation occurs at the edges of the circular etch holes and by the supported edges of the diaphragm (Fig. 2). The elastic limit is given by the fracture stress of a (100) silicon wafer and is in the range of several GPa [27]. This exceeds the maximum stress that is expected to be encountered within the working range of the sensor and is given by the applied force at which the sensing diaphragm comes into physical contact with the substrate (corresponding to a maximum displacement of 2  $\mu\text{m}$ ). The resonant frequency of the device was estimated to be 587 kHz. Thus the elementary device is expected to possess a high dynamic range.

### 2.3. Fabrication method

To fabricate the sensors, commercially available Bonded and Etched-Back Silicon-On-Insulator (BESOI) wafers were used as a substrate. The process flow is schematically illustrated in Fig. 3a–e. The device layer (top side) of the BESOI had a thickness of 2  $\mu\text{m}$ , with a 2  $\mu\text{m}$  buried silicon oxide layer and a 300  $\mu\text{m}$  silicon handle layer (back side) (a). The silicon layers were highly arsenic doped (n<sup>+</sup>) with an electrical resistivity lower than 0.006  $\Omega\text{cm}$ . A spin

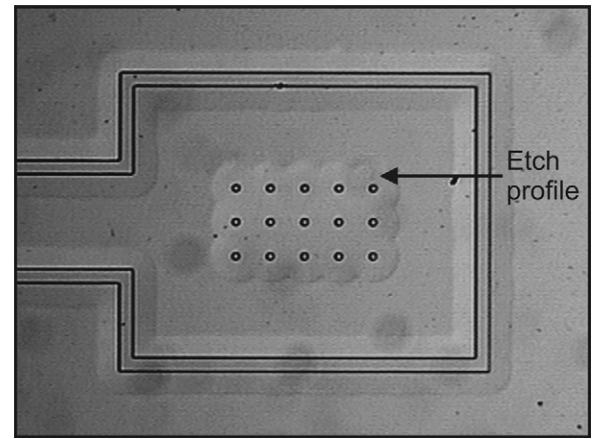


Fig. 4. Optical image showing profile of sensing membrane formed following HF etch.

coated resist on the top side was patterned by using photolithography to define the sensor area and bond pads. Within each defined sensing area, holes of 5  $\mu\text{m}$  radius were included to allow access for subsequent sacrificial etching of selected areas of SiO<sub>2</sub>. These patterns were transferred into the device layer by using Deep Reactive Ion Etching (DRIE, Bosch process) to form the sensing structures and sacrificial etch access holes (b). The wafer was then diced into individual chips of 6 mm  $\times$  6 mm in size which were etched using 40% liquid Hydrofluoric (HF) acid solution (c). This early dicing step prevents damage to the 2  $\mu\text{m}$  thin device layer which could occur following the subsequent sacrificial etching. The timing of the etch process is critical in defining the geometrical dimensions of the sensing diaphragm. Prior to the etching process, the etch rate was established by monitoring the geometric profile formed (Fig. 4) following a specified etch time period. This is possible as 2  $\mu\text{m}$  thin Silicon is optically transparent. Thus the chips were etched until the area defined as the sensing diaphragm had fully released. Following this the chips were rinsed in Isopropyl alcohol and distilled water, and then dried on a hotplate at 115  $^{\circ}\text{C}$ . With this technique, no stiction of the diaphragm occurred in any of the devices. To establish external electrical contacts, the chips were coated with a 200 nm thick gold layer using a thermal evaporation process and a 20 nm thick adhesive titanium layer (d). The sensor was hosted on a standard dual-in-line ceramic package (Spectrum Semiconductor Materials, INC., 24-DIP). The wiring was performed by means of a wire bonder using 25  $\mu\text{m}$  aluminum wires (e). For protection of the wires from damage during testing, they were coated with a UV curable epoxy (Epo-Tek OG142). Fig. 5 shows Scanning Electron Microscopy (SEM) images of the sensor cross section, a plan view of single sensor and the fabricated sensor array.

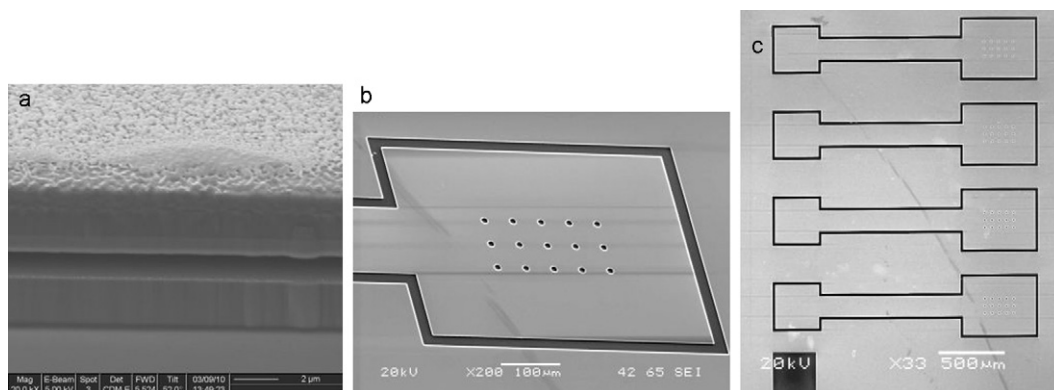
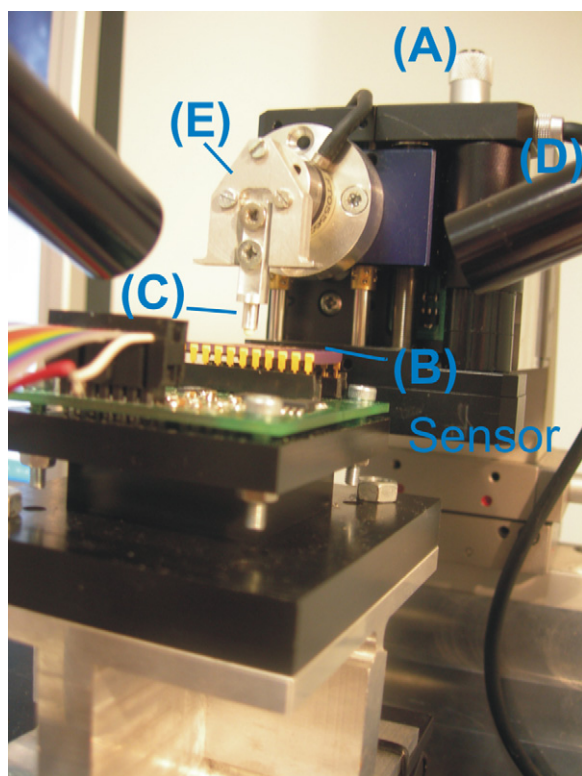


Fig. 5. (a) Scanning Electron Micrograph (SEM) image of sensor cross section, (b) Sensor structure, (c) 4  $\times$  1 linear sensor array.



**Fig. 6.** Experimental setup for probing the sensor with a spherical head. The letters indicate the core components of the setup, as described in the text.

For protecting sensors from mechanical damage, and for forming a conformable, skin like coating over the sensors, Polydimethylsiloxane (PDMS, Sylgard 184) was used. This is a silicon based organic polymer commonly used for embedding or encapsulating electronic components. The polymer is supplied as a two part mix; a monomer and hardener, which are combined at a weight ratio of 10:1. The mixture was then degassed and controlled amounts were dispensed onto the sensor. This was left to cure at 100 °C for 45 min.

### 3. Readout electronics

The readout electronics for the tactile sensor array encompassed high resolution capacitance-to-digital converters (AD7747, Analog Devices) and was implemented on a Printed Circuit Board (PCB). The chosen converter has a nominal resolution down to 20 aF and an accuracy of 10 fF. As reference capacitors were implemented in the device, a differential capacitive readout was used. This allowed elimination of drift and common mode variations due to proximity and parasitic capacitance coupling between the sensor and the probe. Data from the converters were acquired with a soft-core processor (NiosII, Altera) instantiated onboard a FPGA (CycloneII, Altera) by means of I<sup>2</sup>C communication and then transmitted to a PC (running a Graphical User Interface implemented in Labwindows/CVI) by means of Ethernet communication. The devices were configured to work at an update rate of 45 Hz (11.25 Hz each channel).

### 4. Experimental methods and results

For characterising the response of the individual sensors, indentation testing was performed. The experimental setup, shown in Fig. 6, consisted of a loading system, comprising three orthogonal manual micrometric translation stages (A) with crossed roller

bearing (M-105.10, PI, Karlsruhe, Germany). It allowed precise positioning of a loading probe. The experiments were carried out under displacement control using constant velocities (depending on the experimental session) using a Delrin probe with a spherical head ( $\varnothing$  2 mm) (C). Contact between this part and the sensor was obtained by a servo-controlled micrometric translation stage (M-111.1, PI, Karlsruhe, Germany) (D), which allowed the position of the probe to be finely controlled in the normal direction. Two orthogonally located cameras were used for positioning the probe over the required sensing area. In order to measure and record the force applied to the sensor, a six-component load cell (ATI NANO 17 F/T, Apex, NC, USA) (E) was placed at the interface between the loading probe and the servo-controlled micrometric translation stage. The sensors response was related to the applied force rather than pressure as relating it to the latter would require a precise knowledge of the actual contact area between the spherical indenter head and the contact surface.

#### 4.1. Response of bare sensors

The indenter probe was aligned over the bare/unpackaged sensor diaphragm and advanced towards it at constant velocity of 0.34  $\mu\text{m/s}$  gradually increasing the applied load. This loading indentation phase was followed by a steady state phase where the probe was held static for a time period, and an unloading phase at the same constant velocity. The maximum displacement applied to the probe varied between different experimental runs in order to span the working range and to estimate the resolution performance of the devices.

The response of the sensor to aforementioned stimulus is shown in Fig. 7. The upper subplot displays data obtained from the capacitance readout system. The plotted change in capacitance,  $\Delta C$ , is the result of a differential reading obtained from deducting the values of initial and reference capacitance from the capacitance of the sensor at each time instance. Thus any parasitic effects due to capacitive coupling are eliminated. The lower subplot is the superimposition of the raw measurements by the commercial load cell and of data (black) obtained by applying a numeric off-line zero-lag Butterworth filter (using Matlab<sup>®</sup>, having a cutoff frequency at 1 Hz). Results show that the change in capacitance follows the patterns of the applied load. The sensitivity is a non-linear function of applied force, as confirmed by the varying slope of Fig. 7(right), therefore an average sensitivity is specified as 0.035 pF/mN over the experimented load force range. The devices were indented to generate a maximum force in the order of 25 mN. Beyond this the capacitance readout saturated.

The devices demonstrated high force resolution as illustrated in Fig. 8. Here they showed an ability to respond to forces in the sub-mN range, thus representing indentation profiles that are not resolved by the used commercial load cell.

To assess the sensor response to short impulses three subsequent stimuli each having 0.2 s pulse width were applied to the sensor diaphragm via the indentation probe. Testing at shorter stimulus time periods was limited by the probe velocities attainable using the current instrumentation and sampling frequency of the signal acquisition electronics. Fig. 9 shows the sensor response to stimuli of <0.2 s. For the given acquisition frequency, no significant response delay between the force stimulus and the change in capacitance ( $\Delta C$ ) is observed.

#### 4.2. Response of PDMS packaged sensor

##### 4.2.1. Force vs. capacitance characteristic response

For protecting sensors from mechanical damage, the sensors were coated with a 200  $\mu\text{m}$  thick layer of Polydimethylsiloxane (PDMS, Sylgard 184), which is a well-known polymer used for sen-

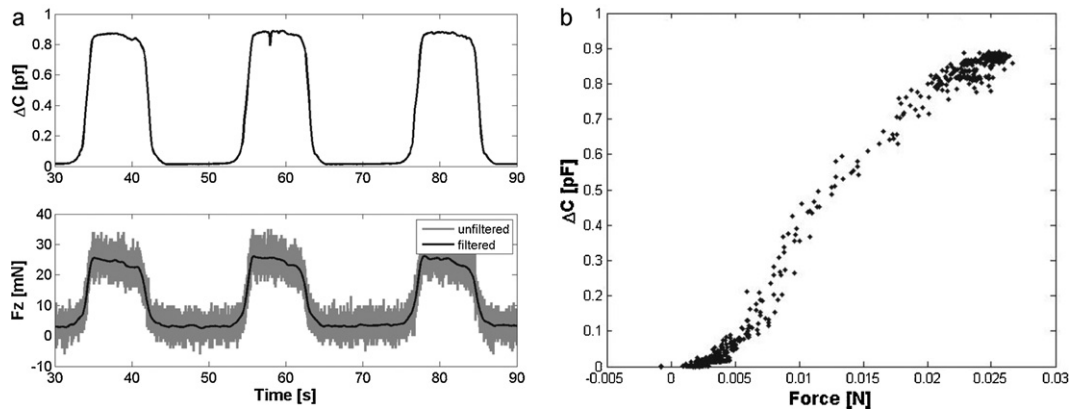


**Fig. 7.** (left) Upper traces: response of the bare sensor to three load–unload indentation cycles applied with a spherical probe under position control. Lower traces: unfiltered and filtered indentation force measurements by the used commercial load cell. A sensitivity of 0.038 pF/mN was experimentally determined. (right) Force vs. change in capacitance ( $\Delta C$ ) graph.

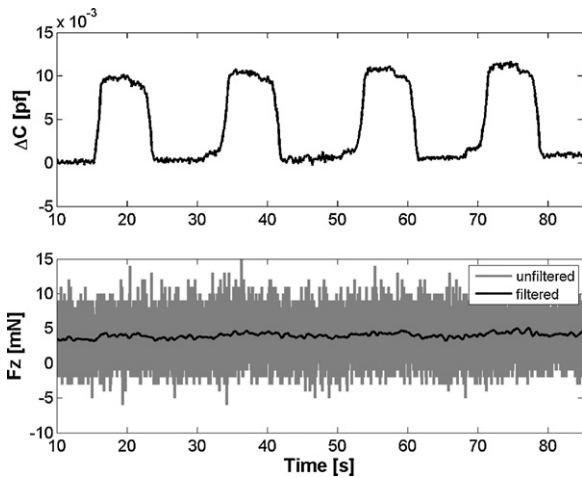


**Fig. 8.** Upper traces: response of a sensor to three “minimum normal force” load–unload indentation cycles. Lower traces: unfiltered and filtered indentation force measurements by the used commercial load cell, that it is not able to resolve the force profile.

sensor packaging. As described in Section 4.1, indentation cycles were applied to the surface of the sensor and response of the sensor simultaneously measured. The influence of the PDMS packaging layer on the response of the sensor can be seen in Fig. 10. For

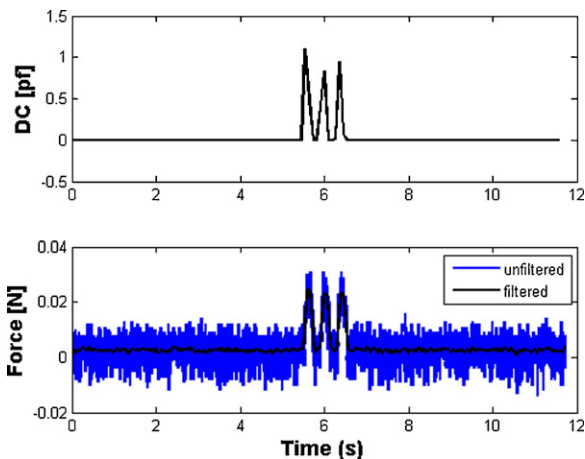


**Fig. 9.** Upper traces: response of a sensor to three fast load–unload indentation cycles applied with a spherical probe under position control. Lower traces: unfiltered and filtered indentation force measurements by the used commercial load cell.

packaged devices, a reduction of the average sensitivity down to 0.068 fF/mN was calculated, in trade-off with the working range, which coherently increased to 1.7 N.

To assess the packaged sensor response to short impulses three subsequent stimuli each having 0.7 s pulse width were applied to the sensor diaphragm via the indentation probe. Testing at shorter stimulus time periods were limited by the probe velocities. Fig. 11 shows the sensor response to the above mentioned stimuli. No significant response delay between the force stimulus and the change in capacitance ( $\Delta C$ ) is observed.

#### 4.2.2. Response to lateral sliding stimuli

A nanotribometer (CSM Instruments) was used to test the response of packaged sensors to lateral sliding stimuli. A spherical probe 2 mm in diameter was indented into the surface of the sensor, generating a force of the order of 100 mN. It was then laterally displaced across the surface to span all the sensor units within the array at a velocity of 0.65 mm/s. A spatio-temporal plot is shown in Fig. 12 which presents the response of each sensor to lateral sliding stimuli. As expected, the distance between peak outputs of each sensor (calculated using the time period between peaks and probe velocity) correlates with the centre-to-centre distance between individual sensing units. The spatial resolution in biological mechanoreceptors is usually described by a parameter known as the receptive field of a receptor. It is the area over the

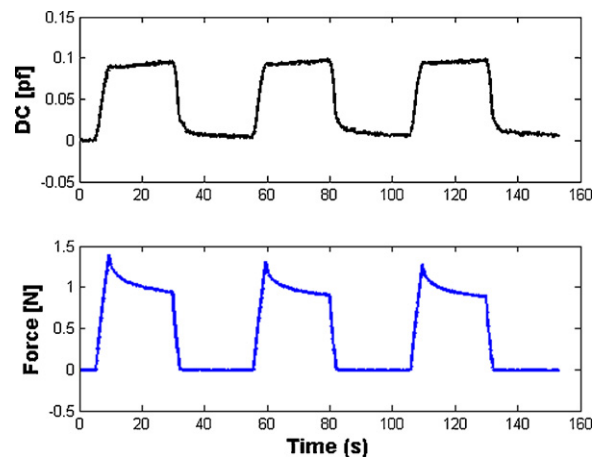


**Fig. 10.** Upper traces: response of the packaged sensor to three load–unload indentation cycles applied with a spherical probe under position control. Lower traces: force measurements by the used commercial load cell. A sensitivity of 0.068 fF/mN was experimentally determined.

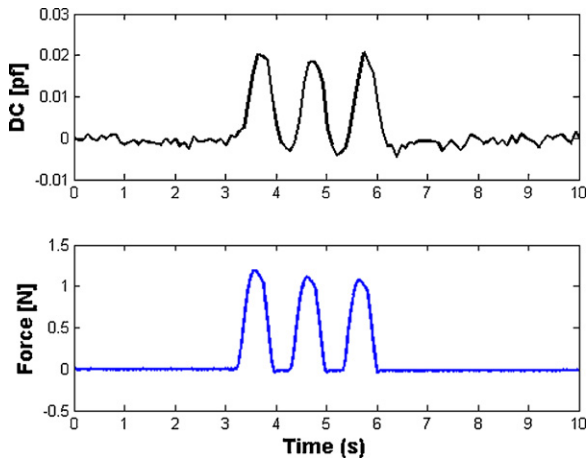


**Fig. 11.** Upper traces: response of a packaged sensor to three fast load–unload indentation cycles applied with a spherical probe under position control. Lower traces: force measurements by the used commercial load cell.

receptor within which a response to mechanical stimulus can be elicited. In a similar manner, the receptive field of mechanical sensors can be described and depends on the stimulus intensity and type of stimulus used. Under the above described loading conditions, the spatial response field in one dimension was calculated (using the time period for which sensor response was generated) to be approximately 1.5 mm.

4.2.3. Spatial mapping of sensor response

In order to map the spatial response field of the packaged sensors, load–unload indentation cycles were applied at six different positions (with a period of 200  $\mu\text{m}$ ) along the horizontal axis of the sensing array. The response of 2 adjacent sensors within an array to increasing forces (generated by indentation testing as described in Section 4.1) at each position is shown in Fig. 13. The receptive field of each sensor is seen to increase with indentation depth as indicated by the widening of the response curve with increasing force. The location where the greatest magnitude of change in capacitance (greatest force sensitivity) is obtained corresponds to the location of the centre of the diaphragm. The distance between regions of maximum sensitivity for 2 adjacent sensors should correspond to the centre to centre distance between them (550  $\mu\text{m}$ ). Approximate locations of diaphragm centres of each sensor can be deduced from the results as illustrated in Fig. 13. A negative response from a sen-

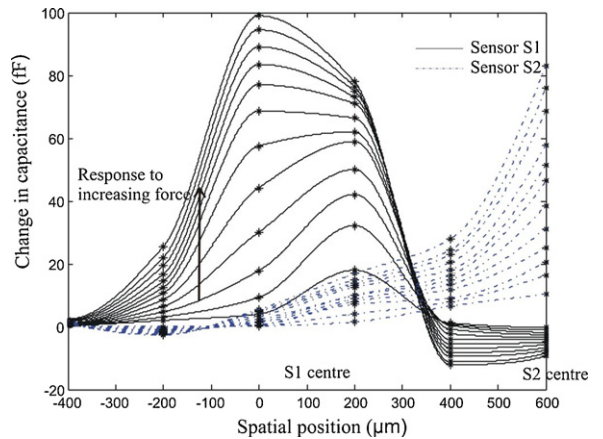


**Fig. 13.** Response of two adjacent sensors S1 and S2 in an array to normal indentation via spherical probe at six positions located 200  $\mu\text{m}$  apart. Centre–centre distance between S1 and S2 is 550  $\mu\text{m}$ , corresponding with the response seen through spatial mapping experimentation.

sor was observed when applying indentations to locations at fixed distances away from the sensor itself. This is most likely related to local changes to the profile of PDMS that occur during indentation. When applying indentations to polymers constrained by a rigid substrate, it has been shown that the indenting probe causes movement of the polymer in the radial direction, perpendicular to the indenter axis [28]. Excess material displaced from the region between the probe and the rigid silicon substrate in turn pushes the surface of the polymer coating upwards in an annular region surrounding the probe tip as there are no constraints to the free surface to restrict this movement. Upward displacement of material will subsequently influence the forces imposed on the sensor generating an inverse response. The inverse response is beneficial in identifying the position of the stimulus with respect to the sensing units.

5. Discussion

A 1  $\times$  4 linear MEMS tactile sensor array was designed and developed. The fabrication process of the sensors was optimized towards a minimum number of processing steps and the sole use of simple standard microfabrication techniques. In comparison with previously reported MEMS based capacitive devices [14,18], the use of BESOI wafers as a substrates allowed for fewer and less complex

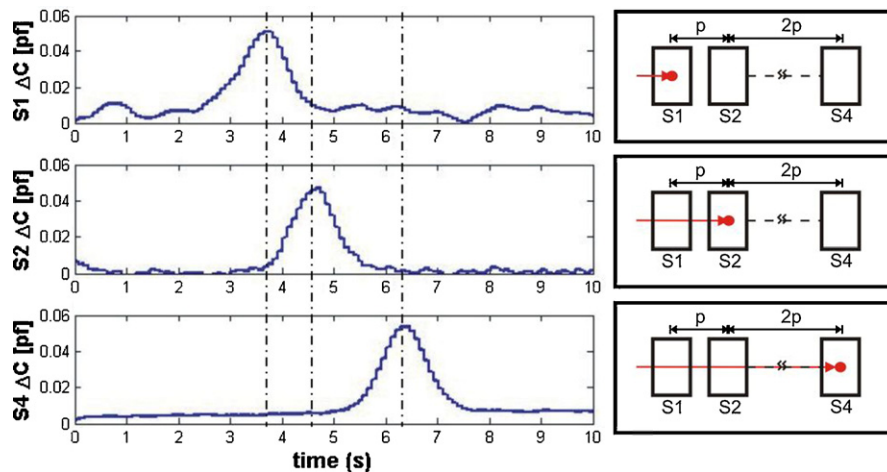


**Fig. 12.** Spatio-temporal event plot showing response of sensors in an array located at distances  $p$  and  $2p$  apart to lateral sliding stimulus via spherical probe displaced at a velocity of 0.65 mm/s.

process steps. Potential difficulties associated with the use of anodic bonding (a commonly used process in capacitive sensor fabrication [29]) were avoided. These include, “snap-down” or sticking of suspended diaphragms due to the presence of electrostatic forces [30,31], introduction of residual stresses in the sensing diaphragm as a result of a mismatch in thermal coefficients of bonding substrates and complexities in accessing electrical connections from the sealed cavity [32,33]. Further, the use of single crystal silicon as the sensing diaphragm material offers advantages over polysilicon (reported by Leineweber et al. [18]) as it does not suffer from stress-related warping that commonly occurs with polysilicon [34,35].

The performance of the sensors was evaluated by applying controlled displacements to the sensor diaphragm via a spherical probe and simultaneous recording of the change in capacitance. The method of applying indentations of controlled amplitudes via punctate probes to the human finger pad has been previously demonstrated for assessing the performance of mechanoreceptors [9]. As expected, the sensor responded to an increase in probe indentation depth with an increase in measured capacitance change. This corresponds with the response of Slowly Adapting (SAI) mechanoreceptors (i.e. the Merkel cells) that respond to an increase in indentation depth of probes with an increase in nerve impulse firing rate [36].

The bare sensor demonstrated high force sensitivity (average of 0.035 pF/mN) and has a dynamic range of 25 mN. Sensors packaged with PDMS showed reduced force sensitivity (average of 0.068 fF/mN) however with an increase in dynamic range to approximately 1.7 N. Previous studies on human perception of touch have shown that the finger contact forces used for discriminating roughness range from 0.8 to 1.6 N with an average of 1 N [37]. The packaged sensors are able to cope with forces within this range.

Bare and packaged sensors were tested to indentation impulses of less than 0.2 s and 0.7 s respectively. For the packaged devices testing at shorter time impulses was limited by the probe speed attainable using the current instrumentation. As the devices are silicon based, they inherently possess high bandwidth as confirmed by the FEM simulation. The bandwidth of the tactile system as a whole is defined by two main factors: The acquisition frequency of the capacitance detection electronics system, which with the currently implemented system is 11.25 Hz per channel of the 4 sensors array, and the response of the PDMS layer.

In their nature of response, the developed sensors particularly imitate the slowly adapting (SAI) mechanoreceptive units i.e. the Merkel cells. These receptors generate responses to mechanical stimuli for as long as a stimulus is present and are hypothesised to be responsible for conveying information regarding surface form and texture [38]. These units have small, well defined receptive fields and are responsible for the high spatial acuity and resolution of the human fingertip which is approximately 1 mm [9]. In tactile sensing, spatial resolution correlates with the distance between sensing elements in an array and sensing range of each unit. Considering the density of elements, the sensors were spaced 170  $\mu\text{m}$  apart with an overall centre-to-centre distance of 570  $\mu\text{m}$ . A high spatial resolution can therefore be anticipated. Additionally with the total sensor unit length of 1840  $\mu\text{m}$  (including the connection pad and the sensing capacitive element), together with the 570  $\mu\text{m}$  centre-to-centre distance (Fig. 5c), a density of about 95 channels/cm<sup>2</sup> can be achieved. This is comparable to the innervations density of SAI units in the distal part of the finger pad which is about 70 per cm<sup>2</sup> [39].

The receptive field of each sensor was experimentally assessed analogous to receptive fields of biological mechanoreceptors. Similarities were demonstrated between receptive field characteristics of the mechanoreceptors and sensors. As in the case of mechanoreceptors, the sensors demonstrate a point of maximum sensitivity

(also termed Hot Spot) [40], when the stimulus is applied to the centre of the sensors receptive field (see Figs. 12 and 13). The response was shown to progressively decrease as the probe is indented at locations away from this region. Similar to the patterns of response found in SA I mechanoreceptive afferents [40], with an increase in indentation amplitude or stimulus intensity, the size of the receptive field and the area of overlap between receptive fields of adjacent sensors in the array tends to increase. Studies conducted on receptive fields of mechanoreceptive afferents have shown that nearly half of the mechanoreceptor afferents exhibit elliptical receptive fields [36]. In this work, the designed sensing membranes were rectangular; due to this asymmetrical design it is expected that the response field would be elliptical rather than circular.

A key design feature in the presented sensing array is the inclusion of reference capacitors that were implemented in close proximity to each sensing element. This design choice enhanced the stability of sensor outputs eliminating the effects of stray capacitance, which is a commonly reported problem in capacitive sensors.

## 6. Conclusions

A silicon based MEMS capacitive tactile sensor array was designed and fabricated by means of a cost efficient process, suitable for batch manufacturing. Sensors were successfully coated with skin-like PDMS polymer. The performance of bare and packaged devices were characterised by means of test methods that have previously been used in assessing the performance of biological mechanoreceptors. This included indentation testing and applications of lateral sliding stimuli. Patterns of sensor response were compared to that of the mechanoreceptors.

Future work will focus on implementing a tactile array incorporating the sensor elements with varying geometrical dimensions. This would give rise to a wider dynamic range of the overall device; the larger sensing units offering higher sensitivity, the smaller units allowing a higher range of detectable forces with the trade-off of a lower sensitivity. It is interesting to note that the population of mechanoreceptor afferents in the fingertip have been shown to demonstrate variations in sensitivities and in the size and structures of their receptive fields [41].

## Acknowledgements

This work was supported by the Commission of the European Union under Contract No. EU-FP6-NMP-033287, Nanobiotact.

## References

- [1] M.H. Lee, Tactile sensing: new directions, new challenges, *The International Journal of Robotics Research* 19 (2000) 636–643.
- [2] Y. Mukaibo, H. Shirado, M. Konyo, T. Maeno, Development of a texture sensor emulating the tissue structure and perceptual mechanism of human fingers, in: *Proceedings of the 2005 IEEE International Conference on Robotics and Automation*, 2005. ICRA 2005, 2005, pp. 2565–2570.
- [3] N. Wettels, V.J. Santos, R.S. Johansson, G.E. Loeb, Biomimetic tactile sensor array, *Advanced Robotics* 22 (2008) 829–849.
- [4] A. Sano, R. Kikuuwe, H. Mochiyama, N. Takesue, H. Fujimoto, A tactile sensing for human-centered robotics, in: *2006 IEEE Sensors*, Vols. 1–3, IEEE, New York, 2006, pp. 819–822.
- [5] L. Beccai, S. Roccella, L. Ascari, P. Valdastris, A. Sieber, M.C. Carrozza, P. Dario, Development and experimental analysis of a soft compliant tactile microsensor for anthropomorphic artificial hand, *IEEE-ASME Transactions on Mechatronics* 13 (2008) 158–168.
- [6] J. Dargahi, S. Najarian, Human tactile perception as a standard for artificial tactile sensing – a review, *International Journal of Medical Robotics and Computer Assisted Surgery* 1 (2004) 23–35.
- [7] R.D. Howe, M.R. Cutkosky, Sensing skin acceleration for slip and texture perception, in: *IEEE International Conference on Robotics and Automation*, 1989, pp. 145–150.
- [8] P. Dario, Tactile sensing – technology and applications, *Sensors and Actuators A: Physical* 26 (1991) 251–256.

- [9] A.W. Goodwin, H.E. Wheat, Physiological responses of sensory afferents in glabrous and hairy skin of humans and monkeys, in: I.B. Allan, et al. (Eds.), *The Senses: A Comprehensive Reference*, Academic Press, New York, 2008, pp. 39–54.
- [10] P. Dario, D. De Rossi, C. Domenici, R. Francesconi, Ferroelectric polymer tactile sensors with anthropomorphic features, in: *IEEE International Conference on Robotics and Automation*, 1984, pp. 332–340.
- [11] S. Omata, Y. Terunuma, New tactile sensor like the human hand and its applications, *Sensors and Actuators A: Physical* 35 (1992) 9–15.
- [12] S.K. Yeung, E.M. Petriu, W.S. McMath, D.C. Petriu, High sampling resolution tactile sensor for object recognition, *IEEE Transactions on Instrumentation and Measurement* 43 (1994) 277–282.
- [13] D.J. Beebe, A.S. Hsieh, D.D. Denton, R.G. Radwin, A silicon force sensor for robotics and medicine, *Sensors and Actuators A: Physical* 50 (1995) 55–65.
- [14] Z. Chu, P.M. Sarro, S. Middelhoeck, Silicon three-axial tactile sensor, *Sensors and Actuators A: Physical* 54 (1996) 505–510.
- [15] T. Maeno, T. Kawai, K. Kobayashi, Analysis and design of a tactile sensor detecting strain distribution inside an elastic finger, in: *IEEE/RSJ International Conference on Intelligent Robots and Systems*, 1998, pp. 1658–1663.
- [16] J. Dargahi, A piezoelectric tactile sensor with three sensing elements for robotic, endoscopic and prosthetic applications, *Sensors and Actuators A: Physical* 80 (2000) 23–30.
- [17] T. Mei, W.J. Li, Y. Ge, Y. Chen, L. Ni, M.H. Chan, An integrated MEMS three-dimensional tactile sensor with large force range, *Sensors and Actuators A: Physical* 80 (2000) 155–162.
- [18] M. Leineweber, G. Pelz, M. Schmidt, H. Kappert, G. Zimmer, New tactile sensor chip with silicone rubber cover, *Sensors and Actuators A: Physical* 84 (2000) 236–245.
- [19] L. Beccai, S. Roccella, A. Arena, F. Valvo, P. Valdastri, A. Menciaci, M.C. Carrozza, P. Dario, Design and fabrication of a hybrid silicon three-axial force sensor for biomechanical applications, *Sensors and Actuators A: Physical* 120 (2005) 370–382.
- [20] K. Hosoda, Y. Tada, M. Asada, Anthropomorphic robotic soft fingertip with randomly distributed receptors, *Robotics and Autonomous Systems* 54 (2006) 104–109.
- [21] J. Scheibert, S. Leurent, A. Prevost, G. Debregeas, The role of fingerprints in the coding of tactile information probed with a biomimetic sensor, *Science* 323 (2009) 1503–1506.
- [22] Y.S. Lee, K.D. Wise, A batch-fabricated silicon capacitive pressure transducer with low temperature sensitivity, *IEEE Transactions on Electron Devices* 29 (1982) 42–48.
- [23] J.C. Greenwood, Silicon in mechanical sensors, *Journal of Physics E: Scientific Instruments* 21 (1988) p1114.
- [24] C.M. Oddo, L. Beccai, M. Felder, F. Giovacchini, M.C. Carrozza, Artificial roughness encoding with a bio-inspired MEMS-based tactile sensor array, *Sensors* 9 (2009) 3161–3183.
- [25] S.P. Timoshenko, S. Woinowsky-Krieger, *Theory of Plates and Shells*, 2nd ed., McGraw-Hill, 1959.
- [26] F. Bitsie, W.P. Eaton, D.W. Plummer, J.H. Smith, A New Analytical Solution for Diaphragm Deflection and its Application to a Surface-Micromachined Pressure Sensor, 1999.
- [27] J. Vedde, P. Gravesen, The fracture strength of nitrogen doped silicon wafers, *Materials Science and Engineering B* 36 (1996) 246–250.
- [28] Y.C. Lu, D.M. Shinozaki, Effects of substrate constraint on micro-indentation testing of polymer coatings, *Materials Science and Engineering A* 396 (2005) 77–86.
- [29] R. Puers, Capacitive sensors: when and how to use them, *Sensors and Actuators A: Physical* 37–38 (1993) 93–105.
- [30] H. Yu, G. Zhou, F.S. Chau, Yield improvement for anodic bonding with suspending structure, *Sensors and Actuators A: Physical* 143 (2008) 462–468.
- [31] R. Puers, D. Lapadatu, Electrostatic forces and their effects on capacitive mechanical sensors, *Sensors and Actuators A: Physical* 56 (1996) 203–210.
- [32] D.C. Catling, High-sensitivity silicon capacitive sensors for measuring medium-vacuum gas pressures, *Sensors and Actuators A: Physical* 64 (1998) 157–164.
- [33] I. Sadaba, C.H.J. Fox, S. McWilliam, An investigation of residual stress effects due to the anodic bonding of glass and silicon in MEMS fabrication, in: P.S. Keogh (Ed.), *Proceedings, Modern Practice in Stress and Vibration Analysis VI*, vols. 5–6, Trans Tech Publications Ltd., Stafa-Zurich, 2006, pp. 501–508.
- [34] A.Y. Usenko, W.N. Carr, SOI technology for MEMS applications, in: P.L.F. Hemment (Ed.), *Proceedings of the Ninth International Symposium on Silicon-on-Insulator Technology and Devices*, vol. 99, Electrochemical Society Inc., Pennington, 1999, pp. 347–352.
- [35] Y. Matsumoto, M. Iwakiri, H. Tanaka, M. Ishida, T. Nakamura, A capacitive accelerometer using SDB-SOI structure, *Sensors and Actuators A: Physical* 53 (1996) 267–272.
- [36] A.P. Sripati, S.J. Bensmaia, K.O. Johnson, A continuum mechanical model of mechanoreceptive afferent responses to indented spatial patterns, *Journal of Neurophysiology* 95 (2006) 3852–3864.
- [37] S.A. Jones, S.J. Lederman, *Human Hand Function*, Oxford University Press, 2006.
- [38] D.T. Blake, S.S. Hsiao, K.O. Johnson, Neural coding mechanisms in tactile pattern recognition: the relative contributions of slowly and rapidly adapting mechanoreceptors to perceived roughness, *Journal of Neuroscience* 17 (1997) 7480–7489.
- [39] A.B. Vallbo, R.S. Johansson, Properties of cutaneous mechanoreceptors in the human hand related to touch sensation, *Human Neurobiology* 3 (1984) 3–14.
- [40] F. Vega-Bermudez, K.O. Johnson, SA1 and RA receptive fields, response variability, and population responses mapped with a probe array, *Journal of Neurophysiology* 81 (1999) 2701–2710.
- [41] M. Knibestöl, Stimulus-response functions of rapidly adapting mechanoreceptors in the human glabrous skin area, *The Journal of Physiology* 232 (1973) 427–452.

## Biographies

**H.B. Muhammad** received a B.Eng. (Hons.) in medical engineering from Bradford University in 2001 and an M.Sc. in biomedical engineering from the University of Surrey in 2003. She underwent the clinical scientist training, specialising in the field of rehabilitation engineering until 2007 (Dip. IPeM). She is currently pursuing a Ph.D. in microengineering. Her main research interests are in MEMS tactile sensors and in the field of medical device design and development.

**C.M. Oddo** was born in 1983. He received, all with summa cum laude, the B.Sc. EE (2005) and the M.Sc. EE (2007) from University of Pisa, Italy, and the Industrial and Information Engineering First (2006) and Second (2009) level degrees from Scuola Superiore Sant'Anna. He is currently a 3rd year Ph.D. student in BioRobotics and is involved in related international and national projects. He is author of more than 10 papers in referred international journals and conferences. He was finalist for the Best Student Paper Award at the IEEE RoBio 2009 conference. His current research interests are in the design and experimentation of tactile sensors, with specific attention to artificial roughness encoding.

**L. Beccai** is team leader at the Center for Micro-BioRobotics IIT@SSSA, from November 2009. Since 1999 she performed research at both CRIM and ARTS laboratories of Scuola Superiore Sant'Anna where, from 2008, she had a temporary position of assistant professor in bioengineering. She has matured expertise in biomechanics and microsystem engineering in the biomedical field and contributed to many international projects. She is member of the IEEE and her scientific interests are related to investigate innovative sensing, actuation and locomotion strategies in robotics using inspiration from Nature. Current focus is on, soft tactile sensors, bio-hybrid sensing systems and soft bodied microrobots.

**C. Recchiuto** was born in 1984. He received the master degree in electronic engineering from the University of Pisa, Italy, in December 2008. Since March 2009 he joined the Advanced Robotic Technology and System (ARTS) Lab of the Scuola Superiore Sant'Anna in Pisa as a Research Fellow. His main research interests are in the fields of microsystems, sensors and signal conditioning.

**C.J. Anthony** received the B.Sc. degree in physics with optoelectronics from the University of Surrey in 1993 and the Ph.D. degree in electronic engineering from Newcastle University in 2006. From 1993 to 2005 he worked at the QinetiQ Malvern technology centre. His research focussed on the reliability of high temperature and high power electronic devices, uncooled thermal imaging technology and microsystems. He is currently a lecturer in the MicroEngineering group in the School of Mechanical Engineering at the University of Birmingham. His research interests are in the field of microsystems engineering; focused on coupled/non-linear resonator systems, autonomous oscillators, energy harvesting for mobile/remote sensors and bio-MEMS tactile sensors.

**M.J. Adams** joined the School of Chemical Engineering at the University of Birmingham in 2004. He was previously a senior scientist with Unilever R&D. He is a fellow of the Royal Academy of Engineering, the Institution of Chemical Engineers, the Royal Society of Chemistry and the Institute of Physics. In 1999 he was awarded the Donald Julius Groen Prize by the IMechE for outstanding contributions to interfacial engineering. His research interests are concerned with the behaviour of complex material systems including the tribological, adhesive and mechanical properties of biological materials such as human skin.

**M.C. Carrozza** is full professor of biomedical engineering and robotics at Scuola Superiore Sant'Anna (SSSA). Since November 2007 she is director of SSSA. She has scientific and coordination responsibilities within several European, national and regional research projects. She leads a group of about 35 researchers, Ph.D. students and research assistants. She authored more than 60 ISI journal papers, more than 100 papers in referred conference proceedings and 12 patents. Her research interests are in ambient assisted living, biorobotics, rehabilitation engineering, bionics, cybernetic hands, humanoid robotics, functional replacement and augmentation systems, biomechatronic interfaces, tactile sensors, artificial skin and renewable energy.

**D.W.L. Hukins** holds degrees from the Universities of London (Queen Mary and King's College) and the University of Manchester and is a fellow of the Royal Society of Edinburgh. He has held academic and research posts at Purdue University, University of Oxford, University of Aberdeen (where he was MacRobert Professor of Physics) and the University of Birmingham (where he is currently professor of bio-medical engineering and head of the School of Mechanical Engineering). His research covers a range of topics in biomedical engineering including the potential application of MEMS devices.

**M.C.L. Ward** obtained his physics degree from Imperial College in 1981 and subsequently was awarded his Ph.D. from Warwick University for his EXAFS study on the passivation of stainless steels. In 1985 he joined RSRE Malvern where he worked for IR detectors, image processing, SOI electronics and MEMS before joining the university of Birmingham in 1999. He is currently senior lecturer in microsystem engineering with research interest in noise, non-linear mechanics and microfluidics.



## A capacitive tactile sensor array for surface texture discrimination

H.B. Muhammad<sup>a,\*</sup>, C. Recchiuto<sup>b</sup>, C.M. Oddo<sup>b</sup>, L. Beccai<sup>c</sup>, C.J. Anthony<sup>a</sup>, M.J. Adams<sup>a</sup>,  
M.C. Carrozza<sup>b</sup>, M.C.L. Ward<sup>a</sup>

<sup>a</sup>Bio-medical and Micro Engineering Research Centre, School of Mechanical Engineering, University of Birmingham, Edgbaston, Birmingham, United Kingdom

<sup>b</sup>Advanced Robotics Technology and Systems Laboratory, Polo Sant'Anna Valdera – Scuola Superiore Sant'Anna, Pontedera, PI 56025, Italy

<sup>c</sup>Center for Micro-BioRobotics@SSSA, Istituto Italiano di Tecnologia (IIT), Pontedera, PI 56025, Italy

### ARTICLE INFO

Article history:  
Available online xxx

Keywords:  
MEMS  
Tactile sensor  
Biomimetic  
Capacitive sensor

### ABSTRACT

This paper presents a silicon MEMS based capacitive sensing array, which has the ability to resolve forces in the sub mN range, provides directional response to applied loading and has the ability to differentiate between surface textures. Texture recognition is achieved by scanning surfaces over the sensing array and assessing the frequency spectrum of the sensor outputs.

© 2011 Elsevier B.V. All rights reserved.

### 1. Introduction

The discrimination of textures is an essential feature of artificial tactile sensing with applications in robotics, minimal invasive surgery and manufacturing industries. Work on tactile sensor development is inspired by the performances of the mechanoreceptors (biological sensors) of the human finger pad [1–3]. Challenges lie in the development of devices that are comparable to the mechanoreceptors in terms of sensitivity, spatial acuity, directional response to applied force and texture detection. Recently, Oddo et al. demonstrated a piezoresistive based bio-inspired tactile sensor array for artificial roughness encoding [4]. The device successfully discriminated between ridged surfaces with spatial periods from 2.6 mm to 4.1 mm. De Boissieu et al. also demonstrated the performance of a similar piezoresistance based device for recognition of papers and fabrics [5].

The authors have recently described a linear array of MEMS based tactile sensors intended for incorporation into a robotic finger [6]. The sensing principle was capacitance based because of their advantages in terms of higher sensitivity, long term drift stability, lower temperature sensitivity and power consumption as compared to piezoresistive devices that have been used in previous works [7].

Currently there is no consolidated agreement in the literature regarding the neural mechanisms underlying texture perception in humans. Hollins and Risner [8] proposed a duplex mechanism supporting Katz's hypothesis, i.e. a vibrotactile mechanism accounting for the perceived roughness of fine textures and a spatial coding mechanism for perception of coarse textures. Conversely, Yoshioka

and colleagues proposed a unified paradigm via the spatiotemporal modulation of the neural activity of SAI afferents [9]. However, an established finding is the enhanced discrimination sensitivity obtained as a consequence of relative motion between the finger and the surface. While detecting textures, humans tend to slide their finger over the surface of interest; this relative motion, eliciting vibratory mechanical waveforms at finger–object interface, is hypothesised to be a requirement for the perception of fine textures [10], whether the neural encoding mechanism is actually temporal [8] or spatiotemporal [9]. Studies on texture perception often employ gratings of alternating ridges and grooves as moving stimulus to the finger pad while simultaneously recording the responses of the mechanoreceptors and subjects perceptions [9,11]. The main focus of the current work is to demonstrate the ability of the MEMS sensors in recognition of different textures, using protocols inspired by such experiments.

### 2. Sensor description

A linear array of 4 MEMS based capacitive sensors was designed and fabricated using a bonded and etched-back silicon-on-insulator (BESOI) wafer as a substrate. Each sensor incorporates an upper 2 μm thick highly doped single crystal silicon diaphragm (resistivity <0.006 Ω cm), a 2 μm air cavity formed by sacrificial layer releasing and a lower electrode consisting of highly doped silicon (Fig. 1a). Individual sensing elements have dimensions of 500 μm × 400 μm and are separated by 150 μm (Fig. 1b). The device was packaged with a 200 μm thin layer of PDMS (Sylgard 184) to protect the chip from damage and to provide a skin-like covering for transmitting applied loads to the sensing diaphragm. For acquiring signal response from the sensors, the readout

\* Corresponding author. Tel.: +44 0121 4144217; fax: +44 0121 4143958.  
E-mail address: [hbm768@bham.ac.uk](mailto:hbm768@bham.ac.uk) (H.B. Muhammad).

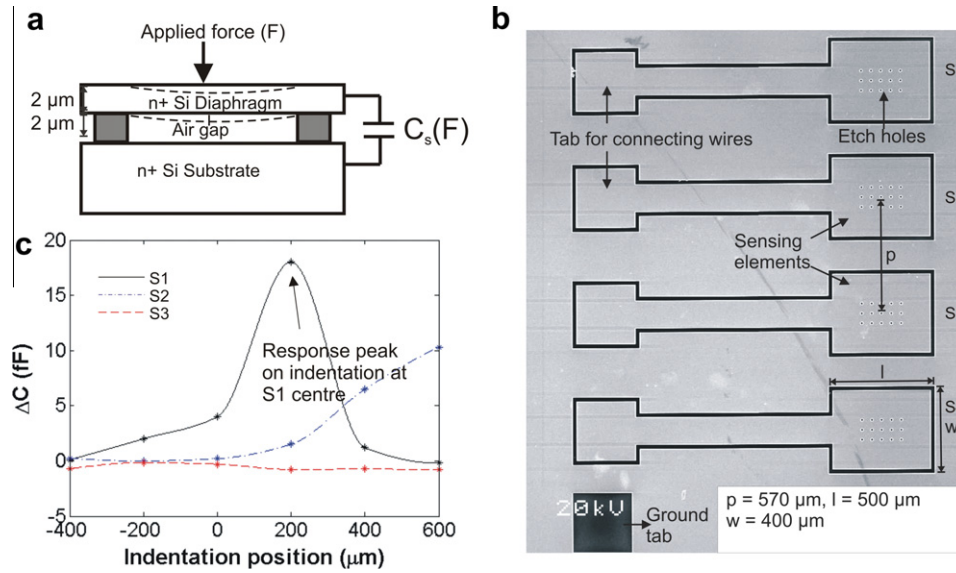


**Fig. 1.** (a) Schematic of cross sections of single sensor, (b) SEM image of  $1 \times 4$  linear tactile sensor array showing geometrical dimensions of device, and (c) Response of sensors in an array to spatially varying stimuli.

electronics was implemented with four capacitance-to-digital converters (Analog Devices, AD7747). These devices have a resolution down to 20 aF and an accuracy of 10 fF. Data from the converters were acquired with a soft-core processor (NiosII, Altera) instantiated onboard a FPGA (CycloneII, Altera). The devices were configured to work at an update rate of 45 Hz (11.25 Hz each channel).

The performance of sensors has previously been evaluated by applying controlled displacements to the diaphragm via a 2 mm  $\varnothing$  spherical probe at different locations across the width of the sensing elements and simultaneously recording the capacitance change [6]. Fig. 1c shows sensor outputs for stimuli applied at specific points along the sensing axis. The greatest magnitude of response corresponds to the indentation at the centre of the diaphragm; then the sensor output decreases in magnitude with increasing distances from this point. Given the response behavior, a comparison of the sensing units can be attempted to the Slowly Adapting type I (SA-1) mechanoreceptive units, which generate responses to mechanical stimuli for as long as a stimuli is present and are hypothesised to convey information regarding surface form and texture [12].

Variation in responses of sensors in an array can be used to identify spatial features of a surface. However, such approach could lack in accuracy when exploring surfaces with spatial features finer than the spacing between neighbouring sensors. Another option, which is pursued in the following, is to introduce a relative motion (resulting in a dynamic touch protocol) between the tactile array and the stimuli, and to analyse the vibrational patterns arising in sensor outputs. In principle such an approach may be effective with a single sensor, but the availability of an array offers several advantages such as a wider sensorised contact area and the possibility of identifying irregular texture patterns differing along the specimen. Therefore, experimental results under a dynamic touch protocol are presented in the next section. Gratings varying in spatial periodicity from 400  $\mu\text{m}$  to 1200  $\mu\text{m}$  (Section 3.1) and fabrics (Section 3.2) were evaluated.

### 3. Experimental methodology and results

#### 3.1. Discrimination of gratings varying in spatial periodicity

Five gratings varying in spatial periodicity were fabricated using multi jet modeling (MJM) technology [13]. The ridge width and

ridge height were kept constant at 200  $\mu\text{m}$  and 400  $\mu\text{m}$ , respectively. The groove width varied from 200 to 1000  $\mu\text{m}$  in increments

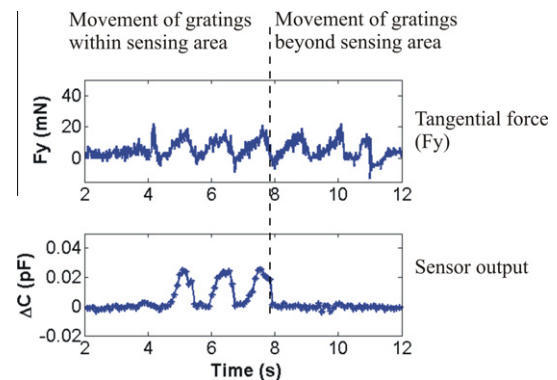


**Fig. 2.** Temporal plots showing the recorded tangential force ( $F_y$ ) and the change in capacitance ( $\Delta C$ ) by a sensor of the array in response to an applied stimulus via a grating with a 600  $\mu\text{m}$  spatial period.

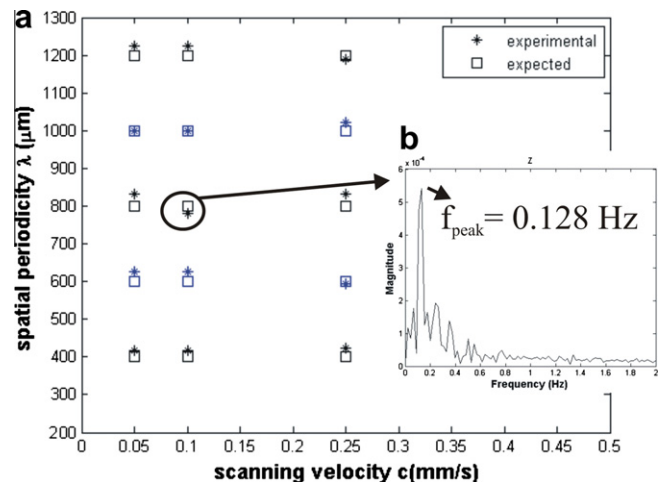


**Fig. 3.** (a) Expected and experimentally determined grating spatial periodicity at three different scan velocities and (b) FFT spectrum for single measurement showing peak frequency ( $f_{\text{peak}}$ ).

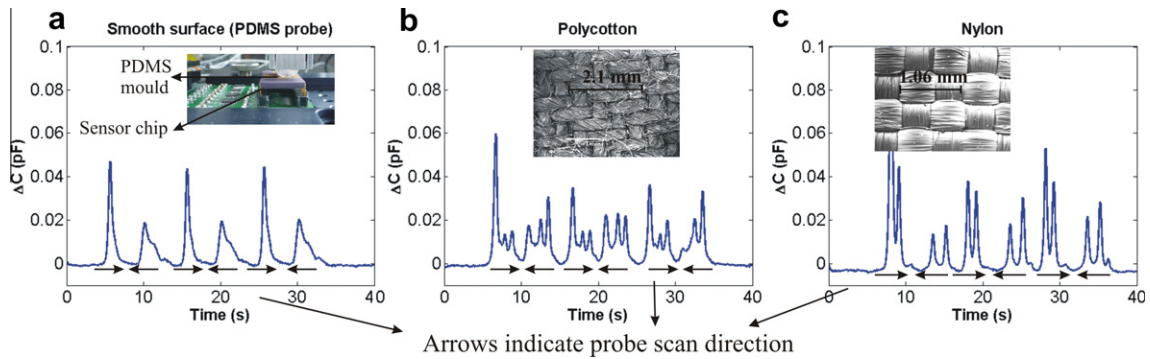


Fig. 4. Results showing sensor output ( $\Delta C$ ) with time to applied stimulus of (a) smooth PDMS surface, (b) polycotton and (c) nylon.

of 200  $\mu\text{m}$  thus generating a range of textures from fine to coarse. The gratings were tangentially displaced over the sensor surface at velocities ranging from 0.05 mm/s to 4 mm/s with an average normal force ( $F_z$ ) of 10 mN. Low velocities were experimented due to the limited acquisition frequency of signal recording electronics (11.25 Hz/channel). To deliver the stimulus to the sensors, a custom built mechatronic platform which allowed two degrees of freedom for movement was used. The gratings were mounted to the moving arm and applied forces were recorded via a commercial ATI load cell.

Both temporal and spectral domains of sensor signals generated in response to applied gratings were assessed. A typical temporal trace of results can be seen in Fig. 2 where the output of a single sensor follows the variations of the tangential contact force component ( $F_y$ ). Further, the FFT spectrum of the signals from the sensors was calculated for each experimental run and the peak frequency was determined. Fig. 3a shows the experimentally determined spatial periodicity of gratings for measurements made using three different velocities. The spatial periodicity ( $\lambda$ ) is calculated from the scanning velocity ( $c$ ) and peak frequency ( $f_{\text{peak}}$ ) (Fig. 3b) according to the equation  $\lambda = c/f_{\text{peak}}$ . The results (Fig. 3) showed that the sensor array was able to distinguish between all the gratings and good correlation was found between calculated and experimentally obtained values.

### 3.2. Discrimination of fabrics

After the successful discrimination of gratings, the tactile sensing device was evaluated with fabrics varying in texture (including polycotton and nylon). Each fabric was attached to a cylindrical PDMS probe which was then mounted onto the moving arm of a tribometer, loaded using a weight of 40 g, and tangentially displaced across the sensor surface. The sensors response to a smooth surface was also tested in a similar manner using the PDMS probe directly. Three subsequent experimental runs were carried out with each run comprising scanning the probe with a velocity of 1 mm/s across the sensors in one direction followed by a subsequent scan in the opposite direction. Time domain sensor outputs, shown in Fig. 4, reveal characteristic responses for each material. In particular, specific features were observed in peak density and in the spatial period (determined from the measurement of the time lag between peaks in capacitance change and from the knowledge of the scan velocity). These particular features in sensor outputs

could be related to the spatial periodicity of tested fabrics as determined using SEM (Fig. 4). A directional response to applied tangential loading was also observed through an apparent enhanced sensitivity in one scan direction. This can be attributed to factors such as non-uniform thickness of the packaging layer and an uneven surface topology which can lead to differences in stress propagation through the material dependent on the scan direction.

## 4. Conclusions

A MEMS based capacitive sensing array was demonstrated for texture recognition applications. Using periodic gratings and fabrics, the performance of sensors for discrimination of coarse to fine textures (with feature spacing down to 0.2 mm) was successfully demonstrated. The availability of an array of tactile sensors will allow a combined spatio-temporal approach for the discrimination of textures, by considering the spectral content of each single sensor output and the variation in responses of spatially located sensors. Further experimental work will investigate scanning of fabrics in multi directions in order to explore non-periodic/random topologies.

## Acknowledgements

This work was supported by the Commission of the European Union under Contract No. EU-FP6-NMP-033287, Nanobiotact. The authors would like to thank Satoshi Endo for his assistance in fabrication of the gratings.

## References

- [1] N. Wettels et al., *Advanced Robotics* 22 (2008) 829–849.
- [2] A. Sano et al., *Sensors* (2006) 819–822.
- [3] L. Beccai et al., *IEEE ASME Transactions on Mechatronic* 13 (2008) 158–168.
- [4] C.M. Oddo et al., *Sensors* 9 (2009) 3161–3183.
- [5] De Boissieu et al., *Robotic Science System*, 2009.
- [6] H.B. Muhammad et al., *Sensors and Actuators A: Physical* 165 (2011) 221–229.
- [7] Y.S. Lee et al., *IEEE Transactions on Electronic Devices* 29 (1982) 42–48.
- [8] M. Hollins et al., *Perception and Psychophysics* 62 (4) (2000) 695–705.
- [9] T. Yoshioka et al., *Journal of Neuroscience* 21 (17) (2001) 6905–6916.
- [10] B. Hughes, G. Jansson, *Human Movement Science* 13 (1994) 301–333.
- [11] K. Sathian et al., *Journal of Neuroscience* 9 (4) (1989) 1273–1279.
- [12] D.T. Blake et al., *Journal of Neuroscience* 17 (19) (1997) 7480–7489.
- [13] S. Upcraft et al., *Assembly Automation* 23 (4) (2003) 318–330.

# A Biomimetic MEMS-based Tactile Sensor Array with Fingerprints integrated in a Robotic Fingertip for Artificial Roughness Encoding

Calogero M. Oddo, Lucia Beccai, *Member, IEEE*, Giovanni G. Muscolo, and Maria Chiara Carrozza, *Associate Member, IEEE*

**Abstract**—This work shows the accomplishment of a full integration of a biomimetic 2x2 tactile array and related electronics in an artificial fingertip. The technological approach is based on merging 3D MEMS sensors and skin-like artificial materials that are moulded mimicking human epidermal ridges. Experimental results using a mechatronic tactile stimulator for indenting periodic gratings (spatial periodicity from 400  $\mu\text{m}$  to 1900  $\mu\text{m}$ ) and sliding them at constant speeds (from 5 mm/s to 40 mm/s) under regulated normal contact forces (between 100 mN and 400 mN) show that the developed sensing technology is suitable for fine roughness encoding: a frequency shift of the principal spectral component arising from sensor outputs was observed coherently with the spatial periodicity of the used ridged stimuli and their sliding velocity. Such phenomenon is pointed out with fine gratings particularly when the stimulation is operated along the proximal-distal direction of the finger (i.e. with sliding motion of the ridges of the stimulus across the ridges of the packaging) showing a more marked frequency locked behavior if compared to the radial-ular stimulation (i.e. with sliding motion of the ridges of the grating along the ridges of the packaging).

## I. INTRODUCTION

ROUGHNESS encoding and perception are enhanced by movement [1]. Texture related vibrations generated during dynamic touch exploratory tasks are fundamental for the discrimination of tactile stimuli [2]-[4].

Finite element analyses using human finger model during dynamic touch showed that spatial information of the textured surface are related to temporal frequency changes at the position of tactile receptors [5]. In touch activities, if humans have the ability to estimate somehow the relative hand velocity  $v$  between the textured surface and the exploring finger, the spatial period  $\Delta p$  of the surface can be perceived by detecting the temporal frequency of the vibration [5], such that:

$$f = \frac{v}{\Delta p} \quad (1)$$

In artificial touch, when considering technological

Manuscript received July 31, 2009. This study was funded by the NANOBIOCONTACT project (EU-FP6-NMP-033287).

C. M. Oddo is with the ARTS Lab of Scuola Superiore Sant'Anna, Pontedera, PI 56025 Italy (e-mail: oddoc@sssup.it).

L. Beccai is with the ARTS Lab of Scuola Superiore Sant'Anna and with the Center for Micro-BioRobotics, Italian Institute of Technology (IIT), Pontedera, PI 56025 Italy (phone: 0039-050-883-064; fax: 0039-050-883-101/497; e-mail: l.beccai@sssup.it).

G. G. Muscolo is with the ARTS Lab of Scuola Superiore Sant'Anna, Pontedera, PI 56025 Italy (e-mail: g.muscolo@sssup.it).

M. C. Carrozza is with the ARTS Lab of Scuola Superiore Sant'Anna, Pontedera, PI 56025 Italy (e-mail: carrozza@sssup.it).

approaches in which mechanical sensing elements are embedded in skin-like elastomeric matrices that mimic human skin, such vibrations should be elicited by stimulus-skin interface, by motion dynamics and by contact mechanics, and then gathered by the sensing units located under the covering material [6]-[8].

Stimuli have to be encoded with high sensitivity and discrimination capability. The surface conditions, e.g. morphology, roughness, hardness etc..., of the skin-like materials play a major role and strongly affect the deformation of the sensor elements embedded therein. Especially stimuli applied in the horizontal direction against the surface of the skin-like tactile arrays may result in a more effective deformation of the sensor element with a fingerprint-type surface than that with a smooth surface [8].

In parallel, the type of artificial sensor used is a crucial choice since the sensor must have a design that allows technological coupling with skin-like polymeric packaging and also capable of detecting the induced deformation by the external mechanical stimuli correspondent to the tactile event to be encoded or detected. It has been shown that MEMS based tactile sensors can be designed and built with a 3D structure that can adequately be packaged with skin-like polymeric materials so that the sensor and soft packaging become a new tactile sensible element like the Soft and Compliant Tactile Microsensor reported in [9]. Such integration can thus yield to a robust yet highly sensitive device offering the possibility to provide information about static contact forces and dynamic events with one tactile element. This technological approach was also ascertained for roughness encoding by building tactile sensor arrays [4].

In this work, the development of a MEMS based biomimetic sensor array with polymeric fingerprint-type surface is presented. This approach is proposed for promoting texture related vibrations when applying stimuli having medium-fine periodic ridged structure. Surface ridges were purposely introduced in the packaging design for achieving spectral selection and amplification of tactile information as has been supposed to happen in the human finger [8]. A bi-layer packaging, with increasing hardness going from the inner layer to the external surface, was used in order to enhance biomimeticity to human skin. The biomimetic tactile sensor array and dedicated readout electronics were integrated in a distal phalanx of a robotic fingertip [10], [11] (which in a previous design hosted one

single sensor [12]) which was investigated by means of preliminary experimental protocols aimed at studying its capability to encode texture related cues.

## II. MATERIALS

### A. MEMS sensor array and electronics for integration in a robotic finger

An improved version of the MEMS presented in [13] was employed and the array was built by connecting by flip-chip bonding four microsensors by means of a micro-soldering paste directly on a rigid-flex board which was concurrently designed with the distal phalanx of an artificial finger in order to achieve the following results:

- a 2x2 array of microsensors integrated in an artificial fingertip with robust (both mechanical and electrical) connection and with all the conditioning electronics integrated on board;
- a 2x2 sensing array that could be suitably packaged with skin-like materials without affecting the tactile array itself nor compromising the integration in the artificial fingertip.

The bare sensor array, depicted in Fig. 1, had 16 channels as total tactile sensor outputs, and it had a pitch of 2.36 mm. Unlike the previous approach [4] the wire bonding could be avoided in this case because of the usage of the rigid-flex board solution. With respect to the previous study a new version of the electronics was used; the number of discrete components could be reduced because of the improved design of the MEMS sensor, enabling the full integration in the distal phalanx of a robotic finger. Each piezoresistor-resistor arm was supplied by means of a 5V DC regulated voltage, and the node between each piezoresistor and the completing integrated resistor was directly acquired without pre-amplification by means of a 16-channel 24-bit Analog to Digital Converter (ADS1258, Texas Instruments). The sampling frequency was set to 350 Hz. The data acquisition system was based on Field Programmable Gate Array technology (CycloneII, Altera) and the acquisition of each channel had a time reference with resolution of 20 ns. Data was acquired by a soft-core processor (NiosII, Altera), parallel to a second processor by means of which the mechatronic stimulator used in experiments (see Section 3-A) was controlled. Data was transmitted in real-time to a PC by means of Ethernet protocol with full digital synchronization of stimulus force and position.

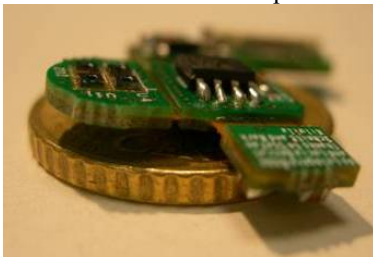


Fig. 1. The developed rigid-flex board integrating the 2x2 array of MEMS sensors.

### B. Packaging with ridges: design, fabrication and integration in a robotic finger

Biomimeticism was pursued by designing a bi-layer packaging with increasing hardness going from the inner layer to the external surface, by introducing ridges, by mimicking the positioning of type I human mechanoreceptors and by allowing the design to be compatible with a thin protective layer mimicking stratum corneum of the human skin.

Figure 2 shows a model of the packaged sensor array and the fabricated prototype, having concentric ridges with groove width set to 0.7 mm and ridge width to 0.5 mm and curvature radius between 9.75 mm and 15.75 mm. PDMS (Sylgard 184, Dow Corning, USA) was used as an external layer, stacked over an inner film of Dragon Skin (Smooth-On, USA).

The result of the integration of the packaged tactile sensor array in the distal phalanx of the robotic finger is shown in Fig. 3.

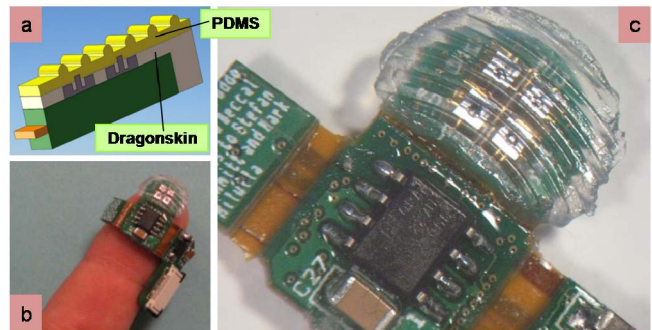


Fig. 2. a) Cross-section of the sensor array showing the sensors positioning and the packaging structure. b) Rigid-flex board with sensor array and packaging wrapped around a human index finger distal phalanx. c) Close-up view of a fabricated prototype with bi-layer packaging and ridges.

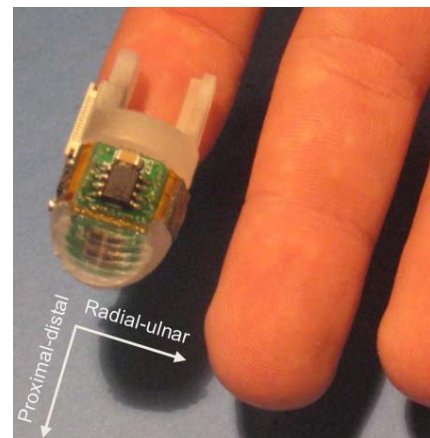


Fig. 3. Integration of the fabricated prototype in the distal phalanx of the robotic fingertip; the proximal-distal and radial-ulnar directions are shown.

## III. METHODS

### A. Experimental protocol

The distal phalanx of the finger was mounted on a mechatronic tactile stimulator capable of indenting the tactile sensor with force feedback control and stroking a

stimulus over it with precise position control. Figure 4 shows a diagram of the overall experimental set-up.

The robotic finger integrating the tactile sensor array was oriented in such a way to provide stimulus motion selectively along the proximal-distal direction or along the radial-ulnar direction.

Six types of medium-fine ridged stimuli, built with TUFSET Rigid Polyurethane thermosetting plastics, were used with spatial periods  $\Delta p$  ranging from a minimum of 320  $\mu\text{m}$  to a maximum of 1900  $\mu\text{m}$ , as detailed in Table 1.

Data acquisition started prior to the phase during which the stimulus contacted the sensor array (phase A). In a second phase of the experiment, the stimulator was commanded to contact the tactile sensor (phase B). Three different stimulation combinations with regards to the finger-stimulus contact force were tested; the sensor array was loaded with a sequence of 100 mN, 200 mN or 400 mN as the references of the normal force feedback controller.

The loading resulted in a contact spike in the signals gathered from the MEMS array. The target force level was held for 2 s. After that, the sliding of stimulus started (phase C) along the proximal-distal or radial-ulnar directions (see Fig. 3) depending on the chosen stimulation condition, while maintaining enabled the force feedback controller, thus obtaining a stimulation with regulated normal force  $F_z$ , and tangential force  $F_y$  depending on the contact mechanics and on the motion dynamics.

Four different stimulus sliding velocities (5 mm/s, 10 mm/s, 20 mm/s and 40 mm/s) were chosen for overlapping with the range commonly used in related neurophysiological studies [14]. The sign of velocity and the starting absolute position were not varied. The sliding was applied for 60 mm, providing dynamic stimulations of 12 s, 6 s, 3 s or 1.5 s depending on the applied velocity. At the end of the sliding motion there was a steady state of 2 s with contact force held (phase D) at the reference value, i.e. 100 mN, 200 mN or 400 mN as reported above, for the specific session and, finally, the tactile sensor array was unloaded (phase E).

TABLE I  
GRATING GROOVE WIDTH ( $GW$ ), RIDGE WIDTH ( $RW$ ) AND SPATIAL PERIOD ( $\Delta p$ ) WITH RESPECT TO THE SAMPLE TYPE.

Grating number	1	2	3	4	5	6
$gw$ ( $\mu\text{m}$ )	220	300	380	500	985	1487
$rw$ ( $\mu\text{m}$ )	100	100	100	399	413	413
$\Delta p$ ( $\mu\text{m}$ )	320	400	480	899	1398	1900

### B. Processing

The acquired channels underwent a Fast Fourier Transform (FFT) in order to perform a pilot evaluation of the capabilities of the developed artificial finger to retrieve

the fundamental spatio-temporal frequency of the system. Such operation was performed windowing the acquired data, including in the FFT the complete sliding motion (phase C) with 100 mN, 200 mN or 400 mN reference contact force. On one side, this choice ensured low quantization error, while on the other the procedure was not suitable as is for being used in real-time applications. Table 2 points out the expected principal frequency from sensor outputs as a function of the spatial periodicity of the grating and of its sliding velocity. It is remarkable to observe that, with regards to the value of the principal frequency, the contact force was supposed to have no effect provided that it was in the adequate range for eliciting the mechanical vibration and for allowing such periodic wave to be gathered by the sensing units.

TABLE II  
EXPECTED PRINCIPAL FREQUENCY FROM SENSOR OUTPUTS DEPENDING ON THE SPATIAL PERIODICITY ( $\Delta p$ ) AND ON THE SLIDING VELOCITY ( $v$ ) OF THE APPLIED GRATING.

Expected frequency vs. $\Delta p$ and $v$	$\Delta p = 320$ $\mu\text{m}$	$\Delta p = 400$ $\mu\text{m}$	$\Delta p = 480$ $\mu\text{m}$	$\Delta p = 899$ $\mu\text{m}$	$\Delta p = 1398$ $\mu\text{m}$	$\Delta p = 1900$ $\mu\text{m}$
$v = 5$ mm/s	15.625 Hz	12.5 Hz	10.417 Hz	5.562 Hz	3.577 Hz	2.632 Hz
$v = 10$ mm/s	31.25 Hz	25.0 Hz	20.833 Hz	11.124 Hz	7.153 Hz	5.263 Hz
$v = 20$ mm/s	62.5 Hz	50.0 Hz	41.667 Hz	22.247 Hz	14.306 Hz	10.526 Hz
$v = 40$ mm/s	125.0 Hz	100.0 Hz	83.333 Hz	44.494 Hz	28.612 Hz	21.053 Hz

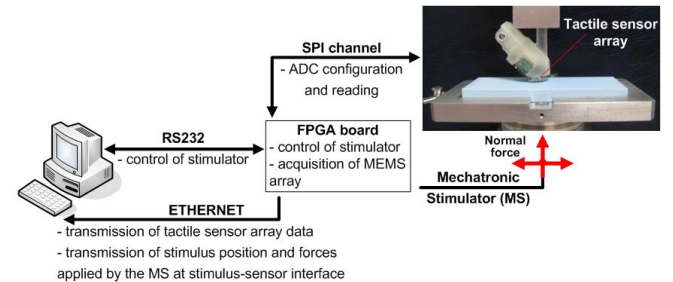


Fig. 4. Block diagram of the experimental setup implementing the control of the tactile stimulator together with the acquisition of data from the MEMS sensor array and high-speed transmission of synchronized data by means of the Ethernet. The picture on the top-right shows the stimulus-finger interface in the proximal-distal stimulation condition with a grating having 480  $\mu\text{m}$  spatial period.

## IV. EXPERIMENTAL RESULTS

This Section presents some of the experimental results, in the form of time and frequency domain plots, obtained by using the stimulation combinations reported in Table 2, with both proximal-distal and radial-ulnar stimulation directions. For the objectives of this analysis, a single piezoresistor of the 16 channels of the 2x2 array was considered.

### A. Proximal-distal stimulation

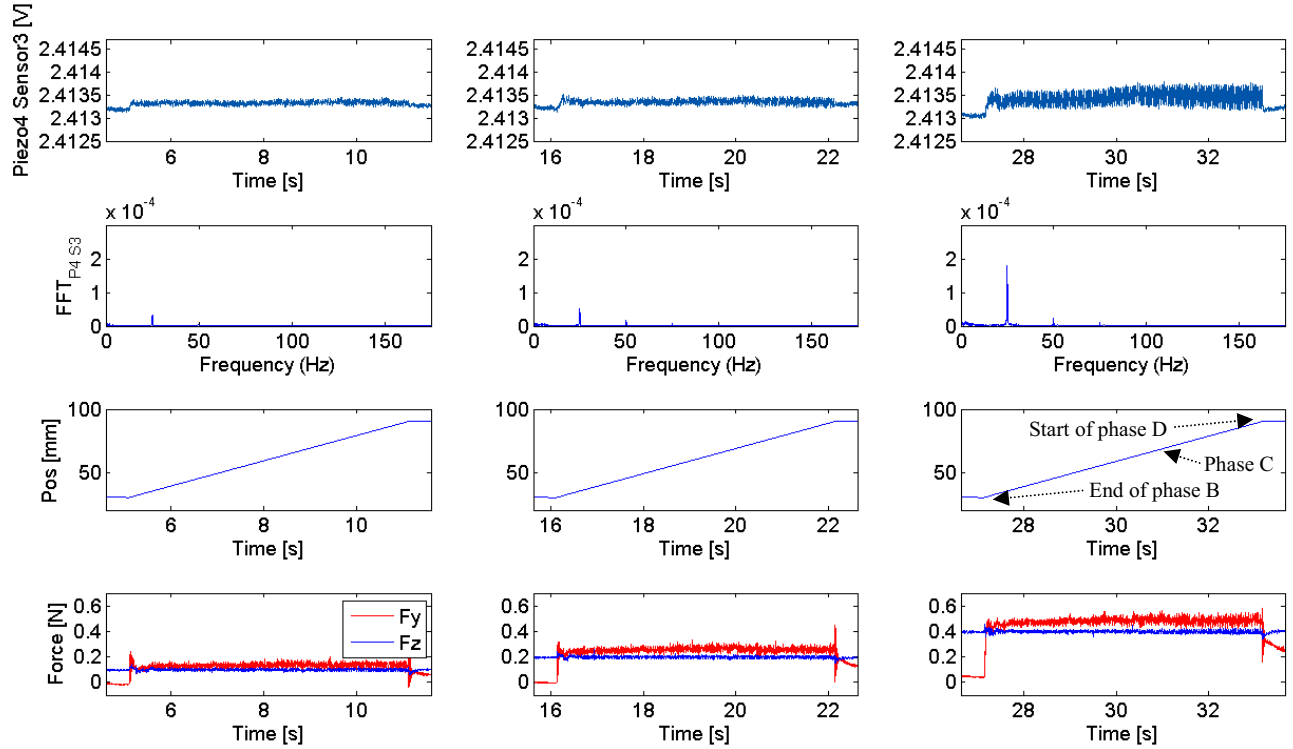


Fig. 5. From the first row: time domain plots of the voltage acquired from a piezoresistor of the array; single-sided amplitude spectrum of each of the plots shown in the first row during phase C; horizontal position of the stimulus (accounting for the sliding motion); normal and tangential (along the direction of the sliding motion) components of the contact force at stimulus-artificial finger interface, measured by means of a 6 axis F/T load cell. In the first column the normal component of the contact force is set to 100 mN, in the second to 200 mN and in the third to 400 mN. Some phases of the experimental protocol are indicated. The plots refer to stimulation in the proximal-distal direction with a surface having spatial period of 400  $\mu\text{m}$  and sliding velocity of 10 mm/s.

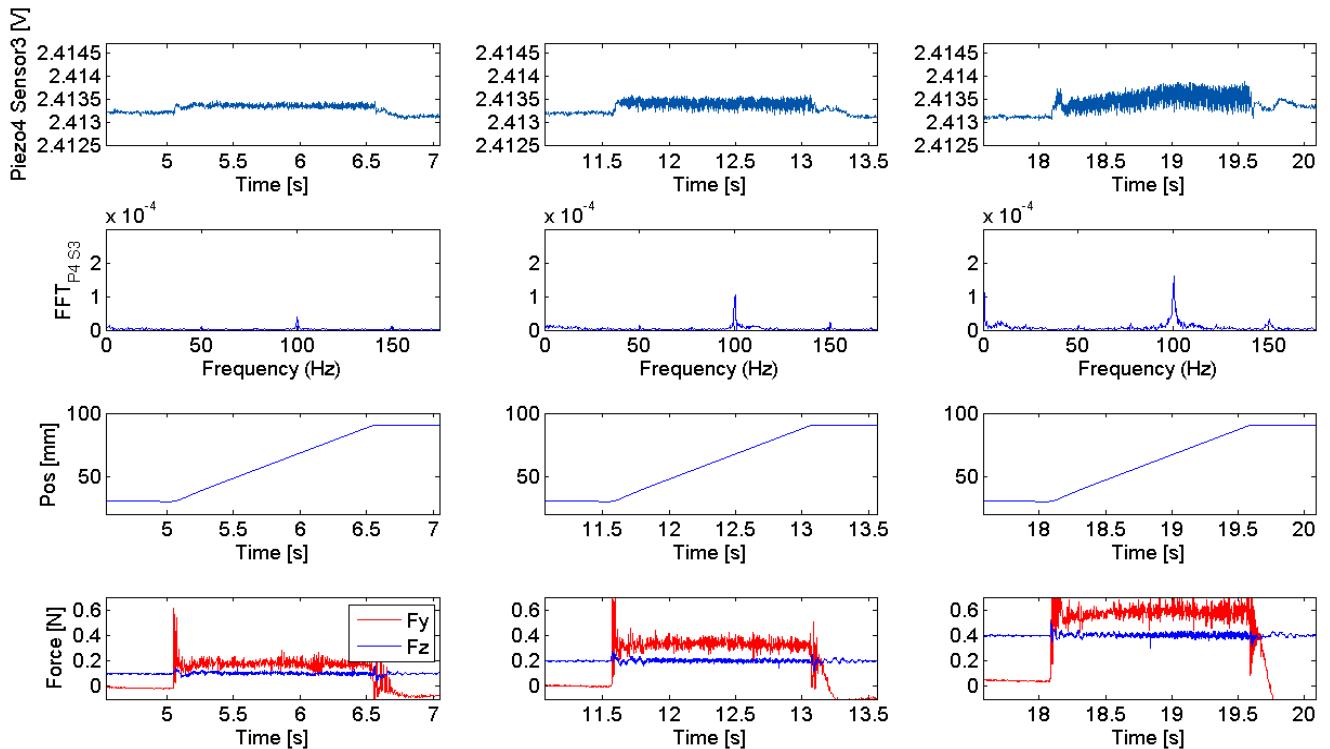


Fig. 6. Refer to Fig. 5 for an explanation of the subplots. The plots refer to stimulation in the proximal-distal direction with a surface having spatial period of 400  $\mu\text{m}$  and sliding velocity of 40 mm/s.

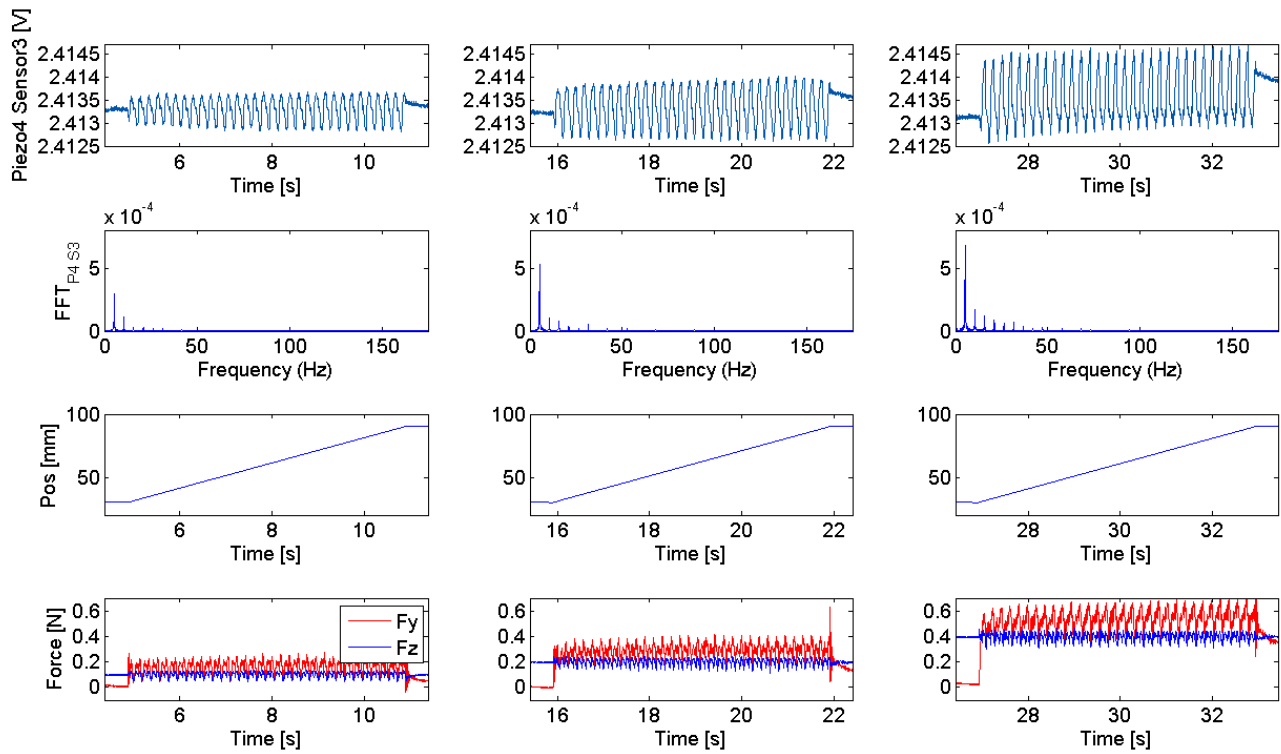


Fig. 7. Refer to Fig. 5 for an explanation of the subplots. The plots refer to stimulation in the proximal-distal direction with a surface having spatial period of 1900  $\mu\text{m}$  and sliding velocity of 10 mm/s.

### B. Radial-ulnar stimulation

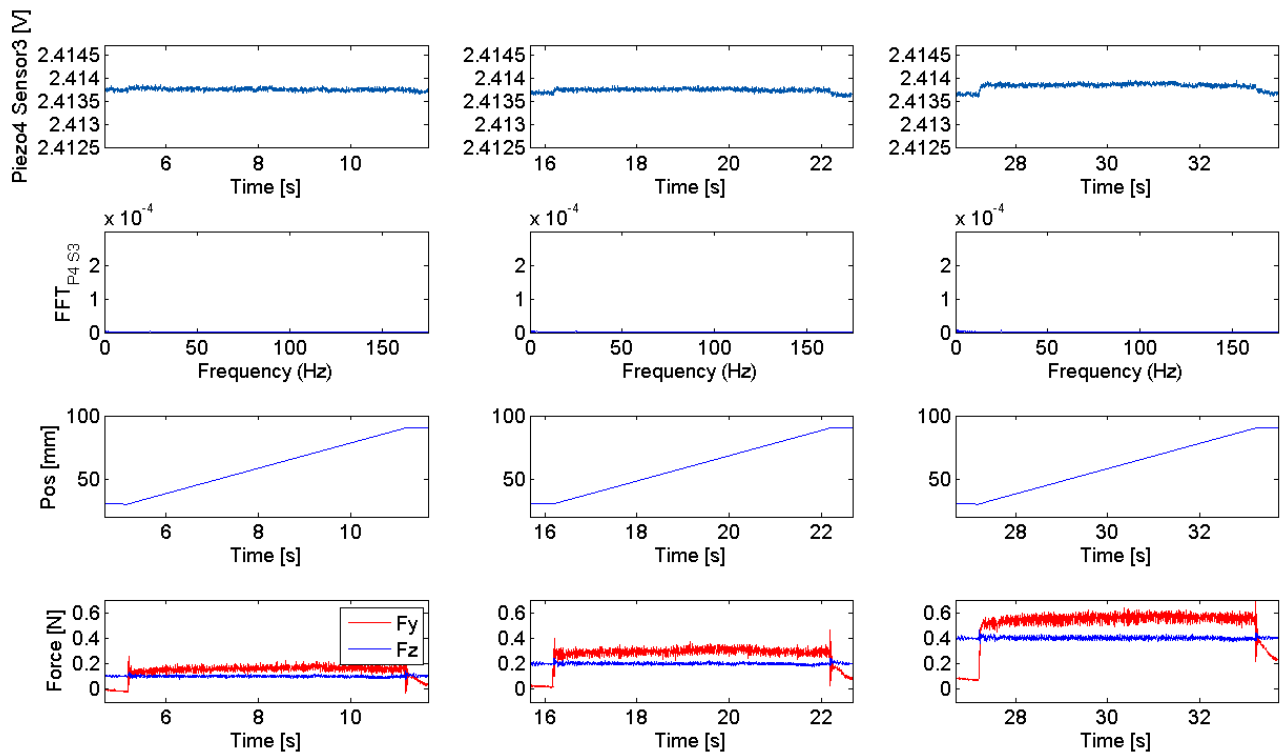


Fig. 8. Refer to Fig. 5 for an explanation of the subplots. The plots refer to stimulation in the radial-ulnar direction with a surface having spatial period of 400  $\mu\text{m}$  and sliding velocity of 10 mm/s.

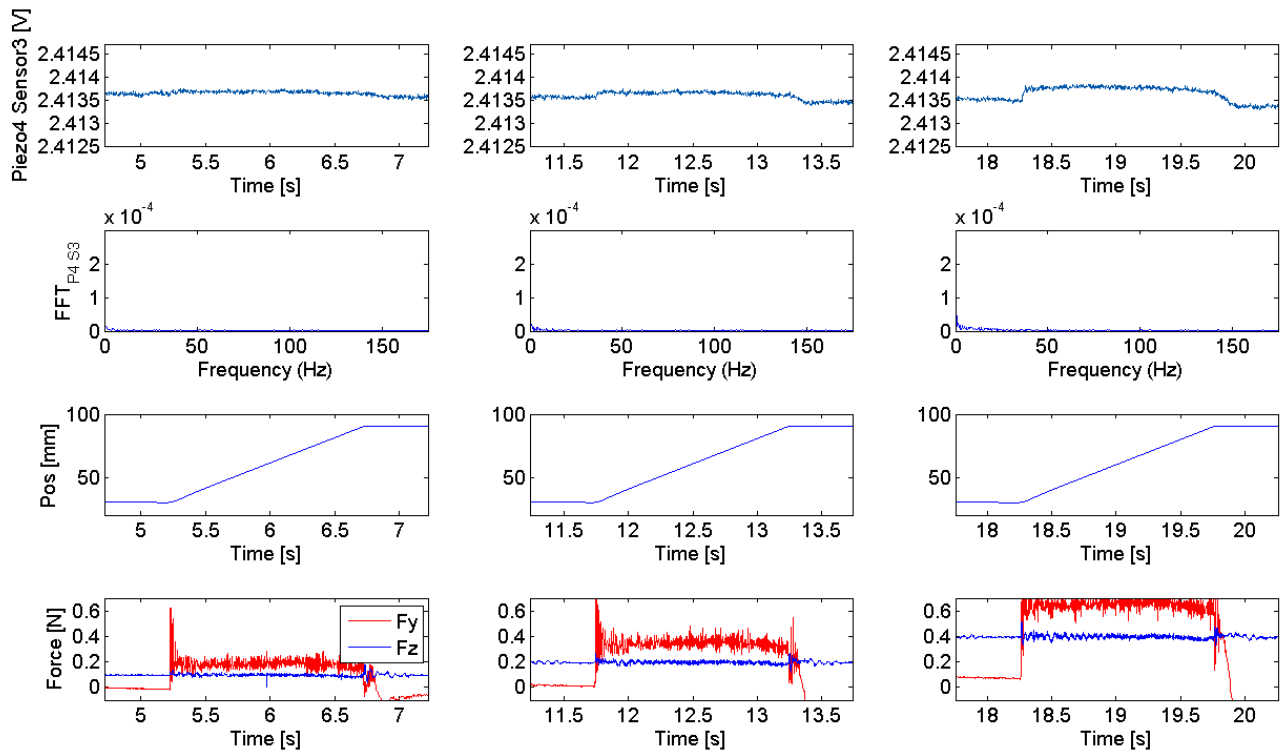


Fig. 9. Refer to Fig. 5 for an explanation of the subplots. The plots refer to stimulation in the radial-ulnar direction with a surface having spatial period of 400  $\mu\text{m}$  and sliding velocity of 40 mm/s.

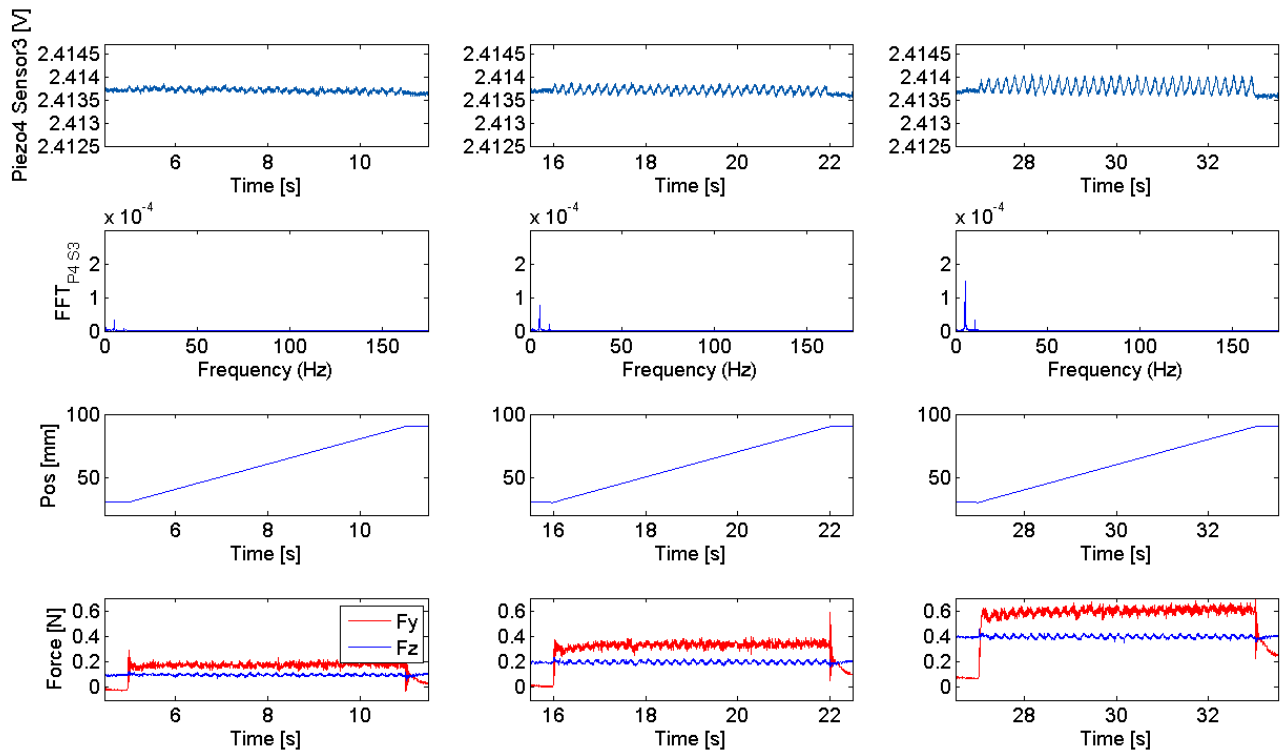


Fig. 10. Refer to Fig. 5 for an explanation of the subplots. The plots refer to stimulation in the radial-ulnar direction with a surface having spatial period of 1900  $\mu\text{m}$  and sliding velocity of 10 mm/s.

## V. DISCUSSION

The experimental results shown in Section 4 confirmed that the design of the ridges for the packaging of the artificial fingertip enabled the promotion of stimulus related vibrations when medium-fine periodic ridged stimuli were used. Moreover, in case of fine stimuli (such as gratings 1, 2 and 3 of Table I), the results pointed out a more evident frequency locking with each expected frequency (Table II) when the stimulation was along the proximal to distal direction, instead of along the radial to ulnar one (see Fig. 5, 6 and 7 vs. Fig. 8, 9 and 10). According to (1), the frequency locking behavior consisted in a decreasing value of the frequency of the vibration while increasing the stimulus spatial period, and in a frequency value increasing together with the stimulus sliding velocity.

This phenomenon was evident in the form of appreciable time-domain vibrations during proximal to distal stimulus sliding motion, or in the form of a principal tone coherent with the expected one in the frequency domain. As a matter of fact, due to the radius of curvature of the artificial ridges of the fingertip, in the proximal to distal stimulation condition the sliding motion of the ridges of the grating was mainly across the ridges of the packaging, while in the radial to ulnar the sliding motion of the ridges of the grating was mainly along the ridges of the packaging. This is the reason why with the proximal to distal motion the packaging ridges behaved as vibration promoters enhancing the artificial roughness encoding capabilities of the artificial finger. The vibrations arose in the radial-ulnar direction only for coarser stimuli and always showed lower amplitude than with the distal-proximal stimulation condition. Moreover, it is noteworthy to point out, as a qualitative comment to the obtained results with respect to contact mechanics, that the friction coefficient (which can be evaluated looking at the lower subplots from Fig. 5 to Fig. 10) was slightly lower with the proximal-distal stimulation condition than with the radial-ulnar one.

Finally, the time and frequency domain plots shown from Fig. 5 to Fig. 10 pointed out an increasing value of the vibration amplitude by increasing the normal contact force or by increasing the spatial period.

## VI. CONCLUSION

The obtained results were remarkable in terms of both tactile sensing technology development and assessment for roughness encoding of medium-fine ridged stimuli. This research approach will be investigated for what concerns smart positioning of transducers, in order to achieve hyper tactile spatial resolution, and packaging geometry in order to define modeling and processing techniques for the classification of roughness information related to the applied tactile stimuli.

## ACKNOWLEDGMENT

The authors would like to thank Simon Johnson and Bill Ranken from Unilever R&D, Port Sunlight, for providing the stimuli for experiments; Mark Mitulla from Institute of Microtechnology, Mainz, for collaboration in sensor bonding; Marco Controzzi from ARTS Lab of Scuola Superiore Sant'Anna, Pisa, for input on robotic finger design.

## REFERENCES

- [1] J. W. Morley, A. W. Goodwin, and I. Darian-Smith, "Tactile Discrimination of Gratings," *Exp. Brain Res.*, vol. 49, 1983, pp. 291-299.
- [2] L. A. Jones, and S. J. Lederman, "Tactile Sensing," in *Human Hand Function*, L. A. Jones, and S.J. Lederman, Eds. New York: Oxford University Press, 2006, pp. 44-74.
- [3] A. Prevost, J. Scheibert, and G. Debrégeas, "Effect of fingerprints orientation on skin vibrations during tactile exploration of textured surfaces," *Communicative & Integrative Biology*, vol. 2, Sept.-Oct. 2009, pp. 1-3.
- [4] C. M. Oddo, L. Beccai, M. Felder, F. Giovacchini, and M. C. Carrozza, "Artificial Roughness Encoding with a Bio-inspired MEMS Tactile Sensor Array," *Sensors*, vol. 9, Apr. 2009, pp. 3161-3183.
- [5] M. Konyo, T. Maeno, A. Yoshida, and S. Tadokoro, "Roughness sense display representing temporal frequency changes of tactile information in response to hand movements," In *Proc. of the First Joint Eurohaptics Conference and Symposium on Haptic Interface for Virtual Environment and Teleoperator Systems*, 2005, pp. 609-610.
- [6] V. Maheshwari, and R. F. Saraf, "Tactile devices to sense touch on a par with a human finger," *Angew Chem. Int. Edit.*, vol. 47, 2008, pp. 7808-7826.
- [7] Y. Mukaibo, H. Shirado, M. Konyo, and T. Maeno, "Development of a texture sensor emulating the tissue structure and perceptual mechanism of human fingers," In *Proc. of the IEEE International Conference on Robotics and Automation*, Barcellona, 2005, pp. 2565-2570.
- [8] J. Scheibert, S. Leurent, A. Prevost, and G. Debrégeas, "The role of fingerprints in the coding of tactile information probed with a biomimetic sensor," *Science*, vol. 323, Jan. 2009, pp. 1503-1506.
- [9] L. Beccai, S. Roccella, L. Ascari, P. Valdastris, A. Sieber, M. C. Carrozza, and P. Dario, "Development and Experimental Analysis of a Soft Compliant Tactile Microsensor for Anthropomorphic Artificial Hand," *IEEE-ASME Trans. Mechatron.* 13, 2008, pp. 158-168.
- [10] M. C. Carrozza, G. Cappiello, S. Micera, B. B. Edin, L. Beccai, and C. Cipriani, "Design of a cybernetic hand for perception and action," *Biol. Cybern.*, vol. 95, 2006, pp. 629-644.
- [11] M. Controzzi, C. Cipriani, and M. C. Carrozza, "Mechatronic Design of a Transradial Cybernetic Hand," In *Proc. of the IEEE/RSJ Int. Conf. on Intelligent Robots and Systems IROS*, Nice, 2008.
- [12] L. Beccai, S. Roccella, C. Oddo, and M. C. Carrozza, "Sensing fingertip for bio-inspired tactile encoding," in *Proceedings of the First Italian Conference on Bioengineering*; Burattini, R., Contro, R., Dario, P., Landini, L., Eds.; Patron editore: Bologna, Italy, 2008; p. 787.
- [13] L. Beccai, S. Roccella, A. Arena, F. Valvo, P. Valdastris, A. Menciassi, M. C. Carrozza, and P. Dario, "Design and fabrication of a hybrid silicon three-axial force sensor for biomechanical applications," *Sens. Actuator A-Phys.*, vol. 120, Feb. 2005, pp. 370-382.
- [14] I. Darian-Smith, and L. E. Oke, "Peripheral neural representation of the spatial frequency of a grating moving across the monkey's finger pad," *J. Physiol.-London*, vol. 309, 1980, 117-133.

Article

## **Roughness encoding in human and biomimetic artificial touch: spatiotemporal frequency modulation and structural anisotropy of fingerprints**

**Calogero Maria Oddo**<sup>1,\*</sup>, **Lucia Beccai**<sup>2</sup>, **Johan Wessberg**<sup>3</sup>, **Helena Backlund Wasling**<sup>3</sup>, **Fabio Mattioli**<sup>2</sup> and **Maria Chiara Carrozza**<sup>1</sup>

<sup>1</sup> The BioRobotics Institute, Scuola Superiore Sant'Anna, Polo Sant'Anna Valdera / Viale Rinaldo Piaggio 34, 56025 Pontedera, PI, Italy; E-Mails: oddoc@sssup.it (C.M. O.); chiara.carrozza@sssup.it (M.C. C.)

<sup>2</sup> Center for Micro-BioRobotics@SSSA, Istituto Italiano di Tecnologia (IIT) / Viale Rinaldo Piaggio 34, 56025 Pontedera, PI, Italy; E-Mails: lucia.beccai@iit.it (L. B.); fabio.mattioli@iit.it (F. M.)

<sup>3</sup> Department of Physiology, University of Gothenburg / Medicinaregatan 11, SE-40530 Goteborg, Sweden; E-Mails: wessberg@physiol.gu.se (J. W.); helena.backlund@physiol.gu.se (H. B.W.)

\* Author to whom correspondence should be addressed; Email: oddoc@sssup.it; Tel.: +39-050-88-3136; Fax: +39-050-88-3101/497

---

**Abstract:** The influence of fingerprints and their curvature in tactile sensing performance is investigated by comparative analysis of different design parameters in a biomimetic artificial fingertip, having straight or curved fingerprints. The strength in the encoding of the principal spatial period of ridged tactile stimuli (gratings) is evaluated by indenting and sliding the surfaces at controlled normal contact force and tangential sliding velocity, as a function of fingertip rotation along the indentation axis. Curved fingerprints guaranteed higher directional isotropy than straight fingerprints in the encoding of the principal frequency resulting from the ratio between the sliding velocity and the spatial periodicity of the grating. In parallel, human microneurography experiments were performed and a selection of results is included in this work in order to support the significance of the biorobotic study with the artificial tactile system.

**Keywords:** MEMS tactile sensor array; fingerprints; biomimetic fingertip; roughness encoding; artificial touch; mechanoreceptors; microneurography; human touch; biorobotics.

---

## 1. Introduction

In this work we investigate the specific role of fingerprints in artificial touch by building tactile systems, inspired to the biological model, that embed artificial fingerprints with different geometries while leaving unchanged the other design features. This comparative approach is fundamental to define design parameters in developing bioinspired sensory systems but it could be also useful to provide hints and suggestions to develop experimental protocols and models in neurophysiology. Biorobotics offers the possibility to develop emulator of the human subjects [1], with different characteristics and design parameters, as in the work presented in this paper we selectively modify a specific parameter (the curvature of fingerprints) to evaluate the related effect. In order to support the significance of the artificial touch results, in parallel we present a selection of electrophysiological studies by means of microneurographic recordings of the activity of single, identified afferent units in the fingertips of healthy human volunteers [2].

We address roughness encoding, which is a major independent component of texture (together with softness, while stickiness is a minor component) [3,4]. Roughness is associated to the spatial modulation of the surface (i.e. spatial coarseness) and its perception is severely degraded in case of lack of tangential motion between the fingertip and the tactile stimuli (i.e. dynamic vs. static touch) [5,6].

The biomimetic fingertip experimented for artificial roughness encoding was designed and built by means of a MEMS based technological approach, integrating an array of microscale tactile sensors and polymeric fingerprint-like packaging. Biomimetism was achieved by reaching a density similar to the innervation of type I mechanoreceptors in humans (e.g., SAI have a density of about 70 units/cm<sup>2</sup> [7]), by having a fine skin-like packaging layer above the MEMS sensors, as for the positioning of slowly adapting type I (SAI; Merkel) and rapidly adapting (RA; Meissner) units, and by mimicking the coarseness of human fingerprints (between-ridge distance typically comprised within 0.3 mm and 0.5 mm [8]).

To make a comparative analysis between the human subject and the artificial system, the same class of tactile stimuli is presented to both the biomimetic fingertip and to human subjects via dynamic passive touch protocols implemented through a mechatronic platform that can indent the stimuli to the fingertip and slide them in a smooth tangential fashion. We use periodic ridged stimuli (namely gratings, which can be considered as a kernel of more realistic polyharmonic surfaces used in various studies [9,10]) in order to show, in artificial touch, that the structure of fingerprints affects the directional isotropy in the encoding of the principal spatiotemporal frequency of stimuli. In this attempt we get inspiration from previous observations with monkey subjects providing evidence that gratings locally oriented parallel to the finger ridges elicit stronger response than tactile stimuli oriented along the orthogonal direction [11].

The working principle of our artificial touch system was explained in [12] and, coherently with other human or artificial touch studies [13,14,15], considers the spectral content of the mechanical vibrations elicited by textured surfaces. Briefly, when a relative motion occurs at finger-stimulus interface, provided that it is possible to estimate somehow the relative velocity  $v$ , the spatial period  $\Delta p_s$  of the grating is in inversely proportional relationship with the principal frequency  $f_{princ}$  of the elicited mechanical vibration [16], such that:

$$f_{princ} = \frac{v}{\Delta p_s} \quad (1)$$

The effectiveness in roughness encoding via dynamic artificial touch is in the capability to elicit such vibrations by stimulus-skin interface, by motion dynamics and by contact mechanics, and then to gather them via the sensing units located under the covering material [15,17,18,19].

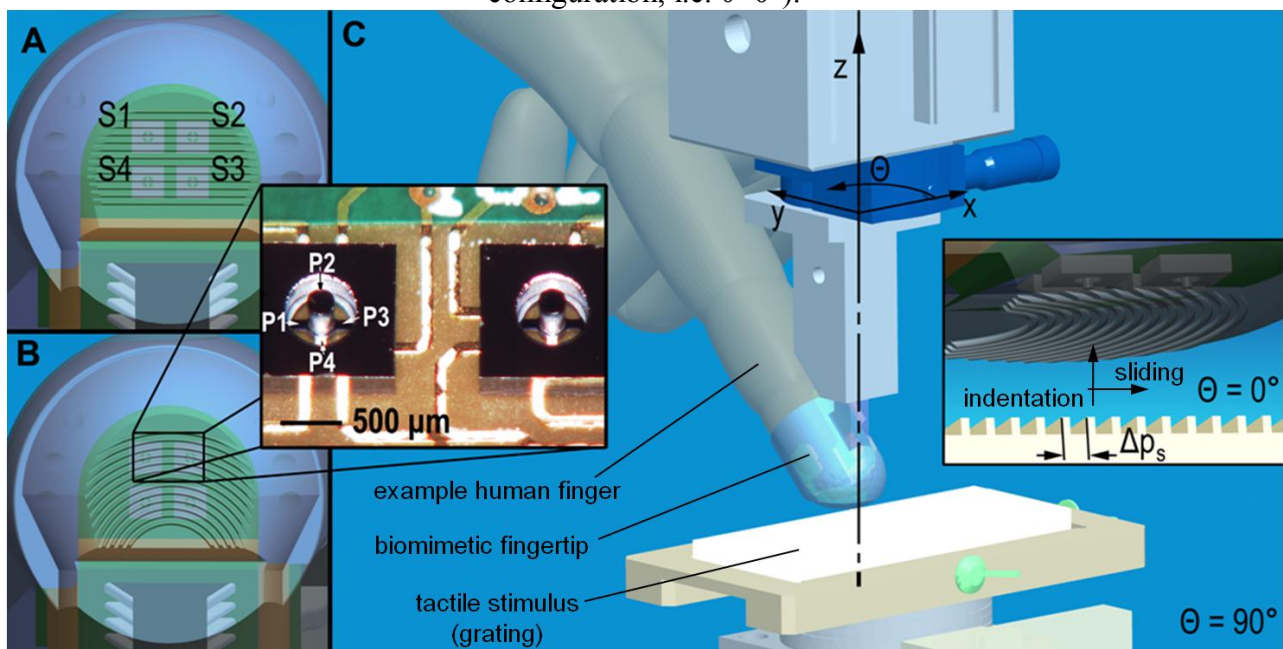
Recently it has been asserted that human fingerprints contribute to the encoding of fine textures as they may perform spectral selection and amplification of tactile information in the frequency band, centered at about 250 Hz, of optimal sensitivity of Pacinian afferents [20]. In such work, Scheibert and colleagues, by experimenting an artificial tactile sensing technology, showed a principal frequency differing from Equation 1, since the spatial period  $\Delta p_f$  of fingerprints appeared (instead of  $\Delta p_s$ ) in the dominant vibrations gathered by the tactile sensor, resulting in  $f_{princ} = v/\Delta p_f$ . In our opinion, in [20] the dominance of finger skin geometry ( $\Delta p_f$ ) on stimulus surface features ( $\Delta p_s$ ) in the retrieved principal spectral component was (1) activated by the used stimulus, whose edges were positioned randomly (white-noise 1D patterning, i.e. extremely polyharmonic), and (2) gathered thanks to the quite wide receptive field of the sensor due to the relatively thick 2 mm packaging layer (a relevant related analysis is provided in [21]) mimicking the positioning of deeply located (i.e. type II) Pacinian mechanoreceptors.

As stated above, here the design of the tactile system gets inspiration from surface located human type I mechanoreceptors, we demonstrate a principal frequency modulation as from Equation 1, and in parallel we provide evidences of the same mechanism with RA human mechanoreceptors for fine and coarse gratings and with SAI for coarse gratings only (both RA and SAI are type I mechanoreceptors). Following this, we investigate in artificial touch how the shape of fingerprints affects the strength of principal frequency encoding by the embedded sensors. To this aim, we selectively change the morphology of the packaging encapsulating the sensor array (i.e. the curvature of fingerprints embedded in the polymeric skin-like outer layer as depicted in Figure 1A-B) and show the consequences on directional isotropy by means of experiments varying the reciprocal orientation between the artificial fingertip and the presented gratings (Figure 1C).

The manuscript is organized as follows. Section 2 presents the design of the experimented biomimetic fingertips, differing in the curvature of fingerprints, provides a brief description of the microneurography technique for human touch studies, and reports the experimental set-up and protocols. Section 3 introduces the data analysis techniques for human and artificial touch experiments. In Section 4 the experimental results are shown and discussed. Finally, the conclusions are provided in Section 5, together with insights on planned future work.

**Figure 1.** Design of the biomimetic fingertip integrating the rigid-flex board with 2x2 MEMS sensor array and readout electronics. Fingerprints embossed in the polymeric packaging had two curvatures.

**Panel A** shows fingertip *a* design with straight fingerprints. **Panel B** shows fingertip *b* design with curved fingerprints. The inset shows two elements of the array of MEMS sensors. The piezoresistors (P1...P4) and the sensors (S1...S4) of the array are labeled according to the convention used in the text. **Panel C** shows a drawing of the experimental setup for indenting and sliding tactile stimuli in dynamic passive-touch experiments. An example human finger model is overlapped as a comparison to the developed biomimetic fingertip. The finger is rotated in steps of  $10^\circ$  along the  $z$ -axis (stimulus sliding across the distal phalanx in the depicted configuration, i.e.  $\theta=90^\circ$ ). The inset provides a close-up view of stimulus-artificial finger interface (stimulus sliding along the distal phalanx in the depicted configuration, i.e.  $\theta=0^\circ$ ).



## 2. Materials

### 2.1. Biomimetic fingertip

Four MEMS force micro-sensors [22,23] were integrated in a 2x2 array via flip-chip bonding on a rigid-flex board. Each sensor of the array was bonded on the rigid part on the corner of a square with a pitch  $\Delta X$  of 2.36 mm, allowing the 4 tethers of each sensor to be suspended and free to flex under externally applied loads while a rigid support guaranteed stable mechanical bonding. Each sensor integrated 4 piezoresistors as sensing elements at the roots of the tethers forming a cross shape structure equipped with a mesa. This resulted in an array with 16 channels in total for transducing the mechanical interaction with external tactile stimuli. Inscribing each sensor in a square of area 5.57 mm<sup>2</sup>, a 0.72 channels/mm<sup>2</sup> (16 channels / 22.28 mm<sup>2</sup>) density was achieved, which mimics the SAI innervation density in humans (70 units/cm<sup>2</sup>) [7].

The 16 channels of the array were acquired by means of a high resolution (24 bit) Analog to Digital Converter (ADS1258, Texas Instruments, USA). The integration of the ADC onboard the fingertip allowed to reduce the amount of wires between the fingertip and the outer electronics, requiring power supply and a few digital communication channels only, and also guaranteed adequate signal-to-noise ratio due to the limited length of the connections routing analog signals. Data was sampled at 250 Hz per channel since such value was about one order of magnitude higher than the expected fundamental frequencies (as from Equation 1); however, higher sampling frequencies are allowed by 1) increasing the overall conversion rate (this operation will affect the signal to noise ratio, but the achieved S/N levels guarantee that this is feasible) of the ADC lodged onto the fingertip, or 2) by reducing the number of converted channels (this operation will not affect S/N) without changing the overall conversion rate of the ADC. Acquired data was transmitted to a PC via Ethernet protocol by a soft-core processor (NiosII, Altera, USA) instantiated onboard a FPGA (Cyclone II, Altera, USA).

The rigid-flex board with MEMS sensor array and readout electronics was integrated in a rigid fingertip mimicking human anthropometry (Figure 1 and 3B). The fingertip was designed for application to distal phalanges of robotic hands being appropriate for grasping and manipulation tasks in anthropomorphic manner [24,25] and was fabricated with rapid prototyping resin via a 3D printer.

The packaging skin-like layer of the 2x2 array of MEMS sensors was introduced to have a similar function to the epidermal ridges of a human finger that can enhance deformation and frictional properties of the fingertip surface. Significant contributions in the simulative analysis [26,27] and artificial emulation [27,28] of fingerprints were given by Maeno and colleagues, showing that their structure increases the sensitivity in tactile activities with a major effect on surface located type I receptors. Therefore, fingerprints were included in the design of the proposed biomimetic fingertip considering that the epidermal ridges and grooves of an adult human have width in the 100 – 300  $\mu\text{m}$  range, and the typical between-ridge distance is 400  $\mu\text{m}$  [8,26,28].

The encapsulation was performed by means of soft polymeric packaging (Dragon Skin, Smooth-On, USA), having shore A 10 hardness and recovering its original form after a mechanical stimulation. The packaging material was poured directly on the fingertip by means of a mould that allowed to pattern the surface of the skin-like layer on top the sensor array.

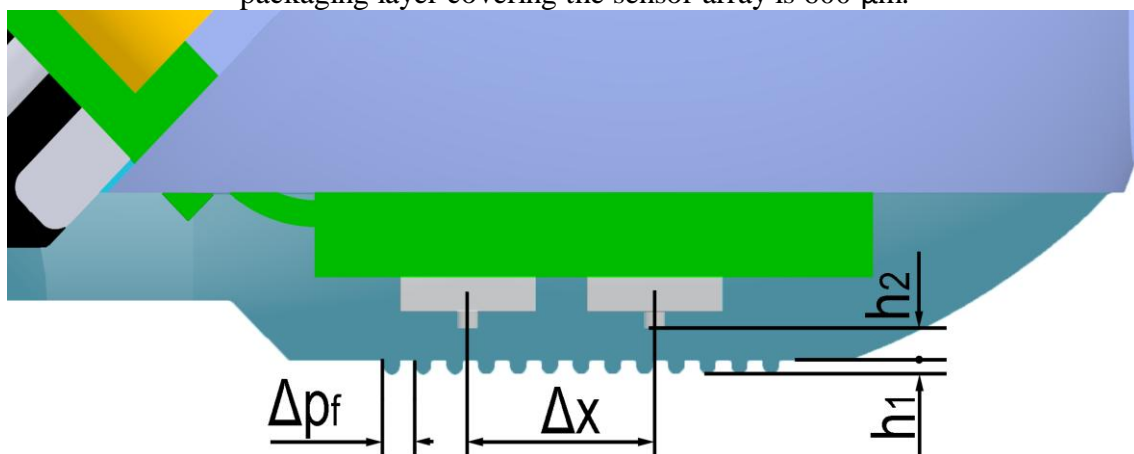
Each single sensor of the array provides local information on the contact interaction at its interface with the surrounding polymeric packaging material, with the advantages of distributed tactile sensing [29]; in addition, our array of tactile sensors provides also directional information by means of the output readings from the four piezoresistors (implanted each at a root of a tether). Therefore, to have four outputs from each sensor increases the informative content on the stress state locally at each sensor site.

In order to investigate the role of the shape of fingerprints in texture encoding, two curvatures were designed (Figure 1A-B). In finger *a*, fingerprints were embossed with straight parallel ridges having between-ridge distance  $\Delta p_f$  set to 400  $\mu\text{m}$ . Finger *b* had concentric fingerprints with groove and ridge widths as for prototype *a*, and the fingerprint passing from the center of the sensor array had curvature radius of 4.8 mm.

As regards the thickness, here we used an artificial epidermal ridge with a height  $h_1$  of 170  $\mu\text{m}$ , while the thickness  $h_2$  of the homogeneous packaging layer covering the sensor array was 600  $\mu\text{m}$  (Figure 2); this resulted in sensing units being located quite close to the surface of the fingertip, similarly to the positioning of type I human mechanoreceptors [26,28].

Preliminary load-unload tests with smooth flat surfaces were performed (not shown in this work) and showed that, for both the fingertip designs, the design of the packaging allows to reach at least up to 8 N normal and 4 N tangential forces without any damage to the encapsulated sensors.

**Figure 2.** Cross section of the biomimetic fingertip, showing two sensors of the array and the structure and dimensions of fingerprints. The array pitch  $\Delta X$  is 2.36 mm, the fingerprints have between-ridge distance  $\Delta p_f$  set to 400  $\mu\text{m}$ , while their thickness  $h_1$  is 170  $\mu\text{m}$ . The thickness  $h_2$  of the homogeneous packaging layer covering the sensor array is 600  $\mu\text{m}$ .



## 2.2. Microneurography technique for human touch studies

Impulses of single tactile afferents in the left index and middle fingers were recorded using the microneurographic technique in 36 human healthy volunteers [2]. The subjects seated comfortably in a dentist's chair, the left arm resting in a vacuum cast for stabilization and maximum comfort. Tungsten needle electrodes were inserted in the left median nerve, 8 cm above the elbow. The nerve signal was band-pass filtered at 200-4000 Hz, sampled at 12.8 kHz together with analog data from the tactile stimulation mechatronic platform, and stored on a PC using the ZOOM/SC system developed at the Department of Physiology, Umeå University, Sweden. Recorded nerve impulses were inspected off-line on an expanded time scale using in-house software implemented in MATLAB (The Mathworks) and were accepted for subsequent analyses only if they could be validated as originating from a single afferent. Before running the experimental protocol, the units' responses and receptive fields were explored using calibrated nylon filaments (von Frey hairs) and were classified as SAI, SAII, RA, or PC according to the adaptation of the response to sustained stimulation and size of the receptive field [30,31].

## 2.3. Experimental set-up and protocol

The study focused on experimenting passive-touch protocols in which periodic ridged stimuli were indented ( $z$  direction, Figure 1C) and slid ( $y$  direction) on the human fingertip and on the two artificial fingertip prototypes (differing in the curvature of fingerprints).

The passive-touch stimulation sequences were implemented by means of a mechatronic platform [32] with which repeatable experiments could be performed (Figures 1C and 3). This consisted in a 2 DoF system that could indent and slide textured stimuli to the fingertip. The system performed a feedback control on the normal contact force (i.e. indentation along the  $z$  direction) and a precise position/velocity control while recording the normal and tangential forces at finger-stimulus interface. The tactile stimulator could present stimuli to the fingertip without being affected by spurious vibrations and covering a range of forces and movement velocities as those that would be used by humans while exploring textures [4,6], i.e. at least from 100 mN up to 5 N indentation force and up to 150 mm/s tangential sliding velocity. The same core mechatronic tactile stimulator was used for human (Figure 3A) and artificial touch (Figure 3B) experiments. Periodic ridged surfaces (gratings), fabricated from tufset rigid polyurethane thermosetting plastics material, were tested as tactile stimuli in both human and artificial touch experiments.

### Human touch experiments

During microneurographic experiments, gratings measuring 32 mm x 35 mm each and mounted in pairs on changeable plates (Figure 1C and Figure 3A) were experimented. The experiments were performed with gratings having spatial period  $\Delta p_s$  (defined in the inset of Figure 1C) between 280  $\mu\text{m}$  and 1920  $\mu\text{m}$ , with normal contact force set to 100 mN, 200 mN, 400 mN or 800 mN, sliding distance of 24 mm and velocity from 5 mm/s up to 40 mm/s among different sessions. Overall, 10 RA, 5 SAI and 3 SAII single afferent units were successfully recorded in the fingerpad with different grating spatial periods, while the platform applied the sliding motions, repeated in runs of 12, across the distal phalanx (i.e.,

according to the reference frame in Figure 1C,  $\theta$  was fixed at  $90^\circ$ ). According to previous studies [33,34], the finger-stimulus contact area monotonically increases (positive first derivative), with decreasing slope (negative second derivative), with respect to the contact force; such previous studies report a contact area lower than  $1 \text{ cm}^2$  at the maximum force loads used in the human touch studies presented in this work. However, the preparatory session with calibrated Von Frey hairs, to characterize the locations and receptive fields of the recorded human tactile units, guaranteed the contact zone with the grating to cover the receptive field of the unit which was recorded during each experimental session.

Human experiments were conducted according the Declaration of Helsinki and the ethics committee at the University of Gothenburg approved the study.

### Artificial touch experiments

The artificial fingertip was fixed to the tactile stimulator by means of a mechanical support, interfaced to a rotational stage with goniometer (07 TRT 508, Melles Griot, USA, depicted in blue in Figure 1C and labeled as 7 in the picture of Figure 3B), that kept the fingertip surface parallel to the stimulus surface. As for human touch experiments, gratings were used as tactile stimuli. Each grating measured  $32 \text{ mm} \times 75 \text{ mm}$ . Therefore, the experimented gratings had approximately double length than those used with human subjects and each was separately (rather than in half-pairs as for human touch experiments) mounted on changeable plates. This choice was operated to test a higher sliding distance for each stimulus, since in artificial touch there is no relevant constraint to acquire as many data as possible within each session, oppositely to the looming risk of missing the nerve signal during human microneurography experiments. Two surfaces were evaluated, with spatial periods  $\Delta p_s$  (defined in the inset of Figure 1C) of  $360$  and  $440 \mu\text{m}$ . The indentation force was  $200 \text{ mN}$ , which is one of the values used in the ongoing human touch study and is within the range used by humans during tactile exploratory tasks [6]; the force level was not varied in this work since related previous artificial touch studies by our group [12,22] showed that a modulation of the contact force in the  $100 \text{ mN} - 1 \text{ N}$  range resulted in a principal frequency being coherent with Equation 1. The velocity was  $10 \text{ mm/s}$ , which is the lower boundary of the range of exploratory velocities typically used by humans [35], and was not varied in this work since previous studies [12,22,36] already showed (up to  $48 \text{ mm/s}$ , in [12]) that a change in velocity coherently modulates the principal frequency according to Equation 1. A more comprehensive investigation is left to future studies, which could investigate the effect on amplitude modulation at the expected principal frequency due to variations in the indentation force or in the sliding velocity.

According to the experimental protocol, the two artificial fingertip prototypes *a* (straight fingerprints, Figure 4-top) and *b* (curved fingerprints, Figure 4-bottom) were evaluated by rotating them from  $\theta=0^\circ$  (stimulus sliding along the distal phalanx, Figure 4-left) to  $\theta=90^\circ$  (stimulus sliding across the distal phalanx, Figure 4-right) in steps of  $10^\circ$ , thus indenting and sliding the ridged stimuli with ten different fingertip orientations. After enabling data acquisition, the stimulator applied the  $200 \text{ mN}$  feedback-regulated indentation force to the biomimetic fingertip. Subsequently, the stimulus was stroked at  $10 \text{ mm/s}$ , with the fingertip oriented along the selected direction, while maintaining enabled the force feedback controller. The sliding distance was set to  $60 \text{ mm}$ , providing a dynamic stimulation (corresponding to surface-fingertip tangential relative motion) for a duration of  $6 \text{ s}$ . Before commanding

the stimulator to unload the fingertip, a steady state was applied, with contact force held at the 200 mN reference value.

In each experimental run a *combination* of stimulus (having spatial period  $\Delta p_s$ ) and of fingertip orientation angle ( $\theta$ ) was used with a fingertip prototype (*a* or *b*). Six runs were repeated per *combination*, resulting in 240 runs in total (2 fingertip designs x 2 gratings x 10 angles x 6 repetitions).

The velocity and the start and stop absolute positions along the sliding direction were not varied among different *combinations* or among repeated runs with the same *combination*.

**Figure 3.** Experimental set-up in human (**Panel A**) and artificial (**Panel B**) touch experiments. 1: core mechatronic tactile stimulation platform; 2: pair of half-gratings; 3: human and biomimetic finger support; 4: first stage of microneurography electronics; 5: display with neural data for experiment monitoring; 6: single full-grating; 7: rotational stage with goniometer.

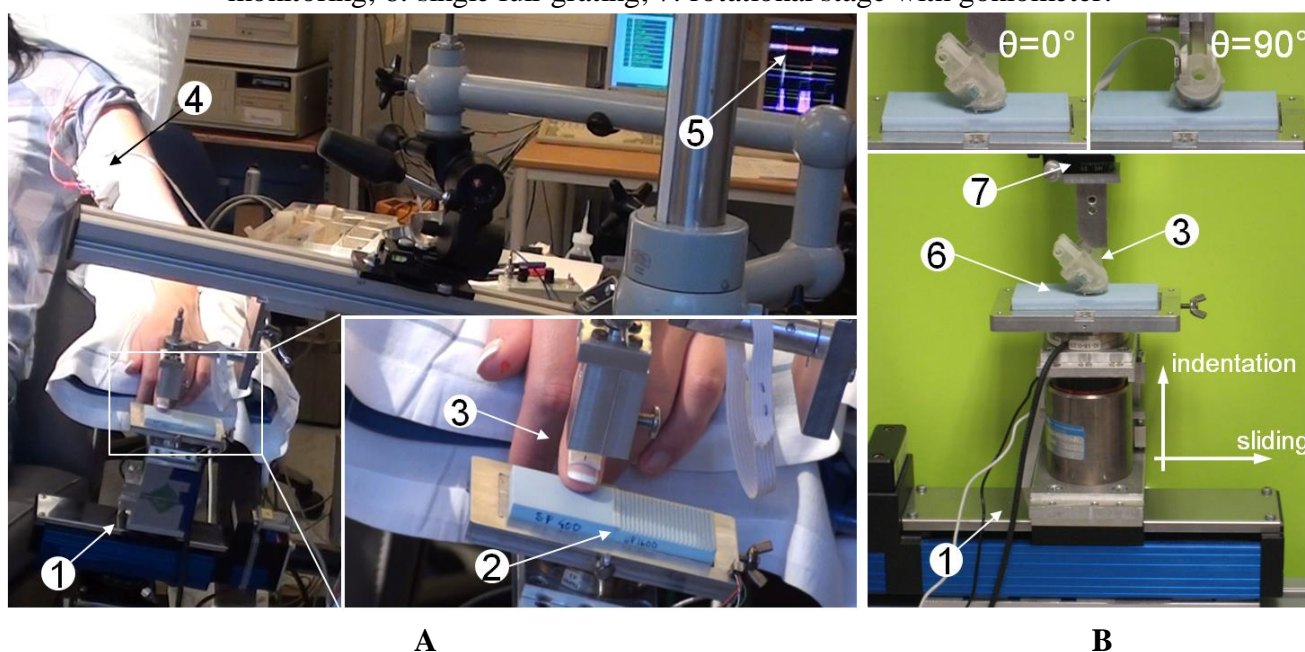
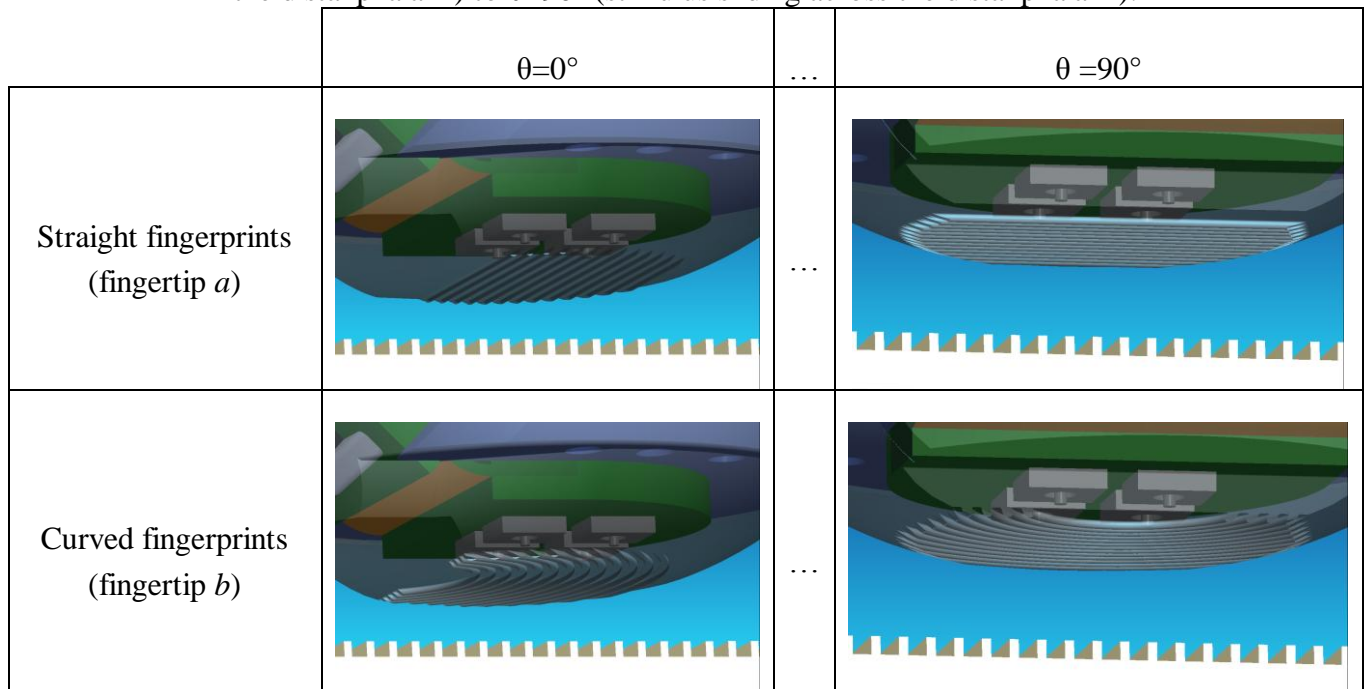


**Figure 4.** Protocol for the artificial touch experiments: the two biomimetic fingertip prototypes, differing in the curvature of fingerprints, were rotated in steps of  $10^\circ$  from  $\theta=0^\circ$  (stimulus sliding along the distal phalanx) to  $\theta=90^\circ$  (stimulus sliding across the distal phalanx).



### 3. Methods

#### 3.1 Human touch data analysis

Neural data was at first inspected and processed in time domain to identify neural events. Then, the identified spikes were analyzed by obtaining spectra of the spike trains from single afferent units using the approach for frequency domain analysis for point processes [37]. For frequency domain analysis, 1.0 second data windows without overlap were used, and spectra were obtained from disjoint windows for all the available data for a specific stimulus condition (i.e., *combination* of sliding velocity, surface type, and normal force). Quantitative analysis was then performed across all the acquired data to evaluate whether or not a specific class of tactile units presented a spectrum with a principal frequency according to Equation (1).

#### 3.2. Artificial touch data analysis

After a preliminary graphical inspection of data from the biomimetic fingertip in time domain, the core analysis was operated in time-frequency domain via Short Time Fourier Transform (STFT) and in frequency domain via Fast Fourier Transform (FFT) over 1024 samples (4.096 s of data at 250 Hz) in the middle of the stimulus sliding phase.

A recent study in active touch showed outstanding repeatability of experimental data by means of the fingertip having curved fingerprints [36]. Those previous results allowed us to directly consider here the aggregated results rather than data on a single run basis, also because real-time is not targeted in this

work. Therefore, the six repeated runs per *combination* were aligned off-line and averaged channel by channel, enhancing their statistical significance and emphasizing their informative content.

For quantitative analysis of biomimetic fingertip experimental results, the principal spectral component  $f_{peak}$  is retrieved from outputs of the sensor array in order to evaluate the matching with the expected frequency  $f_{princ}$  (Equation 1):

$$f_{peak} = \arg \max_{f > f_0} (|FFT(PiSj)|) \quad (2)$$

Where the *argmax* function returns the frequency, provided that it is higher than the lower boundary  $f_0$ , carrying the highest power in the FFT of the output data from piezoresistor  $Pi$  of Sensor  $Sj$ . In the considered analysis,  $f_0$  was set to 2.5 Hz, so to discard the very low-frequency spectral components.

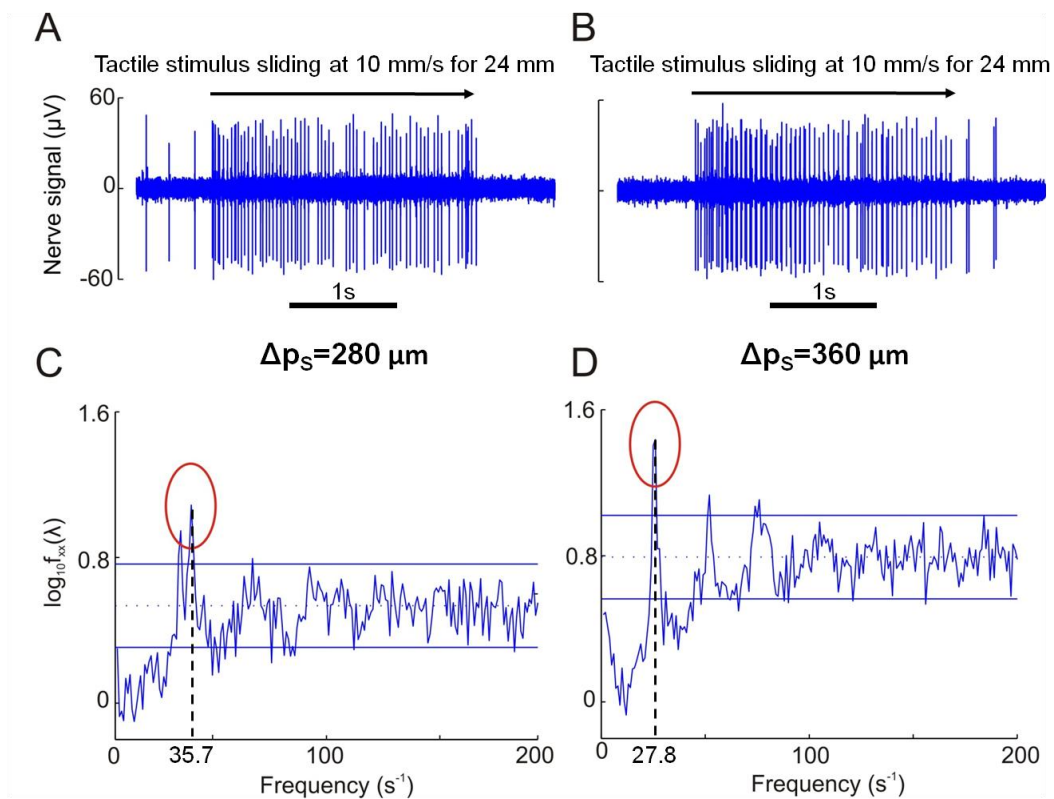
#### 4. Results and Discussion

The presented results from human microneurography experiments (Figure 5) provide evidence of modulation of single unit firing according to Equation 1. The experiments with the biomimetic fingertip show such modulation as well, confirming significance of the presented artificial touch investigation, carried out in parallel to human touch studies. A compared analysis of results from biomimetic fingertip *b* with curved fingerprints (Figures 7 and 8E-H and 9B), and from biomimetic fingertip *a* with straight fingerprints (Figures 8A-D and 9A) shows that the curvature of fingerprints has consequences on isotropy in the encoding of roughness while rotating the fingertip.

##### 4.1 Human touch

Figure 5 shows sample nerve recordings, gathered from the median nerve above the elbow using the microneurographic technique [2], from a human RA receptor during stimulus sliding motion across the distal phalanx (i.e.  $\theta=90^\circ$ ). The subject's fingerprint at the location of the depicted RA unit has a tangent oriented at approximately  $46^\circ$  from the direction parallel to the ridges of the gratings (=  $44^\circ$  degrees from the direction of the sliding motion). Spectral analysis of the nerve discharge patterns [37] showed significant modulation at the frequency determined by the stimulus spatial period  $\Delta p_s$ , according to Equation 1. A similar relationship depending on the stimulus spatial period was observed in the activity of single human mechanoreceptors with receptive fields in the finger tips of the second and third fingers. Particularly, for the tested gratings in the 280-520  $\mu\text{m}$  spatial period range, this frequency-locked modulation was for 8 of 9 RA afferents units where this was tested, but not in any of the SAI units ( $n=5$ ). For gratings in the 1600-1920  $\mu\text{m}$  spatial period range, it was observed in all of the tested RA and SAI units ( $n=7$  and  $5$ , respectively; 10-20 mm/s sliding velocity). The smaller peak at 30.8 Hz in Figure 5C reflects a slight periodic modulation of unit firing that is uncorrelated with the periodicities in the mechanical stimulus. Moreover, it should be noted that the average discharge rates of single tactile afferents never directly reflected the spatial periods of the stimuli. As an example, average discharge rate was 40 Hz for the unit in Figure 5A, and 55.5 Hz for the unit in Figure 5B. Thus, there was no 1:1 (or higher order) locking of the nerve discharges, but the spatial periodicity were reflected as a frequency modulation (Equation 1) of the discharge patterns.

**Figure 5. Panels A and B** show microneurographic recordings from human single tactile RA afferents in the fingertips during stimulation as in Figures 1C and 3A; a 10 mm/s sliding motion was applied across the distal phalanx. **Panels C and D** show spectral analysis of the nerve discharge trains from 12 repeated stimulus runs for the units shown in **A** and **B**. Grating spatial periodicity  $\Delta p_s$  is 280  $\mu\text{m}$  in **A** and **C**, 360  $\mu\text{m}$  in **B** and **D**. Principal frequencies resulting from Equation 1 according to the specific combination of grating spatial periodicity  $\Delta p_s$  and sliding velocity  $v$  are 35.7 and 27.8 Hz for **Panels C** and **D**, respectively, with meaningful coherence with the depicted experimental results. Horizontal lines in **C** and **D** show  $p < 0.01$  confidence limits for significant frequency modulation.



## 4.2 Artificial touch

Figure 6 shows the output signal from a channel of the tactile array over six runs recorded under the same experimental conditions, in order to assess high repeatability of data. Cursory analysis of Figure 6 confirms high similarity among the plots. As a further quantitative assessment, Table I presents the correlation indexes calculated over all the pairs of the runs plotted in Figure 6. All the correlation values reported in Table I are close to 1, confirming high repeatability. Similar repeatable results were obtained from the other channels of the array, for both the fingerprint designs and for all the experimental combinations ( $\theta$  and  $\Delta p$  values). High repeatability allowed to perform the averaging operation for all the following experimental results, as detailed in Section 3.2, in order to provide significant information by means of data recorded under multiple runs.

**Figure 6.** Outputs from P4S2 of the fingertip *b* with curved fingerprints, over six runs under the same experimental conditions ( $\Delta p=440\mu\text{m}$  and  $\theta=0^\circ$ ), showing high repeatability of experimental data.

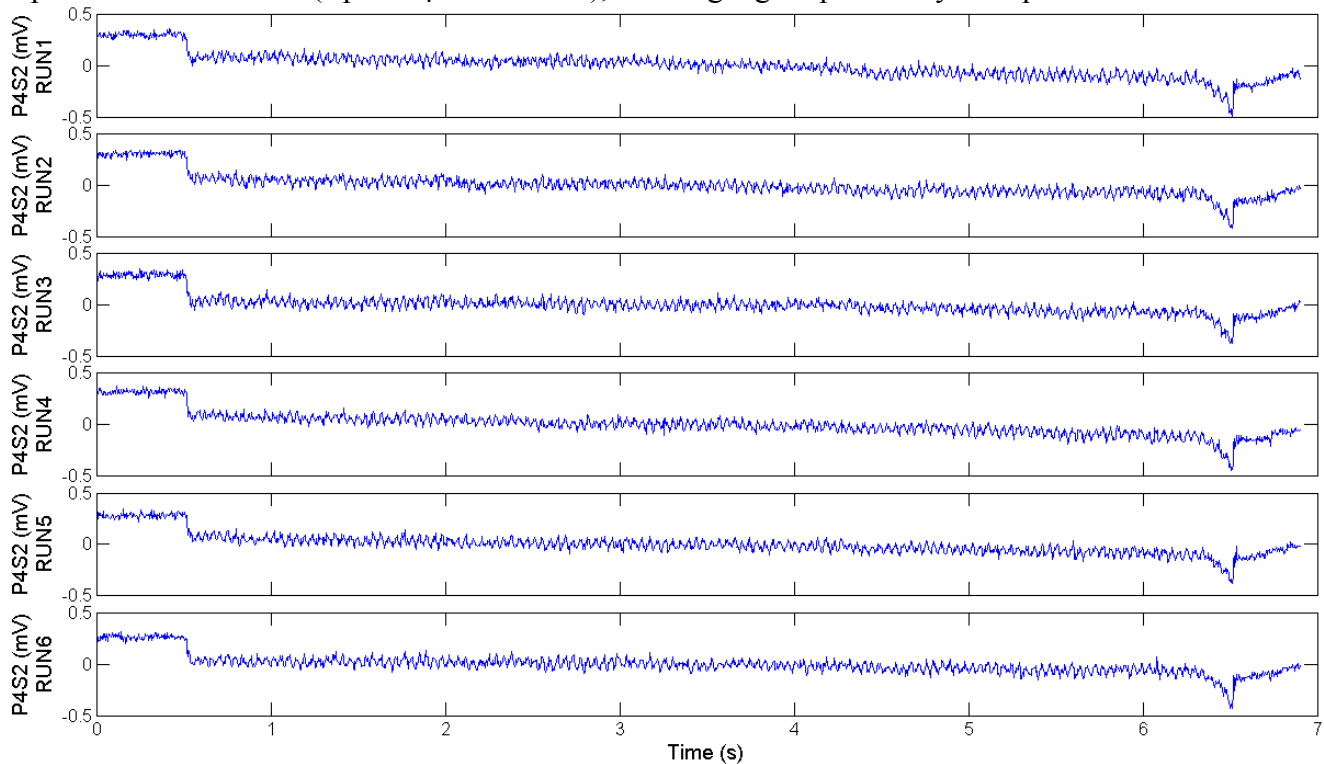


**Table 1.** Correlation indexes for all the pairs of experimental runs shown in Figure 6.

		RUNS					
		1	2	3	4	5	6
RUNS	1	1.00	0.94	0.92	0.95	0.94	0.93
	2	0.94	1.00	0.95	0.95	0.95	0.94
	3	0.92	0.95	1.00	0.94	0.94	0.94
	4	0.95	0.95	0.94	1.00	0.96	0.94
	5	0.94	0.95	0.94	0.96	1.00	0.94
	6	0.93	0.94	0.94	0.94	0.94	1.00

In Figures 7 and 8 time domain data from single channels (Piezoresistor 2 of Sensor 1 and Piezoresistor 4 of Sensor 4, respectively) of the experimented biomimetic fingertip designs is plotted above the related STFT. The insets on the right of the STFT plots show the spectra obtained by applying a FFT to the single channel data highlighted in red in the time domain plots.

Particularly, Figure 7A-B shows time domain traces from Piezoresistor 2 of Sensor 1 in fingertip *b* (see Figure 1 for the labeling of sensors of the tactile array) during stimulation with 360  $\mu\text{m}$  and 440  $\mu\text{m}$  regular gratings rotated at an angle  $\theta = 10^\circ$ . The periodic patterns at 27.8 Hz (360  $\mu\text{m}$  grating) and at 22.7 Hz (440  $\mu\text{m}$  grating) associated to the spatial periodicity of tactile stimuli are clearly visible either in time (vibrational component), in frequency (dominant peak in the FFT, marked with a dotted line) and in time-frequency (red region, marked with a dotted line in the STFT) domains. Since the sliding velocity remains constant in the performed experiments, the dominant frequency of the vibrations elicited by the tactile stimulus is proportional to the inverse of the spatial period of the grating (Equation 1), while the intensity of the vibrations increases with the spatial period. Both these effects appear to be coherent with [13], where the mechanical vibrations recorded in the fingertip of human subjects are shown to scale down in peak frequency and to increase in peak-to-peak amplitude while increasing the spatial period.

The relevance of the dynamic stimulation phase (i.e. the dataset corresponding to surface-fingertip tangential relative motion) to extract vibrational patterns which are correlated to the stimulus surface features is confirmed by the STFT spectrograms depicted below the time domain plots, which show a sudden frequency step at the onset of the stimulus sliding motion. The spectral pattern remains stable while the periodic grating is stroked at constant velocity. More importantly, as confirmed by the FFT spectra, the frequency peak corresponds to the expected value depending on the applied stimulus according to Equation 1, i.e. 27.8 Hz for the 360  $\mu\text{m}$  surface and 22.7 Hz for the 440  $\mu\text{m}$  one. Significantly, this artificial vibrational roughness encoding is coherent with the microneurography results in humans, according to the findings reported in Section 3.1 and to previous studies with monkeys [38].

A comparison between the A-D and the E-H panels in Figure 8 shows the effect of the curvature of fingerprints in the encoding of stimulus spatial features in relation to the rotation of the biomimetic fingertip. The four rows show results for  $\theta = 10^\circ$ ,  $\theta = 20^\circ$ ,  $\theta = 40^\circ$  and  $\theta = 90^\circ$ . There is higher isotropy with the curved fingerprints than with the straight ones, which have a strongly preferred direction when the sliding is closer to the direction along the distal phalanx (i.e. across the fingerprints). As shown in Figure 8A, with straight fingerprints the vibratory patterns are noticeable either in time and frequency domains for  $\theta = 10^\circ$ , while those patterns are considerably reduced and masked by the other spectral components when the fingertip is rotated (Figure 8B-D) so to have a sliding oriented closer to the direction across the distal phalanx (i.e. along the fingerprints).

**Figure 7.** Encoding of stimulus spatial period  $\Delta p_s$  in either time, frequency and time-frequency domains. Data belongs to Piezoresistor 2 of Sensor 1 of the biomimetic fingertip and was acquired while sliding at 10mm/s (200mN indentation force) the 440  $\mu\text{m}$  (**Panel A**) and 360  $\mu\text{m}$  (**Panel B**) periodic stimuli over the biomimetic fingertip with curved fingerprints (shown in Figure 1B). According to Equation 1, the expected principal frequency was 22.7 Hz (**A**) or 27.8 Hz (**B**). The rotation of the fingertip was  $10^\circ$  with respect to the stimulus sliding direction (reference frame shown in Figure 1C).

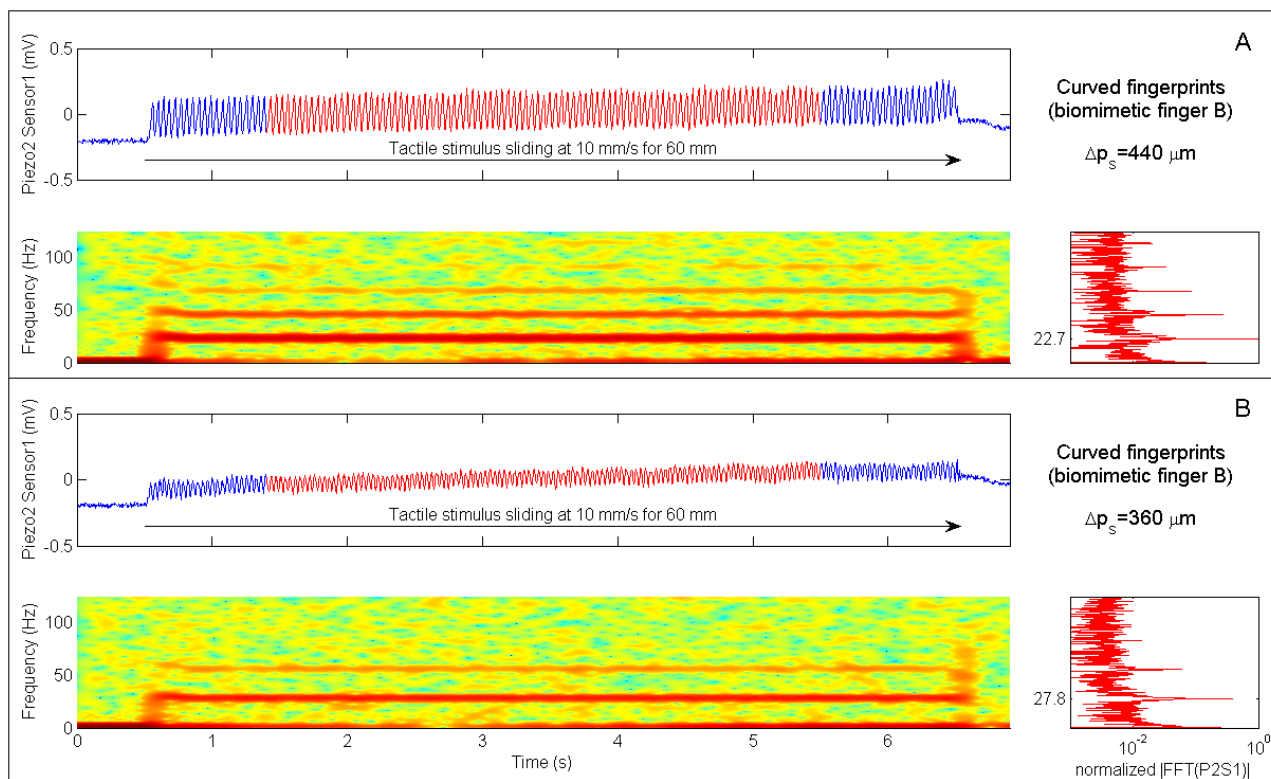
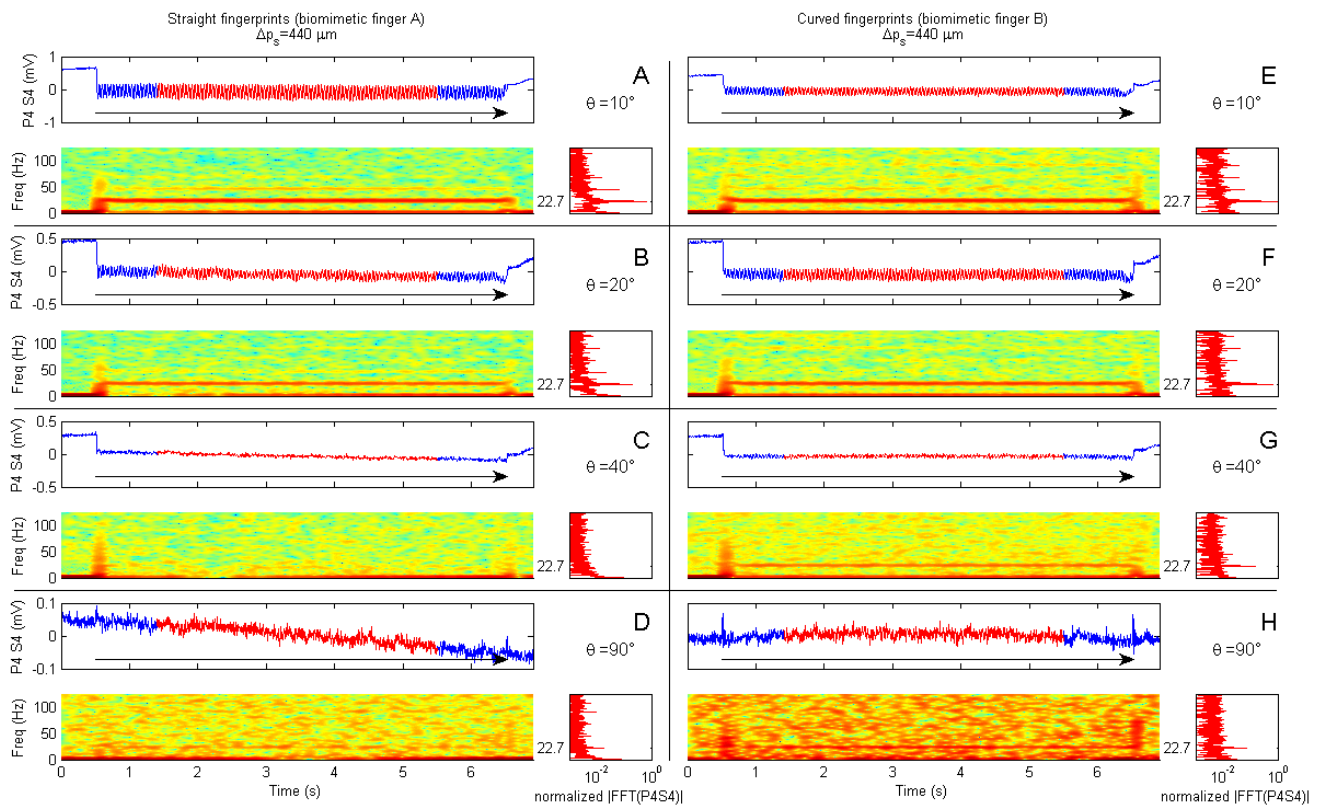


**Figure 8.** Encoding of stimulus spatial period  $\Delta p_s$  as a function of biomimetic fingertip rotation  $\theta$  for both the prototypes with straight and curved fingerprints. Data belongs to Piezoresistor 4 of Sensor 4 of the biomimetic finger and was acquired while sliding at 10 mm/s (200 mN indentation force) the 440  $\mu\text{m}$  periodic stimulus over the biomimetic finger with straight fingerprints (**Panels A to D**) and with curved fingerprints (**Panels E to H**). According to Equation 1, the expected principal frequency was 22.7 Hz. A description of each row of the subplots is provided within Figure 7. The plotted results are obtained by rotating the finger of an angle  $\theta$  set to 10° (**A, E**), 20° (**B, F**), 40° (**C, G**) and 90° (**D, H**) with respect to the stimulus sliding direction.



Extended analysis of the spectrum of readings from both the biomimetic finger designs as a function of the rotation angle  $\theta$  brings evidence of the higher anisotropy anticipated above for straight fingerprints (Figure 9A compared to Figure 9B and Figure 10A compared to Figure 10B). Within the plots shown in Figures 9 and 10, the expected (Equation 1) principal frequency is represented by a straight red line, while the peak arising in the frequency domain for output  $PiSj$  ( $i^{\text{th}}$  piezoresistor of  $j^{\text{th}}$  sensor, according to Figure 1) is detected by applying Equation 2 and the correctly identified ones are marked with red circles in the figures.

It is significant to point out that, differing from Figure 9A (straight fingerprints), in Figure 9B (curved fingerprints) the peak is not at  $\theta=0^\circ$  but at  $\theta=10^\circ$ . This is a consequence of the curvature of fingerprints, which affects the sensitivity of the packaged system in tradeoff with the preferred direction of Piezoresistor P4, hence widening the region of effective roughness encoding as a function of the finger rotation angle  $\theta$ : the tangent to the curved fingerprints at the location of Sensor S4 is orthogonal to the  $x$  axis sliding motion direction (and contemporarily parallel to ridges of the grating) when  $\theta=17.4^\circ$  (i.e.,  $>10^\circ$ ), while piezoresistor P4 shows its maximum sensitivity [23,39] to tangential loads

(reaching the sensor through the packaging material) being oriented along the direction of its tether, which is aligned with the  $x$  axis when  $\theta=0^\circ$  (i.e.,  $<10^\circ$ ).

Considerations similar to those reported above for Figure 9 apply to Figure 10 as well, which depicts spectral data from P2S1 as a function of the rotation angle  $\theta$ . The tangent to the curved fingerprints at the location of Sensor S1 is orthogonal to the  $x$  axis sliding motion direction (and contemporarily parallel to ridges of the grating) when  $\theta=10.9^\circ$ , which is lower than the related value for S4; as a consequence, in Figure 10B the peak at  $\theta=10^\circ$  appear to be more marked than the one at  $\theta=20^\circ$ , if compared with the same pair of peaks in Figure 9B.

For all the channels of the tactile array, the design with straight fingerprints guaranteed an absolute error  $\Delta f = |f_{princ} - f_{peak}|$  in principal frequency estimation (via Equation 2) lower than 0.15Hz for 75% of all the experimental combinations, while the percentage raised to 82.5% for the design with curved fingerprints.

**Figure 9.** Single-sided normalized amplitude spectra as a function of the rotation of the biomimetic fingertip with straight (**Panel A**) and curved (**Panel B**) fingerprints. Data is related to 4.096s subsets gathered from Piezoresistor 4 of Sensor 4 (P4S4) while the stimulus was indented and rubbed tangentially to the finger. Normal stimulus-fingertip contact force was set to 200mN, while the sliding velocity was 10mm/s. According to Equation 1, the expected principal frequency (marked with a red straight line) was 22.7 Hz. The red circles highlight the correctly identified (by applying Equation 2) peak frequency per each stimulation combination. Higher isotropy as a function of the rotation angle is appreciated with the fingertip having curved fingerprints.

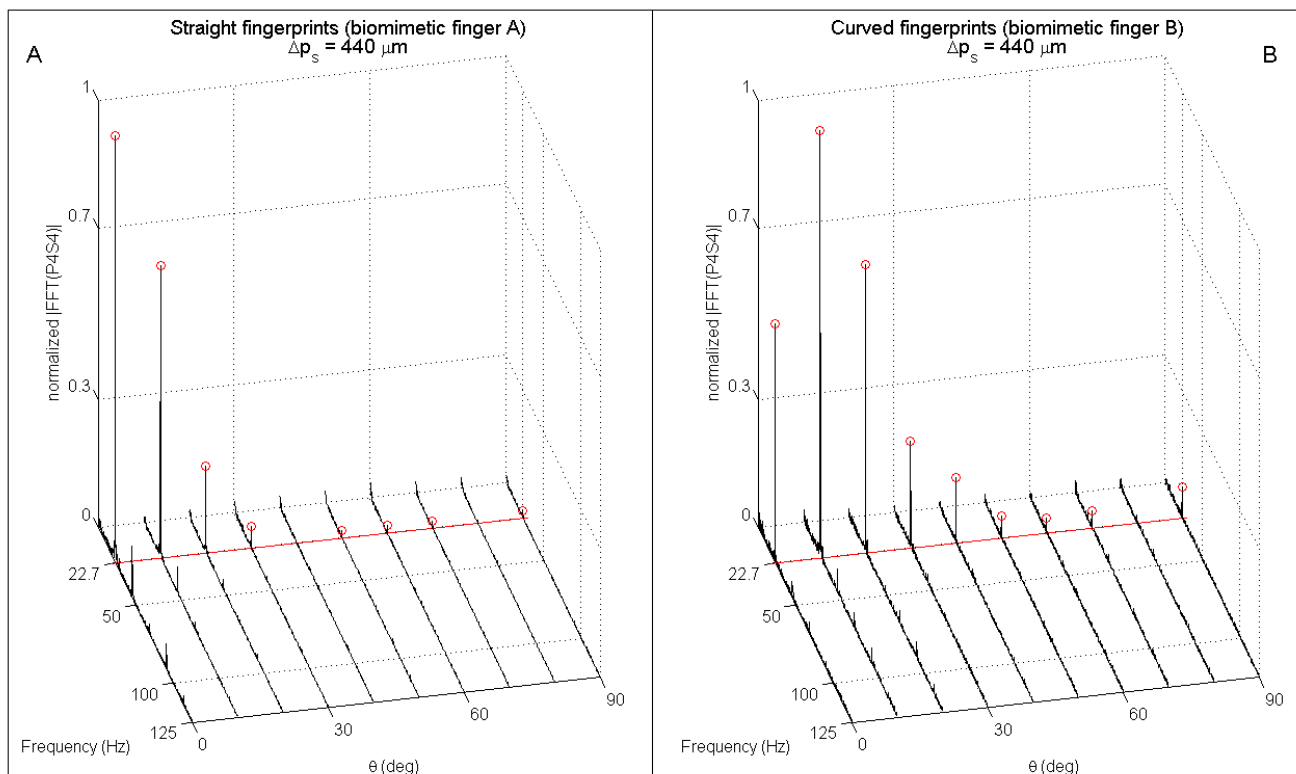
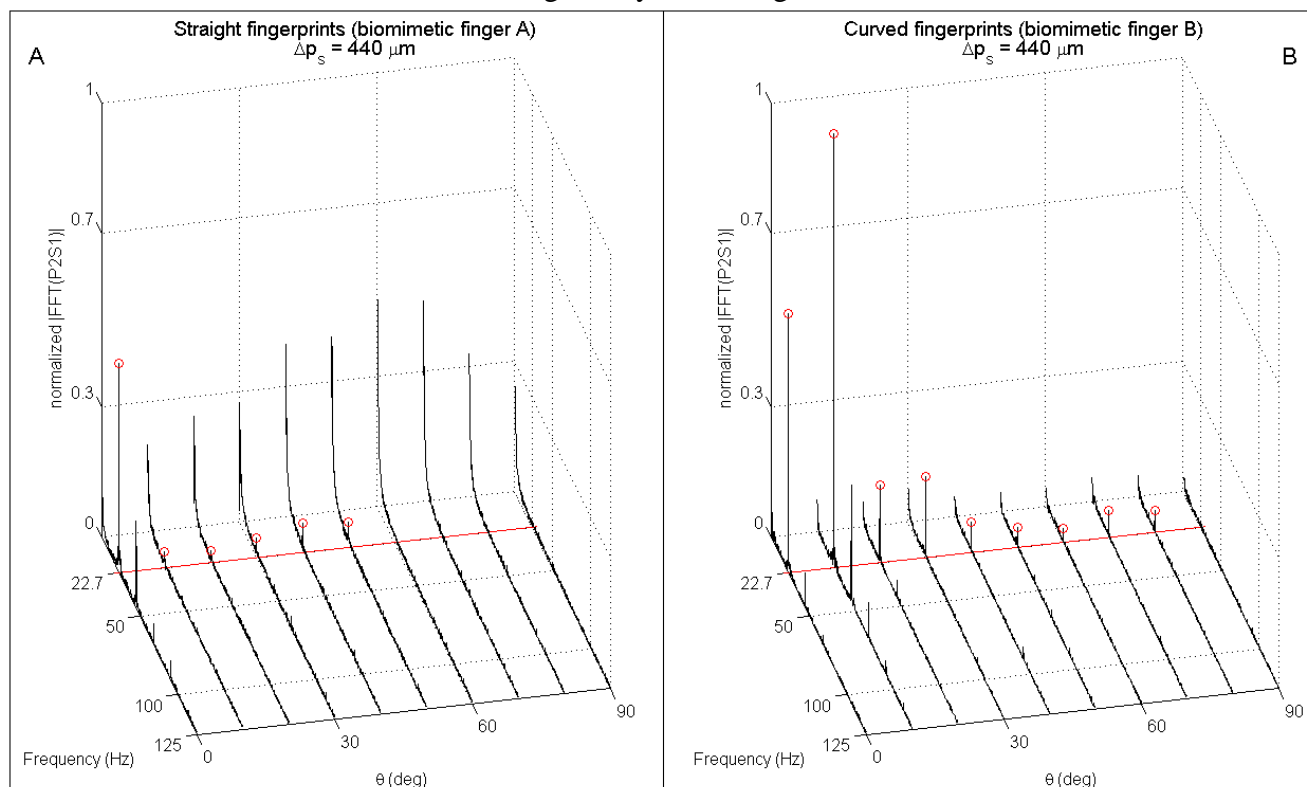


**Figure 10.** Single-sided normalized amplitude spectra as a function of the rotation of the biomimetic fingertip with straight (**Panel A**) and curved (**Panel B**) fingerprints. Data is related to 4.096s subsets gathered from Piezoresistor 2 of Sensor 1 (P4S4) while the stimulus was indented and rubbed tangentially to the finger.



## 5. Conclusions and Future Work

The presented results provide evidence that the stimulus spatial features are encoded in the spectral content (i.e. the principal frequency for a periodic grating) of the firing pattern in human mechanoreceptors and of the outputs of the developed biomimetic artificial fingertip. It is notable that in human touch this was observed for all the tested gratings in a large proportion of recorded RA human mechanoreceptor afferents and that in artificial touch the same roughness encoding mechanism, based on Equation 1, was fully demonstrated. In this work, the observed peak frequency values were at the expected values depending on the tested stimulus spatial period and constant sliding velocity tangential to the fingerpad, while the shape of the fingerprints was shown to have an effect on the possibility to promote and sense such vibrations, not in shifting the peak values on the frequency axis. The results presented here with simple gratings appear to go in the direction of those with more complex surfaces presented in [9] (e.g., see Figure 4 of [9]), since in such work the mechanical vibrations were found to have spectra repeatably related to the surfaces which were experimented with different subjects (therefore, having different fingerprints one to the other) at constant finger-stimulus relative velocity.

The experimental analysis of the artificial fingertip suggests that the structural anisotropy of fingerprints, due to their shape, has a major role in determining the level of anisotropy in the encoding of tactile stimuli spatial features. The sensory systems with straight fingerprints embedded in the skin-like packaging had noticeably higher directional preference, while higher isotropy was observed with curved ones. The obtained results provide inputs for the design of artificial sensory systems to best

encode textural features in case that the target application has or has not a preferred direction for the finger-stimulus relative motion.

Bensmaïa and colleagues raised the open question whether the anisotropy observed in humans is related to the structural anisotropy of the skin or to afferent branching at neural level [40]. In this work the experimented biomimetic artificial fingertips differed in the packaging skin-like layer design only; moreover, the anisotropy was observed on a channel by channel basis, not only as an aggregated effect among different outputs of the array. Therefore, from a robotic point of view the presented results agree with the hypothesis according to which the directional anisotropy is affected by the structure of fingerprints. Starting from these initial results, investigations on a potential concurrent role of afferent branching at neural level may be addressed in future by performing artificial touch experiments in accordance with human touch protocols, while also recording from afferent units by means of the microneurography technique and analyzing the firing modulation as a function of the stimulus sliding direction.

Finally, moving from the observation that humans appear to be able to discriminate tactile stimuli in a wide velocity range (from a few mm/s up to more than a hundred of mm/s) without any significant velocity induced effect on perceived roughness [35,41], future research via parallel artificial and human touch experiments will investigate a possible mechanism for removing the effect of velocity from Equation 1. This work has not addressed the real time discrimination of surfaces neither considered a time-varying velocity during the sliding motion of the tactile stimuli. Constant velocity was used to obtain stationary spectra in the frequency domain, which were analyzed to evaluate the role of the curvature of fingerprints in modulating the strength in the encoding of spatial wavelengths of tactile stimuli. To go towards real time discrimination feasibility under unconstrained non-constant sliding velocities, we will investigate the possibility for our artificial tactile system to implement the hypothetical human model based on coincidence detection of neural spikes, which was discussed in [42,43]. As a matter of fact, we believe that such model is promising in artificial touch as well, since a suitable approach should consider phase relationships between outputs from adjacent sensors of the array (as briefly anticipated in [36]), so to establish a spatio-temporal surface discrimination method, rather than spatial (i.e. taking into account static stimulus representation by distributed sensor units) or temporal (i.e. taking into account the vibrational stimulus representation by single sensor units) only.

## Acknowledgements

This work was supported in part by the NANOBIOACT project (EU-FP6-NMP-033287) and in part by the NANOBIO TOUCH project (EU-FP7-NMP-228844).

The authors thank N. Vitiello, R. Di Leonardo and C. Filippeschi (Scuola Superiore Sant'Anna), K. Göthner (University of Gothenburg) and M. Mitulla and S. Schmitt (Institute of Microtechnology of Mainz, Germany) for technical support. The conversations with S. Roccella (Scuola Superiore Sant'Anna) are gratefully acknowledged. The experimented tactile stimuli were provided by S. Johnson and B. Ranken (Unilever R&D, Port Sunlight).

## References and Notes

1. Dario, P.; Hannaford, B.; Takanishi, A. Guest Editorial Special Issue on Biorobotics. *IEEE T. Robot.* **2008**, *24(1)*, 3-4.
2. Vallbo, A.B.; Hagbarth, K.E.; Wallin, B.G. Microneurography: how the technique developed and its role in the investigation of the sympathetic nervous system. *J. Appl. Physiol.* **2004**, *96(4)*, 1262-1269.
3. Hollins, M.; Faldowski, R.; Rao, S.; Young, F. Perceptual dimensions of tactile surface texture: A multidimensional scaling analysis. *Percept. Psychophys.* **1993**, *54(6)*, 697-705.
4. Johnson, K.O.; Yoshioka, T. Neural mechanisms of tactile form and texture perception. In *The Somatosensory System: Deciphering the Brain's Own Body Image*; Nelson, R.J., Ed.; CRC Press LLC: Boca Raton, USA, 2001; pp. 73-101.
5. Morley, J.W.; Goodwin, A.W. Darian-Smith, I. Tactile Discrimination Of Gratings. *Exp. Brain Res.* **1983**, *49(2)*, 291-299.
6. Jones, L.A.; Lederman, S.J. Tactile Sensing. In *Human Hand Function*; Jones, L.A.; Lederman, S.J., Eds.; Oxford University Press: USA, 2006; pp. 44-74.
7. Johansson, R.S.; Vallbo, Å.B. Tactile sensibility in the human hand: relative and absolute densities of four types of mechanoreceptive units in glabrous skin. *J. Physiol. (Lond.)* **1979**, *286*, 283-300.
8. Peters, R.M.; Hackeman, E.; Goldreich, D. Diminutive Digits Discern Delicate Details: Fingertip Size and the Sex Difference in Tactile Spatial Acuity. *J. Neurosci.* **2009**, *29(50)*, 15756-15761.
9. Bensmaïa, S.; Hollins, M. Pacinian representations of fine surface texture. *Percept. Psychophys.* **2005**, *67(5)*, 842-854.
10. De Boissieu, F.; Godin, C.; Guilhamat, B.; David, D.; Serviere, C.; Baudois, D. Tactile texture recognition with a 3-axial force MEMS integrated artificial finger. In *Proceedings of Robotics: Science and Systems (RSS)* **2009**, 49-56.
11. Wheat, H.E.; Goodwin, A.W. Tactile Discrimination of Gaps by Slowly Adapting Afferents: Effects of Population Parameters and Anisotropy in the Fingerpad. *J. Neurophysiol.* **2000**, *84(3)*, 1430-1444.
12. Oddo, C.M.; Beccai, L.; Felder, M.; Giovacchini, F.; Carrozza, M.C. Artificial roughness encoding with a bio-inspired MEMS based tactile sensor array. *Sensors* **2009**, *9*, 3161-3183.
13. Bensmaïa, S.J.; Hollins, M. The vibrations of texture. *Somatosens Mot Res.* **2003**, *20(1)*, 33-43.
14. Muhammad, H.B.; Recchiuto, C.; Oddo, C.M.; Beccai, L.; Anthony, C.J.; Adams, M.J.; Carrozza, M.C.; Ward, M.C.L. A capacitive tactile sensor array for surface texture discrimination. *Microelectron Eng* **2011**, in press, doi:10.1016/j.mee.2011.01.045.
15. Edwards, J.; Lawry, J.; Rossiter, J.; Melhuish, C. Extracting textural features from tactile sensors. *Bioinspir. Biomim.* **2008**, *3(3)*, 1-12.
16. Konyo, M.; Maeno, T.; Yoshida, A.; Tadokoro, S. Roughness sense display representing temporal frequency changes of tactile information in response to hand movements. In *Proceedings of the First Joint Eurohaptics Conference and Symposium on Haptic Interface for Virtual Environment and Teleoperator Systems* **2005**, 609-610.

17. Mukaibo, Y.; Shirado, H.; Konyo M.; Maeno T. Development of a texture sensor emulating the tissue structure and perceptual mechanism of human fingers. In *Proceedings of the IEEE International Conference on Robotics and Automation* **2005**, 2565-2570.
18. Chen, X.; Sakai, J.; Yang, S.; Motojima, S. Biomimetic Tactile Sensors with Fingerprint-Type Surface Made of Carbon Microcoils/Polysilicone. *Jpn. J. Appl. Phys.* **2006**, *45*, L1019–L1021.
19. Zhang, Y.; Mukaibo, Y.; Maeno, T. A multi-purpose tactile sensor inspired by human finger for texture and tissue stiffness detection. *Proceedings of the IEEE International Conference on Robotics and Biomimetics* **2006**, 159–164.
20. Scheibert, J.; Leurent, S.; Prevost, A.; Debregeas, G. The role of fingerprints in the coding of tactile information probed with a biomimetic sensor. *Science* **2009**, 323(5920), 1503–1506.
21. Vásárhelyi, G.; Ádám, M.; Vázsonyi, É.; Bársony, I.; Dücső, C. Effects of the elastic cover on tactile sensor arrays. *Sens. Actuator A-Phys.* **2006**, *132*, 245-251.
22. Oddo, C.M.; Beccai, L.; Muscolo, G.G.; Carrozza, M.C. A biomimetic mems-based tactile sensor array with fingerprints integrated in a robotic fingertip for artificial roughness encoding. In *Proceedings of the IEEE International Conference on Robotics and Biomimetics* **2009**, 894–900.
23. Beccai, L.; Roccella, S.; Arena, A.; Valvo, F.; Valdastrì, P.; Menciassi, A.; Carrozza, M.C. Design and fabrication of a hybrid silicon three-axial force sensor for biomechanical applications. *Sens. Actuator A-Phys.* **2005**, *120*, 370-382.
24. Carrozza, M.C.; Cappiello, G.; Micera, S.; Edin, B.B.; Beccai, L.; Cipriani, C. Design of a cybernetic hand for perception and action. *Biol. Cybern.* **2006**, *95*(6), 629-644.
25. Controzzi, M.; Cipriani, C.; Carrozza, M.C. Mechatronic design of a transradial cybernetic hand. In *Proceedings of the IEEE/RSJ International Conference on Intelligent Robots and Systems* **2008**, 576–581.
26. Maeno, T.; Kobayashi, K.; Yamazaki, N. Relationship Between Structure of Finger Tissue and Location of Tactile Receptors, *JSME International Journal* **1998**, *41*(1), 94-100.
27. Yamada, D.; Maeno, T.; Yamada, Y. Artificial Finger Skin having Ridges and Distributed Tactile Sensors used for Grasp Force Control, *Journal of Robotics and Mechatronics* **2002**, *14*(2), 140-146.
28. Hidaka, Y.; Shiokawa, Y.; Tashiro, K.; Maeno, T.; Konyo, M.; Yamauchi, T. Development of an Elastic Tactile Sensor Emulating Human Fingers for Tele-Presentation Systems. In *Proceedings of the IEEE SENSORS 2009 Conference* **2009**, 1919-1922.
29. Hosoda, K.; Tada, Y.; Asada, M. Anthropomorphic robotic soft fingertip with randomly distributed receptors. *Robotics and Autonomous Systems* **2006**, *54*, 104–109.
30. Vallbo, A.B.; Johansson, R.S. Properties of cutaneous mechanoreceptors in the human hand related to touch sensation. *Hum. Neurobiol.* **1984**, *3*, 3-14.
31. Chambers, M.R.; Andres, K.H.; Von Duering, M.; Iggo, A. The structure and function of the slowly adapting type II mechanoreceptor in hairy skin. *Q. J. Exp. Physiol.* **1972**, *57*, 417-445.
32. Oddo, C.M.; Beccai, L.; Vitiello, N.; Backlund Wasling, H.; Wessberg, J.; Carrozza, M.C. A mechatronic platform for human touch studies. *Mechatronics* **2011**, in press, doi:10.1016/j.mechatronics.2011.02.012.

33. Kinoshita, H.; Backstrom, L.; Flanagan, J.R.; Johansson, R.S. Tangential torque effects on the control of grip forces when holding objects with precision grip. *J. Neurophys.* **1997**, *78*(3), 1619-1630.
34. Soneda, T.; Nakano, K. Investigation of vibrotactile sensation of human fingerpads by observation of contact zones. *Tribol. Intl.* **2010**, *43*, 210–217.
35. Lederman, S.J. Tactual Roughness Perception: Spatial and Temporal Determinants. *Canadian Journal of Psychology* **1983**, *37*(4), 498-511.
36. Oddo, C.M.; Controzzi, M.; Beccai, L.; Cipriani, C.; Carrozza, M.C. Roughness encoding for discrimination of surfaces in artificial active touch. *IEEE Trans Robotics* **2011**, *27*(3), in press, doi:10.1109/TRO.2011.2116930.
37. Rosenberg, J.R.; Halliday, D.M.; Breeze, P.; Conway, B.A. Identification of patterns of neuronal connectivity – partial spectra, partial coherence, and neuronal interactions. *J. Neurosci. Meth.* **1998**, *83*, 57-72.
38. Darian-Smith, I.; Oke, L.E. Peripheral neural representation of the spatial frequency of a grating moving across the monkey's finger pad. *J. Physiol.-London* **1980**, *309*, 117-133.
39. Oddo, C.M.; Valdastri, P.; Beccai, L.; Roccella, S.; Carrozza, M.C.; Dario, P. Investigation on calibration methods for multi-axis, linear and redundant force sensors. *Meas. Sci. Technol.* **2007**, *18*(3), 623-631.
40. Bensmaïa, S.J.; Craig, J.C.; Yoshioka, T.; Johnson, K.O. SA1 and RA Afferent Responses to Static and Vibrating Gratings. *J. Neurophysiol.* **2006**, *95*(3), 1771–1782.
41. Meftah, E.M.; Belingard, L.; Chapman, E. Relative effects of the spatial and temporal characteristics of scanned surfaces on human perception of tactile roughness using passive touch. *Exp. Brain Res.* **2000**, *132*, 351-361.
42. Johansson, R.S.; Birznieks, I. First spikes in ensembles of human tactile afferents code complex spatial fingertip events. *Nature Neuroscience* **2004**, *7*(2), 170-177.
43. Johansson, R.S.; Flanagan, J.R. Coding and use of tactile signals from the fingertips in object manipulation tasks. *Nature Rev. Neurosci.* **2009**, *10*, 345–359.

# Roughness Encoding for Discrimination of Surfaces in Artificial Active-Touch

Calogero M. Oddo, Marco Controzzi, *Student Member, IEEE*, Lucia Beccai, *Member, IEEE*, Christian Cipriani, *Member, IEEE*, and Maria Chiara Carrozza, *Associate Member, IEEE*

**Abstract**—A  $2 \times 2$  array of four microelectromechanical system (MEMS) tactile microsensors is integrated with readout electronics in the distal phalanx of an anthropomorphic robotic finger. A total of 16 sensing elements are available in a  $22.3\text{-mm}^2$  area (i.e.,  $72$  units/cm<sup>2</sup>) of the artificial finger, thus achieving a density comparable with human Merkel mechanoreceptors. The MEMS array is covered by a polymeric packaging with biomimetic fingerprints enhancing the sensitivity in roughness encoding. This paper shows the ability of the sensor array to encode roughness for discrimination of surfaces, without requiring dedicated proprioceptive sensors for end-effector velocity. Three fine surfaces with 400-, 440-, and 480-  $\mu\text{m}$  spatial periods are quantitatively evaluated. Core experiments consisted in active-touch exploration of surfaces by the finger executing a stereotyped human-like movement. A time–frequency analysis on pairs of tactile array outputs shows a clustering of the fundamental frequency, thus yielding 97.6% worst-case discrimination accuracy with a  $k$ -nearest-neighbor ( $k$ -NN) classifier. Hence, surfaces differing down to 40  $\mu\text{m}$  are identified in active-touch by both hardware and processing methods based on exteroceptive tactile information. Finally, active-touch results with five textiles (which differ in texture or orientation) are shown as a preliminary qualitative assessment of discrimination in a more realistic tactile-stimulation scenario.

**Index Terms**—Artificial touch, force and tactile sensing, microelectromechanical system (MEMS) sensors array, robotic finger, roughness encoding.

## I. INTRODUCTION

THE development of a tactile sensory system, which is able to mimic the human sense of touch in the encoding of textures and is compact enough to be integrated into articulated artificial fingers, would significantly improve dexterous manipulation (e.g., exploited in industrial, service, or assistive robotics) and upper limb prosthetics [1]–[3]. Within prosthetics, one of the main drawbacks of current commercial systems is the lack

Manuscript received September 19, 2010; revised December 30, 2010; accepted February 14, 2011. This paper was recommended for publication by Guest Editor M. Valle and Editor W. K. Chung upon evaluation of the reviewers' comments. This work was supported by the Nanoengineering Biomimetic Tactile Sensors (NANOBIOTACT) under Project EU-FP6-NMP-033287, by the Nano-resolved multi-scale investigations of human tactile sensations and tissue engineered nanobiosensors (NANOBIOTOUCH) under Project EU-FP7-NMP-228844, and by the OPEN neuro-prosthetic HAND platform (OPENHAND) under Project Italian MiUR PRIN 2008 prot. PMZT2Z.

C. M. Oddo, M. Controzzi, C. Cipriani, and M. C. Carrozza are with The BioRobotics Institute, Scuola Superiore Sant'Anna (SSSA), I-56025 Pontedera, Pisa, Italy (e-mail: oddoc@sssup.it).

L. Beccai is with the Center for Micro-BioRobotics@SSSA, Istituto Italiano di Tecnologia (IIT), I-56025 Pontedera, Pisa, Italy.

Color versions of one or more of the figures in this paper are available online at <http://ieeexplore.ieee.org>.

Digital Object Identifier 10.1109/TRO.2011.2116930

of sensory feedback [4]. As a consequence, the user is unable to *feel* an item held by the hand.

Among the various properties that an artificial tactile system should be able to sense, texture is one of the most challenging and less established. Considering the role that has been hypothesized in humans for high-density surface-located type-I mechanoreceptors [5], [6], gathering information on texture of a surface could take benefit from the implementation of artificial tactile systems that can encode dynamic events with a low threshold in sensitivity and a human-like spatial resolution of taxels [7]. In humans, texture has two major independent dimensions: roughness and softness [8]. Other surface qualities, such as stickiness, warmth, bumpiness, and harshness, were identified. However, these are not independent from the two major dimensions, and there is a consolidated agreement for a primacy of the smooth–rough dimension as a descriptor, even if not unique, of surface textures [8]–[10]. Therefore, taking inspiration from the human sense of touch, in this study, we focus on roughness, which is associated with the spatial modulation of the surface (i.e., spatial coarseness, at both macro- and microscales) [9], and in humans it is mediated by neural mechanisms which are also involved in tactile guidance during dexterous manipulation [5], [11].

The objective of this study is to develop an exploratory artificial finger equipped with tactile microsensors at its fingertip and a method for robust discrimination of surfaces based on roughness encoding during stereotyped movements. Such a system has not been presented so far and may be exploited in future next-generation hand-prostheses [12], [13], with the aim of providing noninvasive or invasive afferent sensory feedback.

To our knowledge, previous works for roughness encoding showed experimental results under passive-touch protocols only, i.e., surfaces were presented to a still sensorized fingertip that was not integrated into an actuated finger, or without relative movements of finger linkages in case of integration. Hosoda *et al.* developed a soft fingertip with a smooth surface embedding strain gauges and PVDF films in a random manner at different depths of the rubber layers, allowing for discrimination of five different types of materials [14]. Wettels *et al.* developed a tactile sensor array consisting of a rigid core surrounded by a weakly conductive fluid contained within an elastomeric skin. The sensor uses the deformable properties of the fingerpad, and tactile information relative to the contact force is retrieved from impedance measurements via embedded electrodes [15], [16]. Dynamic roughness encoding was shown via time–frequency inspection in [17], while manually moving the artificial finger over specimens, by means of a pressure sensor located away

from the skin and functioning as a hydrophone in a fluid. A fingertip-shape tactile sensor integrating a microphone has also been investigated to quantify textural features [18] presented by medium-coarse stimuli producing a square wave that is 1 mm in height, with wavelength varying from 1 to 4 mm with 0.5-mm increments. A fingertip, which is three times larger than the human finger, was developed to provide information on roughness, stiffness, and friction of the object with which it comes into contact [19], [20]. Some other works presented the integration of tactile sensing in actuated robotic fingers, but the focus has mainly been on grasp stabilization rather than on the encoding of spatial coarseness. Examples include the Gifu III Robotic Hand [21] and the DLR Hand II [22] with embedded six-axis force sensors.

We previously presented a bioinspired fingertip with tactile sensors embedded in a viscoelastic packaging with medium-coarse fingerprints, which was suitable for the encoding of surface roughness in the frequency domain under controlled stimuli [23]. To provide the controlled stimuli, we [23] used a 2-degree-of-freedom (DoF) platform presenting tactile specimens to the sensor in a precise and repeatable manner; the fingertip was still, while surfaces were indented with controlled normal contact force and then stroked at known constant velocity tangentially to the fingerpad. Periodic ridged tactile stimuli (i.e., gratings), which can be considered as the kernel of everyday life surfaces, were selected as a class of standardized test surfaces. Gratings are widely used to investigate roughness encoding in neurophysiological studies [6], [24]. We demonstrated that they could be identified by means of spectral analysis on the outputs of the sensor array, since the constant-speed sliding motion of the grating resulted into a stationary fundamental frequency equal to the ratio between the tangential velocity and the spatial period of the scanned stimuli [23].

In this study, we use the same class of tactile stimuli, and we extend the *passive* grating-recognition method to the application with an *active* underactuated [25], [26] robotic finger (see Fig. 1) to emulate the possible behavior of a robotic or prosthetic hand in exploring objects. We integrate a  $2 \times 2$  array of four tactile sensors (resulting in 16 channels in an area of  $22.3 \text{ mm}^2$ , i.e.,  $72 \text{ units/cm}^2$ ) and biomimetic fingerprints in the distal phalanx of a robotic finger [see Fig. 1(a)] being appropriate for the integration within a hand prosthesis [27].

As a control condition, we present the fundamental-frequency modulation under a passive-touch protocol with controlled stimulus scanning velocity. Next, as an experimental condition, the robotic finger actively explores the samples in a preprogrammed trajectory. Three gratings having very close spatial periods (i.e.,  $400$ ,  $440$ , and  $480 \mu\text{m}$ ) are evaluated to demonstrate the working principle and accuracy of the sensor array and its performance. Results demonstrate a surface-identification approach based on 1) the implementation of a stereotyped feedforward exploratory trajectory, 2) time-frequency analysis via wavelet transform (WT) and cross-wavelet transform (XWT) on the outputs of the tactile sensors, and 3)  $k$ -nearest-neighbor ( $k$ -NN) discrimination based on extracted fundamental frequency; this is bioinspired to sensorimotor control models [28], since it is based on planned-motion trajectory rather than continuous feedback from proprioceptive sensors.

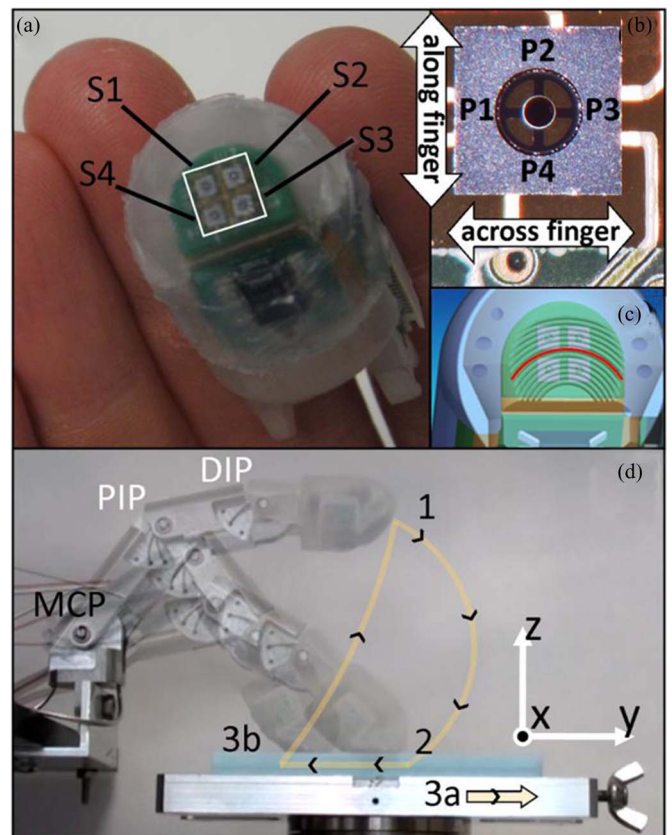


Fig. 1 (a) Distal phalanx of the robotic finger, in comparison with human hand, integrating the  $2 \times 2$  sensor array (S1–S4), electronics, and polymeric packaging with fingerprints; the square with white borders highlights the  $22.3\text{-mm}^2$  area of the array, where a density of  $72 \text{ units/cm}^2$  is reached. (b) (Close-up view) Sensor S4 of the array. The four outputs of the sensor are marked at the roots of the tethers of the cross-shape structure. For all the sensors of the array, P1 and P3 are on tethers that are oriented across the finger, while P2 and P4 are on tethers oriented along the finger. (c) Design of the sensor array showing the fingerprints, having a  $400\text{-}\mu\text{m}$  ridge-to-ridge distance; the curvature radius of the fingerprint highlighted in red is  $4.8 \text{ mm}$ . (d) Setup, reference frame, and phases of the protocol for the passive-touch (1, 2, and 3a) and active-touch (1, 2, and 3b) experiments. The 2 degrees of actuation (DoA) are obtained via independent control of MCP joint and underactuated coupling between the PIP and DIP joints.

This paper is organized as follows. Section II describes the developed finger. Section III details the roughness-encoding approach, the experimental protocol, and the wavelet-analysis technique. Section IV shows 1) passive-touch results, which demonstrate correct operation of the finger in a precisely controlled experiment, and 2) outcomes in an active-touch exploratory task. Finally, insights on future work 1) present the possibility to include phase differences from adjacent sensor outputs as a further discrimination feature and 2) shows preliminary active-touch experimental results with textiles (which differ in texture or orientation) as a proof of discrimination feasibility with everyday life surfaces.

## II. MATERIALS

### A. Underactuated Finger

The robotic finger [see Fig. 1(d)] was human-sized [29], tendon-driven (as given in [12], [13], and [27]), and underactuated, i.e., with more DoFs than actuators. Such property reduces

design complexity and allows self-adaptation and anthropomorphic movements similar to human exploratory tasks [12]. The finger had 3 DoFs (as flexion/extension DoFs of the human finger) and two dc-motor actuators (i.e., model 1727, Faulhaber Minimotor; ratio 14:1) under position control. One motor actuated the flexion/extension of the metacarpophalangeal (MCP) joint, and the other was for the underactuated flexion/extension of the proximal interphalangeal (PIP) and distal interphalangeal (DIP) coupled joints (as Hirose's soft finger [30]).

### B. Tactile Array

A  $2 \times 2$ , with 2.36-mm pitch, array of four microelectromechanical system (MEMS) sensors was connected to a rigid-flex board integrated in the distal phalanx of the robotic finger [see Fig. 1(a)]. The core microsensor [see Fig. 1(b)] is a 3-D high aspect ratio,  $\sim 1.4 \text{ mm}^3$ , MEMS resulting from silicon microstructuring technologies [31]. Each sensor integrated four piezoresistors at the roots of a cross-shape structure equipped with a mesa. This turned out into a 16-channel sensory system for transducing the mechanical interaction with external tactile stimuli in a  $22.3\text{-mm}^2$  area of the fingerpad [see Fig. 1(a)]. Therefore, a density of  $72 \text{ units/cm}^2$  (i.e., 16 channels/ $22.3 \text{ mm}^2$ ) was reached, which is similar to the  $70 \text{ units/cm}^2$  of human Merkel mechanoreceptors [32] which have been shown to encode roughness in studies with monkeys [5].

The sensors of the array are labeled as S1, S2, S3, and S4 according to Fig. 1(a), while the outputs of each sensor are labeled as P1, P2, P3, and P4, as shown in Fig. 1(b). P1 and P3 are related to piezoresistors implanted on the cross-shape structure on tethers oriented across the finger axis, while P2 and P4 are on tethers oriented along the finger axis. The output signals were acquired at  $f_s = 300 \text{ Hz}$  without preamplification by means of a 16-channel 24-bit analog-to-digital converter (ADS1258, Texas Instruments) lodged in the distal phalanx.

The packaging of the MEMS tactile array mechanically filters the physical stimulation applied to the fingertip and is crucial to its bioinspired response. It is known from previous studies that fingerprints enhance tactile sensitivity [33]–[35]. Therefore, the outer packaging layer of the fingertip, which is made of synthetic compliant material (DragonSkin, Smooth-On), had a surface with fingerprints [see Fig. 1(c)] mimicking the human fingerpad. To achieve biomimetism [36], the fingerprints had  $400 \mu\text{m}$  between-ridge distance; their curvature radius was set to 4.8 mm in the center of the sensor array [see the red ridge in Fig. 1(c)], while the artificial epidermal ridge had a height of  $170 \mu\text{m}$ , and the total packaging thickness from the mesa structure of the silicon microsensor was  $770 \mu\text{m}$ .

### C. Experimental Setup

The experimental setup consisted of two main subsystems, as shown in Fig. 1(d): the sensorized robotic finger and a platform under horizontal [see the  $y$ -axis in Fig. 1(d)] position/velocity control, which was a simplified version of a 2-DoF platform [37] used in previous studies [23], [38]. Changeable gratings were housed in a carrier of the platform. A load cell (Nano43, ATI, NC) was integrated under the carrier to verify

TABLE I  
TESTED PERIODIC STIMULI IN BOTH PASSIVE- AND ACTIVE-TOUCH SESSIONS AND EXPECTED FUNDAMENTAL FREQUENCY IN SENSOR OUTPUTS AS A FUNCTION OF THE STIMULUS SPATIAL PERIOD AND SLIDING VELOCITY IN PASSIVE-TOUCH

		Stimulus spatial period $\Delta p$		
		400 $\mu\text{m}$ (runs 1-8)	440 $\mu\text{m}$ (runs 9-16)	480 $\mu\text{m}$ (runs 17-24)
Stimulus sliding velocity $v$	$v_1=6.7 \text{ mm/s}$	16.7 Hz	15.2 Hz	13.9 Hz
	$v_2=10.0 \text{ mm/s}$	25.0 Hz	22.7 Hz	20.8 Hz

that finger–stimulus contact forces were in the range of hundreds of milliNewtons, such as that occurring in typical human tactile exploratory tasks [24].

## III. METHODS

### A. Fundamental Frequency

When a relative motion at speed  $v(t)$  occurs between a finger and a grating having spatial period  $\Delta p$  along the motion direction, a correct roughness encoding by the tactile sensor array should reveal a fundamental tone at frequency  $f_{\text{princ}}(t)$  [37]

$$f_{\text{princ}}(t) = \frac{v(t)}{\Delta p}. \quad (1)$$

### B. Experimental Protocol

The coherence between the theoretical [see (1)] and the experimental *fundamental frequency* is demonstrated at first in passive-touch; stimuli were stroked at controlled known velocity in order to show and evaluate the encoding principle [see (1)] under a protocol allowing to directly decouple the contribution of velocity  $v(t)$  from stimulus spatial coarseness  $\Delta p$ . In a second set of experiments, the approach was evaluated under an active-touch protocol with the robotic finger mimicking the natural exploratory movement by the hand and without measuring the instant sliding velocity. In order to evaluate their discrimination by the artificial finger, three gratings (see Table I) with 400-, 440-, and 480- $\mu\text{m}$  spatial periods  $\Delta p$  were used eight times each with both the protocols, for a total of 48 experiments (runs). The tested spatial periods are in the range of studies on roughness discrimination in humans [38]. Preliminary active-touch experiments were performed with textiles as well and are presented as insights on future work in Section V-B.

1) *Passive-Touch Experiments With Gratings*: The finger was flexed and the fingertip brought into contact with the tactile stimulus [see phases 1 and 2 of Fig. 1(d)]. To show the fundamental frequency dynamically modulating as a function of velocity, a double-ramp sliding motion was then applied to the grating along the positive  $y$ -axis [see phase 3a of Fig. 1(d)] via the platform under position/velocity control: a 10-mm ramp for 1500 ms ( $v_1 = 6.7 \text{ mm/s}$ ) was followed by a 10-mm one in 1000 ms ( $v_2 = 10.0 \text{ mm/s}$ ). This protocol is named passive-touch since the robotic finger is still during the stimulus-sliding motion. Based on (1), Table I shows the theoretical fundamental

frequencies, ranging from 13.9 to 25.0 Hz, in the passive-touch protocol depending on the combination of sliding velocity and tactile stimulus.

2) *Active-Touch Experiments With Gratings*: Active-touch experiments were implemented by controlling the MCP joint to contact the tactile stimulus [see phases 1 and 2 of Fig. 1(d)]; subsequently, the PIP and DIP joints were flexed [see phase 3b of Fig. 1(d)] to scan, along the negative  $y$ -axis, the same spatial portion of stimulus presented with the passive-touch experiments. The finger was actuated to perform a smooth human-like exploratory task lasting for 2 s. The same pattern was provided to the finger for all the active-touch runs, thus implementing a stereotyped [14] exploratory movement.

### C. Data Analysis

1) *Wavelet and Cross-Wavelet Transforms*: The elaboration method should take into account that in the active-touch experiments the end-effector velocity could be time variant. As a consequence, the fundamental frequency would dynamically modulate within each exploratory session, while rubbing the surface. To allow retrieving such dynamic frequency-modulation, the continuous WT is used, thus expanding the output signals from the sensor array into a time–frequency space. Data analysis is performed via the MATLAB wavelet-coherence package (for underlying theory and an application example, see [39]); the default Morlet wavelet function and 100 scales per octave were selected. More reliably than the single-channel WT, the cross WT (XWT) is applied to identify time–frequency regions with high common power between outputs from different sensors of the array, hence establishing a robust elaboration method based on combined processing of pairs of sensor outputs.

Each sensing-element (i.e., piezoresistor) response depends on its orientation with respect to the applied stimulus [31]. Although the MEMS sensor is suitable (both bare [31], [40], or packaged [41]) to solve the contact force, in this study, the raw voltage readings were used. This represents an added value of the system, not only because the contact force is not addressed in this study, but mainly because this turns out into a technique being more robust and less time-consuming for the operator (thereby avoiding periodic recalibration operations). The 16 sensing elements of the array are either aligned in the direction across the finger or along the finger. The analysis via XWT is operated by processing outputs of piezoresistors that are oriented along the same direction. Specifically, of the 16 available channels, three are shown in the following to point out the meaningful information available by processing in combination a pair of outputs belonging to sensors in line across the finger axis [i.e., P1 outputs from sensors S1 and S2, according to the labeling of Fig. 1(b) and (c)] and a pair of outputs from sensors aligned along the finger axis (i.e., P1 outputs from sensors S4 and S1).

The application of the WT and the XWT is graphically represented with colors mapping the normalized power in time–frequency space, where the 5% significance level is highlighted as a thick contour. In addition, the XWT provides information about the local relative phase differences between sensor out-

puts. Phase information obtained via XWT ( $O_1, O_2$ ) is graphically represented by arrows pointing right or left if the signals are in-phase or in anti-phase, pointing down if sensor output  $O_1$  leads  $O_2$  of  $\pi/2$ , and pointing up if  $O_2$  leads  $O_1$ .

2) *Passive-Touch Roughness Encoding Via Vibratory Cues*: To discriminate the gratings via vibratory cues [from (1)], the frequency  $f_{MP}$  carrying the maximum power was identified, as a function of time  $t_k$ , from the XWT applied to pairs of array outputs (which are labeled as  $O_1$  and  $O_2$  for the sake of generalization)

$$f_{MP}(O_1, O_2)(t_k) = \arg \max_f |XWT(O_1, O_2)(t_k, f)|. \quad (2)$$

In passive-touch, the vibrational encoding was expected to last for the entire stimulus sliding. Hence, the frequency  $f_{MP}$  should encode the spatial coarseness of the stimuli whatever be the time instant  $t_k$ , provided that it belonged to the sliding motion at controlled constant velocity.

The mean value  $\bar{f}_{MP}(O_1, O_2)$  of the frequency  $f_{MP}$  carrying the maximum power was calculated on two pairs of array channels (i.e., P1S1–P1S2 and P1S4–P1S1). This was calculated from significant signal slices on each run; in particular, 200 sample windows (with 667-ms duration) were extracted from the 6.7 and 10.0 mm/s sliding motion in order to consider subsets of data belonging to constant-speed phases of the passive-touch protocol. Due to the constant sliding velocity of surfaces, a clustering of  $\bar{f}_{MP}$  data is expected subject to spatial-coarseness encoding being suitable for discrimination of surfaces. Statistical indices on frequency  $f_{MP}$  were calculated across repeated runs (with same grating): double mean  $\bar{\bar{f}}_{MP}(O_1, O_2)$  and standard deviation  $\Delta f_{MP}(O_1, O_2)$  aggregating the eight windows of  $f_{MP}$  across the repeated runs (per grating and velocity), mean-max  $\overline{mf}_{MP}(O_1, O_2)$ , and mean-min  $\underline{mf}_{MP}(O_1, O_2)$  (i.e., the mean across the repeated runs of the maximum/minimum  $f_{MP}$  registered within each window). In passive-touch, the grating was identified by selecting the one yielding in minimum error between theoretical (see Table I) and experimental fundamental frequency.

3) *Active-Touch Roughness Encoding Via Vibratory Cues*: While in passive-touch the vibrational roughness encoding is expected to last for all the sliding of the stimulus, in active-touch, it is expected that each unit of the array best encodes the tactile stimulus in a subset only of the finger exploratory task. In fact, the varying inclination of the fingertip in active-touch generally results in a shift of the center of pressure on the fingerpad. Therefore, it is crucial to identify significant regions in time–frequency space. To this aim, the instant  $t_{MP}$  corresponding to the maximum cross-power between adjacent units is identified run by run from  $f_{MP}$  [as defined in (2)] as a starting point for active-touch data analysis

$$t_{MP}(O_1, O_2) = \arg \max_{t_k} |XWT(O_1, O_2)(t_k, f_{MP}(O_1, O_2)(t_k))|. \quad (3)$$

The mean value  $\bar{f}_{MP}(O_1, O_2)$  of the maximum power frequency  $f_{MP}$  was calculated run by run on two pairs of array channels (i.e., P1S1–P1S2 and P1S4–P1S1) from a

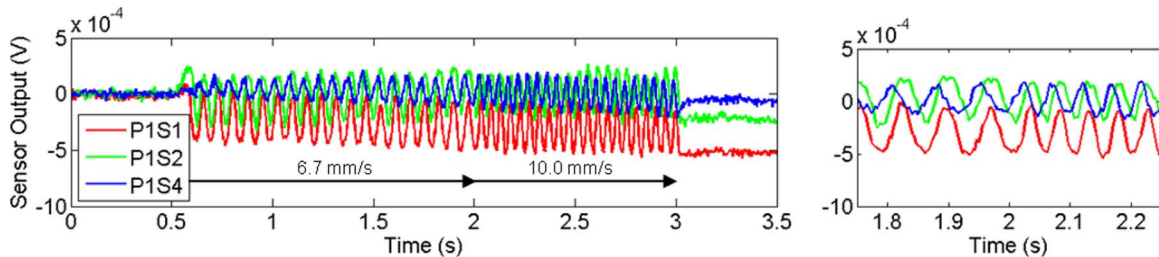


Fig. 2. Time-domain plots under a passive-touch run with 480- $\mu\text{m}$  grating (P1S1, P1S2, and P1S4, according to the labeling of Fig. 1(b) and (c), are shown). The stimulus sliding-motion starts at  $t_1 = 0.5$  s with a 6.7 mm/s velocity up to  $t_2 = 2.0$  s, when the velocity is raised to 10 mm/s. The sliding motion stops at  $t_3 = 3.0$  s. Vibrational encoding of stimulus spatial period is appreciated between  $t_1 = 0.5$  s and  $t_3 = 3.0$  s. The plots on the right show a zoom of the encoding of stimulus-controlled velocity step at  $t_2 = 2$  s. Sensors S1 and S2 are on the distal part of the fingerpad in symmetrical positions with respect to the axis of the finger, and thus, the related P1S1 and P1S2 signals are in-phase during the stimulus sliding-motion. Sensor S4 is more proximal on the fingerpad, and therefore, P1S4 shows a phase difference with respect to P1S1 and P1S2. The phase difference between S4 and S1/S2 outputs is not affected by the varying velocity [see (4)].

20-sample window (67 ms of data) around the instant  $t_{MP}$  (from six samples before to 13 samples after  $t_{MP}$ ). This particular condition was imposed by the short duration of the active-rub (where significant information is found) roughness encoding, as presented below. Statistical indices were calculated across runs. Even in the condition of nonconstant end-effector velocity while actively exploring surfaces, due to the execution of movements being stereotyped across the runs, a clustering of  $\bar{f}_{MP}$  data is expected in the event of spatial-coarseness encoding being applicable to machine-learning classifiers for discrimination of surfaces. The same statistical indices defined for passive-touch in Section III-C2) were calculated across active-touch runs. In active-touch, a  $k$ -NN technique was used for discrimination of gratings by using  $\bar{f}_{MP}$  values from two output pairs as a classification feature. The training and test operation was performed 10 000 times, by using a *leave-M-out* validation for evaluation of discrimination performance:  $M$  experimental runs out of the 24 active-touch ones were randomly selected as a test set, while the others were used to train the  $NN$  classifier, provided that each of the three stimuli appeared with the same number of occurrences, i.e.,  $(24-M)/3$ , in every training set. Therefore, for each train and test operation,  $M = 3$  results in a classifier being trained over seven random runs out of the eight repeated ones per stimulus, down to a single random training run per stimulus with  $M = 21$ . The latter condition is a worst-case evaluation because a training set based on a single experimental observation would be more sensitive to the potential occurrence of outliers.

#### IV. RESULTS AND DISCUSSION

In the following, the results in the control passive- and experimental active-touch conditions are shown. The contact forces at finger–stimulus interface, as recorded by a load cell, are comprised within 100 and 300 mN (not shown in the plots for the sake of graphical clearness) and, thus, belong to the range used in human exploratory tasks [24].

##### A. Passive-Touch Experiments With Gratings

Fig. 2 shows in time domain the vibrational encoding of the 480- $\mu\text{m}$  periodic ridged profile of the grating by three sensor outputs (i.e., output P1 of sensors S1, S2, and S4) during the whole stimulus sliding in the time interval  $t_1 = 0.5$  s to  $t_3 =$

3.0 s. The right inset of Fig. 2 focuses on the velocity step at  $t_2 = 2.0$  s from  $v_1$  (6.7 mm/s) to  $v_2$  (10.0 mm/s), showing excellent dynamic modulation by the tactile sensor array in encoding vibratory cues according to (1). To point out precise coherence in dynamic frequency encoding, such velocity transient at  $t_2 = 2.0$  s is inspected via WT and XWT in Fig. 3, which shows that the frequency carrying the highest power (i.e., colored in red) modulates from 13.9 to 20.8 Hz, according to the expected values (see Table I).

Table II presents statistical indices across all runs, thereby demonstrating stable conditions in passive-touch: the roughness encoding by the sensory system lasted steadily for the whole duration of the sliding stimulus. As an example confirming very low variability, the standard deviation of  $f_{MP}$  was at most 1.6% of its mean value (0.4 Hz/25.0 Hz) and the difference between  $\bar{M}f_{MP}$  and  $\overline{mf}_{MP}$  indices was reduced. Importantly, the experimental fundamental frequencies  $f_{MP}$  were in strict accordance with the expected ones (see Table I). A lookup table, based on theoretical fundamental frequencies (see Table I) and thresholds, guarantees 100% success in classifying the gratings down to the tested 40  $\mu\text{m}$  difference in spatial coarseness.

##### B. Active-Touch Experiments With Gratings

The active stereotyped exploratory task presented a subset lasting about 150 ms, during which the spatial coarseness of the tactile stimuli was encoded with vibrational features by, at least, one unit of the array (cf., Fig. 4). An overlap of about 80 ms was observed [see Fig. 4 (right)] for the combined vibrational activation of distal sensor units (i.e., S1 and S2) and proximal sensor ones (i.e., S3 and S4, with the former not shown for the sake of graphical clearness). Fig. 5 shows WT and XWT applied to P1S4, P1S1, and P1S2, and  $t_{MP}$  resulting from the analysis of signals gathered by pairs of sensor outputs. The shifting of the high-power red zone toward higher frequencies reveals that the end-effector velocity varied (increasing) with time, while rubbing the sample. Variation of end-effector velocity within each active-touch rub is also confirmed by the higher values of the standard deviation of  $f_{MP}$ , which was at most 8.3% of its mean value (5.5 Hz/65.9 Hz; see Table III), and higher difference between  $\bar{M}f_{MP}$  and  $\overline{mf}_{MP}$  indices, in comparison with the constant-velocity passive-touch tests (see Table II).

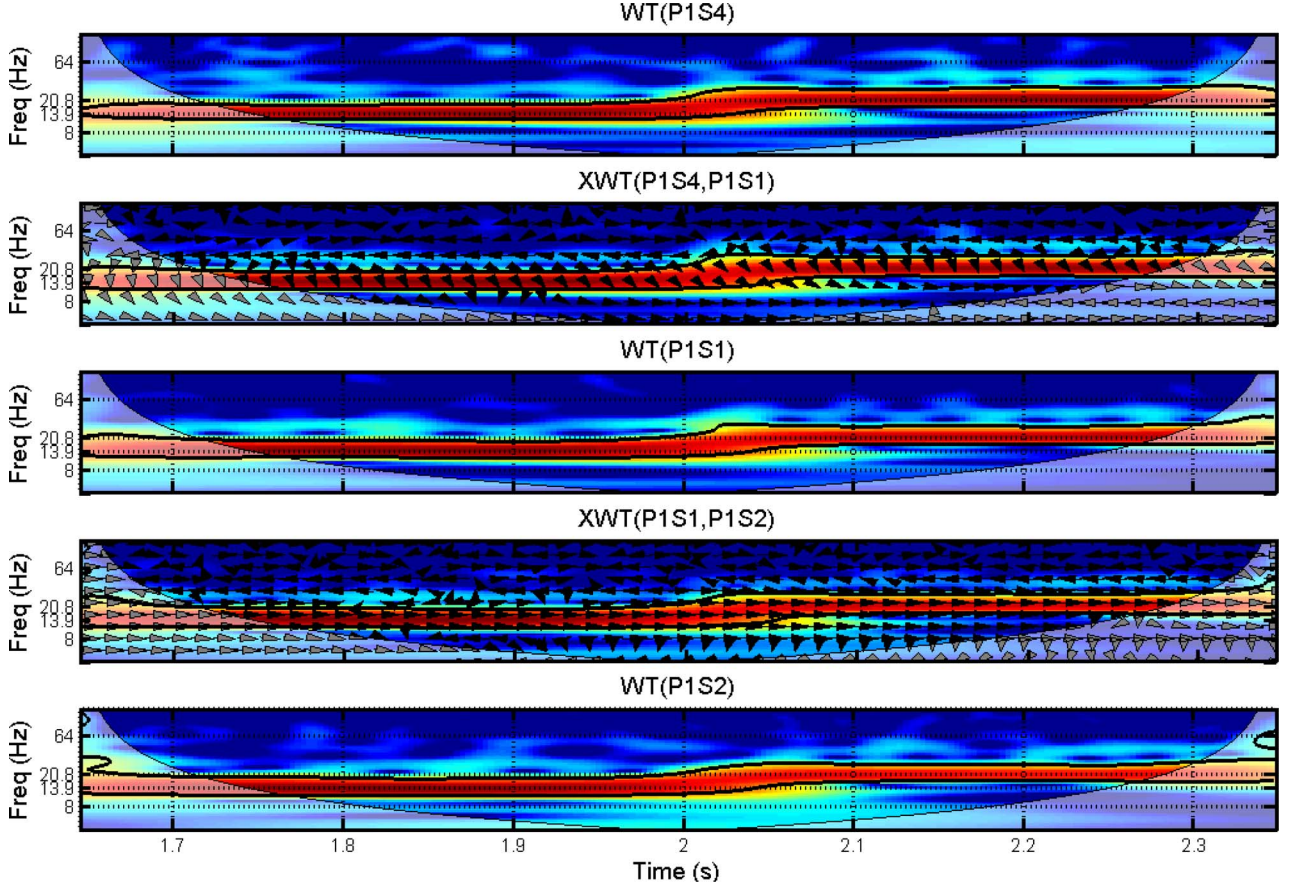


Fig. 3. WT on single channels (i.e., P1S4, P1S1, and P1S2) of the array and XWT on channel pairs P1S4–P1S1 and P1S1–P1S2. The plots focus on the velocity step during the passive-touch presentation of the 480- $\mu\text{m}$  stimulus to the robotic finger, showing the frequency shift from 13.9 to 20.8 Hz according to (1). High-power regions in time–frequency space are colored in red. The thick contour surrounding the red region identifies the 5% significant level. The arrows in the XWT plots are a graphical representation of the phase difference between the pairs of channels (pointing right: in-phase; left: antiphase; down: series 1 leading series 2 by 90°).

TABLE II  
STATISTICAL INDICES IN PASSIVE-TOUCH EXPERIMENTS

Statistical index	O1 O2	Stimulus spatial period $\Delta p$					
		400 $\mu\text{m}$ runs 1-8		440 $\mu\text{m}$ runs 9-16		480 $\mu\text{m}$ runs 17-24	
		Stimulus sliding velocity (mm/s)					
		6.7	10.0	6.7	10.0	6.7	10.0
$\bar{f}_{MP}(O1, O2)$ (Hz)	P1S1 P1S2	16.6	25.0	15.1	22.8	13.7	20.8
	P1S4 P1S1	16.6	25.0	15.1	22.7	13.7	20.8
$\Delta f_{MP}(O1, O2)$ (Hz)	P1S1 P1S2	0.2	0.3	0.1	0.2	0.1	0.2
	P1S4 P1S1	0.1	0.4	0.1	0.2	0.1	0.2
$\overline{Mf}_{MP}(O1, O2)$ (Hz)	P1S1 P1S2	16.9	25.5	15.3	23.1	13.9	21.0
	P1S4 P1S1	16.8	25.9	15.3	23.1	13.8	21.1
$\overline{mf}_{MP}(O1, O2)$ (Hz)	P1S1 P1S2	16.3	24.6	14.9	22.4	13.5	20.5
	P1S4 P1S1	16.3	24.5	14.9	22.3	13.5	20.5

Fig. 7 shows a plot of the 20 samples subset per run of  $f_{MP}(P1S4, P1S1)$  and  $f_{MP}(P1S1, P1S2)$  around  $t_{MP}(P1S4, P1S1)$  and  $t_{MP}(P1S1, P1S2)$ , as defined in (2) and (3). The fundamental frequency  $f_{MP}$ , as shown in Fig. 7, is monotonically modulated from a lower value to a higher one, due to the increasing nonconstant speed, within each run in the considered 20 samples. Despite of overlap of instant fundamental frequencies  $f_{MP}$  arising in active-touch with different gratings, Fig. 7 reveals a clear separation among the three tactile stimuli, as indicated by the black dots representing the mean fundamental frequency  $\bar{f}_{MP}$  run by run per couple of sensor outputs. This is more evident in the scatter plot of  $\bar{f}_{MP}$  values resulting from the two considered channel pairs (cf., Fig. 8), which reveals a clear clustering of the grating spatial period  $\Delta p$  and reduced variance  $\Delta \bar{f}_{MP}$  (across the repeated runs) of the mean fundamental frequency, as confirmed by the depicted ellipses in Fig. 8. It is significant to point out that, coherently with the physical model underlying (1), finer grating spatial periods  $\Delta p$  resulted in higher frequencies in both the axes of Fig. 8. Due to high repeatability, a  $k$ -NN classification applied to data of Fig. 8 guaranteed excellent discrimination performance (see Table IV). A 97.6% identification accuracy was obtained in the worst-case training based on a single run per stimulus and the other runs used as validation set (i.e., leave-21-out). The accuracy raised to 100%

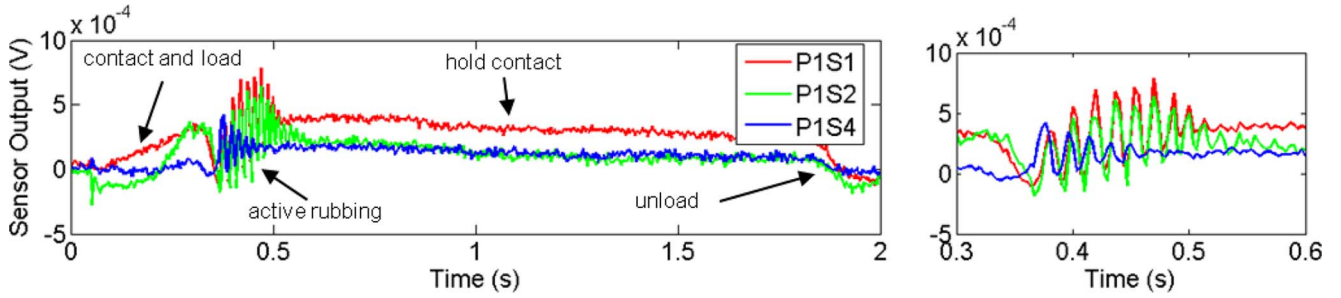


Fig. 4. Time-domain plots under an active-touch experiment with the ridged tactile stimulus having spatial period  $\Delta p = 480 \mu\text{m}$  [P1S1, P1S2, and P1S4, according to the labeling of Fig. 1(b) and (c)]. The graphs show experimental data comprising the load, rubbing, and unload phases of the active-touch exploratory task. The plot on the right focuses on the active rubbing of the ridged stimulus, which shows vibrational encoding of roughness. Similarly to the passive-touch experiment shown in Fig. 2, the signal from P1S1 is in-phase with P1S2 and shows a phase difference with P1S4, as expected from (4).

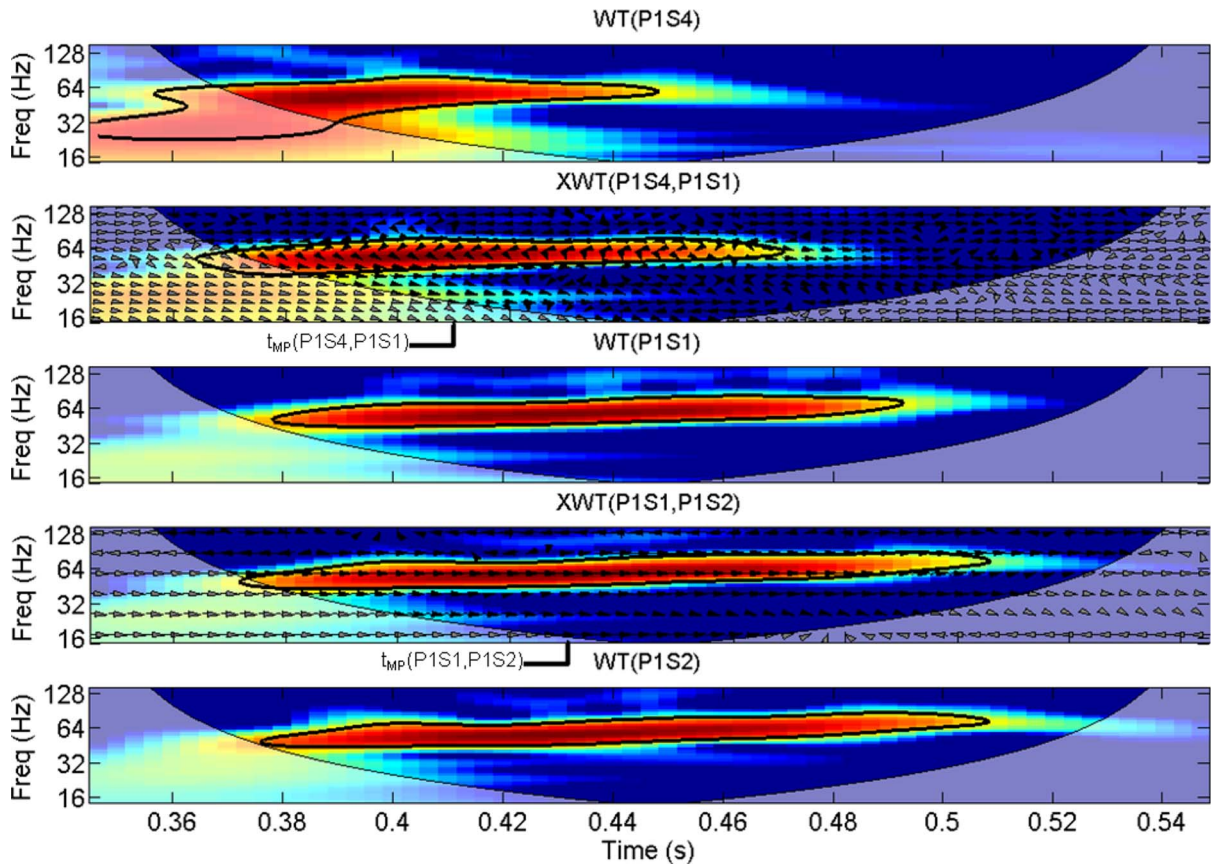


Fig. 5. WT on single channels (i.e., P1S4, P1S1, and P1S2) of the array and XWT on channel pairs P1S4–P1S1 and P1S1–P1S2. The plots focus on the active-touch exploration of the  $480\text{-}\mu\text{m}$  stimulus by the robotic finger, showing the frequency encoding during the rubbing phase, which is a function of the stimulus spatial period and the time-variant velocity according to (1). High-power regions in time–frequency space are colored in red and  $t_{\text{MP}}$  are indicated for both the channel pairs. The thick contour surrounding the red region identifies the 5% significant level. The arrows in the XWT plots are a graphical representation of the phase difference between the pairs of channels (pointing right: in-phase; left: antiphase; down: series1 leading series 2 by  $90^\circ$ ).

with all the gratings by using at least four runs per stimulus as a training set (i.e., leave-12-out).

Velocity was constant and known (either 6.7 or 10.0 mm/s was tested) in passive-touch experiments, while in active-touch, it was not directly measured. However, as a final evaluation of tested velocity range in comparison with typical human exploratory tasks, we can reconstruct this information by inverting (1) via the knowledge of tested stimuli and measured  $\overline{Mf}_{\text{MP}}$  and  $\overline{mf}_{\text{MP}}$  indices (see Table III), thereby resulting in active-touch

velocities monotonically increasing approximately from 22 to 31 mm/s within the significant portion (which is around  $t_{\text{MP}}$ ) of each run. Thus, the tested velocities belong to the wide range (from a few millimeters per second up to more than a hundred of millimeters per second) used, with no significant related effect on perceived roughness, by humans during active exploratory tasks [42].

A compared inspection of the three time-domain plots aligned vertically in Fig. 6 confirms that a change in the grating spatial

TABLE III  
 STATISTICAL INDICES IN ACTIVE-TOUCH EXPERIMENTS

Statistical index	O1 O2	Grating spatial period $\Delta p$		
		400 $\mu\text{m}$ (runs 1-8)	440 $\mu\text{m}$ (runs 9-16)	480 $\mu\text{m}$ (runs 17-24)
$\bar{f}_{MP}(O1, O2)$ (Hz)	P1S1 P1S2	65.9	60.9	58.3
	P1S4 P1S1	66.2	58.4	54.6
$\Delta f_{MP}(O1, O2)$ (Hz)	P1S1 P1S2	5.5	4.3	3.9
	P1S4 P1S1	5.1	2.5	2.4
$\overline{Mf}_{MP}(O1, O2)$ (Hz)	P1S4 P1S2	75.9	68.8	64.5
	P1S4 P1S1	75.8	62.4	58.1
$\overline{mf}_{MP}(O1, O2)$ (Hz)	P1S1 P1S2	57.2	55.9	53.8
	P1S4 P1S1	58.4	54.7	49.8

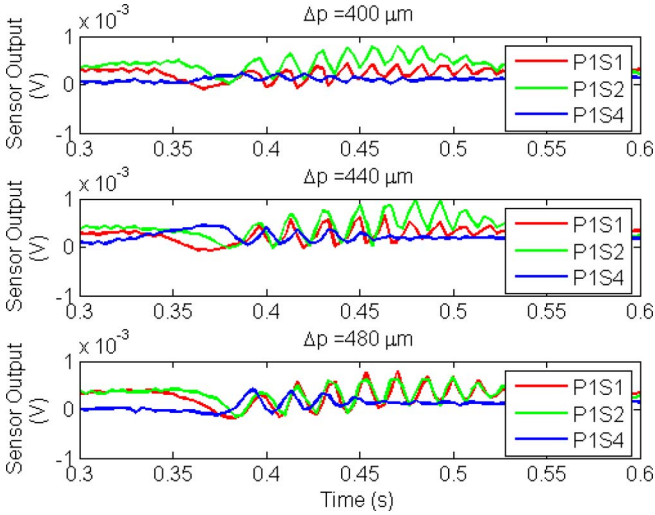


Fig. 6. Active-touch vibrational frequency encoding in time domain of the grating spatial period  $\Delta p$  by sensor outputs P1S1, P1S2, and P1S4. Moreover, P1S1 and P1S2 are always in-phase, while the phase difference with P1S4 varies, depending on the surface (as confirmed by the horizontal shift of the blue trace with respect to the red and green ones, while comparing the plots for the three values of the grating spatial period  $\Delta p$ ), coherently with (4).

period  $\Delta p$  causes a modulation of the vibrational cues in active-touch.

## V. INSIGHTS ON FUTURE WORK

### A. Toward Surface Classification With Nonstereotyped Exploratory Movements: Phase Locking

Phase information was taken into account as a further feature in addition to the fundamental frequency useful for discriminating among surfaces. A qualitative discussion of related results is presented here as a preliminary study for future works addressing passive-touch experiments without the limiting condition on

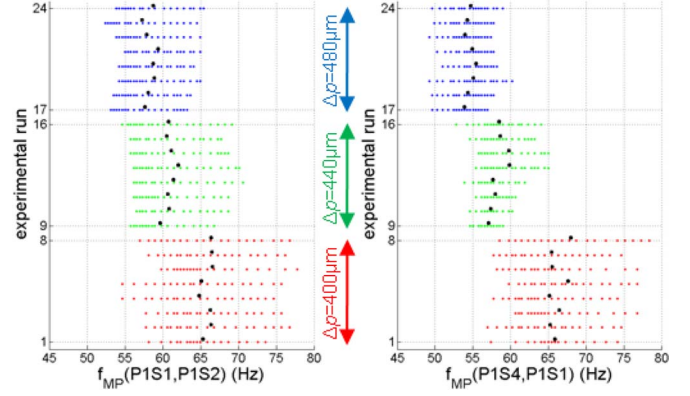


Fig. 7. Maximum-power frequencies  $f_{MP}(P1S4, P1S1)$  and  $f_{MP}(P1S1, P1S2)$  are depicted with colored dots under the active-touch protocol (red:  $\Delta p = 400 \mu\text{m}$ ; green:  $\Delta p = 440 \mu\text{m}$ ; blue:  $\Delta p = 480 \mu\text{m}$ ). A total of 20 samples of  $f_{MP}$  around  $t_{MP}$  are shown per experimental run. A separation between the fundamental-frequency values gathered with the three tactile stimuli can be appreciated. (Black dots) Mean frequency  $\bar{f}_{MP}$  resulting from a run-by-run averaging operation. The wide distribution around the black dots is due to the varying velocity within each active rub session, as confirmed by standard deviation given in Table III.

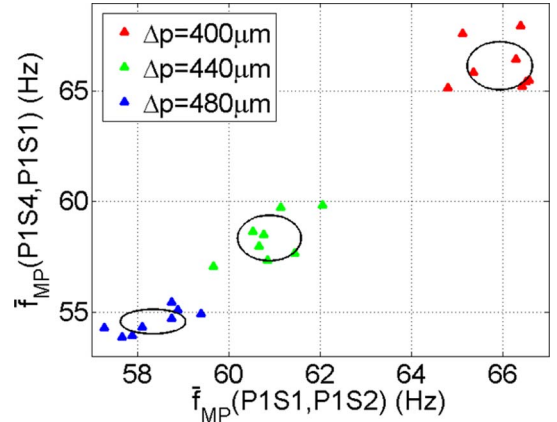


Fig. 8. Scatter plot of the run-by-run mean values of the fundamental frequencies, i.e.,  $\bar{f}_{MP}(P1S1, P1S2)$  and  $\bar{f}_{MP}(P1S4, P1S1)$ , identified by two pairs of sensor outputs under the active-touch protocol. A clear clustering is shown, depending on the explored surface, and coherent frequency-increase while decreasing the spatial period  $\Delta p$  of the grating. The ellipses depict low dispersion of data, as a result of significant repeatability. These are centered on the centroid of each cluster and have axes lengths set to twice the standard deviation of  $\bar{f}_{MP}$  values belonging to each cluster.

constant (or known) stimulus-velocity or active exploration of surfaces under general nonstereotyped trajectories.

Considering piezoresistors belonging to sensor tethers that are oriented along the same direction, we expect the gathered output signals to show vibrational components having a phase difference  $\Delta\varphi_{i,j}$  being independent on the stimulus sliding-velocity

$$\Delta\varphi_{i,j} = 2\pi \frac{\Delta y_{j,i}}{\Delta p} \quad (4)$$

where  $\Delta y_{j,i} = y_i - y_j$  is the difference of the y-coordinates of sensor  $S_i$  and sensor  $S_j$  (while considering sensors aligned along the finger axis, i.e., S1–S4 and S2–S3,  $\Delta y_{j,i}$  corresponds to the 2.36 mm pitch of the array in case that the plane of the

TABLE IV  
PERCENT DISCRIMINATION ACCURACY WITH GRATINGS AS TACTILE STIMULI,  
VIA  $k$ -NN CLASSIFICATION AND LEAVE- $M$ -OUT VALIDATION  
(SEE SECTION III-C3)

	Grating spatial period $\Delta p$		
	400 $\mu\text{m}$ (runs 1-8)	440 $\mu\text{m}$ (runs 9-16)	480 $\mu\text{m}$ (runs 17-24)
$M=3,6,9,12$ (1..4 runs out x 3 surfaces)	100.0%	100.0%	100.0%
$M=15$ (5 runs out x3 surfaces)	100.0%	99.9%	100.0%
$M=18$ (6 runs out x3 surfaces)	100.0%	99.3%	99.8%
$M=21$ (7 runs out x3 surfaces)	100.0%	97.6%	99.3%

sensors is parallel to the stimulus), according to the labeling introduced in Fig. 1(a). This results in signals always in-phase if considering the couple S1–S2 or the couple S3–S4 and with phase differences depending on the tactile stimulus for the other combinations.

In passive-touch, during finger–stimulus contact, sensors S1 and S2 of the array on the distal part of the phalanx were simultaneously aligned under the same ridge of each grating [same  $y$ -coordinate, i.e.,  $\Delta y_{1,2} = 0$ , according to the reference frame in Fig. 1(d)]. Therefore, coherently with (4), the outputs from piezoresistors belonging to sensor tethers which are oriented along the same direction (e.g., P1S1 and P1S2), were in-phase for all the runs, regardless of the grating spatial period. This is also confirmed in time domain in Fig. 2 (in-phase P1S1 and P1S2 signals) and depicted by the horizontal arrows in time–frequency space of the XWT(P1S1,P1S2) plots in Fig. 3. Conversely, a phase difference was observed from sensor units lodged at different positions along the axis of the finger (e.g., P1S1 and P1S4, which are represented with red and blue traces in Fig. 2 and with arrows in the second subplot of Fig. 3). Velocity had no effect on the phase relationships, as shown by the arrows before and after the velocity variation at  $t_2 = 2.0$  s in Fig. 3. This property of *phase locking* is coherent with (4) (since no velocity appears in the equation) and can be applied to remove the velocity dependence of (1). However, a problem occurs with respect to (4): Phase differences can be experimentally measured only in a  $2\pi$  range, thus introducing limiting conditions to invert (4) (i.e.,  $\Delta p > 2\Delta y_{\text{pitch}} = 4.72$  mm or  $\Delta p > \Delta y_{\text{pitch}} = 2.36$  mm, depending on the knowledge of the sign of the relative finger–stimulus velocity). This means that, by just considering two spatially located sensors of a regular array, phase differences can be analytically reconstructed only in case that two sensors are encountered along the rubbing direction within a half- or full-spatial wavelength of the tactile stimulus. Such limiting conditions for spatially distributed sam-

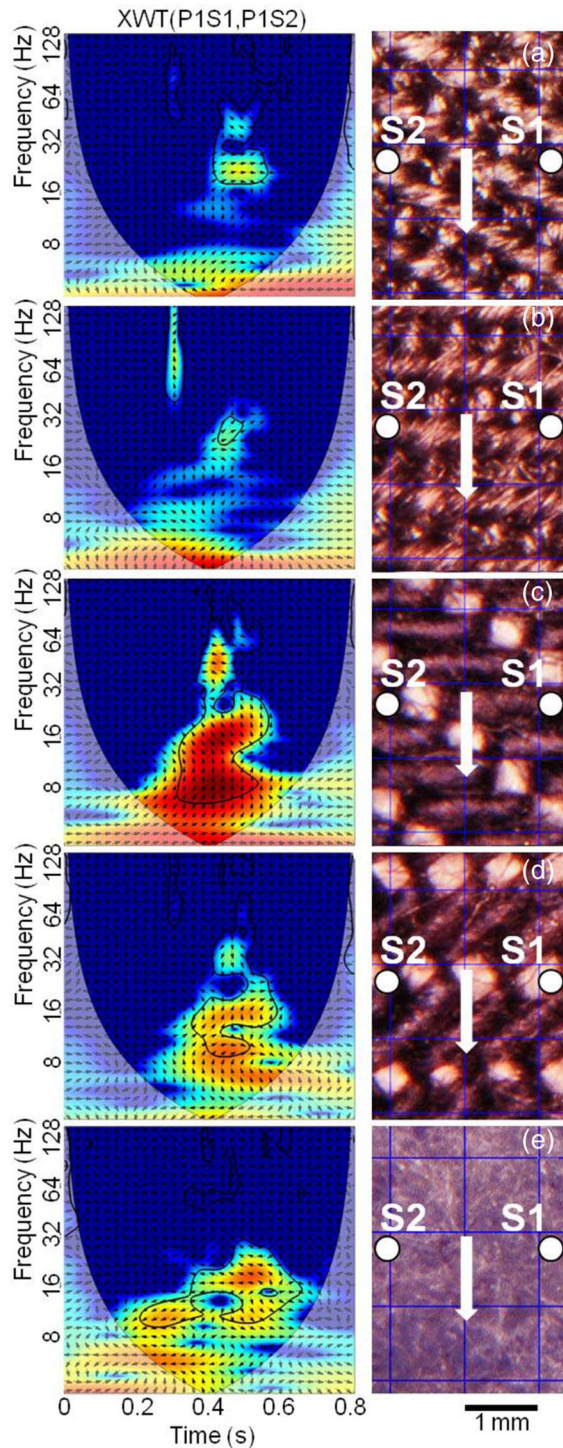


Fig. 9. (Left plots) XWT on channel pair P1S1–P1S2 during active rubbing of five textiles (see Section V-B). The textured structure of each specimen is shown on the right by means of optical microscopy (Hirox KH-7700 digital microscope). The relative positioning of sensors S1 and S2 is marked on the right images, together with an arrow representing the active rubbing direction.

pling are equivalent to the Nyquist theorem for time-domain sampling.

Gratings with different spatial period  $\Delta p$  caused a modulation in the relative phase between units lodged along the direction of the finger axis (e.g., S4 with respect to S1 and S2) in active-touch as well. Consistently with (4), the phase difference between units

aligned across the finger axis (e.g., S1–S2, with  $\Delta y_{1,2} = 0$  mm) did not modulate. As an example from two couples of outputs from the array in both time (i.e., inspecting the relative timing between vibratory peaks in Fig. 4) and time–frequency (i.e., inspecting the arrows in Fig. 5) domains, the signals from P1S1 and P1S2 were in-phase, while a phase difference was observed between P1S4 and P1S1. The same behavior is shown in Fig. 6 for all the three used gratings (varying in  $\Delta p$ ), as confirmed by the horizontal shift of the blue trace with respect to the red and green ones. It is relevant to point out that the phase relationships around the red high-power time–frequency regions (i.e., around  $t_{MP}$ ), as depicted for active-touch in Fig. 5, were consistent with the passive-touch ones (cf., Fig. 3). This is observable by comparing the arrows (equal down-right pointing) in the significant regions of the two figures. Further related results and considerations are left to future works.

### B. Active-Touch Experiments With Textiles

Five textiles were tested in active-touch to preliminarily evaluate discrimination suitability in a more realistic tactile-stimulation scenario with respect to gratings. The five surfaces were a fine-denim cut along two different orientations [see Fig. 9(a) and (b)], a coarse-denim cut along two different orientations [see Fig. 9(c) and (d)], and a nap textile [see Fig. 9(e)]. The active-touch protocol detailed in Section III-B2 was used. For all the runs and textiles, the XWT was calculated on channel pairs to inspect data. Fig. 9 depicts one XWT(P1S1,P1S2) example for each textile. Each surface showed a repeatable *specific pattern* in time–frequency space in all the eight runs. Such repeatability was confirmed calculating the correlation indices for each time-domain raw single-sensor output over all the combinations of pairs of repeated runs with the same textile. As an example, average correlation coefficients for channel P1S1 over repeated runs are  $0.96 \pm 0.01$  for textiles A and E,  $0.97 \pm 0.01$  for textiles B and C and  $0.98 \pm 0.01$  for textile D. All the coefficients are very close to one with a significant confidence interval, thereby demonstrating high repeatability and, thus, confirming the suitability for the discrimination of realistic surfaces. Moreover, average correlation coefficients lower in a range between 0.78 and 0.90, with significant confidence as well, while considering combinations of runs related to pairs of different stimuli.

Textiles present a surface structure being more complex and realistic with respect to gratings. Therefore, a number of spectral components rather than a single fundamental frequency should be taken into account in order to yield high classification performance (up to the full time-varying spectrum to succeed in the discrimination of unspecified tactile stimuli having a very complex surface structure). The extension and generalization of the discrimination technique presented for gratings in Section IV-B will be investigated in future works. Sandpaper tactile stimuli will be experimented as well: despite the fact that sandpaper is not usual in everyday-life tactile experience in comparison with textiles, it represents a significant testbed (as is confirmed by related psychophysical studies [24]) due to its aperiodic, but still standardized (grit size), surface structure.

## VI. CONCLUSION

The vibratory patterns recorded by the sensor array during the sliding motion of gratings at known constant velocity coherently modulated at the expected frequency in passive-touch. The significant results shown under the passive-touch protocol constituted the foundations for the subsequent active-touch investigation. The XWT on outputs from adjacent sensors of the array revealed a fundamental spectral component being a function of time when the robotic finger actively explored the tactile stimuli. Despite of the nonconstant scanning velocity, the finger stereotyped exploratory-movement allowed to encode the spatial coarseness of gratings by identifying, in a 67-ms window (i.e., 20 samples at 300 Hz) of time–frequency space, the set of spectral components conveying the highest cross power between adjacent sensors.

This study showed the capability to discriminate among surfaces having spatial periods differing down to  $40 \mu\text{m}$ , both under passive-touch and under human-like active-touch tasks. Performance in the active-touch discrimination of gratings was excellent, with worst-case accuracy (97.6%; see Table IV) being much higher than the one-third performance in case of random choice. Therefore, the  $40\text{-}\mu\text{m}$  threshold underestimates the potential performance, and the developed technology could ensure better results while being tested with finer stimuli.

The evaluation of the robotic finger was operated with contact forces and velocities in the range used by humans during tactile exploratory tasks. In active-touch experiments with gratings, exteroceptive information (i.e., tactile cues) was enough for the successful coarseness encoding (see Figs. 4–8) and discrimination of surfaces (see Table IV), without the need to consider proprioceptive data (such as end-effector velocity). This could open various possibilities, while pursuing the integration of the developed artificial touch technology into an upper limb prosthesis via noninvasive (e.g., vibrating tactors [43]) or invasive (e.g., direct peripheral neural feedback [44], [45]) interfaces.

The proposed method is neither temporal nor spatial; rather, it is spatiotemporal because it is based on the temporal (i.e., vibrational) roughness encoding by each single sensor and on the combined observation by spatially adjacent units of the array to identify the data subset to focus on for analysis. Phase information (see Section V-A) via neighboring observers distributed on the surface of the fingerpad is associated with spatiotemporal variation as well.

Preliminary experimental results presented in Section V-B with textiles are promising, and future experiments will be oriented toward a quantitative analysis of discrimination accuracy with a wide set of everyday-life surfaces.

In future works, we will investigate more on how to implement classification techniques based on the *phase locking* between signals gathered by adjacent sensors of the array; to this aim, a smartly distributed sensor array and *phase locking* could be applied to emulate the hypothetical human model for coincidence detection shown in [11]. Attention will be paid to smart irregular physical positioning of sensor units, by getting design inputs from the biological model. This would allow to obtain a system of multiple phase relationships to solve, under

general unconstrained exploratory motions, spatial features being finer than the NN spacing of tactile units, as it happens in humans [5]. Therefore, following our aim while moving from passive to stereotyped active-touch protocols, phase relationships could be introduced as a further classification feature to go toward less-structured experimental conditions without requiring the exploratory movement to be stereotyped.

#### ACKNOWLEDGMENT

The authors thank N. Vitiello, F. Mattioli, R. Di Leonardo, and C. Filippeschi (Scuola Superiore Sant'Anna) and M. Mitulla and S. Schmitt (Institute of Microtechnology, Mainz) for technical support. Valuable conversations with J. Wessberg (Department of Physiology, University of Gothenburg) and with L. Pape (Dalle Molle Institute for Artificial Intelligence, Lugano) are gratefully acknowledged. The experimented tactile stimuli were provided by S. Johnson and B. Ranken (Unilever R&D, Port Sunlight). Crosswavelet and wavelet coherence software were provided by A. Grinsted.

#### REFERENCES

- [1] P. Dario, "Tactile sensing-technology and applications," *Sens. Actuators A: Phys.*, vol. 26, pp. 251–261, 1991.
- [2] R. D. Howe, "Tactile sensing and control of robotic manipulation," *Adv. Robotics*, vol. 8, no. 3, pp. 245–261, 1994.
- [3] A. Bicchi, "Hands for dextrous manipulation and powerful grasping: A difficult road towards simplicity," *IEEE Trans. Robot. Autom.*, vol. 16, no. 6, pp. 652–662, Dec. 2000.
- [4] E. Biddiss, D. Beaton, and T. Chau, "Consumer design priorities for upper limb prosthetics," *Disability Rehabil.: Assistive Technol.*, vol. 2, no. 6, pp. 346–357, 2007.
- [5] T. Yoshioka, B. Gibb, A. K. Dorsch, S. S. Hsiao, and K. O. Johnson, "Neural coding mechanisms underlying perceived roughness of finely textured surfaces," *J. Neurosci.*, vol. 21, no. 17, pp. 6905–6916, 2001.
- [6] K. O. Johnson and T. Yoshioka, "Neural mechanisms of tactile form and texture perception," in *The Somatosensory System: Deciphering the Brain's Own Body Image*, Nelson, R. J., Ed. Boca Raton, FL: CRC, 2001, pp. 73–101.
- [7] V. Maheshwari and R. Saraf, "High-resolution thin-film device to sense texture by touch," *Science*, vol. 312, pp. 1501–1504, 2006.
- [8] M. Hollins, R. Faldowski, S. Rao, and F. Young, "Perceptual dimensions of tactile surface texture: A multidimensional scaling analysis," *Percept. Psychophys.*, vol. 54, no. 6, pp. 697–705, 1993.
- [9] T. Yoshioka, S. J. Bensamaïa, J. C. Craig, and S. S. Hsiao, "Texture perception through direct and indirect touch: An analysis of perceptual space for tactile textures in two modes of exploration," *Somatosens. Mot. Res.*, vol. 24, no. 1, pp. 53–70, 2007.
- [10] T. Yoshioka and J. Zhou, "Factors involved in tactile texture perception through probes," *Adv. Robotics*, vol. 23, pp. 747–766, 2009.
- [11] R. S. Johansson and J. R. Flanagan, "Coding and use of tactile signals from the fingertips in object manipulation tasks," *Nature Rev. Neurosci.*, vol. 10, pp. 345–359, 2009.
- [12] M. C. Carrozza, G. Cappiello, S. Micera, B. B. Edin, L. Beccai, and C. Cipriani, "Design of a cybernetic hand for perception and action," *Biol. Cybern.*, vol. 95, no. 6, pp. 629–644, 2006.
- [13] C. Cipriani, M. Controzzi, and M. C. Carrozza, "Objectives, criteria and methods for the design of the smarthand transradial prosthesis," *Robotica*, vol. 28, no. 6, pp. 919–927, 2010.
- [14] K. Hosoda, Y. Tada, and M. Asada, "Anthropomorphic robotic soft fingertip with randomly distributed receptors," *Robot. Auton. Syst.*, vol. 54, pp. 104–109, 2006.
- [15] N. Wettels, V. J. Santos, R. S. Johansson, and G. E. Loeb, "Biomimetic tactile sensor array," *Adv. Robot.*, vol. 22, pp. 829–849, 2008.
- [16] C. H. Lin, T. W. Erickson, J. A. Fishel, N. Wettels, and G. E. Loeb, "Signal processing and fabrication of a biomimetic tactile sensor array with thermal, force and microvibration modalities," in *Proc. IEEE Int. Conf. Robot. Biomimetics*, Dec. 19–23, 2009, Guilin, China, pp. 129–134.
- [17] J. A. Fishel, V. J. Santos, and G. E. Loeb, "A robust micro-vibration sensor for biomimetic fingertips," in *Proc. 2nd IEEE/RAS-EMBS Int. Conf. Biomed. Robot. Biomechatron.*, Oct. 19–22, 2008, Scottsdale, AZ, pp. 659–663.
- [18] J. Edwards, J. Lawry, J. Rossiter, and C. Melhuish, "Extracting Textural Features from Tactile Sensors," *J. Bioinspiration Biomimetics*, vol. 3, pp. 1–12, 2008.
- [19] Y. Mukaibo, H. Shirado, M. Konyo, and T. Maeno, "Development of a texture sensor emulating the tissue structure and perceptual mechanism of human fingers," in *Proc. IEEE Int. Conf. Robot. Autom.*, 2005, pp. 2576–2581.
- [20] Y. Zhang, Y. Mukaibo, and T. Maeno, "Multi-purpose tactile sensor inspired by human finger for texture and tissue stiffness detection," in *Proc. IEEE Int. Conf. Robot. Biomimetics*, 2006, pp. 159–164.
- [21] T. Mouri, H. Kawasaki, K. Yoshikawa, J. Takai, and S. Ito, "Anthropomorphic robot hand: Gifu hand III," presented at ICCAS, Oct. 16–19, 2002, Jeonbuk, Korea.
- [22] H. Huang, L. Jiang, Y. Liu, L. Hou, H. Cai, and H. Liu, "The mechanical design and experiments of HIT/DLR prosthetic hand," in *Proc. IEEE Int. Conf. Robot. Biomimetics*, Dec. 17–20 2006, pp. 896–901.
- [23] C. M. Oddo, L. Beccai, G. G. Muscolo, and M. C. Carrozza, "A biomimetic MEMS-based tactile sensor array with fingerprints integrated in a robotic fingertip for artificial roughness encoding," in *Proc. IEEE Int. Conf. Robot. Biomimetics*, Guilin, China, 2009, pp. 894–900.
- [24] L. A. Jones and S. J. Lederman, "Tactile Sensing," in *Human Hand Function*, L. A. Jones and S. J. Lederman, Eds. New York: Oxford Univ. Press, 2006, pp. 44–74.
- [25] L. Birglen and C. M. Gosselin, "Kinetostatic analysis of underactuated fingers," *IEEE Trans. Robot. Autom.*, vol. 20, no. 2, Apr. 2004, pp. 211–221.
- [26] M. Luo, T. Mei, X. Wang, and Y. Yu, "Grasp characteristics of an underactuated robot hand," in *Proc. IEEE Int. Conf. Robot. Autom.*, 2004, pp. 2236–2241.
- [27] C. Cipriani, C. Antfolk, C. Balkenius, B. Rosén, G. Lundborg, M. C. Carrozza, and F. Sebelius, "A novel concept for a prosthetic hand with a bidirectional interface: A feasibility study," *IEEE Trans. Biomed. Eng.*, vol. 56, no. 11, pp. 2739–2743, Nov. 2009.
- [28] S. H. Scott, "Optimal feedback control and the neural basis of volitional motor control," *Nat. Rev. Neurosci.*, vol. 5, pp. 532–546, 2004.
- [29] B. Buchholz, T. J. Armstrong, and S. A. Goldstein, "Anthropometric data for describing the kinematics of the human hand," *Ergonomics*, vol. 35, no. 3, pp. 261–273, 1992.
- [30] S. Hirose, "Connected differential mechanism and its applications," in *Proc. Int. Conf. Advanced Robotics*, 1985, pp. 319–326.
- [31] L. Beccai, S. Roccella, A. Arena, F. Valvo, P. Valdastrì, A. Menciassi, and M. C. Carrozza, "Design and fabrication of a hybrid silicon three-axial force sensor for biomechanical applications," *Sens. Actuator A: Phys.*, vol. 120, pp. 370–382, 2005.
- [32] R. S. Johansson and Å. B. Vallbo, "Tactile sensibility in the human hand: relative and absolute densities of four types of mechanoreceptive units in glabrous skin," *J. Physiol. (Lond.)*, vol. 286, pp. 283–300, 1979.
- [33] T. Maeno, K. Kobayashi, and N. Yamazaki, "Relationship Between Structure of Finger Tissue and Location of Tactile Receptors," *JSME Int. J.*, vol. 41, no. 1, pp. 94–100, 1998.
- [34] D. Yamada, T. Maeno, and Y. Yamada, "Artificial finger skin having ridges and distributed tactile sensors used for grasp force control," *J. Robot. Mechatron.*, vol. 14, no. 2, pp. 140–146, 2002.
- [35] J. Scheibert, S. Leurent, A. Prevost, and G. Debrégeas, "The role of fingerprints in the coding of tactile information probed with a biomimetic sensor," *Science*, vol. 323, pp. 1503–1506, Jan. 2009.
- [36] R. M. Peters, E. Hackeman, and D. Goldreich, "Diminutive digits discern delicate details: fingertip size and the sex difference in tactile spatial acuity," *J. Neurosci.*, vol. 29, no. 50, pp. 15756–15761, Dec. 2009.
- [37] C. M. Oddo, L. Beccai, N. Vitiello, H. B. Wasling, J. Wessberg, and M. C. Carrozza, "A mechatronic platform for human touch studies," *Mechatronics*, to be published.
- [38] S. J. Lederman, "The perception of surface roughness by active and passive touch," *Bull. Psychon. Soc.*, vol. 18, no. 5, pp. 253–255, 1981.
- [39] A. Grinsted, J. C. Moore, and S. Jevrejeva, "Application of the cross wavelet transform and wavelet coherence to geophysical time series," *Nonlinear Processes Geophys.*, vol. 11, pp. 561–566, 2004.
- [40] C. M. Oddo, P. Valdastrì, L. Beccai, S. Roccella, M. C. Carrozza, and P. Dario, "Investigation on calibration methods for multi-axis, linear and redundant force sensors," *Meas. Sci. Technol.*, vol. 18, pp. 623–631, 2007.

- [41] L. Beccai, S. Roccella, L. Ascari, P. Valdastrì, A. Sieber, M. C. Carrozza, and P. Dario, "Development and experimental analysis of a soft compliant tactile microsensor for anthropomorphic artificial hand," *IEEE/ASME Trans. Mechatron.*, vol. 13, no. 2, pp. 158–168, Apr. 2008.
- [42] S. J. Lederman, "Tactile roughness perception: spatial and temporal determinants," *Can. J. Psychol.*, vol. 37, no. 4, pp. 498–511, 1983.
- [43] K. A. Kaczmarek, J. G. Webster, P. Bach-y-Rita, and W. J. Tompkins, "Electrotactile and vibrotactile displays for sensory substitution systems," *IEEE Trans. Biomed. Eng.*, vol. 38, no. 1, pp. 1–16, Jan. 1991.
- [44] G. Dhillon and K. Horch, "Direct neural sensory feedback and control of a prosthetic arm," *IEEE Trans. Neural Syst. Rehabil. Eng.*, vol. 13, no. 4, pp. 468–472, Dec. 2005.
- [45] P. M. Rossini, S. Micera, A. Benvenuto, J. Carpaneto, G. Cavallo, L. Citi, C. Cipriani, L. Denaro, V. Denaro, G. Di Pino, F. Ferreri, E. Guglielmelli, K. P. Hoffmann, S. Raspopovic, J. Rigosa, L. Rossini, M. Tombini, and P. Dario, "Double nerve intraneural interface implant on a human amputee for robotic hand control," *Clin. Neurophysiol.*, vol. 121, no. 5, pp. 777–783, 2010.



**Calogero M. Oddo** was born in 1983. He received, all *cum laude*, the B.Sc. degree in 2005 and the M.Sc. degree in 2007 in electrical engineering from the University of Pisa, Pisa, Italy, and the first- and second-level degrees, in 2006 and 2009, respectively, in industrial and information engineering from the Scuola Superiore Sant'Anna, Pisa, where he is currently working toward the Ph.D. degree in biorobotics.

In 2006, he participated in the Ninth European Space Agency (ESA) Student Parabolic Flight Campaign, and in 2008, he participated in the First ESA Lunar Robotics Challenge. His current research interests include human and artificial tactile sensing. He has authored or coauthored 21 peer-reviewed scientific papers (with six in ISI journals) and extended abstracts.

Mr. Oddo won the Biorobotics prize, which was established by the Alumni Association of Scuola Superiore Sant'Anna, for his B.Sc. thesis. He was finalist for the Best-Student-Paper Award at the IEEE RoBio09 conference.



**Marco Controzzi** (S'10) received the M.Sc. degree in mechanical engineering from the University of Pisa, Pisa, Italy, in 2008. He is currently working toward the Ph.D. degree in biorobotics with the Scuola Superiore Sant'Anna, Pisa.

In June 2006, he joined the Advanced Robotics Technology and Systems (ARTS) Laboratory, Scuola Superiore Sant'Anna, Pisa, as a Research Assistant. He is a Cofounder of one of the spin-offs of the Scuola Superiore Sant'Anna. He is an author or coauthor of ten peer-reviewed scientific papers and two patents.

His current research interests include the mechanical design of anthropomorphic robotic and prosthetic hands and arms and analytical models for grasping and manipulation.

Mr. Controzzi won the 2009 Antonio d'Auria Award (open to European citizens) from the Italian Robotics and Automation Association.



**Lucia Beccai** (M'08) received the Laurea degree in electronic engineering from the University of Pisa, Pisa, Italy, in 1998 and the Ph.D. degree in microsystem engineering from the University of Rome Tor Vergata, Rome, Italy, in 2003.

Since 1999, she has performed research at both the Center of Research In Microengineering and ARTS laboratories of Scuola Superiore Sant'Anna, Pisa, where, from 2008, she had a temporary position of Assistant Professor of bioengineering. She contributed to many international projects and was responsible for research management activities in several of them, addressing investigations related to biomedical microsystems for in-vivo applications, microelectromechanical systems, bioinspired solutions for bionic hand sensory feedback systems, the understanding of human tactile encoding mechanisms, and the development of artificial systems that can mimic selected tactile functionalities. Since 2009, she has been Team Leader at the Center for MicroBioRobotics@SSSA of Istituto Italiano di Tecnologia, Pontedera, Pisa, Italy, and her current scientific interests are related to the investigation of innovative sensing, actuation, and locomotion strategies in robotics using inspiration from Nature. Focus is on soft-bodied microrobots, biomimetic tactile sensors, and bio-hybrid sensing systems at the microscale. She is the author and co-author of several articles on refereed international journals and of more than 30 papers published in international conference proceedings.

Dr. Beccai is member of the IEEE Engineering in Medicine and Biology Society and the IEEE Robotics and Automation Society.



**Christian Cipriani** (S'06–M'09) received the M.Sc. degree in electronic engineering from the University of Pisa, Pisa, Italy, in 2004 and the Ph.D. degree in biorobotics from the Institutions Markets Technologies Institute for Advanced Studies, Lucca, Italy, in 2008.

He is currently an Assistant Professor of biomedical robotics with The BioRobotics Institute (which was formerly called the ARTS and CRIM Laboratories), Scuola Superiore Sant'Anna, Pisa. He is a Founder of a spin-off company. His current research interests include mechatronic, controllability, and sensory feedback issues of dexterous robotic hands to be used as mind-controlled prostheses.

Dr. Cipriani is a member of the IEEE Robotics and Automation and Engineering in Medicine and Biology Societies. He won the d'Auria Award in 2009 for prototypes of innovative robotic devices to aid the motor disabled from the Italian Robotics and Automation Association.



**Maria Chiara Carrozza** (M'04–A'06) received the M.Sc. degree in physics from the University of Pisa, Pisa, Italy, in 1990 and the Ph.D. degree in bioengineering from Scuola Superiore Sant'Anna, Pisa, in 1994.

She is currently a Professor of biomedical engineering and robotics, and since 2007, she has been the Director of the Scuola Superiore Sant'Anna. She was a Visiting Professor with the Technical University of Wien, Wien, Austria. She is a member of the Scientific Committee of the Italy–Japan Joint Laboratory, ROBOCASA, Waseda University, Tokyo, Japan. Her current research interests include biorobotics, rehabilitation robotics, artificial hands, and tactile sensing. She has authored or coauthored more than 60 papers on ISI Journals, 100 papers in referred conference proceedings, and 12 patents.

Prof. Carrozza is a member of the IEEE Engineering in Medicine and Biology and Robotics and Automation Societies.